Detection of higher visual function deficits and validation of multifocal pupillography in stroke, chiasmal compression and anterior ischemic optic neuropathy.

A thesis submitted for the degree of Doctor of Philosophy

of The Australian National University.

Dr Brendan Tonson-Older

Submitted for examination February 20, 2020

Declaration

I declare that this thesis is entirely my own original work, and that no component has previously been submitted to any university for any award or qualification. I have been the major contributor involved in all aspects in the production of this thesis including: design, data collection, analysis and writing. A portion of the data for the second experimental chapter was collected by persons other than myself to provide the opportunity for reanalysis in combination with my data, but all other analysis and collection of experimental data was carried out by myself. To the best of my knowledge, no component has been previously written or published prior to submission without due acknowledgement.

_____

Brendan Tonson-Older

20th February, 2020

Acknowledgements

Firstly I would like to acknowledge the support of my supevisors, Prof. Ted Maddess for introducing me to the world of ophthalmology and the generous use of his lab and equipment which made this project possible. To my chair Prof. Christian Lueck, who was always there to lend an ear, and whose advise was invaluable both inside and outside of research. To Assoc Prof. Jason Bell, who kindly designed the kinematogram with me, and who I could always rely on to have an open discussion and practical advice. To Dr Corinne Carle, who has invested much of her time helping me to where I am now, teaching me, and showing me the ropes of working in this lab, I also would not be here without your considerable support.

I would also like to especially thank Assoc Prof. Krisztina Valter-Kocsi, who supported me through both my PhD and medical school, through some of my darkest times.

To Diana Perriman and Ms Amelia Maddock, who had helped with numerous questions and concerns, and ensured my financial stability.

To those clinical staff who work on this project:

Emilie Rohan help with slitlamp exams, running the clinical suite, and always with a smile.

Dr Kate Reid, who was kind enough to refer many of the test subjects, and assess all the clinical information to rule out ocular disorders.

Dr Jocelyne Rivero, who first showed me how to use an OCT and the Humphrey devices, and showed me the basics of clinical assessment before the project began.

Dr Shaun Zhai – who referred stroke patients, and assessed neurological deficits in many of the subjects.

Dr Faran Sabeti and Ms Maria Kolic – who showed me many of the devices used in the clinical suite, and aided with my training.

To the various clinical and ANU departments who have supported me along this journey:

Canberra Hospital neurology department, Eye clinic, Calvary stroke ward, and Canberra eye hospital, for all the referrals and advice.

The ANU medical school for training me as a doctor, and supporting my PhD, and for the financial support in stipend and scholarship which allowed me to come here.

I would also like to recognise the excpetional work provided by the professional copy editor Dr Andrew Bell, who helped ensure the quality and continuity of my work.

To my family, especially my mother Jaqui Tonson and my aunt Barbara Tonson, who have always been there to talk and support me through the high and lows.

To my friends who have supported me through this long journey, especially Maree Silling who has kept me level headed and calm in periods of stress, and Hayley Fancourt, who has always been a ear to listen and the shoulder to cry on, and the person who has brought joy to my life just when I need it most.

Abstract

It is well established that neural damage can result in visual dysfunction, both visual field loss and in higher visual function (HVF) loss such as perceptions of depth, colour, motion and faces. This thesis examines these visual deficits in the common neurological diseases of stroke, chiasmal compression, and anterior ischemic optic neuropathy (AION).

While it is established that isolated complete HVF deficits do occur in stroke, they are also known to be rare. However, as HVFs are not routinely tested in clinical practice, it is unknown how common more subtle defects are, and what tools are effective in detecting these. Chapter 3 explores these questions, outlining that colour and depth perceptions are the most commonly affected, that Ishihara (colour) and stereofly and randot (depth), are the most useful tests, and outlines recommendations for improvement in some of these tools.

The relatively new invention of multifocal pupillographic objective perimetry (mfPOP) provides a number of benefits from other forms of perimetry. It measures both eyes at once, allowing measures of direct and consensual responses, it is objective, and it allows repeat measures of each region giving a measure of error. This advancement opens up new opportunities to investigate pupillary physiology in neurological disorders and adds new challenges in how to combine these signals into a single meaningful measure. Chapter 4 investigates the physiology of the pupil in stroke, chiasmal compression, and AION, and investigates how these components can be appropriately combined into a single measure. Results show naso-temporal differences are consistent with known physiology in control subjects and provides evidence that denser nasal retinal input may underpin the greater contraction anisocoria seen in temporal fields than in nasal fields.

With the intention that mfPOP be used in clinical practice, it must demonstrate it can perform as well as traditional perimetry, such as Humphrey and Matrix devices, in a wide range of disorders. Currently mfPOP testing neurological disorders has been very limited, and this represents a large gap in the literature. Chapter 5 compares mfPOP to Humphrey and Matrix perimeters, showing they mfPOP does not correlate well with these devices, and compares their utility in neurological disease. It shows that Humphrey appears the most useful device overall, with Matrix being exceptionally good in chiasmal compression, while mfPOP does not appear effective in these disorders.

With the first mfPOP approach having limitations in its diagnostic ability, a second stimulus protocol was designed using colour opponency with the measure of response latency (rather than amplitude), thought to preferentially stimulate cortical input to the pupil response, and may allow detection of cortical lesions. Chapter 6 investigates this new colour exchange protocol and latency measure, contrasting with the more common luminance approach used in chapter 5. It shows that the colour protocol shows a number of subtle differences compared to the luminance protocol, but does not show any greater utility in neurological disease. It reveals that latency and amplitude appear to have a weak positive relationship, and that mfPOP repeats appear to correlate well, but all measures have substantial variation.

These finding open up a number of future directions, from a larger and more focused HVF study into colour and depth perception, to considering retinal density as contributing towards biases in pupillary components, exploring hemifield ratios as a measure of early detection of chiasmal compression, and trialling other mfPOP methods to determine whether neurological disorders can be detected through pupillometry.

Table of Contents

Glossary: abbreviations

AION	Anterior ischemic optic neuropathy
AMD	Age-related macular degeneration
Amp	Peak amplitude (pupillary response)
ARK-1	Autorefractor and keratometer (Brand name)
AUC	Area under the curve
BCVA	Best corrected visual acuity
BFRT	Benton facial recognition test
BM	Basement membrane
CCC	Central corneal curvature
CCI	Colour confusion index (Farnsworth-Munsell)
CFMT	Cambridge facial memory test
CI	Confidence interval
CIELAB	International Commission of Illumination colour scale
CNIII	Cranial nerve number 3 (Occulomotor nerve)
Con	Consensual pupil response
CT	Computed tomography
D15	Farnsworth-Munsell Dichotomous 15-well test
Dir	Direct pupil response
DTI	Diffusion tensor imaging (Magnetic resonance scan)
DWI	Diffusion weighted imaging
EEG	Electroencephalogram
ETDRS	Early treatment of diabetic retinopathy study (Type of visual acuity chart)
EWN	Edinger-Westphal nuceli
FDT	Frequency doubling technology
FLAIR	Fluid attenuated inversion recovery (Magnetic resonance scan)
FM	Farnsworth-Munsell
FM100	Farnsworth-Munsell Dichotomous 100-well test
FPR	False positive ration
G/R	Bright green stimuli on dim red background
GCA	Giant cell arteritis
GCL	Ganglion cell layer
HFA	Humphrey field analyser
HH	Homonymous hemianopia
HVF	Higher visual function
ICC	Intraclass correlation coeffcient
ICH	Intracranial haemorrhage
ILM	Internal limiting membrane
INL	Inner nuclear layer
IOP	Intraocular pressure
IPL	Inner plexiform layer
ipRGC	intriniscally photoreceptive retinal ganglion cells
IS	Inner segment
Ishi	Ishihara 24-plate set

IT	Inferior temporal
K-cells	Koniocellular cells
Km	Kinematogram
LB	Line bisection (3x horizontal lines)
L-cone	Longwave cone (red)
LGN	Lateral geniculate nucleus
M-cells	Magnocellular cells
M-cone	Mediumwave cone (yellow)
MFA	Humphrey-Matrix field analyser
mfPOP	Multifocal pupillogrpahic objective perimetry
mfVEP	Multifocal visual evoked potentials
MLA	Maximum liklihood analysis
MRI	Magnetic resonance imaging
MT	Middle temporal region
NA-AION	Non-arteritic anterior ischemic optic neuropathy
OCT	Optical coherence tomography
ONH	Optic nerve head
ONL	Outer nuclear layer
OPL	Outer plexiform layer
Opn4	Melanopsin
ORA	Ocular response analyser
OS	Outer segment
P.pole	Posterior pole (Fundoscopy)
PCA	Principal component analysis
P-cells	Parvocellular cells
PON	Pretectal olivery nucleus
PWI	Perfusion weighted imaging
R&R	Relaxing and remitting (Multiple sclerosis)
Randot	Random Dot 3 (Stereoacuity test)
RD	Randot 3 with lea symbols
RDK	Random dot kinematogram
RGC	Retinal ganglion cells
RHT	Retinohypothalamic tract
RMF	Recognition memory test for faces
RNFL	Retinal nerve fibre layer
ROC	Receiver operator characteristics
RPE	Retinal pigment epithelium
SCN	Suprachiasmatic nucleus
S-cone	Shortwave cone (blue)
SD	Standard deviation
SE	Standard error
SF	Stereofly with lea symbols
SITA	Swedish interactive thresholding algorithms
SNR	Signar to noise ratio
Spectralis	Spectral domain optical coherence tomography (Brand name)
TCDS	Total colour difference score (Farnsworth-Munsell)

TTP	Time to peak (pupillary response)
V1	Primary visual cortex
V2-V8	Secondary visual cortices
VEP	Visual evoked potentials
VFD	Visual field defect
VFL	Visual field loss
Y/Y	Bright yellow stimuli on dim yellow background
ZEST	Zippy estimation of sequential testing

Chapter 1: Introduction

1.1. Statement of Purpose

It is well established that neural damage can result in visual dysfunction, both visual field loss and higher visual function[1] (HVF) loss which include facial recognition, motion, and depth and colour perception. While pure and complete HVF losses are rare, patients may also present with more subtle deficits and there is no measure of how commonly these deficits occur in stroke patients, nor which tests are most effective in detecting them. As they are not typically assessed in current clinical practice, they may frequently go undiagnosed, leading to slower recoveries, impaired quality of life, and potentially serious accidents.

The first part of this study is a pilot study investigating higher visual loss in stroke patients to ascertain if any deficits are sufficiently common to warrant further investigation and which tests provide the greatest utility in detection of these disorders.

Another form of visual impairment is visual field loss, which is typically assessed with perimetry. To increase consistency, there has been a transition over the last 25 years from traditional manual perimetry into automated perimetry, with the Humphrey field analyser and Matrix being two of the more commonly used perimeters. Both these machines require users to consciously respond to stimuli, making the test intrinsically subjective. Patients often do not respond appropriately, or in the case of stroke patients, they may have other limitations which prevent reliable testing. To address this, pupillographic perimetry was developed to eliminate

[1] Visial perception which is processed outside of the primary visual cortex. These include all manner of processing of the basic image to include colour, form, motion, recognition, and interpretation.

subjective patient responses and replace them with autonomic pupil responses. Given that it uses the pupil reflex (hundreds of milliseconds) – compared to perception, recognition, and motor output (seconds) – it also means regions can be tested much faster. More recently pupillographic perimetry has been further developed through multifocal methods which allow multiple stimuli to be presented simultaneously, increasing the number of presentations possible in a given time. This multifocal pupillographic objective perimetry (mfPOP) technology has been shown to be useful in a number of retinal disorders, but there has only been limited testing in neural disorders.

The second part of this study aims to investigate how damage to various parts of the visual pathway – anterior (anterior ischemic optic neuropathy, AION), chiasmal (chiasmal compression), and posterior (cortical stroke) – affect mfPOP measures. First, direct and consensual responses are compared to highlight the underlying physiology and determine appropriate means to amalgamate these signals. Secondly, to determine if mfPOP is sensitive enough to neural damage in these conditions, compared to existing Humphrey and Matrix devices, so as to be useful clinically. Lastly, to compare different stimuli protocols and measures to evaluate which approach is most useful and whether any additional information can be gleaned from alternative approaches. In particular, the aim is to determine whether post-lateral geniculate nucleus (LGN) damage (posterior to subcortical pupillary branch point) can be detected by mfPOP, and whether this is best measured with luminance only or colour-exchange protocols, using either size (amplitude) or time (latency) measures.

1.2. Overview of Chapter

There is a wide breadth to cover in this introductory chapter, and readers may come from fairly diverse backgrounds with neurology/neuroscience, ophthalmology/vision science, or both. For this reason, a summary of content is provided here to better allow the reader to skim areas they are familiar with and focus on areas they are not.

The chapter begins with an overview of the visual pathway, from its microscopic origins in the retina including colour encoding and basic cell connections, to the macroscopic pathway of the optic nerve, chiasm, and connection to the occipital cortex. This is provided with the intention to give those without much background in ocular anatomy and physiology sufficient detail to cover more complex topics discussed in the experimental chapters.

In the next section the pupillary pathway is discussed, starting at its microscopic origins in intrinsically photoreceptive retinal ganglions, rods, and cones; followed by the afferent pathway to the pretectal olivary and Edinger-Westphal nuclei, and finally the efferent output via sympathetic and parasympathetic nerves. This is essential to the understanding of the multifocal pupillographic perimetry methods used in the majority of this thesis, and specifically chapter 4 which addresses some of the physiological features of pupil dynamics, and how the anatomy supports these results.

Higher visual functions are then discussed, covering visual neglect, and processing of colour, facial recognition, motion perception, and depth perception; along with their anatomical locations and dual presentation of these deficits in stroke patients. This relates strongly to chapter 3, addressing which higher visual function deficits commonly occur in stroke, and which tests a best used to identify these.

Chapter 1: Overview of chapter

With the visual pathway being covered, including deficits from damage to the cortex, an overview of cortical stroke is first covered, followed by the subcortical diseases used in this research (chiasmal compression and anterior ischemic optic neuropathy). Collectively these represent anterior damage at the optic disc, damage in the middle at the optic radiation, and damage posteriorly in the cortex; allowing a comparison between damage affecting the subcortical pupillary pathway and damage to the cortical input to the pupillary system. This relates to a key element of this research – to determine if multifocal pupillographic perimetry can detect subcortical and cortical damage utilising the pupil response (chapters 5 and 6). Each of these sections also outline their typical visual field loss and progression, to better inform decisions made in methods and analysis, particularly the hemifield ratios used in the analysis of chapter 5.

Visual field testing is then addressed. This section covers confrontational testing and its limitations, the invention of manual Goldmann perimetry, the invention and refinement of both automated Humphrey perimetry and automated Matrix perimetry, and the multifocal methods of visual evoked potentials which led to the development of automated multifocal pupillographic objective perimetry (mfPOP). This history is covered because it is crucial to understanding how and why various aspect of mfPOP were designed they way they are, and because Humphrey and Matrix are directly compared with mfPOP in chapter 5. A more extensive section on mfPOP is then covered, outlining experiments using this technology and refinement of its methods into what is used for these experiments. This is most pertinent to chapter 6, which utilises some new alternative methods informed by previous experiments. Lastly, a summary of experimental results published following commencement of this study are provided to give a sense of where this work fits into the literature.

At the end of the chapter is a summary section, to provide links between the key concepts covered in the introduction and why this led to the research being completed.

1.3. Visual Pathways

1.3.1. Retinal function

Light initially enters the eye through the cornea, which contributes most of the refraction. The iris blocks out extraneous light, allowing the remaining light to be sharply focused on the retina by the variable refractive capacity of the lens. The retina functions to phototransduce light into electrical currents and organise these into a structural framework which can be transmitted and interpreted by the neural networks of the visual cortex and subcortical nuclei.

1.3.1.1. Macroscopic organisation

Macula

The retina can be most generally thought of in terms of high acuity colour sensitive central vision (cone dominant) and low acuity low colour sensitive peripheral vision (rod dominant). Central vision is further subdivided into several regions according to their degree of eccentricity from the most central fovea region. On the surface of the retina, where the image is focused, every degree of visual field approximately corresponds to 0.3 mm (Wandell & Engel, 1995). The central ~10–12° (3 mm) of the retina is called the macula and the central 2–3° (1 mm) the fovea, from which the inner retinal layers are displaced radially (Provis *et al.*, 2013). Within the fovea, the structure of the retina is quite distinctive, containing none of the layers which usually overlay the rods/cones, and forming a depression called the foveal pit (which is also avascular, relying instead on the choroid for blood supply). The foveal connections to the interneurons and retinal ganglion cells (RGCs) are made in the surrounding macula, resulting in a thickening of those layers adjacent to the foveal pit (see Figure 1.1).

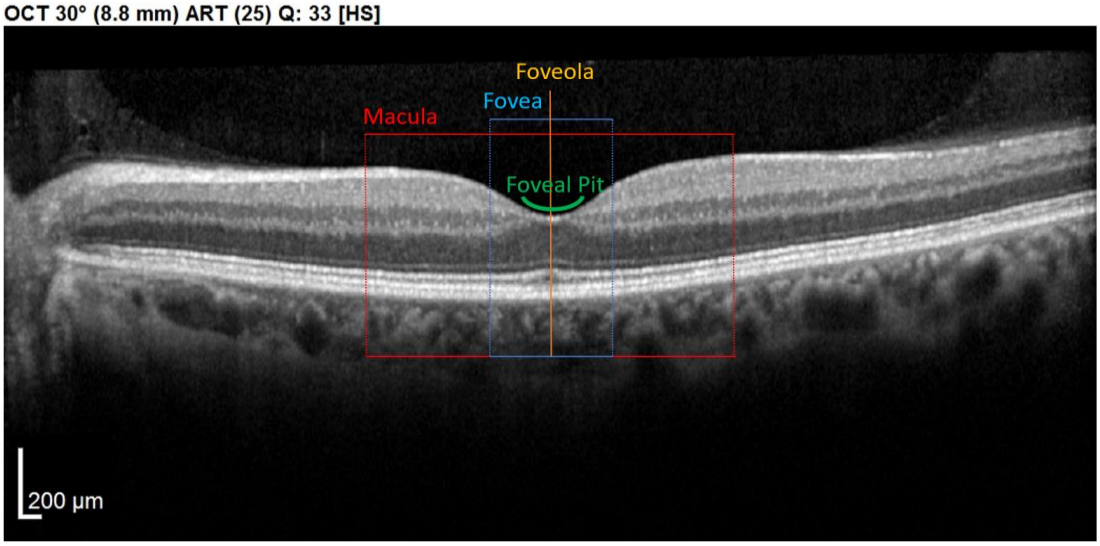

Figure 1.1: Spectralis OCT scan through layers of a normal retina highlighting the foveola, fovea (0.3 mm), and macular (3 mm) regions. Nearby are the avascular foveal pit and a subsequent thickening of the displaced retinal ganglion cells.

Optic nerve head

Another area of structural difference is the optic nerve head (ONH), also known as the optic disc, which is located several millimetres medial to the fovea at an eccentricity of about 15°. This is where the RGC axons exit the eye to form the optic nerve and blood vessels that supply the inside of the eye enter; it is an area containing no light-sensitive cells corresponding to the part of the visual field commonly known as the "blind spot". As all RGCs exit through the ONH, the retinal nerve fibre layer (RNFL) progressively becomes thicker approaching the ONH, as more and more RGC axons are layered together until they all exit, resulting in a depression called the optic cup (see Figure 1.2 and Figure 1.3).

Figure 1.2: (Top) Spectralis OCT digital fundus image of a normal right eye retina. The horizontal line cuts through the fovea and intersects the ONH. (Middle) The resulting cross-section through the retina produced from backscattered light. Note the central foveal pit with no layers preceding the cones and the thickened retinal ganglion cell layer towards the ONH where they exit. The internal limiting membrane (ILM) and basement membrane (BM) are labelled and their difference plotted (Bottom) as retinal thickness (µm).

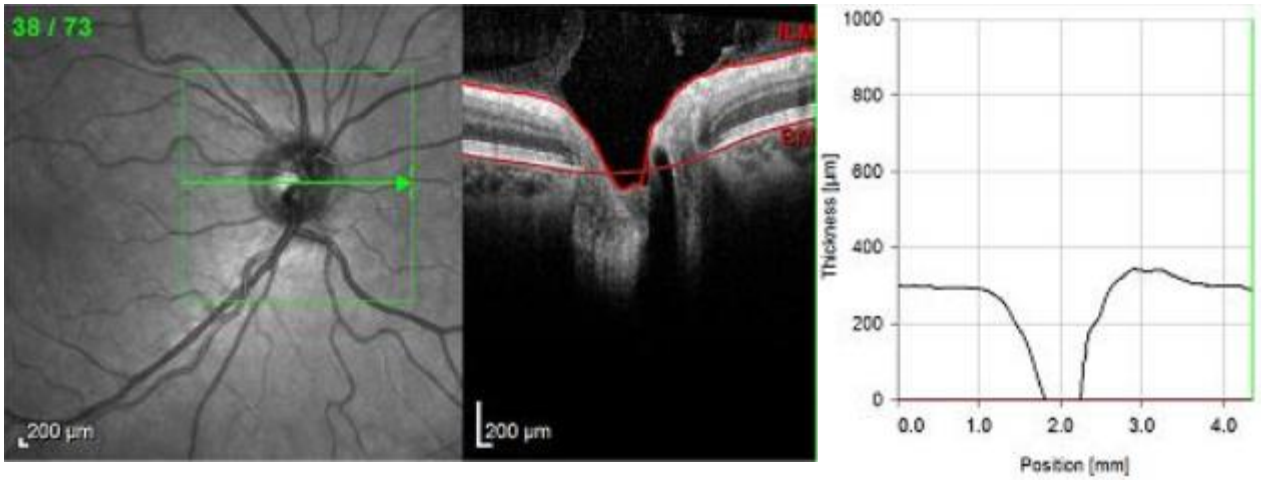

Figure 1.3: (Left) Spectralis OCT digital fundus image of a normal right eye ONH. The horizontal line cuts through the centre of the ONH. (Middle) The resulting cross-section through the ONH produced from backscattered light. Note the absence of any retinal layers centrally as blood vessels and nerves exit through the optic cup (also known as the *blind spot*). The ILM and BM are labelled, and their difference plotted (Right) as retinal thickness (µm), demonstrating this central hole.

1.3.1.2. Microscopic organisation

Light passes through all the layers of the retina before hitting the rods and cones which have light sensitive photopigments (retinal) attached to plasma membrane proteins (opsins). When light strikes retinal it changes conformation, activating a signal cascade using cGMP which results in closure of Na-channels and hyperpolarisation, closing voltage-gated Ca-channels and thus preventing the release of neurotransmitter glutamate (Hurley, 2009) and signalling the postsynaptic cell. The timing of this activation contributes to the delay in pupillary response after a stimulus by as much as 100 ms of its ~500-600 ms latency (Arshavsky & Wensel, 2013) with the larger bulk of the timing in iris constriction. The response of the postsynaptic cell can be stimulatory or inhibitory, there are a great diversity of RGC receiving different input, and with different extent of dendritic lamination, this facilitates the complex input signals involved in each aspect of vision (Dacey *et al.*, 2003).

Retinal layers

The rod and cones span several layers (see Figure 1.4): the opsin-photopigment compartment within the outer segment (OS), the cell organelles within the inner segment (IS), the outer nuclear layer (ONL) containing the cell bodies, and the outer plexiform layer (OPL) where connections are made with interneurons. Within the inner plexiform layer (IPL) and inner nuclear layer (INL) are the axons and cell bodies of interneurons (amacrine, bipolar, and horizontal cells), which integrate and refine signals from rods/cones and eventually connect through to the RGC in the ganglion cell layer (GCL) (Kolb, 1995). While the complexity of these connections cannot be understated, with numerous subdivisions of cells, generally the rods/cones transmit their signal via bipolar cells to the RGC, while horizontal cells in the OPL integrate a large number of inputs as they are communicated to bipolar cells, and amacrine cells in the IPL integrate a number of bipolar cell outputs as they communicate to the RGC.

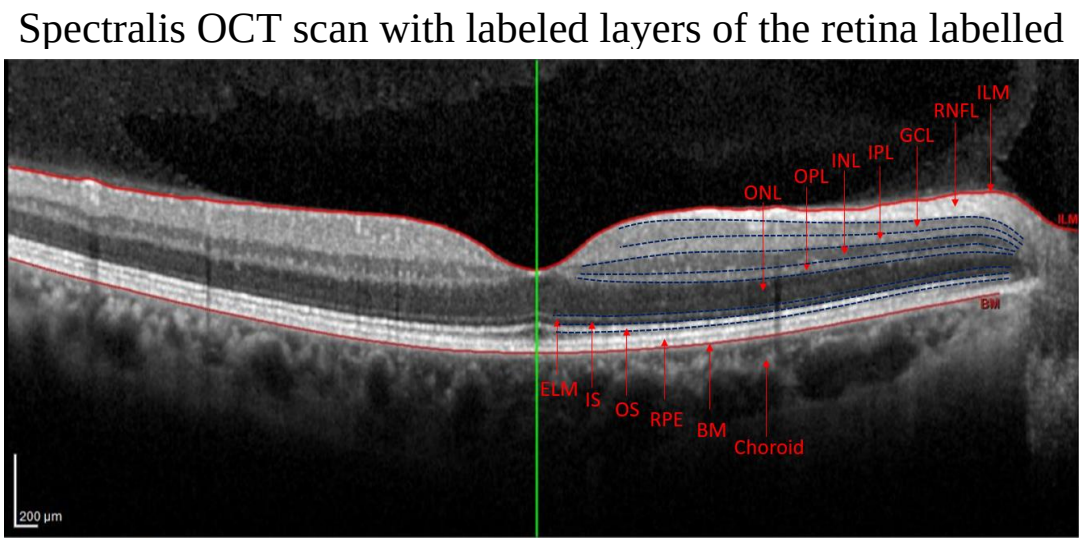

Figure 1.4: Spectralis OCT scan of a normal right eye with labelled layers of the retina. (1) ILM – inner limiting membrane, (2) RNFL – retinal nerve fibre layer, (3) GCL – ganglion cell layer, (4) IPL – inner plexiform layer, (5) INL – inner nuclear layer, (6) OPL – outer plexiform layer, (7) ONL – outer nuclear layer, (8) ELM – external limiting membrane, (9) IS – inner segment, (10) OS – outer segment (11), RPE – retinal pigment epithelium, (12) BM – basement membrane, (13) choroid.

Colour Opponency

As there are approximately 100-fold less RGC than photoreceptor cells, there is a large degree of integration, with multiple bipolar cells signalling a single RGC. This difference in RGC–photoreceptor ratio is most prominent in the rod system, while in the cone system it is closer to 1:1 and cones typically connect to multiple RGC via the colour opponent system (Schein, 1988; Wassle *et al.*, 1989). Neural integration of cones involves an offset of two colour systems and a luminance pathway (see Figure 1.5), with red/green sensitivity being recorded as L – M [long wave (red) minus medium wave (green)], and blue/yellow sensitivity being recorded as S – (L+M) [short wave (blue) minus combination of medium and long (yellow)]. Luminance on the other hand is an integration of all cone types [L+M+S] and is achromatic with a lower resolution, thereby only sampling input from the field it represents (Shevell & Martin, 2017). Given this connectivity in encoding colour, each L-cone (red) and each M-cone (green) need to connect to at least two bipolar neurons, while S-cones (blue) only require one (excluding the luminance pathway). Interestingly, as one progresses from peripheral vision to more central locations, there is an increase in the ratio of RGC to photoreceptor cells, with ~2 RGC per cone at 2.5˚ (Schein, 1988) increasing to >3 RGC in the central 550 µm (Wassle *et al.*, 1989). Centrally, rods are sparse, and while there is a higher density of cones and ganglion cells, there are more than twice as many pedicels[2] as RGC (Wassle *et al.*, 1989), resulting in displacement of the RGC with respect to their associated cone input (Figure 1.6). This particularly high cone density results in significantly higher resolution of central vision in daylight. Additionally, the absence of RGC in the foveal pit, combined with the displacement with respect to their connected cones, results in elongated connections and the apparent thickening of the macula alluded to earlier.

[2] Cone axon terminal where cone synapses with retinal ganglion cell.

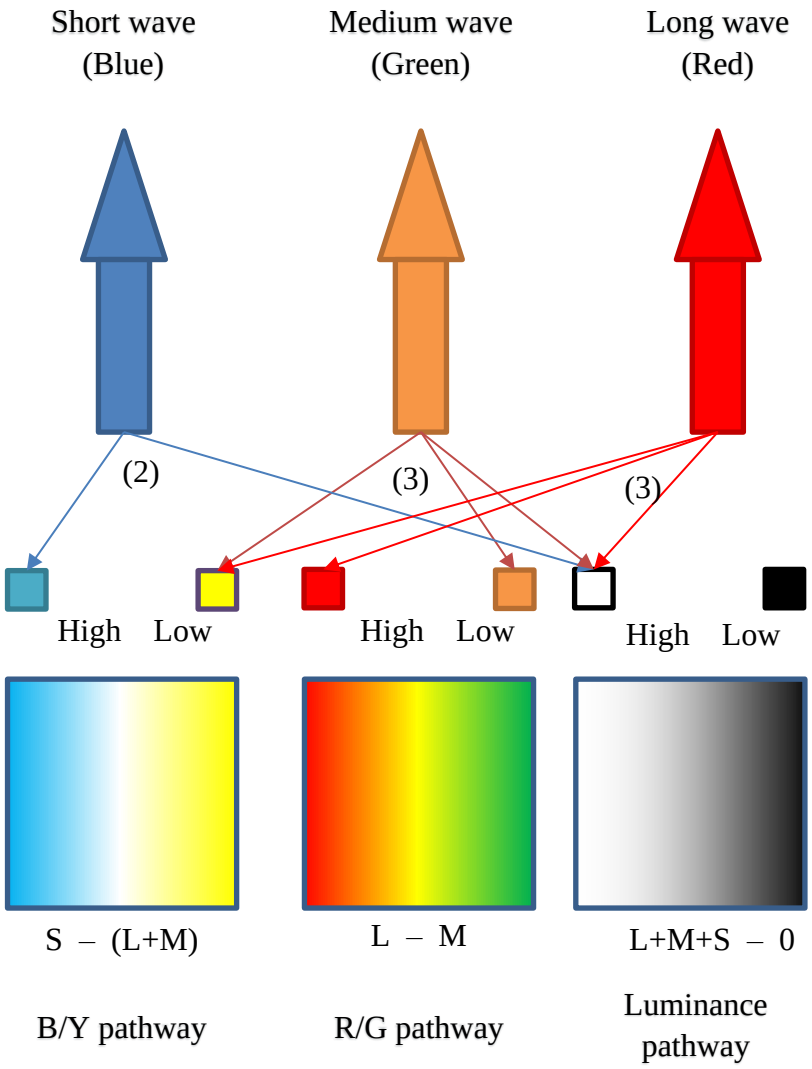

Figure 1.5: Diagram showing the connections of the short-wave (blue), medium-wave (green) and long-wave (red) cones to their respective colour opponency pathways. In the B/Y pathway, firing rate is high with S-wave stimulation and low with either L-wave or M-wave stimulation. In the R/G pathway, firing rate is high with L-wave stimulation and low with M-wave stimulation. In the luminance pathway all cone types provide high firing rates and summate, while absence of input (darkness) results in low firing rate. Note that the S-cones only have two connections, while M-cones and L-cones both have three connections.

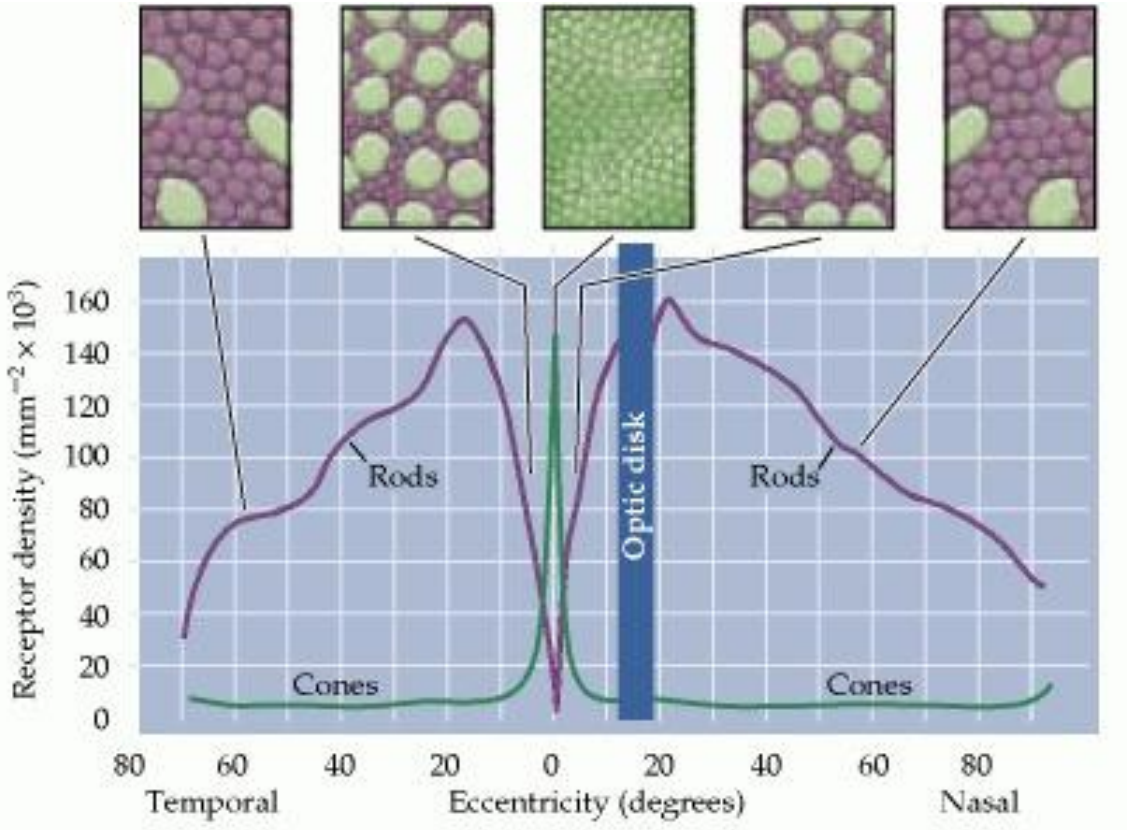

Figure 1.6: Rod and cone densities across the visual field. Cone density sharply peaks in the central foveal region where rods are absent. Rods peak around 18° in the nasal region, while they are slightly offset in the temporal region due to the optic disc and peak at around 22° eccentricity. Relative size of the rods (purple) and cones (green) can also be seen in the top row, highlighting the change in diameter of both rods/cones. Cones are ~3.3 µm in fovea and increase in size to ~10 µm at the extreme periphery. Rods have a size of ~3 µm at peak density and more subtly increase in size to 5.5 µm in the periphery (Jonas *et al.*, 1992; Purves *et al.*, 2001). Reproduced with permission from purves et al., 2001.

1.3.2. Visual pathway

Signals received by the RGC continue in parallel as the optic nerve until they reach the optic chiasm. Here nasal fibres decussate and continue as the contralateral optic tract through the optic radiations to the primary visual cortex (striate cortex) (Walsh, 1990) (See Figure 1.7).

1.3.2.1. Chiasm and optic tract

The optic nerve is highly organised and is separated by hemifield. Fibres which represent the temporal field (nasal retina) decussates at the optic chiasm, while fibres that represent the nasal

field (temporal retina) continues uncrossed. After the chiasm, the optic nerve is then called the optic tract and continues to the LGN. The optic chiasm is about 15 mm wide and 3.5 mm high immediately inferior to the hypothalamus and superior to the pituitary gland (Wagner *et al.*, 1997), making it susceptible to pituitary lesions via compression (Gulsen *et al.*, 2010). Despite the optic chiasm representing a single hemifield of each eye, it represents 53% of the neurons (Kupfer *et al.*, 1967; Ireland & Carter, 2019). This retinotopic organisation is maintained in the optic tract until the LGN is reached, which has its own organisation (discussed below).

1.3.2.2. Lateral geniculate nucleus (LGN)

As shown in Figure 1.8, each LGN is arranged in 6 anatomical layers which separate the information received from each eye, and are arranged in a point-to-point fashion such that adjacent cells represent adjacent regions of the retina (Schneider *et al.*, 2004). Information from the ipsilateral eye projects to LGN layers 2, 3, and 5, while the contralateral eye to layers 1, 4, and 6. Not only is each layer highly topographically organised, but if any point in layers 1, 4, or 6 is selected, the equivalent point in layers 2, 3, and 5 will correspond to the same region of the retina in the other eye (Zeki, 1993). As there are three layers for each eye, each point in the retina is represented three times, but even at this level they have started to become anatomically and functionally distinct. The outer four layers (3–6) generally have small cell bodies, small receptive fields, and red–green colour selectivity (Szmajda *et al.*, 2008), which indicate their involvement in colour vision, fine texture, and patterns – these are called

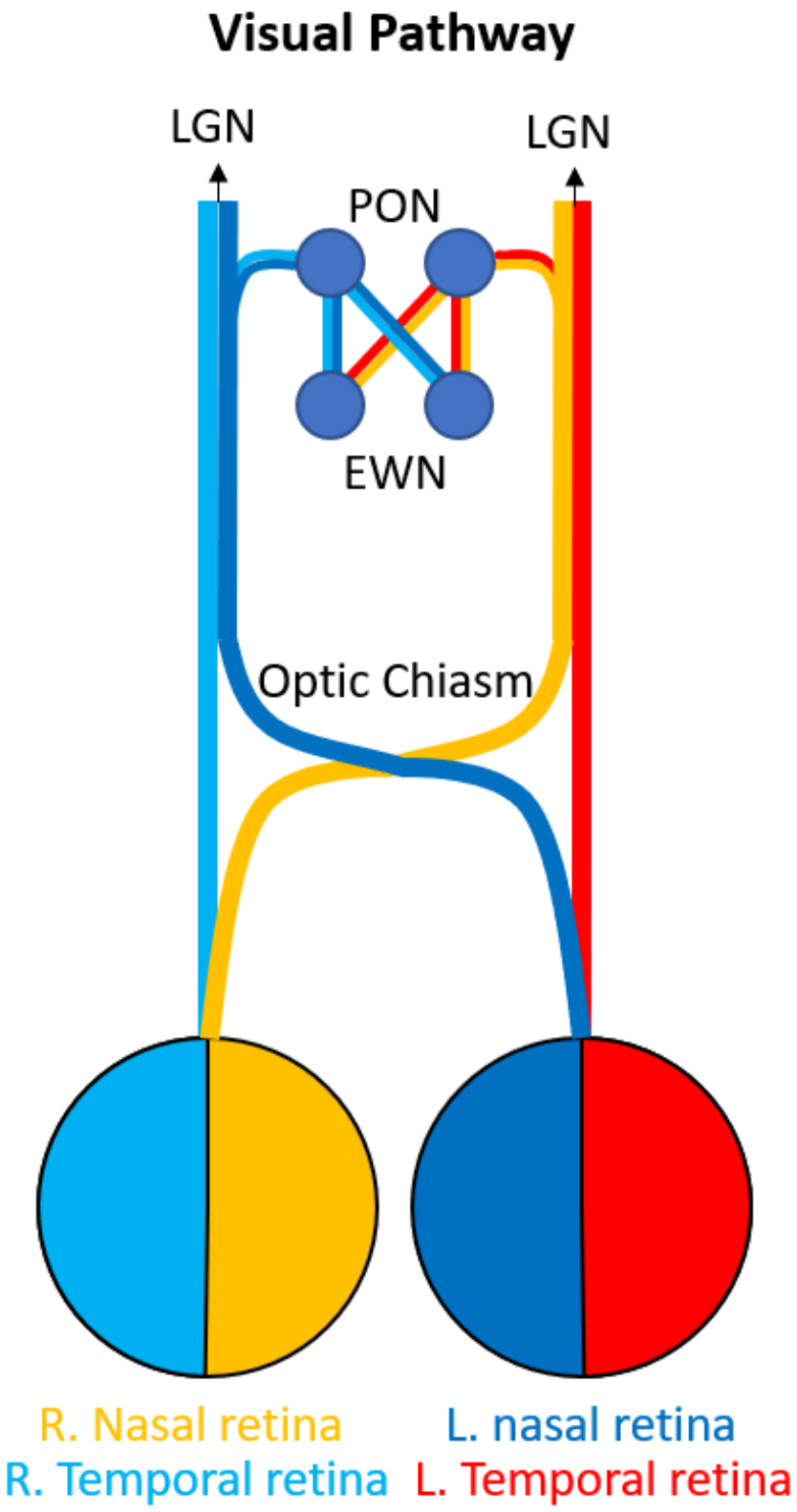

Figure 1.7: Visual pathway from retinal origins, crossing at the optic chiasm, and continuing to the lateral geniculate nucleus (LGN). Highlights branch point off the visual pathway to the subcortical pupillary pathway, leading to the pretectal olivary nucelus (PON) and integrating both fields at the Edinger-Westphal nucleus (EWN) which then innvervates the pupils.

parvocellular cells (P-cells) and receive extensive input from midget RGC. The inner two layers (1 and 2) contain cells with larger cell bodies which have large receptive fields, are contrast sensitive but insensitive to colour, and are responsible for motion detection – these are called magnocellular cells (M-cells) and receive extensive input from parasol RGCs (Szmajda *et al.*, 2008).

Between each of the 6 layers are a third type of cell called koniocellular cells (K-cells) which have very small cell bodies. The function of K-cells and what defines a koniocellular neuron are still up for debate. Evidence from macaques suggests input from both peripheral and central retina (Percival *et al.*, 2013), with three pairs of distinct layers in each LGN: dorsal layer for low-acuity information, middle layer for short-wave (blue) cone sensitivity, and ventral layer tied to the superior colliculus (Hendry & Reid, 2000; Szmajda *et al.*, 2008). A small population of K-cells and P-cells have even been shown to bypass the standard visual pathway and branch off directly to the middle temporal (MT) region which processes motion (Sincich *et al.*, 2004) and, based on evidence in primates, connects directly to V1 (layers 1 and 3B) of the primary visual cortex (Berson *et al.*, 2002).

Taking all this into consideration, it is important to recognise that, despite there only being three types of cone and three apparent anatomical layers in the LGN, there are more than 20 types of RGC, numerous subtypes of interneurons, and complex connectivity from the LGN to other areas of the brain. As pointed out by Kaplan in his updated review of the visual pathways, it would seem remiss to cling to the idea of a simple three-stream pathway when we are consistently presented with evidence that perceptual processing is simply more complex than that (Kaplan, 2013).

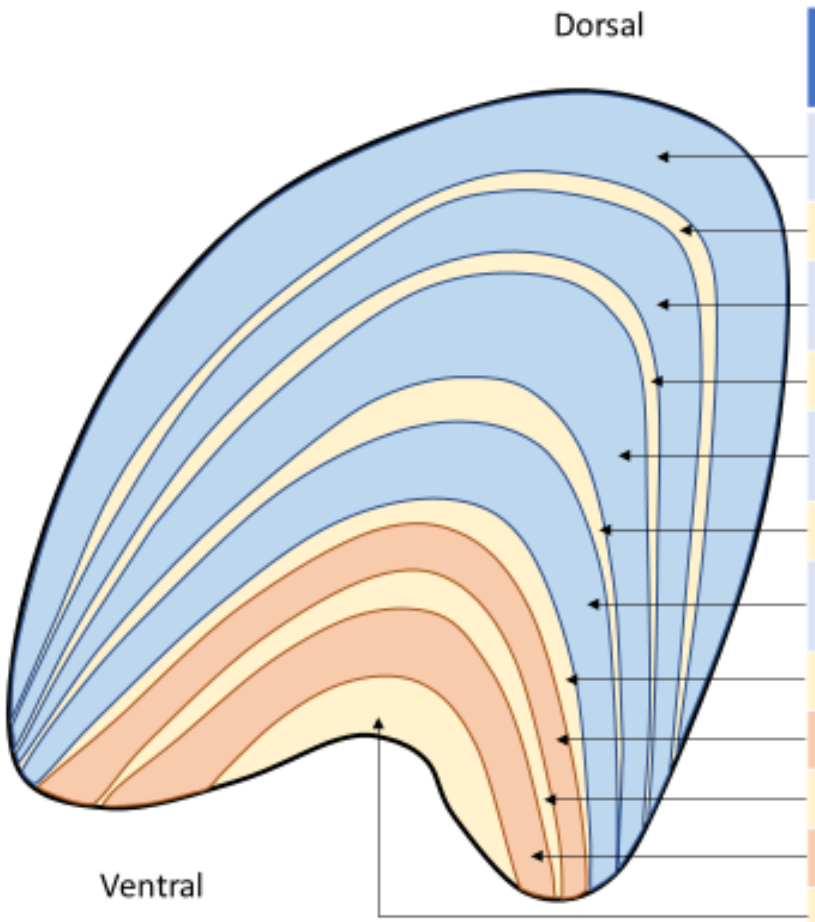

Layer	Pathway	Primary input	Size of Cell	Side	Proposed Function
6	Parvocellular	Midget	Small	Contra	Red/Green & Spatial
K6	Koniocellular	Mixed	Very small	Contra	Low Acuity
5	Parvocellular	Midget	Small	Ipsi	Red/Green & Spatial
K5	Koniocellular	Mixed	Very small	Ipsi	Low Acuity
4	Parvocellular	Midget	Small	Contra	Red/Green & Spatial
K4	Koniocellular	Mixed	Very small	Contra	Blue/Yellow
3	Parvocellular	Midget	Small	Ipsi	Red/Green & Spatial
K3	Koniocellular	Mixed	Very small	Ipsi	Blue/Yellow
2	Magnocellular	Parasol	Large	Ipsi	Contrast / Temporal
K2	Koniocellular	Mixed	Very small	Both	Eye movements
1	Magnocellular	Parasol	Large	Contra	Contrast / Temporal
K1	Koniocellular	Mixed	Very small	Contra	Eye movements

Figure 1.8: Cross-section of the lateral geniculate nucleus with schematic layers. These are labelled as traditional layers 1–6 and koniocellular layers K1–6, with their primary input, relative size, side of retinal input, and proposed function shown in the table. Graphic produced with reference to material from (Millodot, 2009).

1.3.2.3. Visual cortex

The primary visual cortex (V1) is represented in both hemispheres, receiving input from ipsilateral LGN and therefore the contralateral hemifield from both eyes. Similar to the LGN, it is highly retinotopically organised so that nearby points in the cortex map to nearby visual fields. Notably this is not linear – the central 2% of the visual field accounts for 50% of V1 (Adams & Horton, 2003), and the increased density of photoreceptors in the macula only partially accounts for this, as it also shows cortical magnification (Wandell & Engel, 1995). This means that damage to V1 or its immediate input from LGN result in homonymous visual field damage to the contralateral field – that is, damage in the same region on the same side of both eyes but opposite to the side of the lesion. Where damage is incomplete there is frequently a degree of macular sparing, given that it is unlikely to have completely knocked out the entire central vision representation. After V1, information is parcelled out into specialised cortical areas for further analysis of specific aspects of visual information such as colour, motion, spatial location, form and identity (Zeki, 1993), which are further discussed in Section 1.3 (*Higher visual functional deficits*) below.

1.3.3. Pupillary pathway

In the traditional understanding of the pupillary response, some RGC axons branch off the optic tract prior to the LGN to reach the pretectal olivary nucleus (PON) (Walsh, 1990; Tsujimura & Tokuda, 2011). Each of the two PON then project into both oculomotor nuclei to the adjacent Edinger–Westphal Nuclei (EWN), such that despite the earlier separation of the visual field down the two tracts, the full visual field is represented in both the EWN (Carle *et al.*, 2011b; Kozicz *et al.*, 2011). The EWN then produces parasympathetic output, which projects anteriorly through the oculomotor nerves (CNIII) to the ciliary ganglia and, finally, via short ciliary nerves to the iris sphincter muscle to cause pupil constriction. In addition to this standard pupil response, a separate pathway involving colour processing in the cortex has been

postulated to contribute to the pupillary responses (Young & Alpern, 1980). This is further discussed under the multifocal pupillographic objective perimetry (mfPOP) heading (Section 1.5.4.2).

1.3.3.1. Afferent pupillary input

Intrinsically photoreceptive retinal ganglion cells (ipRGC)

Inside the retina there is a recently discovered subpopulation of ~0.2% of RGCs that do not just transmit photoreceptor derived signals, but are intrinsically photosensitive themselves (Fukuda *et al.*, 2012; Munch *et al.*, 2012; Pickard & Sollars, 2012; Munch & Kawasaki, 2013). These intrinsically photoreceptive RGC (ipRGC) express the photopigment melanopsin (Opn4), which is most sensitive to short–medium wavelength light, peaking at ~480 nm (blue) (Pickard & Sollars, 2012; Sand *et al.*, 2012; Munch & Kawasaki, 2013). The ipRGC response to light is relatively slow, taking seconds to build up to maximal response, which is an order of magnitude slower than rods and cones, and it may also persist for minutes after the stimulus has ended (Pickard & Sollars, 2012; Sand *et al.*, 2012). Interestingly though, electron micrographs show that ipRGC also receive input from cones of the retina via amacrine and bipolar cells (Pickard & Sollars, 2012; Sand *et al.*, 2012; Munch & Kawasaki, 2013), allowing a rapid response too.

In determining ipRGC function, it was discovered that they are required for photoentrainment of the circadian rhythm. This was proven by some elegant studies using knockout mice that showed either melanopsin or cones were sufficient, but ipRGC were necessary, for photoentrainment (Pickard & Sollars, 2012; Sand *et al.*, 2012). The pathway was found to travel via the retinohypothalamic tract (RHT) to the suprachiasmatic nucleus (SCN) above the optic chiasm (Munch *et al.*, 2012; Nissila *et al.*, 2012; Pickard & Sollars, 2012; Sand *et al.*, 2012). ipRGC were also implicated in pineal melatonin regulation of the sleep–wake cycle, and in mediating the pupil response (Munch *et al.*, 2012; Pickard & Sollars, 2012; Sand *et al.*,

2012; Carle *et al.*, 2013), either grossly throughout the day (predominantly via melanopsin) or acutely via cone input when a bright flash occurs (Pickard & Sollars, 2012). Animal studies have shown ipRGC branch both directly to the SCN via RHT and also to the intergeniculate leaflet which leads to the SCN via the geniculohypothalamic tract (Morin *et al.*, 2003). In doing these experiments, projections to the pretectal olivary nuclei (PON) were discovered, which is known to regulate the light reflex (Edelstein & Amir, 1999; Pickard & Sollars, 2012). Many more locations were also reported, including ventral subparaventricular zone, lateral preoptic nucleus, medial amygdala, lateral habenula, superior colliculus, and periaqueductal gray matter, which suggest other functional roles which are not yet understood (Pickard & Sollars, 2012).

In macaque retinas, ipRGC were shown to comprise just 0.2% of the RGC (Dacey *et al.*, 2005) with overlapping mesh and very large dendritic fields, particularly in the periphery where they may approach 1 mm (Do & Yau, 2010). Despite being a relatively uncommon RGC type, subtypes have been proposed as M1, M2, and M3. In rodents M1 and M2 appear similar in number at ~45% of total ipRGC each, while M3 comprises only 10% (Berson *et al.*, 2010). Very recently M1 has been further subdivided by expression of a transcription factor (Brn3b), where M1 ipRGC which are Brn3b+ project to the PON and are necessary for the pupillary light reflex, whereas Brn3b– project to the SCN and are sufficient for photoentrainment (Li & Schmidt, 2018). Differences in myelination between ipRGC projecting to SCN and PON showed heavy myelination of PON-projecting neurons, consistent with the necessary time-scales of their responses (Kim *et al.*, 2019).

Rod/Cone

As ipRGC drive the pupillary reflex, rod and cones may only influence pupil response via this pathway. In terms of the intrinsic input (melanopsin) from ipRGC, it contributes significantly to maintenance of pupil constriction in response to light stimuli ≥ 30 seconds in duration, even

when only of small luminance (McDougal & Gamlin, 2010; Lee *et al.*, 2019). Cones contribute over very short durations and quickly adapt, contributing relatively minimally after 30 seconds. Rods are also involved, but do not adapt as much as cones and contribute to steady-state responses at smaller luminances below the threshold at which melanopsin reacts (Lall *et al.*, 2010; McDougal & Gamlin, 2010). Variation in colour input in terms of both wavelength and intensity appears able to selectively target melanopsin (blue), rods (low intensity), or cones (red) (Kardon *et al.*, 2009). It should be noted the final pupil response may include the subcortical, ipRGC-driven pupillary light reflex in addition to cortical inputs to the PON and EWN.

1.3.3.2. Subcortical nuclei

Pretectal olivary nucleus

The pretectal olivary nucleus (PON) receives the retinal input from ipRGC, with the PON firing rate directly related to the intensity of photopic stimulation of the retina (Pintor, 2009). Due to decussation of nasal retinal fibres (temporal field) at the optic chiasm, input to each PON comprises temporal hemiretina from the ipsilateral side and nasal hemiretina from the contralateral side (Carle *et al.*, 2011b). As mentioned earlier, this input is not entirely even, with nasal hemiretina having a greater density of cones (Curcio & Allen, 1990). Primate studies show differences as large as 58% decussate while only 42% do not (Horton & Hocking, 1996; Horton, 1997), and a study of a single human retina showed 53% decussate versus 47% do not (Kupfer *et al.*, 1967; Ireland & Carter, 2019). Recent evidence suggests that this difference is small relative to the differences in PON connection with the Edinger–Westphal nucleus (Carle *et al.*, 2019) (discussed below).

Edinger–Westphal Nucleus (EWN)

There is bilateral input from both PON to both EWN, so this is the first point at which the full retinal input is represented in a single region. Interestingly, there is not equal input from

ipsilateral and contralateral PON. In primate studies a notable bias towards contralateral input has been demonstrated (Tigges & O'Steen, 1974; Hutchins & Weber, 1985; Gamlin & Clarke, 1995; Gamlin *et al.*, 1995). This would result in greater direct than consensual responses in the nasal retina (temporal field) and equally greater consensual than direct in the temporal retina (nasal field). Most studies seem consistent in showing that the nasal retina (temporal field) has greater direct responses, while for the temporal retina (nasal field) the results are mixed, with some studies showing marginally greater consensual responses (Cox & Drewes, 1984; Martin *et al.*, 1991) while others show no difference (Smith & Smith, 1980; Wyatt & Musselman, 1981; Schmid *et al.*, 2000; Carle *et al.*, 2011b). This has been suggested to be due to stimulus intensity affecting this anisocoria, with a model proposed to account for this (Carle *et al.*, 2011b). In investigating retinal, PON, and EWN levels for contribution for anisocoria, the level of the PON connection to EWN was highlighted as most influential (Carle *et al.*, 2019).

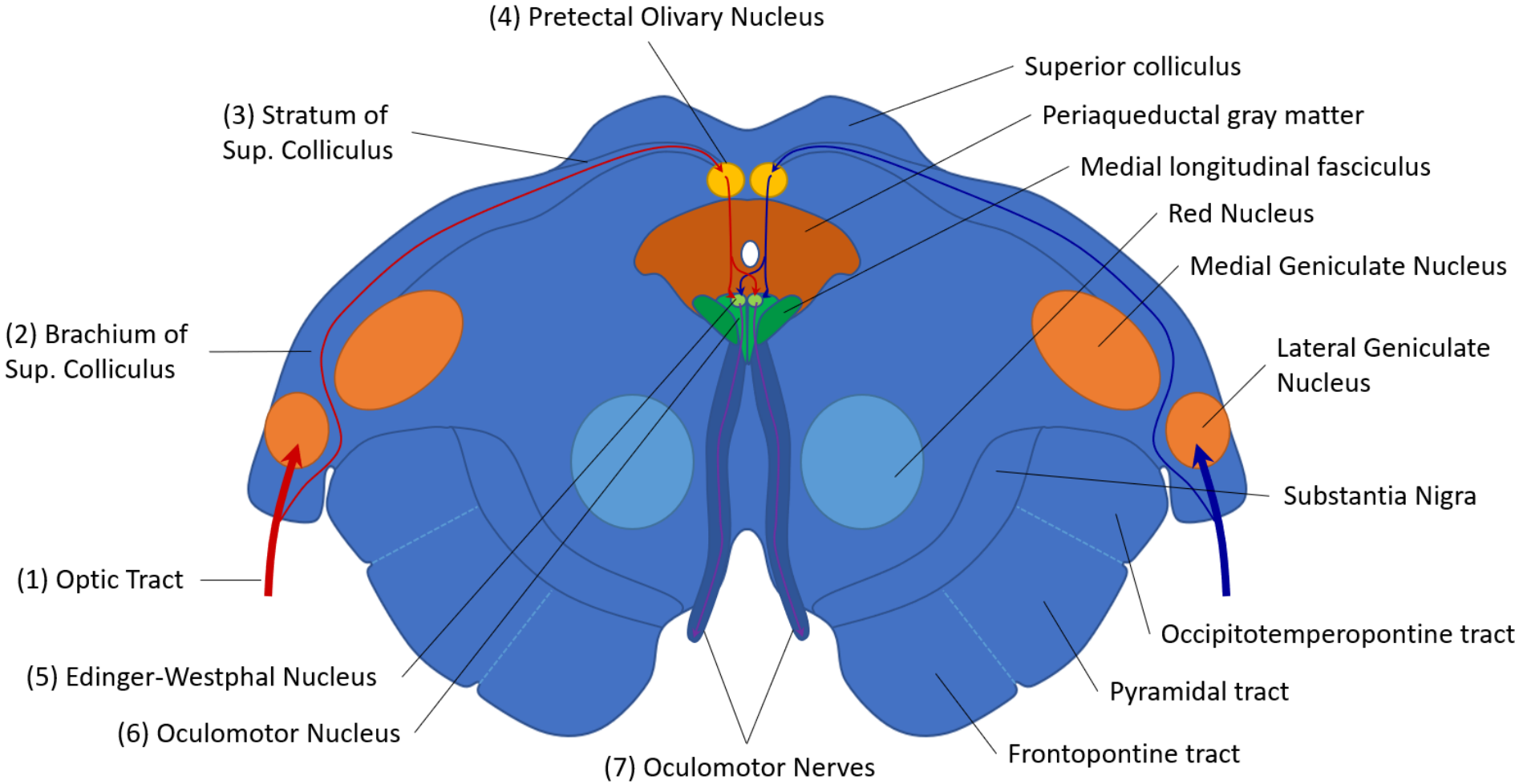

Figure 1.9: Cross-section of midbrain at the level of the superior colliculus. Right side labels show major tracts and nuclei; left side labels show pupillary pathway in order labelled 1–7. (1) Due to decussation at the optic chiasm, the optic tract receives retinal fibres direct from the ipsilateral eye, representing the nasal field, combined with indirect fibres of the contralateral eye representing the temporal field. The large majority of fibres terminate in the lateral geniculate nucleus. (2) Brachium and (3) stratum of the superior colliculus are the continuation of the branch from the optic tract of fibres involved in the pupillary response which terminate in the (4) pretectal olivary nucleus (PON). The PON fibres then bilaterally terminate on both (5) Edinger–Westphal nuclei (EWN), now representing full integration of both streams of visual information. The EWN continues through the (6) oculomotor nucleus where it forms into the parasympathetic component of the pupillary light response and follows the fibres of the (7) oculomotor nerve. Graphic produced with reference to material from (DeArmond *et al.*, 1976).

1.3.3.3. Efferent pupillary output

The iris is comprised of two key components: outer radial muscle that dilates the pupil (controlled by the sympathetic system) and the inner circular muscles that constrict the pupil (parasympathetic control) (McDougal & Gamlin, 2015). These muscles are modulated by the sum of the pupil light response (with greater amounts of light causing constriction of the pupil), the accommodation and convergence response (with near objects resulting in pupil constriction), and arousal from adrenergic responses (causing dilation). The integration of these pathways is what gives rise to the overall pupillary response.

Parasympathetic

The parasympathetic division of the pupillary response begins in the EWN after receiving bilateral input from the PON. Nerves exit the EWN and continue as part of the oculomotor nerve in the dorsal sheath to reach the ciliary ganglion, where neurons synapse and continue as postganglionic neurons to innervate the sphincter pupillae muscle of the iris to cause constriction (McMinn, 1998).

Sympathetic

The sympathetic component of the pupillary response begins in the posterolateral hypothalamus. Neurons exit the hypothalamus, traverse the brainstem laterally adjacent to the spinal lemniscus, and descend the spinal column to the level of T1. Here they exit the lateral horn and enter the sympathetic chain via the white ramus communicans and ascend to the superior cervical ganglion. They then synapse and become postganglionic neurons, which enter the skull with the internal carotid and branch into the pupillary and eyelid components. The pupillary component enters the ophthalmic branch of the trigeminal nerve and is finally distributed to the eye via the nasociliary and long ciliary branches to innervate the dilator pupillae muscle of the iris (McMinn, 1998).

1.4. Higher Visual Functional Deficits

Higher visual functions (HVFs) are visual processes that rely on complex integration of visual information to generate perception beyond that of the raw image itself. They include extrastriate vision that includes things like colour perception, depth perception, motion, and facial recognition. These functional processes are often taken for granted and may occur without the person themselves even being aware of their deficit (anosognosia). Due their specialised nature, they tend not to be tested in clinical settings. There are a variety of case studies presenting various degrees of HVF deficits (presented below), which tend to represent the more severe end of the spectrum. Pure HVF deficits rather rare, but more subtle defects may occur, and without standard clinical testing it is hard to know if they also have a low incidence or rather a low detection rate due to infrequent testing. To try and assess this question, we have noted a range of tests which attempt to assess HVF deficits: visual neglect[3], achromatopsia[4], prosopagnosia[5], akinetopsia[6], and astereopsis[7]. This study does not attempt to definitively define the prevalence of these in the stroke population, but rather to act as a pilot to suggest which might be worth pursuing in future studies, and which tests appear useful. For the detailed list of tests, reasoning for selection, and their administration – please refer to the *General Methods* (Chapter 2).

[3] Visual pathway remains intact, but does not consciously acknowledge items on side contralateral to lesion unless particular attention is drawn to it (inattention).
[4] Inability to recognise colours, seeing the world in grey, following a cortical lesion. More subtle defects may diminish colour sensitivity without being blind to colour.
[5] Inability to recognise faces and unique features of faces, following a cortical lesion. In the most severe cases, they cannot recognise their own face, while more subtle defects may make discerning between faces difficult.
[6] Inability to decern motion either generally (seeing all motion as series of static images) or in motion coherence (cannot detect cohesive motion from noise).
[7] Inability to use binocular vision to produce three-dimensional percept. May reply on other feautres or in severe cases perceive the world as flat.

1.4.1. Extrastriate visual areas

There are many reported areas of visual processing in the brain, with an even more variable set of mapping to cortices. While this is not the focus on this study, a brief overview of these seems fitting before discussing deficits which refer to these regions. As discussed in the sections below – there are numerous cases of those with selective deficits, which would strongly imply selective processing areas of the cortex. Perhaps what make this less clear is that multiple areas are frequently reported as having similar activity when presented with selective stimuli – for example motion stimuli have reported activity in V1, V2, V3, and V5 (McKeefry *et al.*, 1997; Furlan & Smith, 2016), and numerous connections have been described (Vanni *et al.*, 2020). Perhaps a more balanced view is to say that multiple areas partake in *processing* of visual features, while more selective areas are necessary to consciously produce the final visual percept. This would allow for a more subtle range of deficits to present, where any processing region is impaired, while selective loss of perception entirely remains rare (Vaina, 1995). With this in mind, the areas which appear necessary for perception are discussed, along with their anatomical locations, although they may not be the only regions involved in these precepts. To aim with visualisation, a schematic diagram of the visual association areas is included as Figure 1.10.

The primary visual cortex, or striate cortex (V1), is a well mapped area at the occipital pole enveloping inwards. It is necessary for visual field, and while limited perception has been demonstrated in its absence (‘blindsight’) (Vaina, 1995; Vakalopoulos, 2005; Smits *et al.*, 2019), there is minimal visual perception in areas where this has been damaged. Encapsulating and surrounding V1 is V2, which is implicated in higher order contour, shape and form (Roe & Ts'o, 2015). V3 and VP (ventroposterior) have been described superior and inferior (respectively) to V2, each with input from only quarter of a hemifield (Burkhalter & Van Essen, 1986). This has been challenged as actually being two sides of V3 (Sereno *et al.*, 1995; DeYoe

et al., 1996; Lyon & Kaas, 2001) based on similar function selectivity and mirror images of retinotopic maps in humans (Shipp *et al.*, 1995; Zeki, 2003), which certainly seems the stronger argument. More recently it has been suggested that both V3 and V4 play a critical role in transmitting information to higher order areas (Arcaro & Kastner, 2015), such that ventral V3 (VP) has greater colour selectivity (Burkhalter & Van Essen, 1986) in heading towards the colour centre, and that posterior V3 (V3A) has greater motion selectivity (Tootell *et al.*, 1997) in heading toward the motion centre. In a similar set of logic to dividing V3, the colour centre V4 was proposed to be comprised of V4v (Sereno *et al.*, 1995; Tootell *et al.*, 1996) and newly found area V8 (Hadjikhani *et al.*, 1998), which appeared to actually be overlapping with the previously defined V4 (Zeki *et al.*, 1991; McKeefry & Zeki, 1997; Wade *et al.*, 2002; Zeki, 2003). This may correspond closely to the posterior aspect of the interior temporal (IT) region which has also been suggested as the colour processing centre (Heywood *et al.*, 1998; Conway & Tsao, 2009), while others have suggested it relates to colour learning (Cowey *et al.*, 2001). The middle temporal (MT) visual area was coined in owl monkeys (Allman & Kaas, 1971) while the same area was concurrently discovered in macaques and coined V5 (Dubner & Zeki, 1971), hence the persistent use of both terms which can be considered interchangeable. Continued work described V5 in humans, with understanding of V5 has evolved through the years, being sensitive to motion in an integrative sense, focusing on cohesion in noise and filtering objects from background scenery (Born & Bradley, 2005). The V7 and LO (lateral occipital) has not been associated with distinct clinical syndromes, and so are of limited relevance in this context.

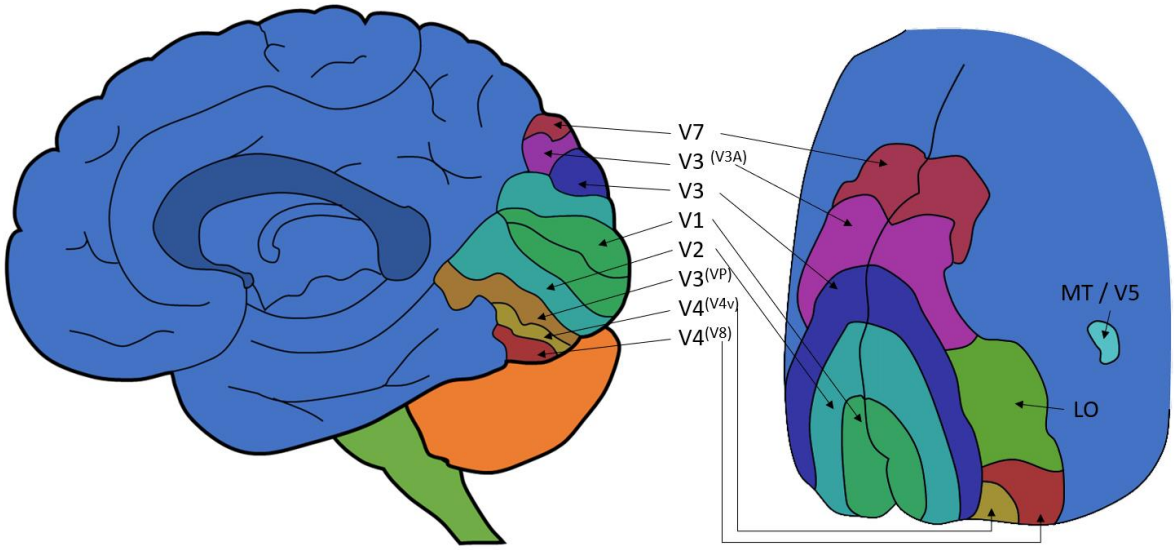

Figure 1.10: Schematic illustration of visual areas of the human brain, with saggital section (left) and posterior oblique surface (right). These show areas V1 (primary visual cortex), V2, V3/3A, V4, V5/MT (middle temporal), V7, V8, VP (ventroposterior), and LO (lateral occipital) regions. Regions V3, V3A and VP are in superscript as they have been argued to all be parts of the collective V3, likewise V4v and V8 as parts of the collective V4. MT and V5 are interchangeable terms, with V5 preferred in humans and MT in other primates within this text. Graphic produced with reference to (Barrett *et al.*, 2011) and (Zeki, 2003)

1.4.2. Visual neglect

Visual neglect may be described as an inattention disorder in which patients have an intact visual system, but ignore objects that appear in one side of their vision unless expressly emphasised (Ting *et al.*, 2011). Although it presents similarly to visual field deficits, it is distinct in that there is no perceptual damage but rather a lack of awareness of what is seen. Visual neglect (or hemineglect) is very common after acute stroke, reportedly affecting 43% of right hemisphere strokes and 20% of left hemispheric strokes (Ringman *et al.*, 2004), with the affected side contralateral to the side of the lesion. This asymmetry in visual neglect presentation is consistently reported (Bowen *et al.*, 1999; Beis *et al.*, 2004; Azouvi *et al.*, 2006) and is suggested to be due to the right hemisphere (allotting attention to both hemispheres) while the left is more selective (Heilman & Van Den Abell, 1980; Heilman *et al.*, 1983). Using standard tests for visual neglect (like line star cancellation and line bisection), retest variability is good when retest is done within the same hour (Bailey *et al.*, 2004), while resolution occurs

in the majority of cases over the following weeks to months (Jehkonen *et al.*, 2000; Lundervold *et al.*, 2005)

1.4.3. Achromatopsia

Damage to cortical areas beyond V1 may not damage the visual field but can result in selective loss of the ability to process features such as colour perception, motion perception, depth perception, and facial recognition. Cases of cerebral achromatopsia have been described from as early as the 1800s (Zeki, 1990), with many case reports continuing in the modern literature (Setala & Vesti, 1994; Cowey *et al.*, 2008; von Arx *et al.*, 2010; Pagani *et al.*, 2012; Carota & Calabrese, 2013; Bartolomeo *et al.*, 2014; Zhou *et al.*, 2018). Reports demonstrate that lesions tend to occur in the inferior occipital–temporal cortex near the reported V4, which has been confirmed in a meta-analysis of the overlapping damaged regions in 92 cases of cerebral achromatopsia (Bouvier & Engel, 2006).

1.4.4. Prosopagnosia

Prosopagnosia is the inability to recognise the distinct features of a person's face that allow that person to be identified. Cerebral deficits in facial recognition have been demonstrated in the modern literature (Lu *et al.*, 2005; Lang *et al.*, 2006; Fox *et al.*, 2011; Heutink *et al.*, 2012), with a meta-analysis of 100 cases showing the commonly reported region being adjacent to V4. Given the regions for prosopagnosia and achromatopsia are so close, it is not surprising that roughly half of achromatopsia patients have prosopagnosia and half of prosopagnosia patients have achromatopsia (Bouvier & Engel, 2006).

1.4.5. Akinetopsia

Compared to colour and facial recognition, descriptions of cerebral deficits in motion perception are more recent, with the first case of isolated motion impariement without field defects (as a consequence of a cerebral lesion) published in 1983 (Zihl *et al.*, 1983). Unlike the

colour centre in achromatopsia, which took many years to be accepted, a motion centre was readily accepted, with the term *akinetopsia* being coined (Zeki, 1991) – although it should be noted that the term akinetopsia refers to impairment or loss of any of the motion domains rather than complete loss of all motion perception. Since then akinetopsia has been described in a number of patients (Shipp *et al.*, 1994; Rizzo *et al.*, 1995; Barton *et al.*, 1996; Vaina *et al.*, 2001; Pelak & Hoyt, 2005; Vaina *et al.*, 2010; Cooper *et al.*, 2012; Otsuka-Hirota *et al.*, 2014). As to the location of the damage, V5 has been suggested - based on transcranial magnetic stimulation (Zihl & Heywood, 2015), and lesions demonstrating an inability to determine the direction of global dot motion stimuli when noise is added (random dot kinematograms) (Shipp *et al.*, 1994; Vaina *et al.*, 2010), or to track motion (Cooper *et al.*, 2012). Further, in a larger group of 57 stroke patients, it was demonstrated that many had enduring motion deficits, with damage in V5 (n = 10) resulting in markedly decreased ability to detect motion coherence ipsilaterally or contralaterally, although more substantially contralaterally (Vaina *et al.*, 2010).

1.4.6. Astereopsis

Astereopsis is the inability to judge depth from the disparity between images projected onto both retinas, with affected persons forced to rely upon other less sensitive monocular cues to judge depth; some individuals are unable to perceive depth at all. A description of 'seeing the world as flat' was published in the early 1900s in which a complete loss of stereovision perception was described (Holmes, 1918, 1919; Holmes & Horrax, 1919). More recent literature has also described stereoscopic damage from lesions (Ross, 1983; Takayama & Sugishita, 1994; Miller *et al.*, 1999; Schaadt *et al.*, 2014); MRI imaging has highlighted activity in the area immediately posterior to V5 during motion tasks (Senior *et al.*, 2000).

Interestingly, many of those with damage to V5 (and who lack motion sensitivity) also lack depth perception (40%), while damage to the nearby occipitoparietal region gave rise to 65% of patients having depth perception (stereopsis) affected (Vaina *et al.*, 2010).

1.5. Diseases of the Visual Pathways

1.5.1. Anterior ischemic optic neuropathy (AION)

AION typically presents as a relatively sudden loss of vision in a single eye, associated with oedema of the optic disc and evolving over several months into optic atrophy with a permanent visual field defect (VFD) (Hayreh, 1974). AION is the most common acute optic nerve disease in those aged over 50, with a reported incidence of 2.3–10.3 per 100,000 (Johnson & Arnold, 1994; Hattenhauer *et al.*, 1997; Kerr *et al.*, 2009; Lee *et al.*, 2011b; Arda *et al.*, 2013). It results from disruption of blood flow to one or more of the short posterior ciliary arteries which progress anteriorly from their branch off the ophthalmic artery and pass into the back of the eye, surrounding the optic nerve and optic disc (Kerr *et al.*, 2009). Ischemia of the optic nerve gives rise to inflammation causing swelling, compression, and hypoxic damage (Matson & Fujimoto, 2011). AION most commonly presents with an altitudinal defect predominantly affecting either the superior or inferior field of a single eye (depending on which ciliary artery is affected). In classifying AION, it may be described as either arteritic or non-arteritic.

1.5.1.1. Arteritic AION

The pathogenesis of the less common arteritic form (Johnson & Arnold, 1994) is well understood and is almost exclusively caused by giant cell arteritis (GCA) (Matson & Fujimoto, 2011). GCA is a form of systemic vasculitis in which medium to large arteries become inflamed with macrophages and giant multinuclear cells, causing thickening of the wall and narrowing of the lumen which may result in disruption to blood flow. Arteritic AION is considered a ocular emergency because further visual field loss (VFL) may be prevented by treating with corticosteroids (Hayreh, 2009; Matson & Fujimoto, 2011).

1.5.1.2. Non-arteritic AION

The exact pathogenesis of non-arteritic AION (NA-AION) has been suggested as lacking by some (Matson & Fujimoto, 2011; Punjabi *et al.*, 2011; Arda *et al.*, 2013). However, extensive work by Hayreh over the last 40 years (who incidentally named AION), suggests that the cause is complex and multifactorial in nature (Hayreh, 1974, 2001b, a, 2009, 2011). Some contributing factors include intraocular pressure, crowded optic discs, vascular resistance, and impaired vessel autoregulation, in addition to the more traditional vascular risk factors such as hyperlipidaemia, hypertension, diabetes, and obstructive sleep apnoea (Hayreh, 2009; Kerr *et al.*, 2009; Matson & Fujimoto, 2011; Arda *et al.*, 2013).

Once a patient has presented with AION in a single eye, the risk of recurrence in the same eye is relatively low (5.8% at 2 years) (Hayreh *et al.*, 2001). This has been proposed to be due to a thinning of the nerve fibre layer, making more space available within the optic disc, so there is less crowding and room for expansion in future ischemic events. However, this is still in contention. That being said, having NA-AION in a single eye puts a patient at high risk of an event in the fellow eye (15–24% over 5 years) (Beck *et al.*, 1997). This is likely due to having the same risk factors and structural commonalities that predisposed the first eye, and this risk is further compounded in the arteritic group to almost double that of NA-AION (Beri *et al.*, 1987). Systematically reducing and eliminating the risk factors appears to be the main option in minimising risk of recurrence.

1.5.2. Pituitary tumours

Each optic nerve passes through their respective optic foramen and converges at the optic chiasm just posterior to the bone of the tuberculum sellae. The chiasmic tract continues directly superior to the pituitary gland and tilts upward 45^{o} to the lamina terminalis, forming an indent in the third ventricle called the anterior optic recess (Walsh, 1990). The pituitary gland (hypophysis) is a small endocrine gland about the size of a pea found inferior to the optic chiasm within the bone cavity of the sella turcica. It is a very common place for tumours to

develop, with pituitary adenomas accounting for 12–17% of all intracranial tumours (Okamoto *et al.*, 2008; Wang *et al.*, 2008; Kasputyte *et al.*, 2013), with a prevalence in autopsy studies as high as 16.7% (Jahangiri *et al.*, 2012). When sufficiently large, they can press on the optic chiasm and cause visual field loss (Figure 1.11).

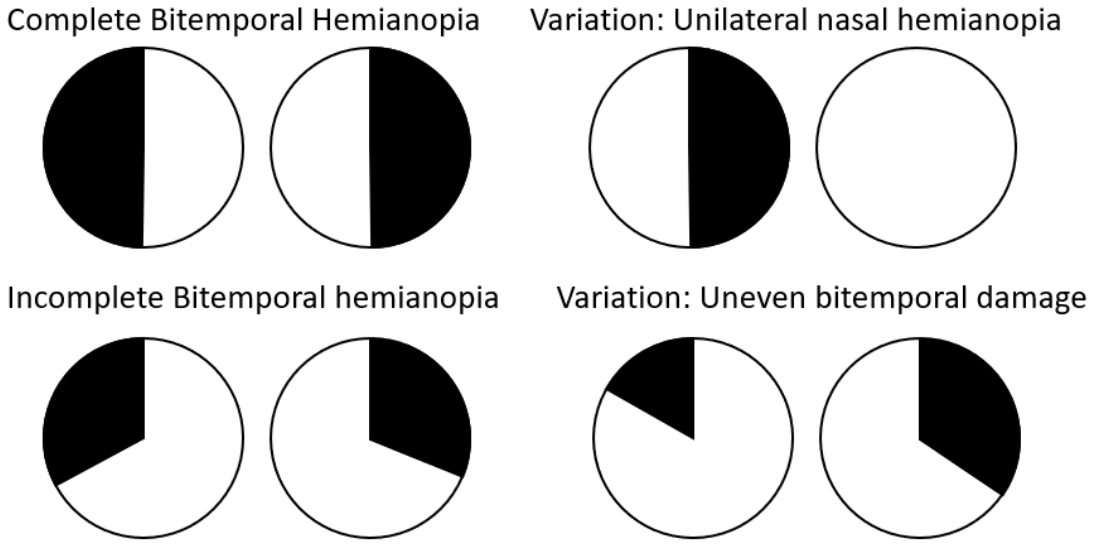

Figure 1.11: Typical presentations for pituitary tumours. Complete and incomplete bitemporal hemianopia (left) occur for complete and partial compression of the optic chiasm nerves. This may be uneven (lower right) and present with asymmetric damage. Rarely, if pressing more lateral to the optic chiasm, it may damage ipsilateral nerves on one side, causing unilateral nasal hemianopia (upper right).

1.5.2.1. Pituitary adenomas

These tumours are classified according to their size as microadenomas (≤10 mm) or macroadenomas (>10 mm). As the pituitary is almost surrounded by the sella turcica, tumours tend to grow superiorly towards the optic chiasm. The 8–13 mm gap between the pituitary gland and the optic chiasm means that small microadenomas do not result in visual damage, while macroadenomas often compress the optic chiasm or may impair blood supply, resulting in visual field defects (VFDs) (Walsh, 1990; Wang *et al.*, 2008; Kasputyte *et al.*, 2013). The nasal retinal fibres which cross through the optic chiasm appear particularly vulnerable to pressure, so a common presentation is loss of the temporal (lateral) half of vision in both eyes,

termed bitemporal hemianopia, which may partially or fully resolve once pressure is alleviated by excision or debulking. Because pituitary adenomas approach the chiasms inferiorly, it is more common to see superior visual field loss progressing inferiorly, within the borders of a temporal hemianopia (Walsh, 1990). Depending on the shape of the tumour, it may also less commonly press more laterally and cause unilateral nasal deficits (Poon *et al.*, 1995; Lee *et al.*, 2011a). In addition to VFD, loss of colour contrast has been reported as one of the early and prognostic signs of pituitary adenomas and may have a role in early diagnosis (Kasputyte *et al.*, 2013).

1.5.2.2. Craniopharyngiomas

The second most common suprasellar tumour, which accounts for 2–4% of all intracranial tumours, are craniopharyngiomas (Chen *et al.*, 2003a; Gautier *et al.*, 2012). These are derived from the remnants of pituitary embryonic tissue that formed the craniopharyngeal duct (Rathke's cleft) (Chen *et al.*, 2003a; Overly, 2009; Gautier *et al.*, 2012). These tumours are most commonly found in children <10 years and those in their 50s–70s (Chen *et al.*, 2003a; Overly, 2009). Craniopharyngiomas also frequently cause compression of the optic chiasm, but differ from pituitary adenomas in that they are typically superior to the chiasm and press on its superior aspect. This may present with predominantly inferior visual field loss, progressing superiorly within the confines of bitemporal hemianopia (Walsh, 1990; Chen *et al.*, 2003a).

Both varieties of pituitary tumour are most commonly diagnosed through non-invasive imaging such as MRI, with treatment options including partial or complete surgical resection, radiotherapy, or drug regimens (Sughrue *et al.*, 2011; Gautier *et al.*, 2012; Roelfsema *et al.*, 2012; Davies *et al.*, 2013). Recurrence in pituitary adenomas varies depending on how aggressive it is, but ranges between 10 and 20% (Roelfsema *et al.*, 2012), while

craniopharyngioma recurrence is reportedly even higher (35.7%) (Gautier *et al.*, 2012). It is therefore common to arrange for periodic radiological images to monitor for regrowth.

1.5.3. Stroke

Stroke is Australia's second highest cause of death and a leading cause of disability, affecting an estimated 375,000 Australians (Wang *et al.*, 2012). Most fundamentally, stroke is a lack of blood flow to the brain, resulting in death of neural tissue. There are two kinds of stroke: ischemic and haemorrhagic. Their most characteristic visual outcome is the homonymous visual field defect as shown in Figure 1.12.

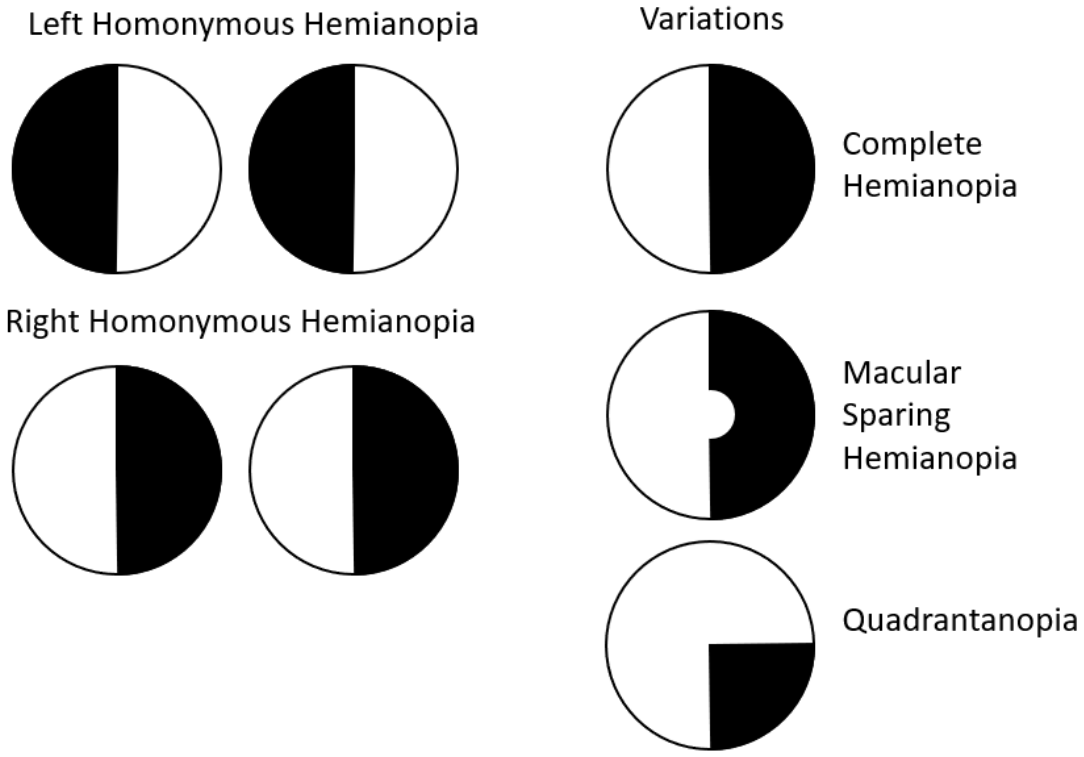

Figure 1.12: Common forms of field damage in stroke. Homonymous defects are most common (left). These may present as complete (top right), with macular sparing (right middle) or smaller portions such as quadrantanopia (lower right).

1.5.3.1. Ischemic stroke

Ischemic stroke accounts for ~80% of all strokes (Boehme *et al.*, 2017) and is most commonly caused by a clot or embolism, preventing blood flow to tissues downstream of the blockage.

Any part of the visual pathway may be affected depending on the location of the infarct. When anterior pre-chiasmal optic nerve(s) are affected due to ciliary artery blood flow disruption, this is classified as AION. The optic nerve is supplied by the ophthalmic artery and internal carotid pial vessels, and the optic chiasm by the circle of Willis; these may present unilateral or bitemporal damage, however both these presentations are rare (Pula & Yuen, 2017). Congruous homonymous hemianopia[8] (HH) is the most common form of field loss following stroke (Rowe *et al.*, 2013; Glisson, 2014) with Rowe et al. reporting complete and partial HH in 73.5% of stroke patients with field loss, and quadrantanopias[9] in another 15.2%. HH is predominantly caused from occipital lobe lesions (54%), optic radiations (33%), or the optic tract (6%) (Rowe *et al.*, 2013). These are supplied by the posterior cerebral artery, which may also have collateral supply from the temporo-occipital sylvian artery (Pula & Yuen, 2017).

1.5.3.2. Haemorrhagic stroke

Haemorrhagic stroke makes up the remaining ~20% of presentations, with a variety of types depending on the layer of the bleed. The most common types are intracerebral haemorrhage (ICH) (~10–15%) and subarachnoid haemorrhage (~5%) (Qureshi *et al.*, 2001; de Rooij *et al.*, 2007; An *et al.*, 2017). Risk factors are those similar to that of ischemic stroke: hypertension, smoking, excessive alcohol intake, old age, and male sex – but also Asian ethnicity and anticoagulants (An *et al.*, 2017). ICH is mostly caused by long-standing hypertension resulting in degeneration of blood vessels and aneurisms, which then rupture. Haemorrhagic stroke has poorer outcomes than other strokes, with a 1-month mortality rate of 40% and 1-year of ~60% (Qureshi *et al.*, 2001; An *et al.*, 2017). Unlike ischemic stroke, peripheral damage may occur

[8] Complete visual field loss covering half the field but not crossing the vertical meridian, affecting the same side of both eyes. Some fields may not affect the whole hemifield, but the damage in one eye matches the other, which are said to have homonrmous field loss, but are not hemianopias.
[9] Visual field loss that is homonymous (see above footnote), but only affects approximately a quarter wedge of the vision in each eye.

due to mass-effect and compression of surrounding structures; therefore almost any region can be affected and result in visual impairment.

1.5.3.3. Imaging

While clinical signs are well known, given the opposing natures of treatment for ischemic and haemorrhagic stroke, imaging is often necessary. According to the American Academy of Neurology, a computed tomography (CT) scan should usually done to distinguish between ischemic and haemorrhagic because it is quick, cheap, and readily available. Magnetic resonance imaging (MRI) may be done later and it can better define the stroke, can detect ischemic regions, and predict infarct more accurately – either acutely using diffusion or perfusion weighted images (DWI, PWI), or chronically using fluid attenuated inversion recovery (FLAIR) to visualise past strokes (Schellinger *et al.*, 2010). While mostly used in the research currently, diffusion tensor imaging (DTI) can also provide information about the particular tracts which are damaged.

1.5.3.4. Visual impairment after stroke

Stroke can affect any part of the body – including movement, sensation, and perception. Visual impairment in stroke patients is very common with an estimated prevalence of 20–74% (Rowe *et al.*, 2009; Pollock *et al.*, 2011b; Hayes *et al.*, 2012; Ali *et al.*, 2013). Persistent visual impairment is particularly significant as it can be associated with loss of mobility, reading deficits, inability to drive, depression, anxiety, social isolation, and falls (Jones & Shinton, 2006; Hayes *et al.*, 2012; Sand *et al.*, 2013). Visual deficits have also been correlated with impaired rehabilitation of other functional deficits (Shrestha *et al.*, 2012). The more commonly detected impairments are visual field defects and eye-movement disorders, although it is also possible for stroke to cause disorders of higher-order functions of perception such as colour

vision, stereo vision, motion detection, and facial recognition. These are not routinely tested for in the clinical setting and hence are not typically detected (Rowe, 2016).

Due to the structure of the visual pathway and the associated blood vessel networks, it is common for a single hemisphere, and thus only one of the two optic tracts, to be damaged. If damage occurs anterior to the optic chiasm, then all visual loss occurs on the side of the damage. However, if the damage occurs post-chiasmally, then half the vision of each eye on the side contralateral to the affected tract is lost. This is termed a homonymous defect as it manifests on either the left or right side of both eyes. When the whole tract is damaged, a full half of the vision on the same side of each eye is lost, with a line down the vertical meridian separating the damaged from the intact vision – this is termed homonymous hemianopia (HH) and occurs in about 8–10% of stroke patients (Zhang *et al.*, 2006; Chen *et al.*, 2009; Gall *et al.*, 2010; Luu *et al.*, 2010). If the hemianopia is "complete" then the central macular vision is split in both eyes, which makes it particularly difficult for the patient to read, the visual loss will also preclude them from driving, and give rise to other lifestyle problems (Zhang *et al.*, 2006). If there is "macular sparing" then the HH damage has left the central ~5º or more of vision intact (Walsh, 1990), which results in less severe disability for daily living. A definitive cause of macular sparing is not known, and may be caused by damage anywhere along the visual pathway (Zhang *et al.*, 2006), indicating that it is not due to collateral blood supply to the occipital pole. Another stream of thought was that the central macular region might be bilaterally represented: there is evidence to suggest that the central *foveal* region is bilaterally represented (Leff, 2004; Marzi *et al.*, 2009); however, the overlap is very small (≤1º) and so cannot explain the extent of macular sparing in most patients. The leading belief is simply that – because of the dense representation of the macular region in the cortex [with 2% of visual field accounting for 50% of V1 (Adams & Horton, 2003) plus cortical magnification (Wandell & Engel, 1995)] – any damage that is incomplete is more likely to spare a component of the

macula than any other region. Interestingly, damage along any part of the visual pathway results in degeneration of connected neurons, which can later be shown on either neural imaging or retinal nerve fibre layer (RNFL) scans. It has long been established that damage to the retina or optic nerve results in die-back (anterograde degeneration) of neurons to the cortex (You *et al.,* 2012), while the reverse has also been demonstrated (retrograde degeneration), where damage to the cortex results in die-back to the retina over several years (Park, 2013).

Cortical plasticity and reorganisation are topics often broached in the literature surrounding strokes, and it is worth mentioning its limitations within the adult visual system. It is well established that vision in early development is plastic, with simple rat models of monocular light depravation resulting in an increase in acuity and large bias of cortical connections from the unaffected eye (Maffei, 2002; Greifzu *et al.,* 2011). This plasticity has also been shown generally in human studies of neonatal stroke, with more favourable prognosis than in older children or adults (Lynch *et al.*, 2002; Boardman *et al.,* 2005), and in visual field defects in young brains resulting in greater anatomical expansion of extrastriate visual network (Guzzetta *et al.,* 2010). Focusing on the visual system, damage to the visual pathways early in the third trimester has been shown compatible with normal vision, while merely a few weeks later, permanent visual dysfunction (Guzzetta *et al.,* 2001a; Guzzetta *et al.*, 2001b; Guzzetta, 2010; Jacobson *et al.*, 2010). These coping mechanisms do not appear to be available in adult stroke (Guzzetta *et al.*, 2010), which appears far less plastic (Spolidoro *et al.*, 2009; Zhou *et al.*, 2017). In terms of visual recovery, maximum improvement is seen during the first 30 days (Cassidy *et al.,* 2001; Ali *et al.,* 2013) and little recovery is typically seen after 3 months (Ijaola & Kausar, 2009; Ali *et al.*, 2013). It is therefore important that patients receive a check-up at this time to equate their expectations with reality, and to provide possible coping mechanisms for any visual disorders that have not resolved.

1.5.3.5. Detection and referral after stroke

Visual field defects occur in ~50% of stroke patients and the UK national guidelines recommend stroke patients have a professional ocular assessment or referral. In practice, a survey of occupational therapists indicated that even basic confrontational field testing was only assessed 67% of the time and an ophthalmologist referral for an identified field problem only 45% of the time (Pollock *et al.*, 2011a). Row et al. (2011) report the most common cause for a referral was visual field loss (26.3% referrals), but that 56% of visual diagnoses made before formal assessment were incorrect (Rowe & Grp, 2011). Confrontational testing frequently misclassifies people, with two authors reporting (1) sensitivity of 88% and specificity of only 23% using a wide set of 7 tests (Kerr *et al.*, 2010) and (2) sensitivity of 27% and specificity of 93.4% (Johnson & Baloh, 1991). These suggest that either broad tests can be used to produce high sensitivity at the cost of many false positives, or that high thresholds in testing can improve specificity but at the cost of many false negatives. Overall, the result is that many stroke patients are not assessed, are misdiagnosed, or simply not referred and therefore go without formal field assessment.

1.5.4. Visual field defects

Visual field defects (VFDs) occur in any disease that results in damage to the retinal cells, their projections to the primary visual cortex, or to the visual cortex itself. In pituitary tumours, these changes to the visual field are often very gradual. It has been suggested that it is this slow progression which account for why patients find it difficult to recognise changes in their visual fields. Conversely, in stroke and AION, there is often a sudden loss of visual field, followed by the potential for some degree of recovery over weeks to months. However, even in the case of stroke, sudden and obvious visual field loss such as hemianopia or quadrantanopia is not necessarily obvious to the patient and may be missed unless specifically looked for (Rowe, 2009). This was demonstrated by the Blue Mountains Eye Study in which 3,654 Sydney

residents over 49 years old were recruited and had their visual fields tested; only 4 of the 13 patients diagnosed with stroke (30%) were aware of their extensive homonymous field defect and of those without a diagnosed history of stroke, none were aware of their deficit (Gilhotra *et al.*, 2002). When discussing those affected by visual deficits, it is important to remember that VFDs impact on many aspects of daily living. Those with HH have orientation and navigation problems, leading to social isolation, increased institutional care, and reduced autonomy (Sand *et al.*, 2013). VFD may prevent driving, inhibit reading ability, and increase the chances of falls and depression (Riggs *et al.*, 2007; Khan *et al.*, 2008; Sand *et al.*, 2013). Stroke-related visual problems have even been associated with reduced responsiveness to general therapeutic programs, reducing their overall functional rehabilitation (Riggs *et al.*, 2007). As VFDs are commonly unnoticed by the patients themselves, it is very important that they are specifically tested for.

1.6. Visual Field Testing

Traditional visual field testing has focused on testing perception rather than structure. This may be useful practically in identifying patient limitations, but is intrinsically subjective in nature, and will therefore always result in some errors when trying to measure and classify it. In the case of Goldmann perimetry (manual perimetry), the accuracy depends on both the examiner and respondent. Although automated perimetry removes the examiner, and so the variation they contribute, it still suffers from subjectivity in patient responses. This is reflected in the substantial variability in repeat testing (Heijl *et al.*, 1989; Artes *et al.*, 2002). Assuming perceptual deficits arise primarily from structural damage, then a measure of functional damage (such as diminished pupillary responses) which linearly correlates to structural damage of the optic tracts could be used to imply visual perception loss. This is the premise behind objective pupillographic perimetry – using pupil responses to measure pupillary functional

deficits to the visual pathway and imply that damage to visual field perception concurrently occurs due to both relying on the same underlying structures.

In the context of neurological disease, it is frequently necessary to assess visual fields. Traditionally this was done with confrontational testing, a relatively crude method where a clinician assesses visual fields by the bedside. While the study of perimetry appears to have started with Hermann Aubert (Aubert & Foerster, 1857), it has opened a broad and extensive domain of investigation. Advances in technology have refined these devices, with more modern devices adopting two testing approaches: manual or automated. In each case, two stimuli can be used: fixed (static) or moving (kinetic). Goldmann perimetry is a form of manual kinetic perimetry which became widely accepted after invention of the Goldmann device (Goldmann, 1946). Goldmann perimetry remains in use today, and in the hands of an experienced professional can be faster and more dynamic than automated perimetry, as the test locations are not fixed. However, manual perimetry does suffer from the intrinsic issue of variability between assessors; it also requires an experience technician to complete, and, being hand-drawn, it is hard to directly compare between cases or sequential visits. Automated perimetry, in the context of readily accessible computers, was designed to address these consistency problems and create a standardised approach where the assessor may complete testing with minimal training. Recently, automated perimetry has become the standard (Johnson *et al.*, 2011). There is substantial variation in which perimeter device or assessment is selected for each ocular or neurological disease; however, a literature review of devices used for conditions in this study revealed the Humphrey perimeter was the most commonly used in cases of stroke, chiasmal compression, and optic neuropathy (Hepworth & Rowe, 2018). While substantially less commonly used, frequency doubling perimetry (also known as Matrix perimetry) has also been used in these conditions (Hepworth & Rowe, 2018). Multifocal pupillographic objective perimetry (mfPOP) is a relatively new technology originating from work on visual evoked

potentials; it attempts to provide the benefits of automated perimetry while addressing some of their flaws – notably the subjectivity of patient responses to stimuli. Patient response are eliminated by utilising their autonomic pupillary light reflex and measuring its amplitude and latency.

Each of these visual field devices, their approach, and adaptations over time are discussed below.

1.6.1. Confrontational testing

Confrontational testing is considered a routine part of the neurological assessment, where the clinician compares their own visual field with that of the patient (Elliott *et al.*, 1997). While there are many variants (Pandit *et al.*, 2001; Connolly & Oczkowski, 2010), in practice this commonly involves having the clinician and patient close one eye; the clinician then either wiggles a finger and asks if the patient can see the movement (kinetic), or raises a select number of fingers and asks the patient to report how many they see (static) in each of four quadrants. While especially quick and easy, this test was soon recognised to have significant limitations, with "wiggling finger" movement said to be easily detectable even in the presence of moderate field suppression (Reader & Harper, 1976). Next is the concern with only testing a very crude and inconsistent set of regions. While large defects like hemianopias (such as stroke and chiasmal defects) may have a sensitivity of 42–75% (Trobe *et al.*, 1981; Johnson & Baloh, 1991; Shahinfar *et al.*, 1995), for smaller arcuate lesions this drops markedly to 20% (Shahinfar *et al.*, 1995), and for irregular defects such as in optic nerve damage to <11% (Trobe *et al.*, 1981) with a high rate of false negatives. Any of the common confrontational approaches (individually or in combination) continue to have either low sensitivity or low specificity, such that none are particularly effective (Connolly & Oczkowski, 2010; Kerr *et al.*, 2010; Danesh-Meyer & Gamble, 2011; Prasad & Cohen, 2011). An adaptation using automated confrontational testing was trialled, using eight coloured test regions: this was shown in

glaucoma to have higher sensitivity than finger-counting confrontation (Bass *et al.*, 2007), which principally is just a simpler form of automated perimetry. The point here is that confrontational testing is not good enough in neurological disorders where visual field defects are likely, meaning formal perimetry becomes necessary. Despite the often low sensitivity of confrontational testing, it remains a quick and easy screening tool and, provided its limitations are understood, it may be useful in some cases where stroke-related disabilities prevent patients from undertaking the higher sensitivity automated perimetry (Sand *et al.*, 2013).

1.6.2. Goldmann perimetry

For many years Goldmann perimetry was the gold standard, only challenged by the invention of standard automated perimetry in the form of the Humphrey perimeter. When the two were initially compared, it was found that the devices showed similar results for the majority of fields. Although Humphrey tended to suggest marginally worse fields than Goldmann, it had a higher rate of inadequate fixation (Beck *et al.*, 1985), and 25% longer test time in glaucoma patients (Trope & Britton, 1987). While patients tended to prefer Goldmann to Humphrey ~3:1, technicians heavily preferred Humphrey over Goldmann 5:1 (Trope & Britton, 1987), so Humphrey naturally began to gain traction. In terms of application to neurological deficits, discussion comparing the older version of Humphrey to Goldmann has mixed results, with some suggesting concordance and other suggesting inability to localise the blind spot may have resulted in unrepresentative fields for some patients (Wong & Sharpe, 2000; Coyle, 2001; Kuritzky, 2001). While manual Goldmann perimetry is still in use for neurological disorders, it has become less popular compared to automated perimetry (Hepworth & Rowe, 2018). More modern iterations of Humphrey have made significant improvements, suggesting it now performs similarly or better to Goldmann perimetry and is a promising successor (Bevers *et al.*, 2019). It should be noted that in rare cases, some individuals show blind visual fields to static perimetry (as used in Humphrey) but not to kinetic stimuli (as used in Goldmann), so-

called statokinetic dissociation (Riddoch Phenomenon) (Zappia *et al.*, 1971; Hayashi *et al.*, 2017). While this effect may account for some of the differences noted between devices, in terms of practical function, they remain functionally blind.

1.6.3. Automated perimetry

There are a range of automated perimetry devices on the market, including the Humphrey (Carl Zeiss AG, Germany) and Octopus (Haag Streit International, Switzerland) devices which use luminance stimuli, and the Humphrey-Matrix (Carl Zeiss Meditec, Dublin CA) devices which use contrast gratings. In this study, Humphrey II (HFA) and Humphrey-Matrix (MFA) devices were used, so discussion will be limited to these devices.

1.6.3.1. Humphrey

The Humphrey Field Analyser II (HFA) (Carl Zeiss Meditech AG, Jena, Germany) is one of the most commonly used automated visual field machines for all manner of visual field assessments, and is the most commonly used visual field device for the visual assessment of stroke, chiasmal compression, and optic neuropathy (Hepworth & Rowe, 2018), with a third model recently being released. All Humphrey models use Goldmann size III stimuli (0.43°) on a stimulus grid with equally spaced points 6° apart and use the Weber formula of contrast ((L_{max} – L_{back}) / (L_{back})) where the background luminance is 10 cd/m^2 and the minimal luminance above background 0.0255cd/m^2 up to maximum above background of 3178 cd/m^2, providing 5.1 log units of range. These are then converted into dB using $10*\log_{10}$(Contrast) (Fredette *et al.*, 2015) and reported as stimulus attenuation from the largest contrast possible (in dB). Thus, the poorest response is where a person does not detect the stimulus at L_{max}, resulting in 0 dB score, and the best response is where a person detects minimal background change, resulting in a 51 dB score, while in practice this is limited to ~40 dB.

In the first edition (HFA I), there was the option to complete two grid types: 30-1, which placed stimuli directly down the meridians at six-degree offsets, or the 30-2, which placed stimuli three-degrees either side of the meridian at six-degree offsets (Rudnicka & Edgar, 1995, 1996) (see Figure 1.13). Practically, the intention was that both tests could be run sequentially and therefore by testing alternate locations improve resolution to 4.2°, but in reality it was more common to use only a single test (Weber & Dobek, 1986). Comparing the combined results with individual results for 30-1 and 30-2, the 30-2 test substantially outperformed the 30-1 for correct detection of defects in glaucoma (Weber & Dobek, 1986) and the 30-2 test became standard practice with the release of the second version of the device in 1990 (Hepworth & Rowe, 2018). This also provided an advantage in testing conditions that result in hemianopias affecting vertical meridians (such as stroke and chiasmal compression): the 30-2 test can accurately detect damage offset 3° laterally (Johnson & Baloh, 1991), whereas testing points right on the edge of defects may not (Spenceley & Henson, 1996).

Continued testing revealed that peripheral fields in glaucoma had lower reliability in both HFA (Berezina *et al.*, 2011) and with similar devices (Pearce & Maddess, 2016). This reduced peripheral reliability, and combined with pressure to complete tests more rapidly due to fatigue effects (Wild *et al.*, 1991), resulted in the creation of a 24-2 version – using the same test points as 30-2 but only extending to 24°. In testing optic neuropathy and chiasmal compression, the 24-2 approach is more commonly used than 30-2, and in stroke they are equally used (Hepworth & Rowe, 2018). For clarity, it should be noted that while it is commonly stated that 30-2 extends to 30° and 24-2 extends to 24°, this is a horizontal average, with both tests placing extra points nasally (at 33° and 27° respectively) while their temporal and vertical points extend 6° less (27° and 21° respectively) (Figure 1.13).

The test regions are not the only factor that has evolved throughout the Humphrey releases, with the method of sampling also being altered. The first approach, called full-threshold, used

a starting value determined from normative data, and then varied stimuli by 4 dB until there was a response reversal; thereafter the variation was 2 dB with the last recognised stimulus used as the final threshold estimate (Spenceley & Henson, 1996; Artes *et al.*, 2002). This approach has provided some redundancy, such that if the starting test position (based on normalised data) is far from the patient's true value, or there is a single response error for a given test point, it does not produce any greater error in the result (although it does take longer to complete the test) (Johnson *et al.*, 1992). This makes the test fairly robust, but at the expense of long test durations, which then have the potential problem of enhanced fatigue effects (Wild *et al.*, 1991). A newer more complex algorithm called Swedish Interactive Thresholding Algorithms (SITA) was trialled to provide shorter test times, with the SITA-standard reducing 30-2 test times by up to 50% (Bengtsson *et al.*, 1998), and the SITA-fast being even shorter (Bengtsson & Heijl, 1998). It achieves this by Bayesian inference and removal of false positive catch trials (Schiefer *et al.*, 2009). SITA-standard showed similar or better detection in glaucomatous fields, similar mean defects (Musch *et al.*, 2005), reduced test–retest variability (Artes *et al.*, 2002), and reduced learning effects (Yenice & Temel, 2005), although it may underestimate false positives as they are no longer formally tested (Newkirk *et al.*, 2006). When SITA-standard was compared to full threshold in optic neuropathies and hemianopias typical of stroke or pituitary lesions, SITA-standard performed at least as well (Wall *et al.*, 2001).

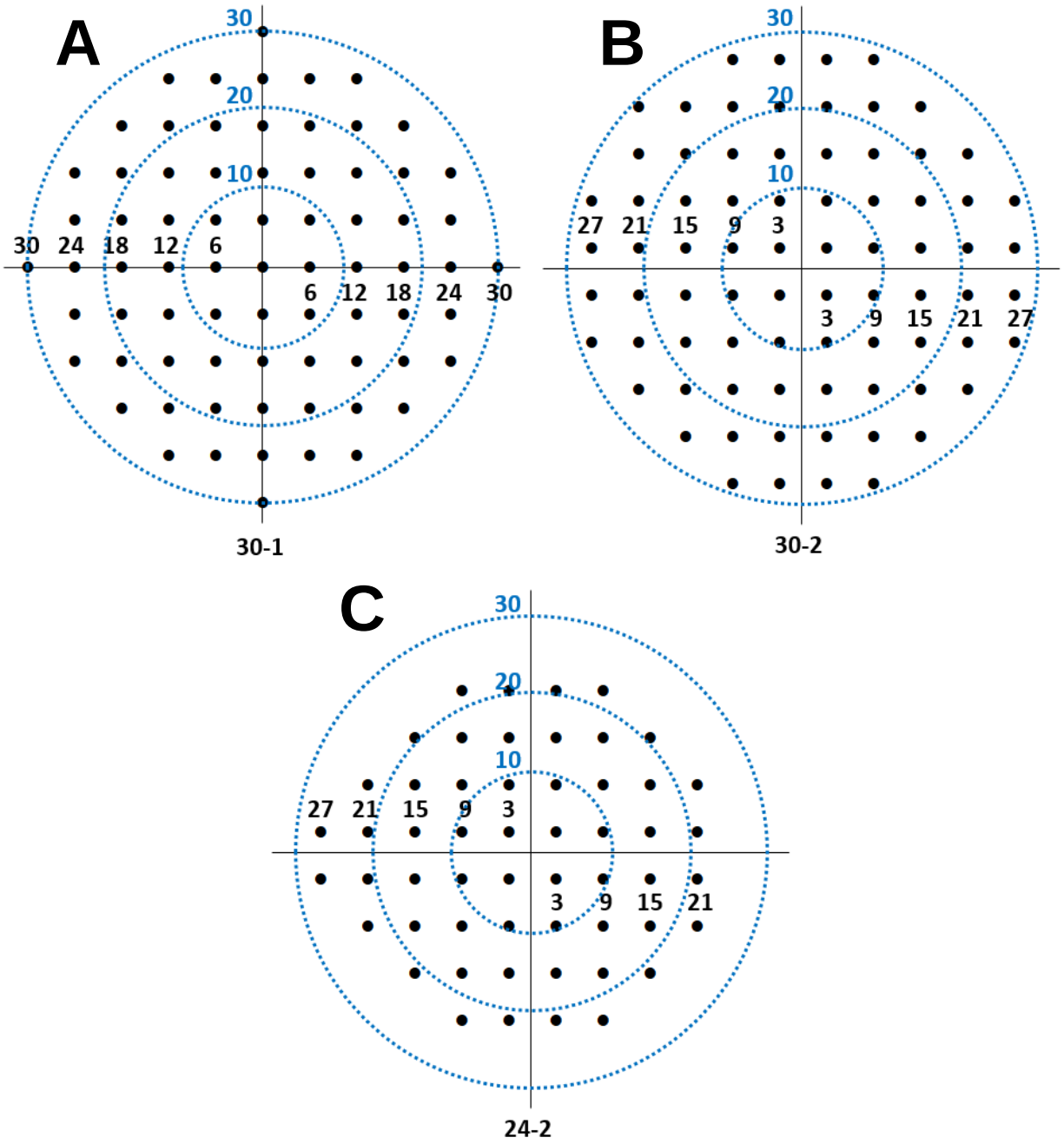

Figure 1.13: Humphrey stimuli for 30-1, 30-2, and 24-2 grids of the right eye, with each dot separated by 6°. (A) Grid for 30-1, which is vertically and horizontally symmetrical, with central dot and stimuli across the meridians extending out to 30°. (B) Grid for 30-2 which is also veritcally and horizontally symmetrical, but with 3° offset from the meridians, extending to 27°. (C) Grid for 24-2, which is vertically symmetrical, but asymmetric horizontally, with points extending to 21° temporally while two additional points extend nasally to 27°.

1.6.3.2. Matrix

MFA is a less commonly used perimeter (Hepworth & Rowe, 2018), using frequency doubling technology: low spatial frequency sinusoidal gratings flickering at high temporal frequency give the illusion of a doubling of the spatial frequency (Anderson & Johnson, 2002). It was developed with the intention on improving on a weakness in HFA regarding its highly variable glaucomatous fields. The belief was that there was preferential stimulation of magnocellular (M) cells and specifically a subpopulation (M_y cells) (Maddess & Henry, 1992), and that with fewer M-cells distributed in the retina, it might be more sensitive to glaucomatous loss with less redundancy (Johnson, 1994; Johnson & Samuels, 1997; Wall *et al.*, 2002; Yoon *et al.*, 2012). While the frequency doubling effect has been demonstrated to occur at frequencies and contrast levels utilised by the MFA (Maddess & Kulikowski, 1999; McKendrick *et al.*, 2003), it does not rely on the apparent frequency in any way, only asking subjects to identify if the stimulus is visualised or not. It was later proposed that the effect was mediated by multiple cells (White *et al.*, 2002), although the stimuli were not the only modifications made. Several changes from the HFA design make it more similar to mfPOP, and therefore of interest. As mentioned earlier, HFA had poor reproducibility over glaucomatous fields (Heijl *et al.*, 1989; Artes *et al.*, 2002), particularly peripherally (Berezina *et al.*, 2011). Another suggestion for this has been the relatively small stimuli (0.43°) and a relatively small cap in the maximal luminance the display can produce, leading to a small dynamic range for the device, which is also shown to improve when larger stimuli are used (Wall *et al.*, 2013; Gardiner *et al.*, 2015; Numata *et al.*, 2017). Further, the technique has relatively wide spacing (6°) between stimuli, resulting in under-sampling and aliasing (Weber & Dobek, 1986; Maddess, 2011, 2014). The size issue was addressed in the first iteration of Matrix (C-20 FDT) in which the central 40° of field was measured using much larger stimuli 10° in diameter but with only 17 test locations (4 in each quadrant and 1 centrally) (Yoon *et al.*, 2012). This approach had success in detecting

anterior pathway damage with both AION and chiasmal compression, showing similar sensitivities to HFA (Wall *et al.*, 2002; Girkin *et al.*, 2004; Monteiro *et al.*, 2007). However it also suffered from some of the same drawbacks as the 30-1 HFA in that targets were along the meridian and so performed poorly in hemianopias (Wall *et al.*, 2002; Noval *et al.*, 2005). Likewise, while the stimuli are much larger, the number of regions tested is much smaller, meaning under-sampling remained an issue. The second iteration solved these issues by halving the stimuli size to 5° and adopting the same 30-2 (68 test locations) and 24-2 (54 test locations) approach as HFA, while additionally retaining its central test region (Yoon *et al.*, 2012). The method for threshold detection was also upgraded from its modified binary search strategy (Tyrrell & Owens, 1988) to Zippy Estimation by Sequential Testing (ZEST) which showed promise on early testing (Anderson & Johnson, 2006) but causes all results to converge on only 15 unevenly spaced values (Fredette *et al.*, 2015), which may contribute to its reduced variability. When the modern versions of both devices were compared against each other in homonymous hemianopic fields typical of stroke (Biousse *et al.*, 2005) using a 24-2 map, there was no statistically significant difference between MFA and HFA in terms of sensitivity or specificity (Taravati *et al.*, 2008). However, it should be noted that HFA did have higher sensitivity, reportedly due to MFA presenting with a greater number of scattered abnormal field defects incongruent with expectations of the disease. When chiasmal compression damage measured by MFA was compared to prior diagnosis from HFA, it only detected 75% of bitemporal hemianopias (Noval *et al.*, 2005).

1.6.4. Multifocal methods

Multifocal pupillographic object perimetry (mfPOP) evolved from multifocal visual evoked potentials (mfVEP) over the last 20 years and so it seems appropriate to cover advances in mfVEP which lead to mfPOP.

1.6.4.1. Multifocal visual evoked potentials

mfVEP has been use for many years to assess the afferent visual pathway, with some results in compressive lesions showing greater sensitivity than subjective Goldmann perimetry (Halliday *et al.*, 1976a; Halliday *et al.*, 1976b; Flanagan & Harding, 1988). Typically, mfVEP employs pattern reversal stimuli, such as a black and white checkerboard which undergoes inversion, and responses are measured from electroencephalogram (EEG) recording on the scalp near the occipital cortex (Fishman *et al.*, 2001). It was known that stimuli responses varied according to their cortical representation, with central vision invoking large responses and those at greater eccentricities showing smaller responses (for a fixed stimulus size). To account for these differences, maps were designed with small central stimuli and larger peripheral stimuli (Sutter & Tran, 1992; Baseler *et al.*, 1994). Further, there were issues of electrode placement affecting the quality of the signal throughout the visual field (Kikuchi *et al.*, 2002), with typical occipito–frontal placement resulting in a bias towards inferior fields (Klistorner *et al.*, 1998). Despite these limitations, mfVEP was directly compared with HFA 24-2 visual fields, showing decreased amplitude responses, on average, in areas associated with field loss, but showing significant noise; this meant that small mfVEP amplitudes were not *uniquely* associated with poor fields, but rather depended on their signal-to-noise ratio (SNR) (Hood *et al.*, 2002). It was noted that the anterior pathway could be assessed with electroretinograms, while the posterior pathway with mfVEP, providing a means to better demarcate these processes where visual fields alone cannot (Hood *et al.*, 2003a). Naturally, because of correlation of mfVEP and HFA, it was trialled in glaucoma and showed promise (Graham & Klistorner, 1999; Hood *et al.*, 2003b), with the repeat reliability being similar or better than that of HFA (Chen *et al.*, 2003b). When the new and improved SITA approach for HFA was utilised, while both tests had high test–retest variability, mfVEP was shown to have greater variability (Bjerre *et al.*, 2004). In addition to amplitude measures, latencies were also examined in glaucoma. With conventional visual evoked potentials (cVEP), assessing the field as a whole showed large latencies

averaging 28 ms greater than controls (Parisi *et al.*, 2006), while mfVEP showed latencies only greater by 3–5 ms, with only 40% of patients showing delays (Rodarte *et al.*, 2006). While latencies did not show great utility for clinical practice in glaucoma, it was noted that this disease is not characterised by demyelination (Graham, 2006), while in disorders where this is typical – multiple sclerosis (Fraser *et al.*, 2006a), optic neuritis (Fraser *et al.*, 2006b), and compressive optic neuropathies (Danesh-Meyer *et al.*, 2006) – there were larger latencies and high sensitivities. When investigating hemianopia in which visual field damage was occipital in nature, results were discordant between mfVEP and visual field assessment (Watanabe *et al.*, 2007), suggesting this technique may not be sensitive to cortical damage. Colour stimuli began to be used with trials of blue on yellow showing improvements on traditional black and white checkerboards (Klistorner *et al.*, 2007; Arvind *et al.*, 2009), and it was shown that slowing the presentation rate to make stimuli more temporally sparse resulted in greater amplitudes and shorter latencies (Martins *et al.*, 2004). During this period of trials with alternative variants of traditional mfVEP methods, the Maddess group (who would eventually produce the mfPOP approach) were looking at temporal sparseness and alternative contrast mechanisms. They showed that relatively temporally sparse stimuli with low spatial frequency, appeared to keep the visual system in a state of high contrast gain, producing better responses (Maddess *et al.*, 2002; James *et al.*, 2003; Maddess *et al.*, 2003; Maddess *et al.*, 2004; James *et al.*, 2005a). It was shown that dichoptic presentation at the slower presentation rate of 6/s, compared to more traditional faster rates of 25/s, could achieve a similar level of reliability in a 60% shorter test duration (James *et al.*, 2005b). This approach was trialled in multiple sclerosis and optic neuritis with promising results, especially in terms of response latencies (Ruseckaite *et al.*, 2004a, b, 2005, 2006). Roughly around this stage, mfPOP was trialled for the first time, utilising many of the methods developed from mfVEP and quickly responding to the more recent advances developed in this field.

1.6.4.2. Multifocal pupillographic objective perimetry (mfPOP)

The device for mfPOP (about to enter the market in 2020) has been refined over many years, with the first publication addressing its methods and utility in 2007 in which 20 stimulus protocols were investigated in normal subjects (Maddess *et al.*, 2007). The approach clearly incorporated lessons from previous devices: (1) HFA – stimuli not crossing the vertical or horizontal meridians and using luminance contrast; (2) MFA – having relatively large stimuli balanced with the number of test regions (24 were used) and which are spatially low-pass filtered; and (3) mfVEP – using temporally sparse stimuli with dichoptic presentation and trialling both checkerboard, flicker, and chromatic variations (Maddess *et al.*, 2007).

Initial development and refinement of mfPOP

The mfPOP approach produces direct and consensual pupil responses with both amplitude and temporal delays, and results of variants have been compared. Of note is that the multifocal method has a *presentation rate* (referring to how many stimuli, from any location, are presented in 1 second), and a *presentation interval* (referring to the delay between successive stimulations of any individual test region, as not all regions are stimulated simultaneously). Since the pupil response occurs in about 500 ms, in order to keep stimuli temporally sparse for a given location the minimum *presentation interval* must allow for the pupil to have fully responded before restimulating the same region. Compared to responses to 1 stimulus per second, amplitudes were larger for 4/s and much larger for 0.25/s presentation rates, while flicker and 4 checks per region variations decreased amplitude (Maddess *et al.*, 2007). The next version had increased resolution, with 44 test regions extending to 30° eccentricity, and trialled presentation intervals of 1 s or 4 s per region, while attempting to balance luminance across retinal regions according to sensitivity, such that more responsive regions receive less light than less responsive regions (Maddess *et al.*, 2007). Luminance balancing appeared to increase sensitivity and could identify moderate–severe glaucoma subjects from controls using the 3 regional amplitudes

most deviating from the normative data (Maddess *et al.*, 2007). In another glaucoma experiment, single checker (region on or off) was found to be more effective than four-checker stimuli (consistent with initial trials) and stimuli rates of 133 ms (6/s) or 266 ms (3.8/s) were only subtly different depending on number of damaged regions used in the analysis, with all results having receiver operator characteristics (ROC) area under the curve (AUC) values in the range 72–81% for amplitude (Maddess *et al.*, 2009). Further refinement of how sparse the timing presentation interval needs to be in order to maximise sensitivity revealed that very sparse stimuli (mean 16 seconds) were best, followed closely by moderately sparse (mean 4 seconds) and less sparse (mean 1 second) – all achieving ROC AUC values between 89–100% for moderate–severe glaucoma and diagnostic accuracy similar to HFA and MFA (Carle *et al.*, 2011a). Given that both direct and consensual responses are recorded, these were compared and showed systematic differences according to hemifield, with temporal fields showing that direct responses exceeded consensual responses (contraction anisocoria) relatively uniformly, while nasal responses were roughly even between components (Carle *et al.*, 2011b). This provided a model suggesting differential input to the pupillary nuclei according to hemifield and gave a direct insight into how components might be amalgamated, suggesting that the simple 'mean' might not be the best approach.

Having now some more established methods for mfPOP, and demonstrating its utility in glaucoma, a focus was put on reducing variability between subjects, perhaps in applications involving other conditions. The issues of response saturation and variable blue light absorbance in the lens (due to brunescence) were investigated, showing that high luminance stimuli should be avoided as they mask mild field defects (Maddess *et al.*, 2011; Shean *et al.*, 2012), and that blue filtered light (yellow or red stimuli) showed similar response amplitudes and SNRs to mixed (white) light (Maddess *et al.*, 2011). Investigation using yellow/yellow (Y/Y) and green-on-red (G/R) stimuli were trialled in glaucoma, and shown to correlate with anatomical damage

in the form of retinal nerve fibre layer (RNFL) thinning based on optical coherence tomography (OCT) scans (Chain *et al.*, 2012; Kolic *et al.*, 2013), implying it may be useful in other retinal disorders which cause retinal thinning.

Trials of mfPOP in age-related macular degeneration (AMD) revealed smaller constriction amplitudes and high ROC AUC values of 0.84–0.96 for moderate to severe damage (Sabeti *et al.*, 2011; Rosli *et al.*, 2012). Trials in diabetic retinopathy showed reasonable ROC AUC values between 87–95% in diabetics with damage for >10 years, whereas notably poorer values (49–72%) were found in those who had had diabetes for shorter durations (0–10 years) (Bell *et al.*, 2010).

With many of the parameters now constant, including stimulus location and luminance balancing, there still remained some variability in methodology – namely in stimulus duration, brightness, and mean interval between stimuli. An experiment addressing these variables was performed, demonstrating that larger mean intervals (4 seconds), smaller luminance (150 cd/m^2), and duration of 133 ms were optimal (James *et al.*, 2012). A final seminal paper which was published prior to commencing my study which heavily influenced its design took a more comprehensive look at the difference between stimuli of various colours. This showed that (1) isoluminant colour exchange produces a response with either red-on-green (R/G) or green-on-red (G/R) stimuli, although larger responses are noted in the G/R; and (2) that a greater colour component with a smaller luminance component results in longer latencies with differences as large as 60 ms (Carle *et al.*, 2013). While it might be intuitive to think a smaller luminance component with its smaller amplitudes might simply have a greater time to peak (latency) because its waveform has a slow velocity, this is not the case. While pupillary response velocity scales with amplitude (Bremner, 2012), the waveform is isomorphically scaled – that is, every component of its shape remains constant (Semmlow & Stark, 1973; Semmlow *et al.*, 1975;

Maddess, 2012), which shows that response delays are not simply due to widening of the pupillary response, but actually represent a true delay in reaching the peak.

Neurological studies using mfPOP after this study commenced

The design of this study was in part to fill a gap in knowledge of how mfPOP fares in various neurological conditions, being aware that damage to the nerves used to carry the signal might be different to those obtained from damage to the source of the signals, as in retinal damage. After design of this thesis project, there have been further developments in mfPOP in terms of neurological assessment. Trials in multiple sclerosis have been completed showing pupillary peak amplitudes decreased by an average of 0.69 dB; large changes in TTP, with average latencies 25 ms longer; and good demarcation from controls with ROC AUC of 70% for the relapsing remitting (R&R) subtype and 86% for the progressive subtype (Ali *et al.*, 2014). Further testing in multiple sclerosis has shown that mfPOP can detect the R&R subtype even when patients have not experienced optic neuritis, suggesting changes in myelination outside of acute attacks (Maddess & Lueck, 2017) which is also supported by detection with mfVEP (Maddess & Lueck, 2019; Narayanan *et al.*, 2019).

Assessment in those with frequent migraines provided no evidence that stimulation with mfPOP induced migraine, while also showing those with a *recent* migraine (within 2 weeks) had significantly decreased response amplitudes (Lueck *et al.*, 2014). In a recent study looking at the effects of attention using mfPOP, it was demonstrated that yellow stimuli have delays ~20 ms shorter than either white or blue stimuli (Rosli *et al.*, 2018), suggesting that the increased delays in G/R stimuli as compared with Y/Y might partly be due to Y/Y having smaller latencies than other colours, rather than increased latency in G/R. In terms of neuronal gain control, an elegant study utilising multiple mfPOP methods to isolate input to the pretectal olivary nucleus (PON) and the Edinger–Westphal nucleus (EWN) demonstrated that the

majority of gain control occurs at the level of the EWN where the signal is integrated from input of both eyes (Carle *et al.*, 2019).

Retinal studies using mfPOP after this study commenced

Regarding retinal advances in mfPOP after this study commenced, additional studies in AMD, diabetic retinopathy, and glaucoma have been published and are briefly summarised below. In AMD, mfPOP was able to demonstrate a significant change in sensitivity with progression, with the reassuring result that central rings showed the greatest losses, consistent with disease pathology. Comparing Age-Related Eye Disease Study (AREDS) classifications 1–4, the study showed ROC AUC values of 43%, 60%, 60%, and 92% (within eye) and 62%, 74%, 81%, and 100% (between eye) for the best protocol (Sabeti *et al.*, 2014), on par with previous studies in AMD (Sabeti *et al.*, 2011; Rosli *et al.*, 2012). Examination of diabetic retinopathy patients showed mfPOP mean amplitude was smaller in subjects with retinopathy, while surprisingly the longest delays (latency) were in patients without retinopathy. By comparing asymmetry between eyes for TTP (latency), sensitivity reached 100% at 0% FPR in separating diabetes (with or without retinopathy) from controls (Sabeti *et al.*, 2015), a notable improvement from previous work (Bell *et al.*, 2010). In glaucoma, testing the intrinsic component of intrinsically photoreceptive retinal ganglion cells (ipRGC) (blue wavelength sensitivity) compared to their cone input (yellow), showed similar diagnostic accuracy but with blue light being more variable in advanced disease and less sensitive to scotomas (Carle *et al.*, 2015). This is consistent with previous studies involving brunescence, which contributes to variability between individuals (Maddess *et al.*, 2011; Shean *et al.*, 2012). A study of the effects of the dilating agent tropicamide (frequently used in ophthalmic examinations) revealed both pupillary delays and amplitude decreased initially, with pupil delays fully recovered after 8 h, while amplitudes were aberrant for 48 h (Rai *et al.*, 2019).

1.7. Summary – addressing gaps in the literature

1.7.1. Chapter 3 – Higher visual function loss and it assessment in stroke

This introduction has covered the visual pathways from the retina to the visual cortex and its distribution into other cortical centres, any of which may be damaged by disease. Extrastriate visual areas were shown to have areas of specialised processing, with cortical damage resulting in a range of deficits of higher visual function (HVF). It was established that pure higher visual function (HVF) deficits are rare, but that more subtle defects largely go unreported, leaving it unclear whether subtle HVF deficits occur commonly, which tests are most appropriate, and whether these warrants standard testing in clinical practice. Chapter 3 begins this discussion by piloting a study of heterogenous stroke patients who completed a range of HVF testing using multiple measures, and reporting which deficits appear to be worth further investigating and which tests appear most useful.

1.7.2. Chapter 4 – Pupillometry direct and consensual responses in stroke, chiasmal compression and AION

The origin of the pupil response in intrinsically photoreceptive retinal ganglion cells (ipRGC) and their combined intrinsic and cone inputs were discussed, along with their afferent pathways, and input to pupillary nuclei. The direct and consensual pupillary outputs were discussed, specifically covering their differences in the nasal and temporal fields. These features have been reported multiple times in control patients, but have not been reported in neurological disease. Chapter 4 compared direct and consensual pupillary outputs in stroke, chiasmal compression, and AION; addressing whether the same features are controls exist, or whether they may be characteristic differences which can better differentiate these conditions. Further, to enable a direct point-to-point comparison between visual field devices, direct and

consensual signals must be combined, and this chapter considered how best to combine these without bias.

1.7.3. Chapter 5 – Visual field comparison of standard automated perimetry and pupillomgrey in stroke, chiasmal compression and AION.

The introduction covered the history and developments of standard automated perimetry devices (HFA and MFA), covering their strengths, weaknesses, and output format. Likewise the history and development of mfPOP was covered in detail, leading up to the protcols used in these experiements. While mfPOP has been tested in a number of retinal disorders, its testing in neurological disorders remains limited, and it has not been tested in stroke, pituitary tumour, or AION conditions. As disucssed – these are common conditions and it is important that field devices can accurately identify and characterise damage, which may inform treatment or suggest limitations on activities that have becomes dangerous, such as driving. If mfPOP is to be used in clinical practice, it is important to assess how well it performs against devices which are used in clinical practice. This chapter compares HFA, MFA and mfPOP and assesses their relative effectiveness.

1.7.4. Chapter 6 – Analysis of pupillometry response waveform time-to-peak and comparison with amplitude in stroke, chiasmal compression and AION

A range of mfPOP protocols were discussed, including different output measures such as amplitude and time-to-peak (latency) of the response waveform. These previous experiments inform the new protocol used in this chapter, using green on red (G/R) stimuli and yellow on yellow (Y/Y) stimuli, with amplitude and latency measures. These are further justified within the chapter, but follow from the seminal paper by Carle et al., 2013 discussed above. As delays have been demonstrated in G/R colour-exchange stimuli consistent with cortical processing, it was thought that a G/R may be a more sensitive measure to cortical damage in stroke. This

chapter explores that possibility, while also discussing outcomes in chiasmal compression and AION.

References

Adams DL & Horton JC. (2003). A precise retinotopic map of primate striate cortex generated from the representation of angioscotomas. *J Neurosci* **23,** 3771-3789.

Ali EN, Maddess T, James AC, Voicu C & Lueck CJ. (2014). Pupillary response to sparse multifocal stimuli in multiple sclerosis patients. *Mult Scler* **20,** 854-861.

Ali M, Hazelton C, Lyden P, Pollock A, Brady M & Collaboration V. (2013). Recovery from poststroke visual impairment: Evidence from a clinical trials resource. *Neurorehab Neural Re* **27,** 133-141.

Allman JM & Kaas JH. (1971). A representation of the visual field in the caudal third of the middle tempral gyrus of the owl monkey (aotus trivirgatus). *Brain Res* **31,** 85-105.

An SJ, Kim TJ & Yoon BW. (2017). Epidemiology, risk factors, and clinical features of intracerebral hemorrhage: An update. *J Stroke* **19,** 3-10.

Anderson AJ & Johnson CA. (2002). Mechanisms isolated by frequency-doubling technology perimetry. *Invest Ophthalmol Vis Sci* **43,** 398-401.

Anderson AJ & Johnson CA. (2006). Comparison of the asa, mobs, and zest threshold methods. *Vision Res* **46,** 2403-2411.

Arcaro MJ & Kastner S. (2015). Topographic organization of areas v3 and v4 and its relation to supra-areal organization of the primate visual system. *Vis Neurosci* **32,** E014.

Arda H, Birer S, Aksu M, Ismailogullari S, Karakucuk S, Mirza E, Gumus K & Oner A. (2013). Obstructive sleep apnoea prevalence in non-arteritic anterior ischaemic optic neuropathy. *Brit J Ophthalmol* **97,** 206-209.

Arshavsky VY & Wensel TG. (2013). Timing is everything: Gtpase regulation in phototransduction. *Invest Ophthalmol Vis Sci* **54,** 7725-7733.

Artes PH, Iwase A, Ohno Y, Kitazawa Y & Chauban BC. (2002). Properties of perimetric threshold estimates from full threshold, sita standard, and sita fast strategies. *Invest Ophth Vis Sci* **43,** 2654-2659.

Arvind H, Graham S, Leaney J, Grigg J, Goldberg I, Billson F & Klistorner A. (2009). Identifying preperimetric functional loss in glaucoma: A blue-on-yellow multifocal visual evoked potentials study. *Ophthalmology* **116,** 1134-1141.

Aubert H & Foerster R. (1857). Untersuchungen über den raumsinn der retina. *Archiv für Ophthalmologie* **3,** 1-37.

Azouvi P, Bartolomeo P, Beis JM, Perennou D, Pradat-Diehl P & Rousseaux M. (2006). A battery of tests for the quantitative assessment of unilateral neglect. *Restor Neurol Neurosci* **24,** 273-285.

Bailey MJ, Riddoch MJ & Crome P. (2004). Test-retest stability of three tests for unilateral visual neglect in patients with stroke: Star cancellation, line bisection, and the baking tray task. *Neuropsychol Rehabil* **14,** 403-419.

Barrett KE, Barman SM, Biotano S & Brooks HL. (2011). *Ganong's review of medical physiology*. McGraw-Hill Education, USA.

Bartolomeo P, Bachoud-Levi AC & Thiebaut de Schotten M. (2014). The anatomy of cerebral achromatopsia: A reappraisal and comparison of two case reports. *Cortex* **56,** 138-144.

Barton JJS, Sharpe JA & Raymond JE. (1996). Directional defects in pursuit and motion perception in humans with unilateral cerebral lesions. *Brain* **119,** 1535-1550.

Baseler HA, Sutter EE, Klein SA & Carney T. (1994). The topography of visual evoked response properties across the visual field. *Electroencephalogr Clin Neurophysiol* **90,** 65-81.

Bass SJ, Cooper J, Feldman J & Horn D. (2007). Comparison of an automated confrontation testing device versus finger counting in the detection of field loss. *Optometry* **78,** 390-395.

Beck RW, Bergstrom TJ & Lichter PR. (1985). A clinical comparison of visual field testing with a new automated perimeter, the humphrey field analyzer, and the goldmann perimeter. *Ophthalmology* **92,** 77-82.

Beck RW, Hayreh SS, Podhajsky PA, Tan ES & Moke PS. (1997). Aspirin therapy in nonarteritic anterior ischemic optic neuropathy. *Am J Ophthalmol* **123,** 212-217.

Beis JM, Keller C, Morin N, Bartolomeo P, Bernati T, Chokron S, Leclercq M, Louis-Dreyfus A, Marchal F, Martin Y, Perennou D, Pradat-Diehl P, Prairial C, Rode G,

Rousseaux M, Samuel C, Sieroff E, Wiart L, Azouvi P & French Collaborative Study Group on Assessment of Unilateral N. (2004). Right spatial neglect after left hemisphere stroke: Qualitative and quantitative study. *Neurology* **63,** 1600-1605.

Bell A, James AC, Kolic M, Essex RW & Maddess T. (2010). Dichoptic multifocal pupillography reveals afferent visual field defects in early type 2 diabetes. *Invest Ophth Vis Sci* **51,** 602-608.

Bengtsson B & Heijl A. (1998). Sita fast, a new rapid perimetric threshold test. Description of methods and evaluation in patients with manifest and suspect glaucoma. *Acta Ophthalmol Scand* **76,** 431-437.

Bengtsson B, Heijl A & Olsson J. (1998). Evaluation of a new threshold visual field strategy, sita, in normal subjects. Swedish interactive thresholding algorithm. *Acta Ophthalmol Scand* **76,** 165-169.

Berezina TL, Khouri AS, Kolomeyer AM, Clancy PS & Fechtner RD. (2011). Peripheral visual field thresholds using humphrey field analyzer program 60-4 in normal eyes. *Eur J Ophthalmol* **21,** 415-421.

Beri M, Klugman MR, Kohler JA & Hayreh SS. (1987). Anterior ischemic optic neuropathy .7. Incidence of bilaterality and various influencing factors. *Ophthalmology* **94,** 1020-1028.

Berson DM, Castrucci AM & Provencio I. (2010). Morphology and mosaics of melanopsin-expressing retinal ganglion cell types in mice. *J Comp Neurol* **518,** 2405-2422.

Berson DM, Dunn FA & Takao M. (2002). Phototransduction by retinal ganglion cells that set the circadian clock. *Science* **295,** 1070-1073.

Bevers C, Blanckaert G, Van Keer K, Fils JF, Vandewalle E & Stalmans I. (2019). Semi-automated kinetic perimetry: Comparison of the octopus 900 and humphrey visual field analyzer 3 versus goldmann perimetry. *Acta Ophthalmol* **97,** e499-e505.

Biousse V, Kedar S, Zhang XJ, Lynn M & Newman NJ. (2005). Homonymous hemianopia in stroke. *Neurology* **64,** A14-A14.

Bjerre A, Grigg JR, Parry NR & Henson DB. (2004). Test-retest variability of multifocal visual evoked potential and sita standard perimetry in glaucoma. *Invest Ophthalmol Vis Sci* **45,** 4035-4040.

Boardman JP, Ganesan V, Rutherford MA, Saunders DE, Mercuri E & Cowan F. (2005). Magnetic resonance image correlates of hemiparesis after neonatal and childhood middle cerebral artery stroke. *Pediatrics* **115,** 321-326.

Boehme AK, Esenwa C & Elkind MS. (2017). Stroke risk factors, genetics, and prevention. *Circ Res* **120,** 472-495.

Born RT & Bradley DC. (2005). Structure and function of visual area mt. *Annu Rev Neurosci* **28,** 157-189.

Bouvier SE & Engel SA. (2006). Behavioral deficits and cortical damage loci in cerebral achromatopsia. *Cereb Cortex* **16,** 183-191.

Bowen A, McKenna K & Tallis RC. (1999). Reasons for variability in the reported rate of occurrence of unilateral spatial neglect after stroke. *Stroke* **30,** 1196-1202.

Bremner FD. (2012). Pupillometric evaluation of the dynamics of the pupillary response to a brief light stimulus in healthy subjects. *Invest Ophthalmol Vis Sci* **53,** 7343-7347.

Burkhalter A & Van Essen DC. (1986). Processing of color, form and disparity information in visual areas vp and v2 of ventral extrastriate cortex in the macaque monkey. *J Neurosci* **6,** 2327-2351.

Carle CF, James AC, Kolic M, Essex RW & Maddess T. (2015). Blue multifocal pupillographic objective perimetry in glaucoma. *Invest Ophthalmol Vis Sci* **56,** 6394-6403.

Carle CF, James AC, Kolic M, Loh YW & Maddess T. (2011a). High-resolution multifocal pupillographic objective perimetry in glaucoma. *Invest Ophth Vis Sci* **52,** 604-610.

Carle CF, James AC & Maddess T. (2013). The pupillary response to color and luminance variant multifocal stimuli. *Invest Ophth Vis Sci* **54,** 467-475.

Carle CF, James AC, Rosli Y & Maddess T. (2019). Localization of neuronal gain control in the pupillary response. *Frontiers in neurology* **10,** 203.

Carle CF, Maddess T & James AC. (2011b). Contraction anisocoria: Segregation, summation, and saturation in the pupillary pathway. *Invest Ophth Vis Sci* **52,** 2365-2371.

Carota A & Calabrese P. (2013). The achromatic 'philosophical zombie', a syndrome of cerebral achromatopsia with color anopsognosia. *Case Rep Neurol* **5,** 98-103.

Cassidy TP, Bruce DW & Gray CS. (2001). Visual field loss after stroke: Confrontation and perimetry in the assessment of recovery. *J Stroke Cerebrovasc Dis* **10,** 113-117.

Chain AYH, Carle CF, James AC & Maddess T. (2012). Multifocal pupillographic perimetry and ocular coherence tomography measurements in glaucoma. *Clin Exp Ophthalmol* **40,** 136-137.

Chen C, Okera S, Davies PE, Selva D & Crompton JL. (2003a). Craniopharyngioma: A review of long-term visual outcome. *Clin Exp Ophthalmol* **31,** 220-228.

Chen CS, Hood DC, Zhang X, Karam EZ, Liebmann JM, Ritch R, Thienprasiddhi P & Greenstein VC. (2003b). Repeat reliability of the multifocal visual evoked potential in normal and glaucomatous eyes. *J Glaucoma* **12,** 399-408.

Chen CS, Lee AW, Clarke G, Hayes A, George S, Vincent R, Thompson A, Centrella L, Johnson K, Daly A & Crotty M. (2009). Vision-related quality of life in patients with complete homonymous hemianopia post stroke. *Top Stroke Rehabil* **16,** 445-453.

Connolly B & Oczkowski W. (2010). Individual and combined confrontation visual field tests performed poorly as a screen for visual field abnormalities. *Ann Intern Med* **153**.

Conway BR & Tsao DY. (2009). Color-tuned neurons are spatially clustered according to color preference within alert macaque posterior inferior temporal cortex. *Proc Natl Acad Sci U S A* **106,** 18034-18039.

Cooper SA, Joshi AC, Seenan PJ, Hadley DM, Muir KW, Leigh RJ & Metcalfe RA. (2012). Akinetopsia: Acute presentation and evidence for persisting defects in motion vision. *J Neurol Neurosur Ps* **83,** 229-230.

Cowey A, Alexander I, Heywood C & Kentridge R. (2008). Pupillary responses to coloured and contourless displays in total cerebral achromatopsia. *Brain* **131,** 2153-2160.

Cowey A, Heywood CA & Irving-Bell L. (2001). The regional cortical basis of achromatopsia: A study on macaque monkeys and an achromatopsic patient. *Eur J Neurosci* **14,** 1555-1566.

Cox TA & Drewes CP. (1984). Contraction anisocoria resulting from half-field illumination. *Am J Ophthalmol* **97,** 577-582.

Coyle JT. (2001). Goldmann vs. Humphrey perimetry for occipital lobe lesions. *Ophthalmology* **108,** 241-242.

Curcio CA & Allen KA. (1990). Topography of ganglion cells in human retina. *J Comp Neurol* **300,** 5-25.

Dacey DM, Liao HW, Peterson BB, Robinson FR, Smith VC, Pokorny J, Yau KW & Gamlin PD. (2005). Melanopsin-expressing ganglion cells in primate retina signal colour and irradiance and project to the lgn. *Nature* **433,** 749-754.

Dacey DM, Peterson BB, Robinson FR & Gamlin PD. (2003). Fireworks in the primate retina: In vitro photodynamics reveals diverse lgn-projecting ganglion cell types. *Neuron* **37,** 15-27.

Danesh-Meyer HV, Carroll SC, Gaskin BJ, Gao A & Gamble GD. (2006). Correlation of the multifocal visual evoked potential and standard automated perimetry in compressive optic neuropathies. *Invest Ophthalmol Vis Sci* **47,** 1458-1463.

Danesh-Meyer HV & Gamble GD. (2011). Diagnostic accuracy of confrontation visual field tests reply from the authors. *Neurology* **76,** 1193-1193.

Davies JM, Trinh VT, Sneed PK & McDermott MW. (2013). Radiotherapy for recurrent epidermoid cyst. *J Neuro-Oncol* **112,** 307-313.

de Rooij NK, Linn FH, van der Plas JA, Algra A & Rinkel GJ. (2007). Incidence of subarachnoid haemorrhage: A systematic review with emphasis on region, age, gender and time trends. *J Neurol Neurosurg Psychiatry* **78,** 1365-1372.

DeArmond SJ, Fusco MM & Dewey MM. (1976). *Structure of the human brain: A photographic atlas*. Oxford University Press, USA.

DeYoe EA, Carman GJ, Bandettini P, Glickman S, Wieser J, Cox R, Miller D & Neitz J. (1996). Mapping striate and extrastriate visual areas in human cerebral cortex. *Proc Natl Acad Sci U S A* **93,** 2382-2386.

Do MT & Yau KW. (2010). Intrinsically photosensitive retinal ganglion cells. *Physiol Rev* **90,** 1547-1581.

Dubner R & Zeki SM. (1971). Response properties and receptive fields of cells in an anatomically defined region of the superior temporal sulcus in the monkey. *Brain Res* **35,** 528-532.

Edelstein K & Amir S. (1999). The role of the intergeniculate leaflet in entrainment of circadian rhythms to a skeleton photoperiod. *J Neurosci* **19,** 372-380.

Elliott DB, North I & Flanagan J. (1997). Confrontation visual field tests. *Ophthal Physl Opt* **17,** S17-S24.

Fishman GA, Birch DG, Holder GE & Brigell MG. (2001). *Electrophysiologic testing in disorders of the retina, optic nerve, and visual pathway*. American academy of ophthalmology, San Francisco.

Flanagan JG & Harding GF. (1988). Multi-channel visual evoked potentials in early compressive lesions of the chiasm. *Doc Ophthalmol* **69,** 271-281.

Fox CJ, Hanif HM, Iaria G, Duchaine BC & Barton JJS. (2011). Perceptual and anatomic patterns of selective deficits in facial identity and expression processing. *Neuropsychologia* **49,** 3188-3200.

Fraser C, Klistorner A, Graham S, Garrick R, Billson F & Grigg J. (2006a). Multifocal visual evoked potential latency analysis: Predicting progression to multiple sclerosis. *Arch Neurol* **63,** 847-850.

Fraser CL, Klistorner A, Graham SL, Garrick R, Billson FA & Grigg JR. (2006b). Multifocal visual evoked potential analysis of inflammatory or demyelinating optic neuritis. *Ophthalmology* **113,** 323 e321-323 e322.

Fredette MJ, Giguere A, Anderson DR, Budenz DL & McSoley J. (2015). Comparison of matrix with humphrey field analyzer ii with sita. *Optometry and vision science : official publication of the American Academy of Optometry* **92,** 527-536.

Fukuda Y, Higuchi S, Yasukouchi A & Morita T. (2012). Distinct responses of cones and melanopsin-expressing retinal ganglion cells in the human electroretinogram. *J Physiol Anthropol* **31**.

Furlan M & Smith AT. (2016). Global motion processing in human visual cortical areas v2 and v3. *J Neurosci* **36,** 7314-7324.

Gall C, Franke GH & Sabel BA. (2010). Vision-related quality of life in first stroke patients with homonymous visual field defects. *Health Qual Life Out* **8**.

Gamlin PD & Clarke RJ. (1995). The pupillary light reflex pathway of the primate. *J Am Optom Assoc* **66,** 415-418.

Gamlin PD, Zhang H & Clarke RJ. (1995). Luminance neurons in the pretectal olivary nucleus mediate the pupillary light reflex in the rhesus monkey. *Exp Brain Res* **106,** 169-176.

Gardiner SK, Demirel S, Goren D, Mansberger SL & Swanson WH. (2015). The effect of stimulus size on the reliable stimulus range of perimetry. *Transl Vis Sci Technol* **4,** 10.

Gautier A, Godbout A, Grosheny C, Tejedor I, Coudert M, Courtillot C, Jublanc C, De Kerdanet M, Poirier JY, Riffaud L, Sainte-Rose C, Van Effenterre R, Brassier G, Bonnet F, Touraine P & Grp CS. (2012). Markers of recurrence and long-term morbidity in craniopharyngioma: A systematic analysis of 171 patients. *J Clin Endocr Metab* **97,** 1258-1267.

Gilhotra JS, Mitchell P, Healey PR, Cumming RG & Currie J. (2002). Homonymous visual field defects and stroke in an older population. *Stroke* **33,** 2417-2420.

Girkin CA, McGwin G, Jr. & DeLeon-Ortega J. (2004). Frequency doubling technology perimetry in non-arteritic ischaemic optic neuropathy with altitudinal defects. *The British journal of ophthalmology* **88,** 1274-1279.

Glisson CC. (2014). Visual loss due to optic chiasm and retrochiasmal visual pathway lesions. *Continuum (Minneap Minn)* **20,** 907-921.

Goldmann H. (1946). Demonstration unseres neuen projektionskugelperimeters samt theoretischen und klinischen bemerkungen über perimetrie. *Ophthalmologica* **111,** 187-192.

Graham SL. (2006). The effects of glaucoma on the latency of the multifocal visual evoked potential. *The British journal of ophthalmology* **90,** 1077-1078.

Graham SL & Klistorner A. (1999). The diagnostic significance of the multifocal pattern visual evoked potential in glaucoma. *Curr Opin Ophthalmol* **10,** 140-146.

Greifzu F, Schmidt S, Schmidt KF, Kreikemeier K, Witte OW & Lowel S. (2011). Global impairment and therapeutic restoration of visual plasticity mechanisms after a localized cortical stroke. *Proc Natl Acad Sci U S A* **108,** 15450-15455.

Gulsen S, Dinc AH, Unal M, Canturk N & Altinors N. (2010). Characterization of the anatomic location of the pituitary stalk and its relationship to the dorsum sellae, tuberculum sellae and chiasmatic cistern. *J Korean Neurosurg Soc* **47,** 169-173.

Guzzetta A. (2010). Plasticity of the visual system after congenital brain damage: A few weeks can matter. *Dev Med Child Neurol* **52,** 699.

Guzzetta A, Cioni G, Cowan F & Mercuri E. (2001a). Visual disorders in children with brain lesions: 1. Maturation of visual function in infants with neonatal brain lesions: Correlation with neuroimaging. *European journal of paediatric neurology : EJPN : official journal of the European Paediatric Neurology Society* **5,** 107-114.

Guzzetta A, D'Acunto G, Rose S, Tinelli F, Boyd R & Cioni G. (2010). Plasticity of the visual system after early brain damage. *Dev Med Child Neurol* **52,** 891-900.

Guzzetta A, Fazzi B, Mercuri E, Bertuccelli B, Canapicchi R, van Hof-van Duin J & Cioni G. (2001b). Visual function in children with hemiplegia in the first years of life. *Dev Med Child Neurol* **43,** 321-329.

Hadjikhani N, Liu AK, Dale AM, Cavanagh P & Tootell RB. (1998). Retinotopy and color sensitivity in human visual cortical area v8. *Nat Neurosci* **1,** 235-241.

Halliday AM, Halliday E, Kriss A, McDonald WI & Mushin J. (1976a). The pattern-evoked potential in compression of the anterior visual pathways. *Brain* **99,** 357-374.

Halliday AM, Halliday L, Kriss A, McDonald WI & Mushin J. (1976b). Abnormalities of the pattern evoked potential in compression of the anterior visual pathways. *Trans Ophthalmol Soc N Z* **28,** 37-40.

Hattenhauer MG, Leavitt JA, Hodge DO, Grill R & Gray DT. (1997). Incidence of nonarteritic anterior ischemic optic neuropathy. *Am J Ophthalmol* **123,** 103-107.

Hayashi R, Yamaguchi S, Narimatsu T, Miyata H, Katsumata Y & Mimura M. (2017). Statokinetic dissociation (riddoch phenomenon) in a patient with homonymous hemianopsia as the first sign of posterior cortical atrophy. *Case Rep Neurol* **9,** 256-260.

Hayes A, Chen CS, Clarke G & Thompson A. (2012). Functional improvements following the use of the nvt vision rehabilitation program for patients with hemianopia following stroke. *Neurorehabilitation* **31,** 19-30.

Hayreh SS. (1974). Anterior ischemic optic neuropathy .1. Terminology and pathogenesis. *Brit J Ophthalmol* **58,** 955-963.

Hayreh SS. (2001a). Blood flow in the optic nerve head and factors that may influence it. *Prog Retin Eye Res* **20,** 595-624.

Hayreh SS. (2001b). The blood supply of the optic nerve head and the evaluation of it - myth and reality. *Prog Retin Eye Res* **20,** 563-593.

Hayreh SS. (2009). Ischemic optic neuropathy. *Prog Retin Eye Res* **28,** 34-62.

Hayreh SS. (2011). Treatment of non-arteritic anterior ischaemic optic neuropathy. *Brit J Ophthalmol* **95,** 1617-1618.

Hayreh SS, Podhajsky PA & Zimmerman B. (2001). Ipsilateral recurrence of nonarteritic anterior ischemic optic neuropathy. *Am J Ophthalmol* **132,** 734-742.

Heijl A, Lindgren A & Lindgren G. (1989). Test-retest variability in glaucomatous visual-fields. *Am J Ophthalmol* **108,** 130-135.

Heilman KM & Van Den Abell T. (1980). Right hemisphere dominance for attention: The mechanism underlying hemispheric asymmetries of inattention (neglect). *Neurology* **30,** 327-330.

Heilman KM, Watson RT, Bower D & Valenstein E. (1983). [right hemisphere dominance for attention]. *Rev Neurol (Paris)* **139,** 15-17.

Hendry SHC & Reid RC. (2000). The koniocellular pathway in primate vision. *Annu Rev Neurosci* **23,** 127-153.

Hepworth LR & Rowe FJ. (2018). Programme choice for perimetry in neurological conditions (popin): A systematic review of perimetry options and patterns of visual field loss. *Bmc Ophthalmol* **18,** 241.

Heutink J, Brouwer WH, Kums E, Young A & Bouma A. (2012). When family looks strange and strangers look normal: A case of impaired face perception and recognition after stroke. *Neurocase* **18,** 39-49.

Heywood CA, Nicholas JJ, LeMare C & Cowey A. (1998). The effect of lesions to cortical areas v4 or ait on pupillary responses to chromatic and achromatic stimuli in monkeys. *Exp Brain Res* **122,** 475-480.

Holmes G. (1918). Disturbances of visual orientation. *The British journal of ophthalmology* **2,** 506-516.

Holmes G. (1919). Disturbances of visual space perception. *Brit Med J* **2,** 230-233.

Holmes G & Horrax G. (1919). Disturbances of spatial orientation and visual attention with loss of stereoscopic vision. *Arch Neuro Psychiatr* **1,** 385-407.

Hood DC, Greenstein VC, Odel JG, Zhang X, Ritch R, Liebmann JM, Hong JE, Chen CS & Thienprasiddhi P. (2002). Visual field defects and multifocal visual evoked potentials: Evidence of a linear relationship. *Arch Ophthalmol* **120,** 1672-1681.

Hood DC, Odel JG & Winn BJ. (2003a). The multifocal visual evoked potential. *Journal of neuro-ophthalmology : the official journal of the North American Neuro-Ophthalmology Society* **23,** 279-289.

Hood DC, Zhang X & Winn BJ. (2003b). Detecting glaucomatous damage with multifocal visual evoked potentials: How can a monocular test work? *J Glaucoma* **12,** 3-15.

Horton JC. (1997). Wilbrand's knee of the primate optic chiasm is an artefact of monocular enucleation. *Trans Am Ophthalmol Soc* **95,** 579-609.

Horton JC & Hocking DR. (1996). Intrinsic variability of ocular dominance column periodicity in normal macaque monkeys. *J Neurosci* **16,** 7228-7239.

Hurley JB. (2009). Encyclopedia of neuroscience. In *Phototransduction*, ed. Squire LR. Elsevier.

Hutchins B & Weber JT. (1985). The pretectal complex of the monkey: A reinvestigation of the morphology and retinal terminations. *J Comp Neurol* **232,** 425-442.

Ijaola FO & Kausar SA. (2009). Visual impairment following stroke: Do stroke patients require vision assessment ? *Age Ageing* **38,** 629-630.

Ireland AC & Carter BI. (2019). *Neuroanatomy, optic chiasm*. StatPearls Publishing, Treasure Island, Florida.

Jacobson L, Rydberg A, Eliasson AC, Kits A & Flodmark O. (2010). Visual field function in school-aged children with spastic unilateral cerebral palsy related to different patterns of brain damage. *Dev Med Child Neurol* **52,** e184-187.

Jahangiri A, Lamborn KR, Blevins L, Kunwar S & Aghi MK. (2012). Factors associated with delay to pituitary adenoma diagnosis in patients with visual loss. *J Neurosurg* **116,** 283-289.

James AC, Kolic M, Bedford SM & Maddess T. (2012). Stimulus parameters for multifocal pupillographic objective perimetry. *J Glaucoma* **21,** 571-578.

James AC, Maddess T & Bowman E. (2003). Effect of presentation rate and pulse duration on the pattern-pulse multifocal visual evoked potential (ppmvep). *Invest Ophth Vis Sci* **44,** U445-U445.

James AC, Maddess T, Goh XL & Winkles N. (2005a). Spatially sparse pattern-pulse stimulation enhances multifocal visual evoked potential analysis. *Invest Ophth Vis Sci* **46**.

James AC, Ruseckaite R & Maddess T. (2005b). Effect of temporal sparseness and dichoptic presentation on multifocal visual evoked potentials. *Visual Neurosci* **22,** 45-54.

Jehkonen M, Ahonen JP, Dastidar P, Koivisto AM, Laippala P, Vilkki J & Molnar G. (2000). Visual neglect as a predictor of functional outcome one year after stroke. *Acta Neurol Scand* **101,** 195-201.

Johnson CA. (1994). Selective versus nonselective losses in glaucoma. *J Glaucoma* **3 Suppl 1,** S32-44.

Johnson CA, Chauhan BC & Shapiro LR. (1992). Properties of staircase procedures for estimating thresholds in automated perimetry. *Invest Ophthalmol Vis Sci* **33,** 2966-2974.

Johnson CA & Samuels SJ. (1997). Screening for glaucomatous visual field loss with frequency-doubling perimetry. *Invest Ophthalmol Vis Sci* **38,** 413-425.

Johnson CA, Wall M & Thompson HS. (2011). A history of perimetry and visual field testing. *Optometry and vision science : official publication of the American Academy of Optometry* **88,** E8-15.

Johnson LN & Arnold AC. (1994). Incidence of nonarteritic and arteritic anterior ischemic optic neuropathy - population-based study in the state of missouri and los-angeles-county, california. *J Neuro-Ophthalmol* **14,** 38-44.

Johnson LN & Baloh FG. (1991). The accuracy of confrontation visual-field test in comparison with automated perimetry. *J Natl Med Assoc* **83,** 895-898.

Jonas JB, Schneider U & Naumann GO. (1992). Count and density of human retinal photoreceptors. *Graefe's archive for clinical and experimental ophthalmology =*

Albrecht von Graefes Archiv fur klinische und experimentelle Ophthalmologie **230,** 505-510.

Jones SA & Shinton RA. (2006). Improving outcome in stroke patients with visual problems. *Age Ageing* **35,** 560-565.

Kaplan E. (2013). The m, p and k pathways of the primate visual system revisited. In *The new visual neuroscience,* ed. Werner JS & Chalupa LM, pp. 215-227.

Kardon R, Anderson SC, Damarjian TG, Grace EM, Stone E & Kawasaki A. (2009). Chromatic pupil responses: Preferential activation of the melanopsin-mediated versus outer photoreceptor-mediated pupil light reflex. *Ophthalmology* **116,** 1564-1573.

Kasputyte R, Slatkeviciene G, Liutkeviciene R, Glebauskiene B, Bernotas G & Tamasauskas A. (2013). Changes of visual functions in patients with pituitary adenoma. *Med Lith* **49,** 132-137.

Kerr NM, Chew SSL, Eady EK, Gamble GD & Danesh-Meyer HV. (2010). Diagnostic accuracy of confrontation visual field tests. *Neurology* **74,** 1184-1190.

Kerr NM, Chew SSSL & Danesh-Meyer HV. (2009). Non-arteritic anterior ischaemic optic neuropathy: A review and update. *J Clin Neurosci* **16,** 994-1000.

Khan S, Leung E & Jay WM. (2008). Stroke and visual rehabilitation. *Top Stroke Rehabil* **15,** 27-36.

Kikuchi Y, Yoshii M, Yanashima K, Enoki T, Ide T, Sakemi F & Okisaka S. (2002). Multifocal visual evoked potential is dependent on electrode position. *Jpn J Ophthalmol* **46,** 533-539.

Kim KY, Rios LC, Le H, Perez AJ, Phan S, Bushong EA, Deerinck TJ, Liu YH, Ellisman MA, Lev-Ram V, Ju S, Panda SA, Yoon S, Hirayama M, Mure LS, Hatori M, Ellisman MH & Panda S. (2019). Synaptic specializations of melanopsin-retinal ganglion cells in multiple brain regions revealed by genetic label for light and electron microscopy. *Cell Rep* **29,** 628-644 e626.

Klistorner A, Graham SL, Martins A, Grigg JR, Arvind H, Kumar RS, James AC & Billson FA. (2007). Multifocal blue-on-yellow visual evoked potentials in early glaucoma. *Ophthalmology* **114,** 1613-1621.

Klistorner AI, Graham SL, Grigg JR & Billson FA. (1998). Multifocal topographic visual evoked potential: Improving objective detection of local visual field defects. *Invest Ophthalmol Vis Sci* **39,** 937-950.

Kolb H. (1995). Webvision: The organisation of the retina and visual system, ed. Kolb H, Nelson R, Fernandez E & Jones B. University of Utah Health Sciences Center, Salt lake city, Utah.

Kolic M, Chain A, James A, Maddess T & Carle C. (2013). Structure and function in multifocal pupillographic objective perimetry (mfpop). *Invest Ophth Vis Sci* **54**.

Kozicz T, Bittencourt JC, May PJ, Reiner A, Gamlin PDR, Palkovits M, Horn AKE, Toledo CAB & Ryabinin AE. (2011). The edinger-westphal nucleus: A historical, structural, and functional perspective on a dichotomous terminology. *J Comp Neurol* **519,** 1413-1434.

Kupfer C, Chumbley L & Downer JC. (1967). Quantitative histology of optic nerve, optic tract and lateral geniculate nucleus of man. *J Anat* **101,** 393-401.

Kuritzky S. (2001). Goldmann vs. Humphrey perimetry for occipital lobe lesions. *Ophthalmology* **108,** 242.

Lall GS, Revell VL, Momiji H, Al Enezi J, Altimus CM, Guler AD, Aguilar C, Cameron MA, Allender S, Hankins MW & Lucas RJ. (2010). Distinct contributions of rod, cone, and melanopsin photoreceptors to encoding irradiance. *Neuron* **66,** 417-428.

Lang N, Baudewig J, Kallenberg K, Antal A, Happe S, Dechent P & Paulus W. (2006). Transient prosopagnosia after ischemic stroke. *Neurology* **66,** 916-916.

Lee JP, Park IW & Chung YS. (2011a). The volume of tumor mass and visual field defect in patients with pituitary macroadenoma. *Korean J Ophthalmol* **25,** 37-41.

Lee MS, Grossman D, Arnold AC & Sloan FA. (2011b). Incidence of nonarteritic anterior ischemic optic neuropathy: Increased risk among diabetic patients. *Ophthalmology* **118,** 959-963.

Lee SK, Sonoda T & Schmidt TM. (2019). M1 intrinsically photosensitive retinal ganglion cells integrate rod and melanopsin inputs to signal in low light. *Cell Rep* **29,** 3349-3355 e3342.

Leff A. (2004). A historical review of the representation of the visual field in primary visual cortex with special reference to the neural mechanisms underlying macular sparing. *Brain Lang* **88,** 268-278.

Li JY & Schmidt TM. (2018). Divergent projection patterns of m1 iprgc subtypes. *J Comp Neurol* **526,** 2010-2018.

Lu XS, Ye J, Zhou S, Lu BX & Chen XH. (2005). Unilateral spatial neglect, global processing deficit and prosopagnosia following right hemisphere stroke: A case report. *Chinese Med J-Peking* **118,** 1846-1848.

Lueck C, Ali E, Carle C & Maddess T. (2014). Effects of stimulating melanopsin-containing retinal ganglioncells in migraine patients using multifocal objective pupillometry. *J Clin Neurosci* **21,** 2048.

Lundervold AJ, Bergmann N & Wootton C. (2005). Visual neglect in the first weeks after a stroke in the right hemisphere. *Scand J Psychol* **46,** 297-303.

Luu S, Lee AW, Daly A & Chen CS. (2010). Visual field defects after stroke a practical guide for gps. *Aust Fam Physician* **39,** 499-503.

Lynch JK, Hirtz DG, DeVeber G & Nelson KB. (2002). Report of the national institute of neurological disorders and stroke workshop on perinatal and childhood stroke. *Pediatrics* **109,** 116-123.

Lyon DC & Kaas JH. (2001). Connectional and architectonic evidence for dorsal and ventral v3, and dorsomedial area in marmoset monkeys. *J Neurosci* **21,** 249-261.

Maddess T. (2011). The influence of sampling errors on test-retest variability in perimetry. *Invest Ophthalmol Vis Sci* **52,** 1014-1022.

Maddess T. (2012). Pupil dynamics and response amplitude: Only size matters. *Invest Ophth Vis Sci* **53,** 7644-7644.

Maddess T. (2014). Modeling the relative influence of fixation and sampling errors on retest variability in perimetry. *Graefe's archive for clinical and experimental ophthalmology = Albrecht von Graefes Archiv fur klinische und experimentelle Ophthalmologie* **252,** 1611-1619.

Maddess T, Bedford SM, Goh XL & James AC. (2009). Multifocal pupillographic visual field testing in glaucoma. *Clin Exp Ophthalmol* **37,** 678-686.

Maddess T, Goh XL & James AC. (2007). Luminance and chromatic multifocal pupillographic perimetry. In *ARVO annual meeting*, pp. 1628. Investigative ophthalmology and visual science.

Maddess T & Henry GH. (1992). Performance of nonlinear visual units in ocular hypertension and glaucoma. *Clin Vision Sci* **7,** 371-383.

Maddess T, Ho YL, Wong SS, Kolic M, Goh XL, Carle CF & James AC. (2011). Multifocal pupillographic perimetry with white and colored stimuli. *J Glaucoma* **20,** 336-343.

Maddess T, James AC & Bowman EA. (2004). Contrast responses of dichoptic multifocal visual evoked potential responses to contrast reversing and temporally sparse stimuli. *Invest Ophth Vis Sci* **45,** U155-U155.

Maddess T, James AC, Ruseckaite R & Bowman EA. (2003). Hierarchical decomposition of multifocal visual evoked potential responses to dichoptic contrast reversing and temporally sparse stimuli. *Invest Ophth Vis Sci* **44,** U465-U465.

Maddess T & Kulikowski JJ. (1999). Apparent fineness of stationary compound gratings. *Vision Res* **39,** 3404-3416.

Maddess T & Lueck CJ. (2017). Multiple sclerosis seen through new eyes. *Clin Exp Ophthalmol* **45,** 9-11.

Maddess T & Lueck CJ. (2019). Correlating structure with visual function in patients with multiple sclerosis: Where is this leading? *Clin Neurophysiol* **130,** 157-159.

Maddess T, Ruseckaite R & James AC. (2002). Effect of sparseness and dichoptic presentation on multifocal visual evoked potentials. *Invest Ophth Vis Sci* **43,** U1337-U1337.

Maffei L. (2002). Plasticity in the visual system: Role of neurotrophins and electrical activity. *Arch Ital Biol* **140,** 341-346.

Martin TI, Kardon RI & Thompson HS. (1991). Unequal direct and consensual pupillary responses to hemiretinal stimuli. *Invest Ophth Vis Sci* **32,** 1124.

Martins A, Klistorner A, Graham S & Billson F. (2004). Effect of check size and stimulation rate on blue-yellow multifocal visual evoked potentials. *Clin Exp Ophthalmol* **32,** 270-274.

Marzi CA, Mancini F, Sperandio I & Savazzi S. (2009). Evidence of midline retinal nasotemporal overlap in healthy humans: A model for foveal sparing in hemianopia? *Neuropsychologia* **47,** 3007-3011.

Matson M & Fujimoto L. (2011). Bilateral arteritic anterior ischemic optic neuropathy. *Optometry* **82,** 622-631.

McDougal DH & Gamlin PD. (2010). The influence of intrinsically-photosensitive retinal ganglion cells on the spectral sensitivity and response dynamics of the human pupillary light reflex. *Vision Res* **50,** 72-87.

McDougal DH & Gamlin PD. (2015). Autonomic control of the eye. *Compr Physiol* **5,** 439-473.

McKeefry DJ, Watson JDG, Frackowiak RSJ, Fong K & Zeki S. (1997). The activity in human areas v1/v2, v3, and v5 during the perception of coherent and incoherent motion. *Neuroimage* **5,** 1-12.

McKeefry DJ & Zeki S. (1997). The position and topography of the human colour centre as revealed by functional magnetic resonance imaging. *Brain* **120 (Pt 12),** 2229-2242.

McKendrick AM, Anderson AJ, Johnson CA & Fortune B. (2003). Appearance of the frequency doubling stimulus in normal subjects and patients with glaucoma. *Invest Ophthalmol Vis Sci* **44,** 1111-1116.

McMinn RMH. (1998). *Last's anatomy regional and applied*. Elsivier: Churchill Livingstone, Edinburgh, United Kingdom.

Miller LJ, Mittenberg W, Carey VM, McMorrow MA, Kushner TE & Weinstein JM. (1999). Astereopsis caused by traumatic brain injury. *Arch Clin Neuropsych* **14,** 537-543.

Millodot M. (2009). *Dictionary of optometry and visual science*. Butterworth-Heinemann - elsevier, United Kingdom.

Monteiro ML, Moura FC & Cunha LP. (2007). Frequency doubling perimetry in patients with mild and moderate pituitary tumor-associated visual field defects detected by conventional perimetry. *Arq Bras Oftalmol* **70,** 323-329.

Morin LP, Blanchard JH & Provencio I. (2003). Retinal ganglion cell projections to the hamster suprachiasmatic nucleus, intergeniculate leaflet, and visual midbrain: Bifurcation and melanopsin immunoreactivity. *J Comp Neurol* **465,** 401-416.

Munch M & Kawasaki A. (2013). Intrinsically photosensitive retinal ganglion cells: Classification, function and clinical implications. *Curr Opin Neurol* **26,** 45-51.

Munch M, Leon L, Crippa SV & Kawasaki A. (2012). Circadian and wake-dependent effects on the pupil light reflex in response to narrow-bandwidth light pulses. *Invest Ophth Vis Sci* **53,** 4546-4555.

Musch DC, Gillespie BW, Motyka BM, Niziol LM, Mills RP & Lichter PR. (2005). Converting to sita-standard from full-threshold visual field testing in the follow-up phase of a clinical trial. *Invest Ophthalmol Vis Sci* **46,** 2755-2759.

Narayanan D, Cheng H, Tang RA & Frishman LJ. (2019). Multifocal visual evoked potentials and contrast sensitivity correlate with ganglion cell-inner plexiform layer thickness in multiple sclerosis. *Clin Neurophysiol* **130,** 180-188.

Newkirk MR, Gardiner SK, Demirel S & Johnson CA. (2006). Assessment of false positives with the humphrey field analyzer ii perimeter with the sita algorithm. *Invest Ophth Vis Sci* **47,** 4632-4637.

Nissila J, Manttari S, Tuominen H, Sarkioja T, Takala T, Saarela S & Timonen M. (2012). The abundance and distribution of melanopsin (opn4) protein in human brain. *Eur Psychiat* **27**.

Noval S, Contreras I, Rebolleda G, Munoz-Negrete FJ & Ruiz de Zarate B. (2005). A comparison between humphrey and frequency doubling perimetry for chiasmal visual field defects. *Eur J Ophthalmol* **15,** 739-745.

Numata T, Maddess T, Matsumoto C, Okuyama S, Hashimoto S, Nomoto H & Shimomura Y. (2017). Exploring test-retest variability using high-resolution perimetry. *Transl Vis Sci Technol* **6,** 8.

Okamoto Y, Okamoto F, Hiraoka T, Yamada S & Oshika T. (2008). Vision-related quality of life in patients with pituitary adenoma. *Am J Ophthalmol* **146,** 318-322.

Otsuka-Hirota N, Yamamoto H, Miyashita K & Nagatsuka K. (2014). Invisibility of moving objects: A core symptom of motion blindness. *BMJ Case Rep* **2014**.

Overly C. (2009). Bitemporal hemianopia arising from a suprasellar craniopharyngioma. *Optometry* **80,** 621-629.

Pagani R, Bosco G, Dalla Valle E, Capitani E & Laiacona M. (2012). The assessment of colour perception, naming and knowledge: A new test device with a case study. *Neurol Sci* **33,** 801-809.

Pandit RJ, Gales K & Griffiths PG. (2001). Effectiveness of testing visual fields by confrontation. *Lancet* **358,** 1339-1340.

Parisi V, Miglior S, Manni G, Centofanti M & Bucci MG. (2006). Clinical ability of pattern electroretinograms and visual evoked potentials in detecting visual dysfunction in ocular hypertension and glaucoma. *Ophthalmology* **113,** 216-228.

Park HP, YG. Cho, AH. Park, CK. (2013). Transneuronal retrograde degeneration of the retinal ganglion cells in patients with cerebral infarction. *Ophthalmology* **120,** 1292-1299.

Pearce JG & Maddess T. (2016). Retest variability in the medmont m700 automated perimeter. *Optometry and vision science : official publication of the American Academy of Optometry* **93,** 272-280.

Pelak VS & Hoyt WF. (2005). Symptoms of akinetopsia associated with traumatic brain injury and alzheimer's disease. *Neuro-Ophthalmology* **29,** 137-142.

Percival KA, Martin PR & Grunert U. (2013). Organisation of koniocellular-projecting ganglion cells and diffuse bipolar cells in the primate fovea. *Eur J Neurosci* **37,** 1072-1089.

Pickard GE & Sollars PJ. (2012). Intrinsically photosensitive retinal ganglion cells. *Rev Physiol Bioch P* **162,** 59-90.

Pintor J. (2009). Autonomic nervous system: Ophthalmic control. In *Encyclopedia of neuroscience*, ed. Squire LR. Academic Press.

Pollock A, Hazelton C & Brady M. (2011a). Visual problems after stroke: A survey of current practice by occupational therapists working in uk stroke inpatient settings. *Top Stroke Rehabil* **18,** 643-651.

Pollock A, Hazelton C, Henderson CA, Angilley J, Dhillon B, Langhorne P, Livingstone K, Munro FA, Orr H, Rowe FJ & Shahani U. (2011b). Interventions for visual field defects in patients with stroke. *Cochrane Database Syst Rev***,** CD008388.

Poon A, McNeill P, Harper A & O'Day J. (1995). Patterns of visual loss associated with pituitary macroadenomas. *Aust N Z J Ophthalmol* **23,** 107-115.

Prasad S & Cohen AB. (2011). Diagnostic accuracy of confrontation visual field tests. *Neurology* **76,** 1192-1193.

Provis JM, Dubis AM, Maddess T & Carroll J. (2013). Adaptation of the central retina for high acuity vision: Cones, the fovea and the avascular zone. *Prog Retin Eye Res* **35,** 63-81.

Pula JH & Yuen CA. (2017). Eyes and stroke: The visual aspects of cerebrovascular disease. *Stroke Vasc Neurol* **2,** 210-220.

Punjabi OS, Tanna AP & Rosenberg MA. (2011). Optic disk excavation in nonarteritic anterior ischemic optic neuropathy. *J Glaucoma* **20,** 71-73.

Purves D, Augustine GJ, D. F, Katz LC, LaMantia AS, McNamara JO & Williams SM. (2001). *Neuroscience*. Sinaurer Associates, Sunderland (MA).

Qureshi AI, Tuhrim S, Broderick JP, Batjer HH, Hondo H & Hanley DF. (2001). Spontaneous intracerebral hemorrhage. *N Engl J Med* **344,** 1450-1460.

Rai BB, Sabeti F, Carle CF, Rohan EMF, Sarac O, van Kleef J & Maddess T. (2019). Recovery dynamics of multifocal pupillographic objective perimetry from tropicamide dilation. *Graefe's archive for clinical and experimental ophthalmology = Albrecht von Graefes Archiv fur klinische und experimentelle Ophthalmologie*.

Reader AL & Harper DG. (1976). Confrontation visual-field testing. *Jama-J Am Med Assoc* **236,** 250-250.

Riggs RV, Andrews K, Roberts P & Gilewski M. (2007). Visual deficit interventions in adult stroke and brain injury - a systematic review. *Am J Phys Med Rehab* **86,** 853-860.

Ringman JM, Saver JL, Woolson RF, Clarke WR & Adams HP. (2004). Frequency, risk factors, anatomy, and course of unilateral neglect in an acute stroke cohort. *Neurology* **63,** 468-474.

Rizzo M, Nawrot M & Zihl J. (1995). Motion and shape perception in cerebral akinetopsia. *Brain* **118,** 1105-1127.

Rodarte C, Hood DC, Yang EB, Grippo T, Greenstein VC, Liebmann JM & Ritch R. (2006). The effects of glaucoma on the latency of the multifocal visual evoked potential. *The British journal of ophthalmology* **90,** 1132-1136.

Roe AW & Ts'o DY. (2015). Specificity of v1-v2 orientation networks in the primate visual cortex. *Cortex* **72,** 168-178.

Roelfsema F, Biermasz NR & Pereira AM. (2012). Clinical factors involved in the recurrence of pituitary adenomas after surgical remission: A structured review and meta-analysis. *Pituitary* **15,** 71-83.

Rosli Y, Bedford SM, James AC & Maddess T. (2012). Photopic and scotopic multifocal pupillographic responses in age-related macular degeneration. *Vision Res* **69,** 42-48.

Rosli Y, Carle CF, Ho Y, James AC, Kolic M, Rohan EMF & Maddess T. (2018). Retinotopic effects of visual attention revealed by dichoptic multifocal pupillography. *Sci Rep* **8,** 2991.

Ross JE. (1983). Disturbance of stereoscopic vision in patients with unilateral stroke. *Behav Brain Res* **7,** 99-112.

Rowe F. (2009). Letters to the editor: Visual impairment following stroke do stroke patients require visual assessment? *Age Ageing* **35,** 560-565.

Rowe F. (2016). Visual effects and rehabilitation after stroke. *Community Eye Health* **29,** 75-76.

Rowe F, Brand D, Jackson CA, Price A, Walker L, Harrison S, Eccleston C, Scott C, Akerman N, Dodridge C, Howard C, Shipman T, Sperring U, MacDiarmid S & Freeman C. (2009). Visual impairment following stroke: Do stroke patients require vision assessment? *Age Ageing* **38,** 188-193.

Rowe FJ & Grp V. (2011). Accuracy of referrals for visual assessment in a stroke population. *Eye* **25,** 161-167.

Rowe FJ, Wright D, Brand D, Jackson C, Harrison S, Maan T, Scott C, Vogwell L, Peel S, Akerman N, Dodridge C, Howard C, Shipman T, Sperring U, Macdiarmid S & Freeman C. (2013). A prospective profile of visual field loss following stroke: Prevalence, type, rehabilitation, and outcome. *BioMed research international* **2013,** 719096.

Rudnicka AR & Edgar DF. (1995). Automated static perimetry in myopes with peripapillary crescents--part i. *Ophthalmic Physiol Opt* **15,** 409-412.

Rudnicka AR & Edgar DF. (1996). Automated static perimetry in myopes with peripapillary crescents--part ii. *Ophthalmic Physiol Opt* **16,** 416-429.

Ruseckaite R, Maddess T & James AC. (2004a). Comparing multifocal binocular pattern pulse visual evoked potentials in normal and multiple sclerosis patients. *Perception* **33,** 129-129.

Ruseckaite R, Maddess T & James AC. (2004b). Comparing multifocal frequency-doubling illusion, visual evoked potentials, and automated perimetry in normal and optic neuritis patients. *Perception* **33,** 128-128.

Ruseckaite R, Maddess T & James AC. (2005). New methods to detect multiple sclerosis. *Unveiling the Mystery of the Brain: Neurophysiological Investigation of the Brain Function* **1278,** 49-52.

Ruseckaite R, Maddess T & James AC. (2006). Monocular and binocular multifocal visual evoked potentials in normal and multiple sclerosis subjects. *Mult Scler* **12,** S166-S166.

Sabeti F, Maddess T, Essex RW & James AC. (2011). Multifocal pupillographic assessment of age-related macular degeneration. *Optometry Vision Sci* **88,** 1477-1485.

Sabeti F, Maddess T, Essex RW, Saikal A, James AC & Carle CF. (2014). Multifocal pupillography in early age-related macular degeneration. *Optometry and vision science : official publication of the American Academy of Optometry* **91,** 904-915.

Sabeti F, Nolan CJ, James AC, Jenkins A & Maddess T. (2015). Multifocal pupillography identifies changes in visual sensitivity according to severity of diabetic retinopathy in type 2 diabetes. *Invest Ophthalmol Vis Sci* **56,** 4504-4513.

Sand A, Schmidt TM & Kofuji P. (2012). Diverse types of ganglion cell photoreceptors in the mammalian retina. *Prog Retin Eye Res* **31,** 287-302.

Sand KM, Midelfart A, Thomassen L, Melms A, Wilhelm H & Hoff JM. (2013). Visual impairment in stroke patients - a review. *Acta Neurol Scand* **127,** 52-56.

Schaadt AK, Schmidt L, Reinhart S, Adams M, Garbacenkaite R, Leonhardt E, Kuhn C & Kerkhoff G. (2014). Perceptual relearning of binocular fusion and stereoacuity after brain injury. *Neurorehabil Neural Repair* **28,** 462-471.

Schein SJ. (1988). Anatomy of macaque fovea and spatial densities of neurons in foveal representation. *J Comp Neurol* **269,** 479-505.

Schellinger PD, Bryan RN, Caplan LR, Detre JA, Edelman RR, Jaigobin C, Kidwell CS, Mohr JP, Sloan M, Sorensen AG, Warach S, Therapeutics & Technology Assessment Subcommittee of the American Academy of N. (2010). Evidence-based guideline: The role of diffusion and perfusion mri for the diagnosis of acute ischemic stroke: Report of the therapeutics and technology assessment subcommittee of the american academy of neurology. *Neurology* **75,** 177-185.

Schiefer U, Pascual JP, Edmunds B, Feudner E, Hoffmann EM, Johnson CA, Lagreze WA, Pfeiffer N, Sample PA, Staubach F, Weleber RG, Vonthein R, Krapp E & Paetzold J. (2009). Comparison of the new perimetric gate strategy with conventional full-threshold and sita standard strategies. *Invest Ophthalmol Vis Sci* **50,** 488-494.

Schmid R, Wilhelm B & Wilhelm H. (2000). Naso-temporal asymmetry and contraction anisocoria in the pupillomotor system. *Graef Arch Clin Exp* **238,** 123-128.

Schneider KA, Richter MC & Kastner S. (2004). Retinotopic organization and functional subdivisions of the human lateral geniculate nucleus: A high-resolution functional magnetic resonance imaging study. *J Neurosci* **24,** 8975-8985.

Semmlow J, Hansmann D & Stark L. (1975). Variation in pupillomotor responsiveness with mean pupil size. *Vision Res* **15,** 85-90.

Semmlow J & Stark L. (1973). Pupil movements to light and accommodative stimulation: A comparative study. *Vision Res* **13,** 1087-1100.

Senior C, Barnes J, Giampietro V, Simmons A, Bullmore ET, Brammer M & David AS. (2000). The functional neuroanatomy of implicit-motion perception or representational momentum. *Curr Biol* **10,** 16-22.

Sereno MI, Dale AM, Reppas JB, Kwong KK, Belliveau JW, Brady TJ, Rosen BR & Tootell RB. (1995). Borders of multiple visual areas in humans revealed by functional magnetic resonance imaging. *Science* **268,** 889-893.

Setala K & Vesti E. (1994). Acquired cerebral achromatopsia - a case-report. *Neuro-Ophthalmology* **14,** 31-36.

Shahinfar S, Johnson LN & Madsen RW. (1995). Confrontation visual-field loss as a function of decibel sensitivity loss on automated static perimetry - implications on the accuracy of confrontation visual-field (cvf) testing. *Invest Ophth Vis Sci* **36,** S454-S454.

Shean CJW, James AC, Kolic M, Maddess T & Carle CF. (2012). Signal and noise of multifocal pupillographic stimulus response functions. *Clin Exp Ophthalmol* **40,** 122-122.

Shevell SK & Martin PR. (2017). Color opponency: Tutorial. *Journal of the Optical Society of America A, Optics, image science, and vision* **34,** 1099-1108.

Shipp S, de Jong BM, Zihl J, Frackowiak RS & Zeki S. (1994). The brain activity related to residual motion vision in a patient with bilateral lesions of v5. *Brain* **117 (Pt 5),** 1023-1038.

Shipp S, Watson JD, Frackowiak RS & Zeki S. (1995). Retinotopic maps in human prestriate visual cortex: The demarcation of areas v2 and v3. *Neuroimage* **2,** 125-132.

Shrestha GS, Upadhyaya S, Sharma AK & Gajurel BP. (2012). Ocular-visual defect and visual neglect in stroke patients - a report from kathmandu, nepal. *Journal of Optometry* **5,** 43-49.

Sincich LC, Park KF, Wohlgemuth MJ & Horton JC. (2004). Bypassing v1: A direct geniculate input to area mt. *Nat Neurosci* **7,** 1123-1128.

Smith SA & Smith SE. (1980). Contraction anisocoria: Nasal versus temporal illumination. *The British journal of ophthalmology* **64,** 933-934.

Smits AR, Seijdel N, Scholte HS, Heywood CA, Kentridge RW & de Haan EHF. (2019). Action blindsight and antipointing in a hemianopic patient. *Neuropsychologia* **128,** 270-275.

Spenceley SE & Henson DB. (1996). Visual field test simulation and error in threshold estimation. *The British journal of ophthalmology* **80,** 304-308.

Spolidoro M, Sale A, Berardi N & Maffei L. (2009). Plasticity in the adult brain: Lessons from the visual system. *Exp Brain Res* **192,** 335-341.

Sughrue ME, Yang I, Kane AJ, Fang S, Clark AJ, Aranda D, Barani IJ & Parsa AT. (2011). Endocrinologic, neurologic, and visual morbidity after treatment for craniopharyngioma. *J Neuro-Oncol* **101,** 463-476.

Sutter EE & Tran D. (1992). The field topography of erg components in man--i. The photopic luminance response. *Vision Res* **32,** 433-446.

Szmajda BA, Grunert U & Martin PR. (2008). Retinal ganglion cell inputs to the koniocellular pathway. *J Comp Neurol* **510,** 251-268.

Takayama Y & Sugishita M. (1994). Astereopsis induced by repetitive magnetic stimulation of occipital cortex. *J Neurol* **241,** 522-525.

Taravati P, Woodward KR, Keltner JL, Johnson CA, Redline D, Carolan J, Huang CQ & Wall M. (2008). Sensitivity and specificity of the humphrey matrix to detect homonymous hemianopias. *Invest Ophth Vis Sci* **49,** 924-928.

Tigges J & O'Steen WK. (1974). Termination of retinofugal fibers in squirrel monkey: A re-investigation using autoradiographic methods. *Brain Res* **79,** 489-495.

Ting DSJ, Pollock A, Dutton GN, Doubal FN, Ting DSW, Thompson M & Dhillon B. (2011). Visual neglect following stroke: Current concepts and future focus. *Surv Ophthalmol* **56,** 114-134.

Tootell RB, Dale AM, Sereno MI & Malach R. (1996). New images from human visual cortex. *Trends Neurosci* **19,** 481-489.

Tootell RB, Mendola JD, Hadjikhani NK, Ledden PJ, Liu AK, Reppas JB, Sereno MI & Dale AM. (1997). Functional analysis of v3a and related areas in human visual cortex. *J Neurosci* **17,** 7060-7078.

Trobe JD, Acosta PC, Krischer JP & Trick GL. (1981). Confrontation visual-field techniques in the detection of anterior visual pathway lesions. *Ann Neurol* **10,** 28-34.

Trope GE & Britton R. (1987). A comparison of goldmann and humphrey automated perimetry in patients with glaucoma. *The British journal of ophthalmology* **71,** 489-493.

Tsujimura S & Tokuda Y. (2011). Delayed response of human melanopsin retinal ganglion cells on the pupillary light reflex. *Ophthal Physl Opt* **31,** 469-479.

Tyrrell RA & Owens DA. (1988). A rapid technique to assess the resting states of the eyes and other threshold phenomena: The modified binary search (mobs). *Behavior Research Methods, Instruments, & Computers* **20,** 137-141.

Vaina LM. (1995). Akinetopsia, achromatopsia and blindsight: Recent studies on perception without awareness. *Synthese* **105,** 253-271.

Vaina LM, Cowey A, Eskew RT, LeMay M & Kemper T. (2001). Regional cerebral correlates of global motion perception - evidence from unilateral cerebral brain damage. *Brain* **124,** 310-321.

Vaina LM, Sikoglu EM, Soloviev S, LeMay M, Squatrito S, Pandiani G & Cowey A. (2010). Functional and anatomical profile of visual motion impairments in stroke patients correlate with fmri in normal subjects. *J Neuropsychol* **4,** 121-145.

Vakalopoulos C. (2005). A theory of blindsight - the anatomy of the unconscious: A proposal for the koniocellular projections and intralaminar thalamus. *Med Hypotheses* **65,** 1183-1190.

Vanni S, Hokkanen H, Werner F & Angelucci A. (2020). Anatomy and physiology of macaque visual cortical areas v1, v2, and v5/mt: Bases for biologically realistic models. *Cereb Cortex*.

von Arx SW, Muri RM, Heinemann D, Hess CW & Nyffeler T. (2010). Anosognosia for cerebral achromatopsia-a longitudinal case study. *Neuropsychologia* **48,** 970-977.

Wade AR, Brewer AA, Rieger JW & Wandell BA. (2002). Functional measurements of human ventral occipital cortex: Retinotopy and colour. *Philos Trans R Soc Lond B Biol Sci* **357,** 963-973.

Wagner AL, Murtagh FR, Hazlett KS & Arrington JA. (1997). Measurement of the normal optic chiasm on coronal mr images. *AJNR Am J Neuroradiol* **18,** 723-726.

Wall M, Doyle CK, Zamba KD, Artes P & Johnson CA. (2013). The repeatability of mean defect with size iii and size v standard automated perimetry. *Invest Ophthalmol Vis Sci* **54,** 1345-1351.

Wall M, Neahring RK & Woodward KR. (2002). Sensitivity and specificity of frequency doubling perimetry in neuro-ophthalmic disorders: A comparison with conventional automated perimetry. *Invest Ophth Vis Sci* **43,** 1277-1283.

Wall M, Punke SG, Stickney TL, Brito CF, Withrow KR & Kardon RH. (2001). Sita standard in optic neuropathies and hemianopias: A comparison with full threshold testing. *Invest Ophthalmol Vis Sci* **42,** 528-537.

Walsh TJ. (1990). *Visual fields: Examination and interpretation*. Oxford University Press, Oxford, United Kingdom.

Wandell BA & Engel SA. (1995). Fmri measurements of the neural image in area-v1. *Invest Ophth Vis Sci* **36,** S612-S612.

Wang HB, Sun W, Fu Z, Si ZC, Zhu YF, Zhai GD, Zhao GY, Xu SC & Pang Q. (2008). The pattern of visual impairment in patients with pituitary adenoma. *J Int Med Res* **36,** 1064-1069.

Wang L, Guo XL, Sun JF, Jin Z & Tong SB. (2012). Cortical networks of hemianopia stroke patients: A graph theoretical analysis of eeg signals at resting state. *Ieee Eng Med Bio***,** 49-52.

Wassle H, Grunert U, Rohrenbeck J & Boycott BB. (1989). Cortical magnification factor and the ganglion cell density of the primate retina. *Nature* **341,** 643-646.

Watanabe K, Shinoda K, Kimura I, Mashima Y, Oguchi Y & Ohde H. (2007). Discordance between subjective perimetric visual fields and objective multifocal visual evoked potential-determined visual fields in patients with hemianopsia. *Am J Ophthalmol* **143,** 295-304.

Weber J & Dobek K. (1986). What is the most suitable grid for computer perimetry in glaucoma patients? *Ophthalmologica* **192,** 88-96.

White AJ, Sun H, Swanson WH & Lee BB. (2002). An examination of physiological mechanisms underlying the frequency-doubling illusion. *Invest Ophthalmol Vis Sci* **43,** 3590-3599.

Wild JM, Searle AE, Dengler-Harles M & O'Neill EC. (1991). Long-term follow-up of baseline learning and fatigue effects in the automated perimetry of glaucoma and ocular hypertensive patients. *Acta Ophthalmol (Copenh)* **69,** 210-216.

Wong AM & Sharpe JA. (2000). A comparison of tangent screen, goldmann, and humphrey perimetry in the detection and localization of occipital lesions. *Ophthalmology* **107,** 527-544.

Wyatt HJ & Musselman JF. (1981). Pupillary light reflex in humans: Evidence for an unbalanced pathway from nasal retina, and for signal cancellation in brainstem. *Vision Res* **21,** 513-525.

Yenice O & Temel A. (2005). Evaluation of two humphrey perimetry programs: Full threshold and sita standard testing strategy for learning effect. *Eur J Ophthalmol* **15,** 209-212.

Yoon MK, Hwang TN, Day S, Hong J, Porco T & McCulley TJ. (2012). Comparison of humphrey matrix frequency doubling technology to standard automated perimetry in neuro-ophthalmic disease. *Middle East Afr J Ophthalmol* **19,** 211-215.

You Y, Gupta VK, Graham SL & Klistorner A. (2012). Anterograde degeneration along the visual pathway after optic nerve injury. *Plos One* **7,** e52061.

Young RSL & Alpern M. (1980). Pupil responses to foveal exchange of monochromatic lights. *J Opt Soc Am* **70,** 697-706.

Zappia RJ, Enoch JM, Stamper R, Winkelman JZ & Gay AJ. (1971). The riddoch phenomenon revealed in non-occipital lobe lesions. *The British journal of ophthalmology* **55,** 416-420.

Zeki S. (1990). A century of cerebral-achromatopsia. *Brain* **113,** 1721-1777.

Zeki S. (1991). Cerebral akinetopsia (visual-motion blindness) - a review. *Brain* **114,** 811-824.

Zeki S. (1993). *A vision of the brain*. Blackwell Scientific Publications, Oxford.

Zeki S. (2003). Improbable areas in the visual brain. *Trends Neurosci* **26,** 23-26.

Zeki S, Watson JD, Lueck CJ, Friston KJ, Kennard C & Frackowiak RS. (1991). A direct demonstration of functional specialization in human visual cortex. *J Neurosci* **11,** 641-649.

Zhang XJ, Kedar S, Lynn MJ, Newman NJ & Biousse V. (2006). Homonymous hemianopia in stroke. *J Neuro-Ophthalmol* **26,** 180-183.

Zhou C, He Y & Li X. (2018). Cerebral achromatopsia secondary to ischemic stroke. *Neurol India* **66,** 573-575.

Zhou J, Liu Z, Clavagnier S, Reynaud A & Hou F. (2017). Visual plasticity in adults. *Neural Plasticity* **2017,** 8469580.

Zihl J & Heywood CA. (2015). The contribution of lm to the neuroscience of movement vision. *Front Integr Neurosci* **9,** 6.

Zihl J, von Cramon D & Mai N. (1983). Selective disturbance of movement vision after bilateral brain damage. *Brain* **106 (Pt 2),** 313-340.

Chapter 2: General Methods

This chapter outlines recruitment and screening of candidates, experimental procedures for devices, and their rationale for selection. It does not cover methods of analysis specific to any chapter, which are instead presented in that chapter. Note that these methods apply to all experimental data in this study except subject control data for automated perimetry devices (Humphrey Field Analyser and Matrix Field Analyser) used in chapter 5 receiver operator plots, which were instead collected by other researchers in the Maddess Lab for an earlier study, which involved a similar set of screening and testing regimens. In order to clarify which methods apply to which chapter, a table summary is provided here (Table 2.1) with details in

	Chapter 3	Chapter 4	Chapter 5	Chapter 6
Topic	Higher visual function testing	Direct and consensual responses	Visual field testing - comparison of devices	Comparing different mfPOP protocols and repeats
Recruitment	Hospitals, eye clinics.	Hospitals, eye clinics	Hospitals, eye clinics. *Control subjects for mfPOP from CT2g study.	Hospitals, eye clinics
	24 stroke and 26 controls	25 stroke, 11 pituitary compression, and 10 AION	25 stroke, 11 pituitary compression, 10 AION, 26 controls, and 29 control (CT2g for mfPOP)	24 stroke, 11 pituitary compression, and 10 AION
Screening	Questionaire, visual testing, ophthalmologist review			
Stereopsis	Stereofly, Randot	None		
Colour vision	Ishihara, Farnsworth-Munsell D15	None		
Global motion	Random dot stereogram	None		
Facial recognition	Cambridge facial memory test	None		
Visual Field testing	None	None	Humphrey Field Analyser II, Humphrey-Matrix field analyser	None
Multifocal pupillographic objective perimetry	None	Y/Y stimuli, direct and consensual amplitudes, no repeats	Y/Y stimuli, combined amplitude, repeats	Y/Y and G/R stimuli, amplitude, time to peak, direct, consensual & combined, repeats
MRI	None			

Table 2.1: Table summary of which testing methods were used in each experimental chapter. Left side in bold represent headings in the General Methods. Note Y/Y refers to yellow stimuli on yellow background, G/R to green stimuli on red background, and AION to anterior ischemic optic neuropathy.

the headings below. All methods were analysed using Matlab 2016b (The MathWorks, Inc., Natick, USA), Microsoft Excel 2016 and R (Core Team, 2013).

2.1. Recruitment

The primary group of interest are subjects with likely damage to visual pathways, the visual cortex, or surrounding regions. Stroke provides the main target group for these purposes, while anterior ischemic optic neuropathy (AION) and chiasmal compression patients were also recruited to demonstrate chiasmal and anterior damage to the visual pathways and validate and compare pupillometry in these previously untested groups. Subjects were selected who either demonstrated field loss, had pre-treatment field loss and had not been tested post-treatment, or had never been tested. It should be noted that for the purposes of these experiments, 'stroke' was defined as cortical damage, and no patients with demonstrated cerebellar damage or damage anterior to the optic chiasm were included. As discussed in the Introduction 1.4.1, the existence of isolated complete functional deficits suggests functional specialisation of visual processing, although these deficits are rare (Vaina, 1995), and selective stimuli appear to activate multiple areas (McKeefry *et al.*, 1997; Furlan & Smith, 2016), lending itself to distributive processing. In balancing these views, it would seem that some cortical areas are necessary for perception, while other may play a role in processing, but are not essential. Stroke subjects were included, non-selective as to the location of damage, towards looking for more subtle defects, which may occur more frequently and be contributed to by unknown areas. In total, after exclusion criteria, 25 stroke, 11 chiasmal compression, 10 AION, and 26 controls were recruited.

Testing occurred over 3 test sessions, each day being no more than 2 weeks after the last appointment. All subjects attended the first session, which comprised of consent, medical history, screening for pre-existing conditions, and higher visual function testing. Only subjects

within the stroke, chiasmal compression and AION groups continued to sessions 2 and 3, which comprised of testing visual fields. In session 2, Humphrey and two mfPOP version were tested, while in session 3, Matrix and repeats of the mfPOP versions were tested (details in 2.5. Perimetry). One subject in the stroke group, and two subjects in the chiasmal compression group, did not complete session 3 and so have no Matrix reports. Data for these subjects was used where possible, but in producing averages and for direct comparisons, absent results were omitted from the calculation. A demographic breakdown of all included subjects is provided here for reference (Table 2.2).

Table of demographic breakdown of subjects

AION			
Count	ID	Age	Sex
1	mf88101	73	F
2	mf88102	61	M
3	mf88105	39	M
4	mf88106	56	M
5	mf88109	59	F
6	mf88110	50	M
7	mf88112	58	M
8	mf88184	43	M
9	mf88191	43	M
10	mf88193	50	M
Mean	-	**53.2**	2F, 8M

Pituitary Compression			
Count	ID	Age	Sex
1	mf88103	48	M
2	mf88104	72	M
3	mf88115	45	M
4	mf88120	45	F
5	mf88121	41	F
6	mf88122	48	M
7	mf88123	54	M
8	mf88134	43	F
9	mf88161	59	M
10	mf88190	74	M
11	mf88195	57	M
Mean	-	**53.3**	3F, 8M

Stroke			
Count	ID	Age	Sex
1	**mf88108**	62	F
2	**mf88118**	41	F
3	**mf88119**	61	F
4	**mf88125**	69	M
5	**mf88126**	61	F
6	**mf88128**	61	M
7	**mf88130**	72	M
8	**mf88131**	87	M
9	**mf88135**	70	M
10	**mf88136**	93	F
11	**mf88137**	74	M
12	**mf88138**	60	F
13	**mf88139**	87	F
14	**mf88140**	52	M
15	**mf88141**	62	M
16	**mf88142**	71	F
17	**mf88143**	65	M
18	**mf88144**	64	M
19	**mf88146**	75	M
20	**mf88147**	72	F
21	**mf88148**	84	M
22	**mf88151**	84	M
23	**mf88174**	73	F
24	**mf88182**	75	F
25	**mf88150**	61	M
Mean	-	**69.4**	11F, 14M

Table 2.2: Demographics for the 3 groups: AION, chiasmal compression, and stroke. Sex and age are recorded with averages at the bottom. There were 10 AION, 11 pituitary, and 25 stroke subjects. Subject mf88150 was not included in Chapter 3 due to pre-existing colour-defect. Subjects mf88126 (stroke), mf88115 (pituitary), and mf88161 (pituitary) completed day 2 but not day 3 of testing, missing MFA and repeat mfPOP.

2.1.1. Sources of potential subjects

There were five sources of recruitment for those affected by AION, chiasmal compression, or stroke: Canberra Hospital Eye Clinic, Canberra Hospital Neurology Department, Canberra Hospital systematic search of medical record classifications, Canberra Eye Hospital, and Calvary Hospital. The list of potential controls was primarily obtained through a previous lab

study completed two years previously that had already assessed these subjects' vision as being normal at the time and had consented to be contacted for future studies.

2.1.1.1. Canberra Hospital Eye Clinic

A list of potential subjects was obtained from a search of optometrist referral letters to ophthalmologist Dr Kate Reid at The Canberra Hospital Eye Clinic spanning the previous 2 years. Searches used the following keywords: AION, pituitary, stroke, optic neuropathy, and visual field loss. Letters were then assessed and a point score system used to shortlist potential candidates taking into consideration: whether a diagnosis was only suspected or confirmed, whether visual fields had been completed, whether they had sufficient visual acuity for inclusion, and whether they had other diseases that might affect vision. Each case was considered for inclusion given the information provided, excluding those who had visual field testing with normal fields, poor visual acuity, and those with other ocular pathology. This was the source of recruitment for all three disease types. Addresses and phone numbers for these patients were obtained through the ACT Health Medical Records Department.

2.1.1.2. Canberra Hospital Neurology Department

A presentation was given to the neurology staff, outlining the basic inclusion criteria for recruitment which encompassed known or suspected occipital stroke, but with adequate level of cognition and motor skills to complete testing requirements. Suitable subjects were then referred by clinicians including neuro-ophthalmologists, neurologists, and neurosurgeons. This was primarily the source for stroke and pituitary tumour patients. Address and phone numbers for these patients were obtained through the Medical Records Department.

2.1.1.3. Canberra Hospital systematic search of medical records

Regular searches spanning Jan 2011 – July 2014 were completed according to the medical records classification codes. This systematic search included all three patient groups with codes

I60/1/2/3/4 (stroke: ischemic and haemorrhagic), D35.2/3 (pituitary: adenoma and craniopharyngioma), and H47 (AION: other disorders of optic nerve). All shortlisted patients then had their medical records screened for suitability and the refined shortlist of addresses and phone numbers were then obtained from Medical Records.

2.1.1.4. Canberra Eye Hospital

Canberra Eye Hospital is a private specialist treatment centre providing outpatient care for a wide community. In another larger study previously completed by our lab group, participants had been recruited through the Canberra Eye Hospital records. By sorting through the notes from the previous study, a series of potential recruits were shortlisted. Approval to contact was given by their treating physician. They were then screened for applicability through the Canberra Hospital medical records system where such a record existed. Addresses and phone numbers were obtained from both the Canberra Eye Hospital and Canberra Hospital records and the most recent contact details used.

2.1.1.5. Calvary Hospital

During the testing period, a new stroke ward was formed at Calvary hospital in the ACT. To maximise recruitment, the project and its selection criteria were discussed with Dr Shaun Zhai, a registrar working on the Calvary stroke ward. Referrals were sent from the three-month post-stroke follow up clinics, exclusively referring stroke patients. Addresses and phone number were obtained from the physician via Calvary Hospital medical records.

2.1.1.6. Recruitment of controls

Controls were primarily recruited from a previous study list where subjects had been confirmed to have normal vision two years prior and were therefore likely to have maintained normal vision. This study included in its consent form the willingness to be contacted for future studies. 40 potential control subjects were extracted from the original study and their contact details

transferred. There was a good response rate for those that were still contactable, in total 29/40 subjects being recruited.

2.1.2. Selection criteria

In order to assess how the location and character of the neural pathway damage might impact visual fields as measured by the mfPOP device, three locations of damage to the visual pathway were chosen: AION at the optic disc, pituitary tumour at the optic chiasm, and stroke with post-chiasmal damage. AION was selected over other optic disc pathology due to having a more well-defined lesion (as opposed to say glaucoma, which presents with highly variable patchy and less dense damage). Chiasmal compression was selected as a relatively common and well-defined anatomical field loss prior to the pupillary response branch point (subcortical).

All pituitary tumours were diagnosed based on previous MRI or CT scans, stroke subjects by clinical diagnosis in medical records, and AION was diagnosed by clinical judgement of the treating physician (who, after investigation, suggested that it was the most likely explanation for the cause of field loss). 21/27 stroke patients undertook an MRI as part of the study to more explicitly locate lesion(s).

2.1.3. Exclusion criteria

The exclusion criteria for this study were primarily based on either an inability to perform testing adequately or confounding effects from other visual disorders. While visual field testing is relatively insensitive to changes in visual acuity, it is still shown to have a negative relationship with visual field performance (Hawkins *et al.*, 2003) and the suggestion has been made that those with glaucoma with logMAR visual acuity >0.5 (6/19) should be interpreted with caution (Matsuura *et al.*, 2015). Based on these we set the minimum required acuity as acuity ≤6/24, beyond which it would substantially impact on the ability to complete tasks as well as falsely decreasing the visual field sensitivity in unaffected regions. A single stroke

patient was included for visual field analysis, but not higher visual function (HVF) testing, due to a pre-existing red–green colour defect.

Any subject with a pre-existing eye condition that may affect the visual field, such as glaucoma, significant cataracts, age-related macular degeneration, or retinitis, was excluded from the study. As not all the subjects were able to undergo a comprehensive medical records screen prior to testing, this meant some participants were excluded post-testing. Likewise, if any of the participants had eye conditions that would exclude them from a particular component of the HVF testing, such as having only one eye (lack of depth perception), or pre-existing red–green defect (poor colour perception), then their data for that particular test was omitted; however, they were permitted to complete other aspects of the research that would not be dramatically impacted (such as motion and facial recognition). No participants with a single functional eye were included for visual field analysis. Subjects were additionally excluded if they had any underlying neural disorder that may affect conduction speed and pupillary response to light. Given that pupillary responses in Alzheimer's disease (Chougule *et al.*, 2019) and Parkinson's (Micieli *et al.*, 1991) show decreased constriction amplitude and increase latency, patients with concurrent dementia were excluded and were specifically asked if they had any of the following: Parkinson's, Alzheimer's, Huntington's, or any form of dementia. Similarly, due to potential for confounding effects, those with concurrent multiple sclerosis or amyotrophic lateral sclerosis were also excluded as a precaution. For safety reasons current epilepsy was an exclusion, since flashing lights are used, although there is some evidence suggesting mfPOP does not appear to be a trigger for episodes (Ali *et al.*, 2015). Those who were pregnant were also excluded, as this has been shown to result in increased photopic pupil diameter (Altay *et al.*, 2016), and may involve unknown changes to the pupillary response. No subjects were included who concurrently had multiple test conditions (stroke, pituitary tumour, and AION). Those unable, due to field loss, to fixate on the central fixation light when

completing a visual field test were considered to have a single functional eye and their fields were omitted.

2.1.4. Contact

After obtaining preliminary lists of potential subjects from the sources listed above, they were systematically contacted. First contact involved mailing out copies of the information and consent forms, along with a cover letter from their clinician when appropriate. Two weeks later, subjects were called and asked if they were interested in being involved in the study. Candidates who declined were not contacted further, and no privacy complaints have been raised. Those indicating interest were booked in for testing. All were volunteers and no incentive (monetary or other) was used to encourage participation in this study.

2.1.5. Consent

Study approved by ACT Health Human Research Ethics Committee (ETH.5.13.100) and ANU Human Research Ethics Committee (2013/343). Study abides by the principles outlined in the Declaration of Helsinki.

Information and consent forms were included in the approved information pack for subjects to read and sign prior to attending their first appointment and a contact phone number was provided to allow clarification of any points. All consent forms included signature of the investigator, participant, and a witness. Consent detailed that they should not have been involved in any clinical trial or other interventional research within the last 3 months and included consent to view medical records which pertained to this project, allowing review of their medical history.

2.2. Medical History

A questionnaire was completed at the beginning of the first test session to ascertain any ocular conditions or background conditions that may confound the measures made in this research. In

addition to the patient's reported history, a comprehensive summary of their previous medical records held by Canberra Hospital was also made (but omitted from this dissertation so as to maintain confidentiality – see 2.2.2 Hospital).

2.2.1. Questionnaire

A basic medical history for the patients was taken, including both a general history of ocular disorders and a list of specific questions to exclude disorders. Specific questions included presence or absence of: diabetes, cancer, dementia, multiple sclerosis, epilepsy, pregnancy, glaucoma, cataracts, age-related macular degeneration, retinitis, colour vision defects, eye surgery, eye injections, and contacts. This was taken in addition to a structured general history comprising: any diagnosed eye conditions, previous ocular complaints or treatments, family history, full list of medications, and characteristics of the presenting disorder for this study including treatments and investigations sought for this disorder. For demographic and statistical purposes, age, gender, ethnicity, dominant eye, and handedness were also noted.

Any eye condition or ocular history which might cause visual impairment was flagged, and the list of medications was screened by a medical professional for any drugs which may impair normal vision or the pupil response, including interactions that may confound testing.

2.2.2. Hospital records

Permission to access state medical records from Australian Capital Territory Health (ACT health) was included as part of the consent form. Medical records were systematically assessed including all visits to ophthalmology, neurology, neurosurgery, or cardiology wards and any related visits to radiology, emergency department, endocrinology, rehabilitation, or occupational therapy. For each visit, the date and a summary of key information for that visit is provided, including any information received from referrals. All available visual field and optical coherence tomography (OCT) results were included in the summaries. This

supplementary information has sufficient personal information to be considered confidential, and so is not presented as part of this thesis.

2.3. Screening for pre-existing conditions

To ensure any discovered abnormalities in visual function were not caused by another underlying condition, such as retinal disease, all patients were initially screened. This was completed through the set of tests listed below, with their associated chapter section:

- logMAR acuity measured using an ETDRS chart (Kinyoun *et al.*, 1989) (2.3.1.2).
- Intraocular pressure (IOP) with Ocular Response Analyser (Reichert, USA) (2.3.3.2).
- Retroillumination with ARK-1 (Marco, USA) and/or slit lamp examination (2.3.2.1).
- Fundus photo, posterior pole (P.pole), optic nerve head (ONH), and retinal nerve fibre layer (RNFL) scan using Spectralis OCT (Heidelberg Engineering GmbH, Germany) (2.3.3.1).

All results were then assessed by Dr Kate Reid, a senior neuro-ophthalmologist at Canberra Hospital Eye Clinic, for any evidence of retinal disease that might affect the visual field. While the majority of excluded subjects were excluded prior to testing based on medical records and questionnaire, a total of 84 subjects were assessed by Dr Reid and a further 10 subjects were excluded. This gave the final figure of 25 stroke, 11 chiasmal compression, 10 AION, and 26 controls, noting that one stroke patient was only available for visual field testing but not HVF, due to having a pre-existing red-green colour defect and was excluded from Chapters 3 and 6.

2.3.1. Acuity

2.3.1.1. Refraction

Participants that regularly wear reading or distance glasses had their prescription measured with a vertometer and their visual acuity was tested both with and without glasses. The optical prescription was noted for correction of visual myopia, presbyopia, and astigmatism. For those

with acuity worse than 6/12 with glasses, pinhole acuity was also included. The best corrected visual acuity (BCVA) noted through these three assessments was used. A minimum threshold BCVA of 6/24 was used as an exclusion criterion.

2.3.1.2. ETDRS chart

While both Snellen chart and Early Treatment of Diabetic Retinopathy Study (ETDRS) chart report similar acuity in those with mild-to-moderately lowered acuity (Kaiser, 2008), ETDRS acuity at 4 m was chosen as it offers some advantages over the Snellen chart. ETDRS has the same number of optotype letters on each line with approximately the same reading difficulty, increasing its accuracy and reproducibility (Shamir *et al.*, 2016). For consistency, all measures were made by a single assessor, with 3/5 correct in a line considered sufficient to meet that level of acuity. Subjects had one eye covered and were asked to start on the lowest line that they can easily read and then progress down until they either failed the line or were unable to read the line. The right eye was always tested first, and when testing the left eye, they were asked to read the letters in reverse (right to left), to try and minimise their ability to recall letters when reading the same line.

2.3.2. Cataracts

Cataracts are very common, particularly in the elderly population, and can cause dimming of visual fields that are neither of retinal nor neural origin (Lam *et al.*, 1991). As visual fields are a primary focus, it was therefore very important that anyone with a substantial cataract be excluded from the study.

2.3.2.1. ARK-1 retroillumination and slit lamp

To check for cataracts, the ARK-1 autorefractor and keratometer was used as a screening device using its retroillumination test to detect opacities in the optical media of the eye. When the patient reported a history of cataracts or the ARK-1 screening appeared abnormal, a slit

lamp exam was completed by orthoptist Emilie Rohan who characterised and graded the cataract, gauging whether it would impact on central vision. Where there was a discrepancy between the ARK-1 and the slit lamp exam, the slit lamp estimate by the skilled operator was taken as the more definitive.

2.3.2.2. ARK-1 keratometry and central corneal curvature

ARK-1 was also used for keratometry and measurement of central corneal curvature (CCC). The device automatically measures the curvature of the eye using reflection of a flashed light annulus off the cornea. The resulting CCC was noted for input into the Spectralis OCT scan (see below) as a prerequisite for retinal scanning to calibrate the retinal thickness measurements.

2.3.3. Retinal disorders

In order to screen for common retinal disorders, an OCT scan was completed covering central vision and the optic nerve head. In addition, intraocular pressure was measured as a risk factor for glaucoma.

2.3.3.1. Spectralis OCT

The spectral domain optical coherence tomography (Spectralis) uses back-scattered light to generate a digital image of the layers of the retina based on their refractive index/density. The Spectralis takes 40,000 A-scans per second and by scanning in a matrix grid, and a three-dimensional tomographic image is produced. When producing RNFL thickness profiles, a circular scan around the ONH is completed. A series of inbuilt analysis techniques exist to highlight pathology based on the type of scan. Three types of scans were completed for each eye: the posterior pole (P-pole), optic nerve head (ONH), and retinal nerve fibre layer (RNFL), in addition to a digital fundus image using Spectralis widefield addon module.

The ONH scans (Figure 2.2) were centred on the optic disc, while P-pole scans (Figure 2.3) were centred on the fovea. Lines representing the basement membrane (BM) and internal limiting membrane (ILM) were automatically fitted, allowing calculation of thickness profiles for each cross-section and creation of an overall thickness map. The thickness profiles for each slice were visually inspected and manually corrected if required (see Figure 2.5). The resulting colour-coded thickness map, centred on the area of interest (ONH or P-pole), was overlaid on the fundus image and a single cross-section through this region was presented. In addition, a raw fundus image (without overlay) was printed separately to ascertain the cup-to-disc ratio and to more clearly identify any abnormality (see Figures 2.1-2.4 for examples of reports).

Subjects had the RNFL layer as it enters the ONH imaged 3–10 times, depending on quality, and the best image, as defined by central location and quality of resolution, was manually selected before viewing the thickness profile. The thickness profiles for both eyes were then plotted according to their position against normal data to suggest any regions of thinning (Figure 2.4).

These reports were then sent with the other supporting information to ophthalmologist Dr Kate Reid to assess if there were any suspected retinal abnormalities which may affect the visual field. Patients with pathology not in keeping with their neurological disease category, or with retinal pathology likely to affect testing, were excluded.

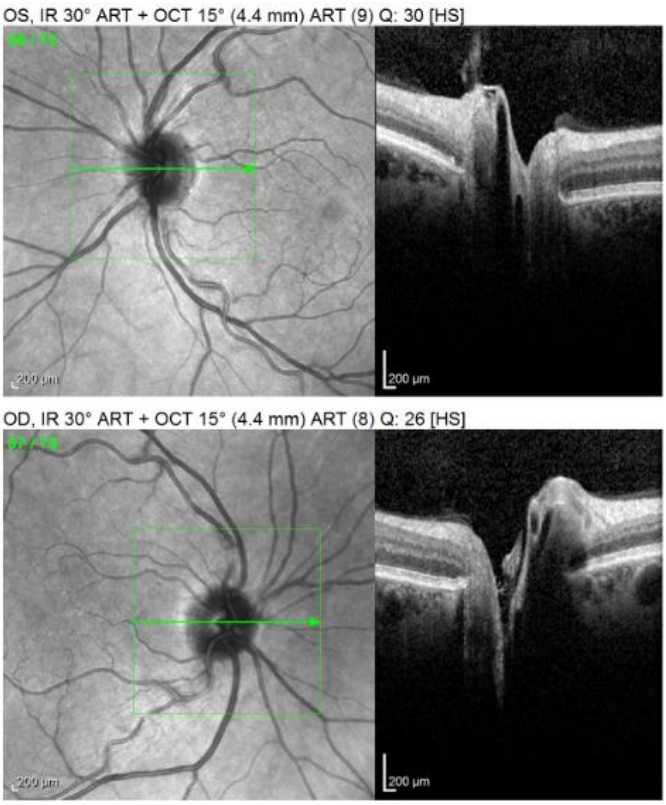

Figure 2.1: Example of optic nerve head (ONH) scans of the left (top) and right (bottom) eyes with the retinal surface highlighted (left) and layers leading to and inserting the ONH (right).

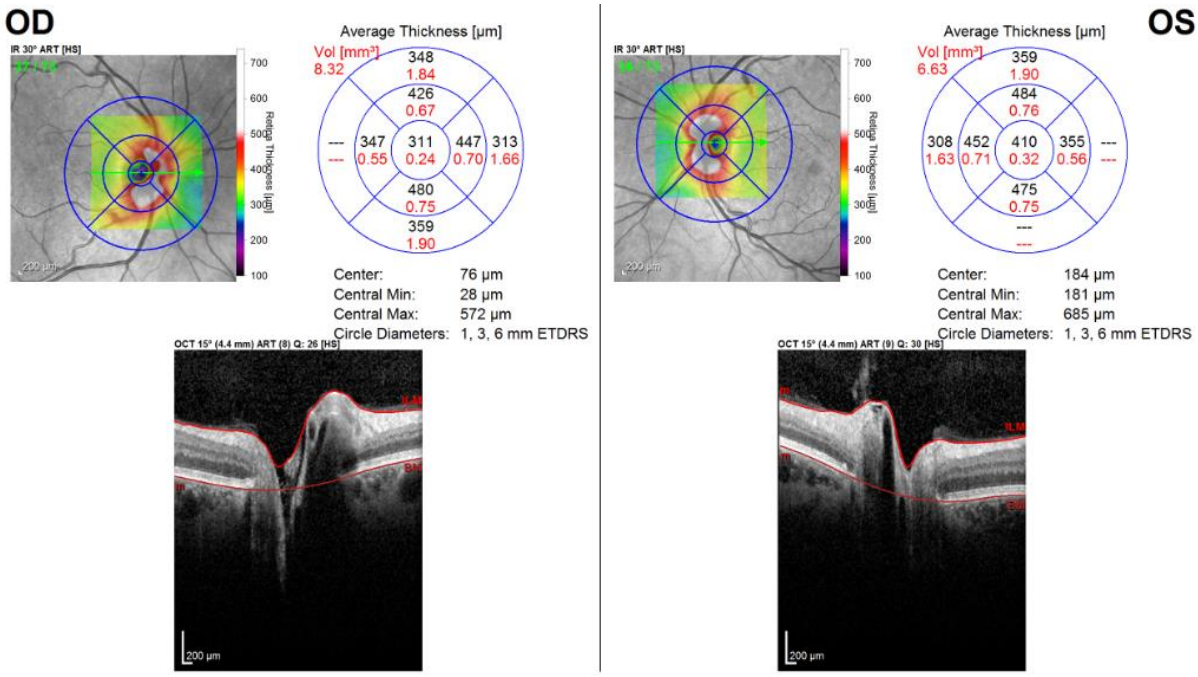

Figure 2.2: Output report from the ONH scan (OD = right eye, OS = left) with automatically fitted lines (bottom images) for the basement membrane (BM) and internal limiting membrane (ILM). These allow calculation of the thickness in all regions surrounding the ONH in terms of a colour map (top left images) and azimuthal averages for each region (top right images).

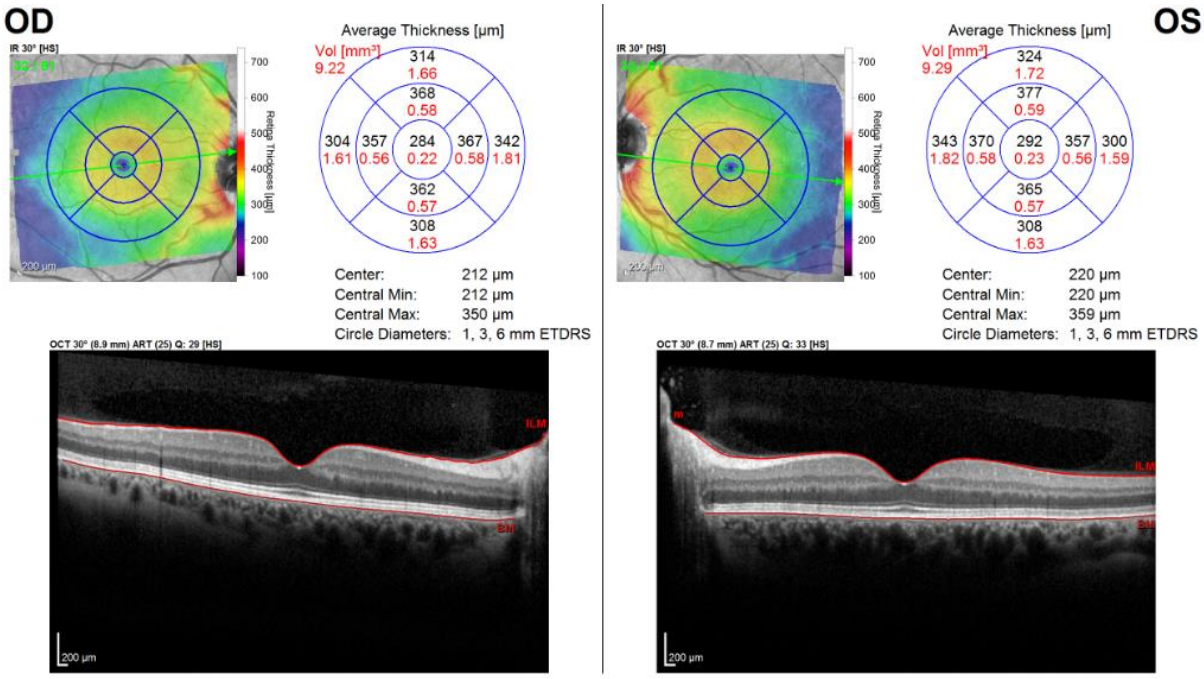

Figure 2.3: Output report from the posterior pole (P pole) scan (OD = right eye, OS = left), which is similar to Figure 2.2 but is instead centred on the fovea. It shows a cross-section through the central fovea (bottom images) with automatically fitted BM and ILM, which allow calculation of the thickness map (top left images), and average azimuth regions (top right images).

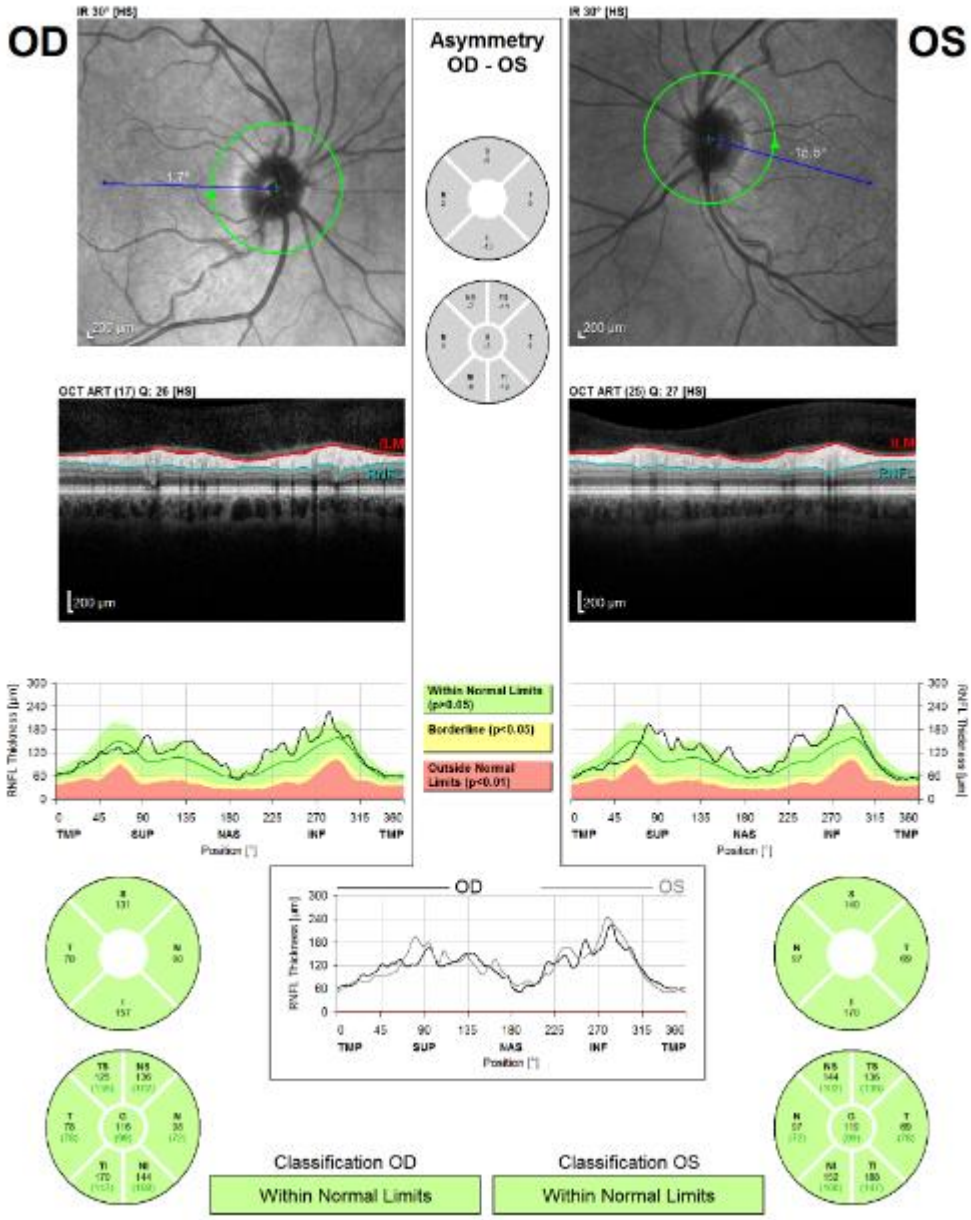

Figure 2.4: Retinal nerve fibre layer (RNFL) ciruclar scan showing the location of the scan (top image) circumferentially equidistant around the ONH, the layers of retina from that scan (middle upper image), plots of thickness on the background of a probability map for normal controls (middle lower image) where green is *within normal limits*, yellow is *borderline* ($p < 0.05$) and red is *outside normal limits* ($p < 0.01$). These plots are then averaged for each central and six peripheral segments and similarly tested for the probability of normal thickness (bottom images) along with superimposed plots matching regional input for comparison.

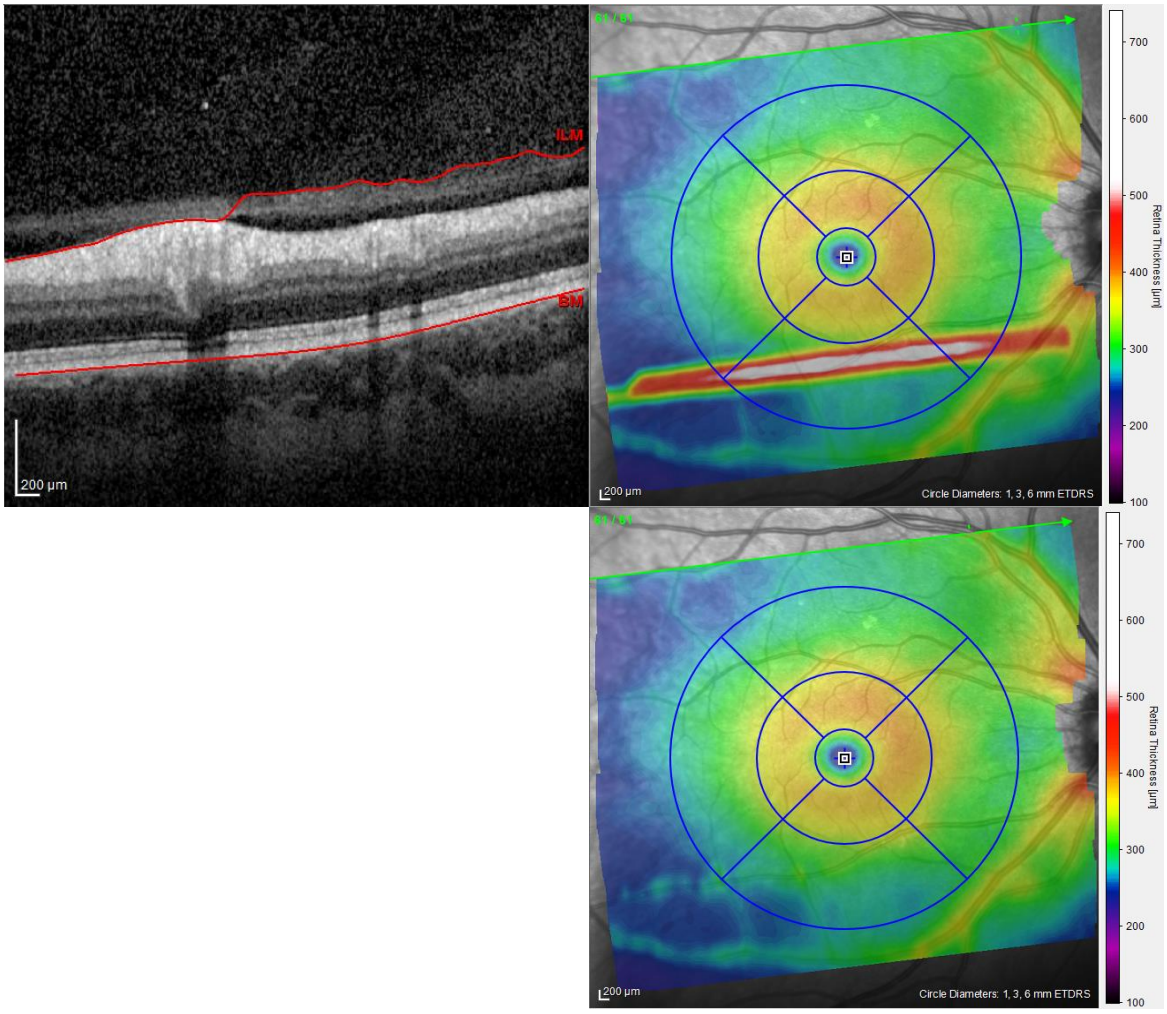

Figure 2.5: Example of a segment with incorrect auto-detection of ILM (top left) resulting in a spurious streak of apparent membrane thickening (top right). Where this occurred for ILM or BM, points were manually corrected to produce the resulting correct thicknesses (bottom right).

2.3.3.2. Ocular Response Analyser (ORA)

The ORA was used as a non-invasive measure of ocular pressure and corneal hysteresis. The principle behind the ORA relies on reflection of laser light off the curved cornea to a receiver (see Figure 2.6). A jet of air is projected onto the eye and as it overcomes the intraocular pressure it begins to flatten the cornea (applanation), causing more light reflection and a peak signal. The pressure causes the cornea to become transiently concave, temporarily lowering the signal. When the pulse of air dissipates, the pressure reduces, and the cornea bounces back

causing a second peak. Based on these measures one can calculate the intraocular pressure and effective elasticity of the cornea, inelasticity being measured by the rate of corneal hysteresis (Radcliffe, 2014). Through extensive evidence that corneal thickness alters the pressure as measured by tonometry (Whitacre *et al.*, 1993; Wolfs *et al.*, 1997; Stodtmeister, 1998; Shah *et al.*, 1999; Bhan *et al.*, 2002), one can calculate a corneal corrected pressure (IOPcc) and a non-corneal adjusted value that correlates with Goldmann tonometry (IOPg), as well as two measures of elasticity, corneal hysteresis (CH) and corneal resistance factor (CRF). During testing, subjects were asked to place their forehead on the forehead rest and look straight ahead. Four red lights in the shape of a diamond with a green dot in the centre are present when the subject is in the correct position. The process was explained to the subject and they were asked to open wide and refrain from squinting as the eye piece moves forward to generate the burst

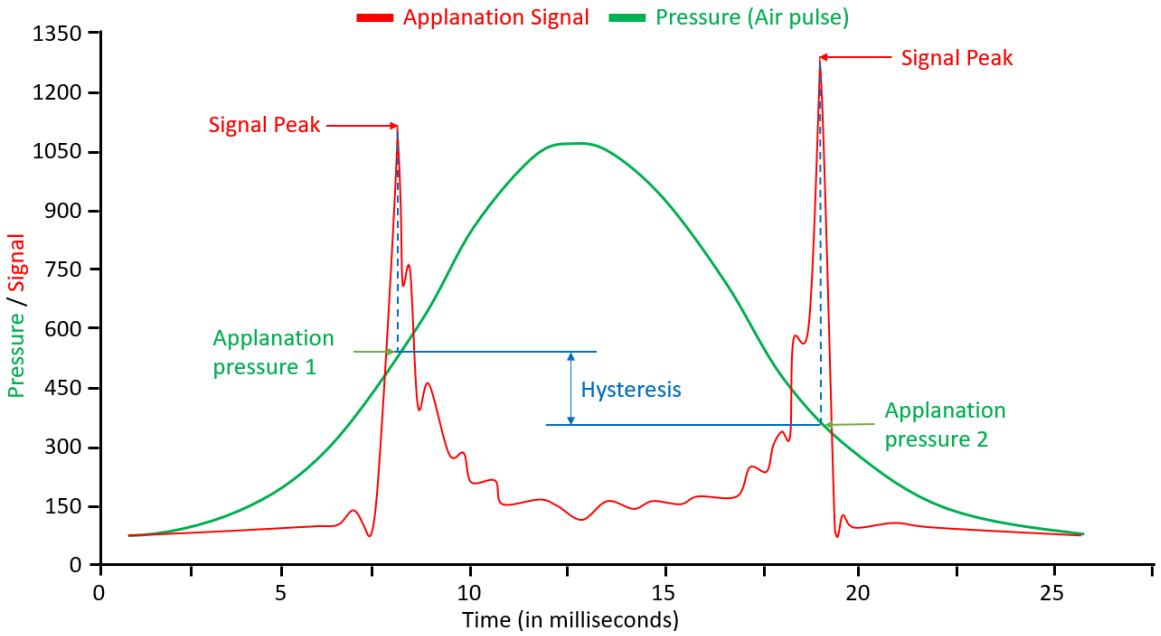

Figure 2.6: Diagram of hysteresis showing the pressure wave (in green) produced by a shot of air, with a smooth increase peaking at 10-15 ms followed by a smooth decrease. In red is the signal from light reflected off the cornea. As air pressure exceeds intraocular pressure (IOP) the cornea flattens resulting in better reflection and a peak in the signal (applanation pressure 1), followed by a period of inversion and, as pressure drops, another peak in signal (applanation pressure 2). Hysteresis is defined as the difference between the pressure at which the airjet applanates the cornea inwards and that at which it applanates outwards, which quantifies the elasticity of the cornea. Produced with reference to (Radcliffe, 2014).

of air. A total of four measures were taken and the recording with the highest quality (as determined by the ORA) was recorded.

2.3.4. Visual neglect

Visual neglect (hemineglect) describes a condition in which there is nothing structurally wrong with the visual system, but patients unconsciously ignore vision on one side unless attention is expressly drawn there. Visual neglect is relatively common immediately after a stroke, with rates reported as 65–82% (depending on side) at 2–3 days post-stroke (Stone *et al.*, 1993) and is also associated with visual field deficits, although double dissociation[10] may occur (Halligan *et al.*, 1990). The difficulty with visual neglect is that patients may not be able to respond to stimuli within the visual field on the affected side. When devices are used that require a perceptual response, such as Humphrey and Matrix field analysers, it is difficult to distinguish it from a true visual field defect (Kooistra & Heilman, 1989). To address this issue, we have both extended the acceptable post-stroke recovery time for inclusion in this study (during which most hemineglect resolves) and have also screened directly using neglect-specific tests. Rates of visual neglect at 3 weeks post stroke are reported to be 8–11%, and significant neglect is rarely observed at 6 months (Sunderland *et al.*, 1987); similarly, a large study of 1281 acute stroke patients found that neglect was markedly reduced at 3 months (Ringman *et al.*, 2004). For our studies, subjects were not recruited until they were allowed a minimum of 3 months recovery time, with many patients well exceeding that period. A number of tests have been devised which allow visual neglect and visual field damage to be distinguished, two of the most common being the line bisection and star cancellation tests (Ferber & Karnath, 2001; Li & Malhotra, 2015).

[10] When two related mental processes present independently of eachother.

2.3.4.1. Line bisection and star cancellation

The line bisection test has three horizontal 19 cm long lines printed on a landscape A4 sheet with the top line placed to the right, the middle line centrally, and the lower line to the left (see Appendix A: Line Bisection Test). Subjects were asked to look at each line in turn and make a mark with a pen where they believed the centre of each line was. The premise behind this test is that those with visual neglect ignore part of the line and so believe it to be shorter, bisecting the line far from the true centre and away from the side with neglect. In comparison, those with a visual field defect, despite not being able to see on one side, realise that the line doesn't end within their vision and they turn their head to make use of their peripheral vision to read the true length of the line. Thus, while those with field defects may perform slightly worse than controls due to peripheral blurring, this is separate from the large consistent bias frequently demonstrated in visual neglect. The output measure for the test is how far the average distance from the true centre is, where left is positive and right is negative. If a bias is made to the left on one line and to the right in another, they will offset each other, resulting in a low mean bias and will not be assessed as having visual neglect (which is characteristically unilateral).

The star cancellation test involves a mixture of a randomly ordered set of 56 small stars, 52 large stars, 13 letters, and 10 words which span an entire A4 sheet (see Appendix B: Star Cancellation Test). The task requires the subject to find and cross out all 56 small stars on the sheet, with the first two stars in the centre being crossed off as part of the initial explanation. The premise is that those with visual neglect will ignore the small stars on one side of the page, while those with an equivalent visual field defect will realise that there is more to the page than they can immediately see and turn their head to ensure they have checked the entire page. The measured output for this test is the degree of laterality, expressed as a fraction of those missed on the left compared with those missed on the right.

When comparing the effectiveness of the line bisection and star cancellation tests, it is first useful to identify a threshold for abnormality. Threshold scores for presence of neglect have been reported as >3 stars on a single side for the star cancellation test, and >14 mm to left or right in the line bisection test (Bailey *et al.*, 2004). Line bisection has a relatively low sensitivity of 53–60% (Halligan *et al.*, 1989; Ferber & Karnath, 2001), which might reflect the fact that a bias also exists in the general population (so-called pseudoneglect) (McCourt & Olafson, 1997; McCourt & Jewell, 1999). Factor analysis of commonly used visual neglect strategies still reveal a relatively high loading factor of 0.85 for a 6-test battery despite a low overall sensitivity of 53%, with star-cancellation having the highest load factor of 0.90 and sensitivity 100% (Halligan *et al.*, 1989). One might conclude that star cancellation is the better option; however, the line bisection and star cancellation tests assess different cognitive skills and may dissociate from each other (Ferber & Karnath, 2001; Rorden & Karnath, 2010), meaning the combination may give better coverage as a screening tool.

2.4. Higher Visual Function Tests

Higher visual functions (HVFs) are visual perceptions which are processed outside of the primary visual cortex. As there are many case studies describing prosopagnosia, akinetopsia, astereopsis, and achromatopsia, but little literature on how commonly more subtle defects present, all these four HVF were explored. Since perception is subjective, there are a range of tests which may assess each HVF. These are described below in more detail, elaborating on why one was chosen over the other options.

2.4.1. Stereopsis

Depth perception can be attributed to several forms of visual processing including both monocular and binocular cues. Monocular cues include motion parallax, optic expansion, and familiar/relative size, some of which incorporate prior known characteristics about the object.

There are intrinsic measures that rely on features of the objects we see, such as occlusion, perspective, and texture/lighting (Stark & Atchison, 2002). Finally, there is the combination of blur and the sense of chromatic aberration with accommodation which can provide a very basic sense of distance (Kruger & Pola, 1986; Stark *et al.*, 2002). However, by far the most accurate measure of judging short-intermediate distances, commonly used for activities of daily living, is binocular vision (stereopsis), which compares slight disparities in vision derived from the offset between our eyes (as well as the muscle strength of convergence when vision is fused and in focus). Stereopsis significantly affects our ability to make correct judgements of size (Zhang *et al.*, 2007), and those with reduced stereopsis perform more poorly on motor skill tasks (O'Connor *et al.*, 2010), may perceive stairs as flat (Humphreys *et al.*, 1989), or perceive cars as on a collision course (Miller *et al.*, 1999). In order to measure stereopsis, a different image must be displayed to each eye to simulate the offset used to judge distance. In these tests, this is often done by providing polarised glasses with different lenses, so that each eye only sees one of the two offset images at high contrast. Because stereopsis is a measure of the difference between the two images, when subjects have blurred or low vision, misaligned eyes (strabismus), or are predominantly monocular, their depth perception may be impaired. Therefore, visual acuity needs to be considered when displaying stereopsis results. The measure of output for these tests is seconds of arc on the retina, where each arcsecond is 1/3600 of a degree subtended at the retina.

2.4.1.1. Stereofly test

The Stereofly test has three components (see Figure 2.7). An initial screening slide with polarised letters (L on the left and R on the right) is used to quantify binocular vision. Subjects are asked to close one eye and determine which letter appears darker, then this is repeated with the other eye. If the letters appear the same, or if only one can be seen, then their vision is too poor to complete the test. The first component is a gross-stereopsis screening measure

presenting a large image of a fly, with each aspect of the fly having an offset of 4800–3000 arcsec. If they do perceive the three-dimensional effect in these more gross examples, then they can proceed to more refined tests on the following test pages. These pages include three lines, each with a series of four basics shapes progressing from 400 down to 100 arcsec. This section of the test is often used to assess children, although it also provides an excellent secondary measure to cover intermediate range stereopsis. In the final section there are ten diamonds, each comprised of four dots (top, bottom, left, right) with only a single circle being the stereopsis stimulus. Participants are asked to identify which circle appears three-dimensional in each example, which progressively become more subtle from 400 to 20 arcsec (fine stereopsis). When a subject can no longer detect any difference or after getting two incorrect, the last correct answer is taken as their threshold. If a subject gets one wrong and then gets at least two correct answers, this is considered an innocent mistake and they are allowed to continue.

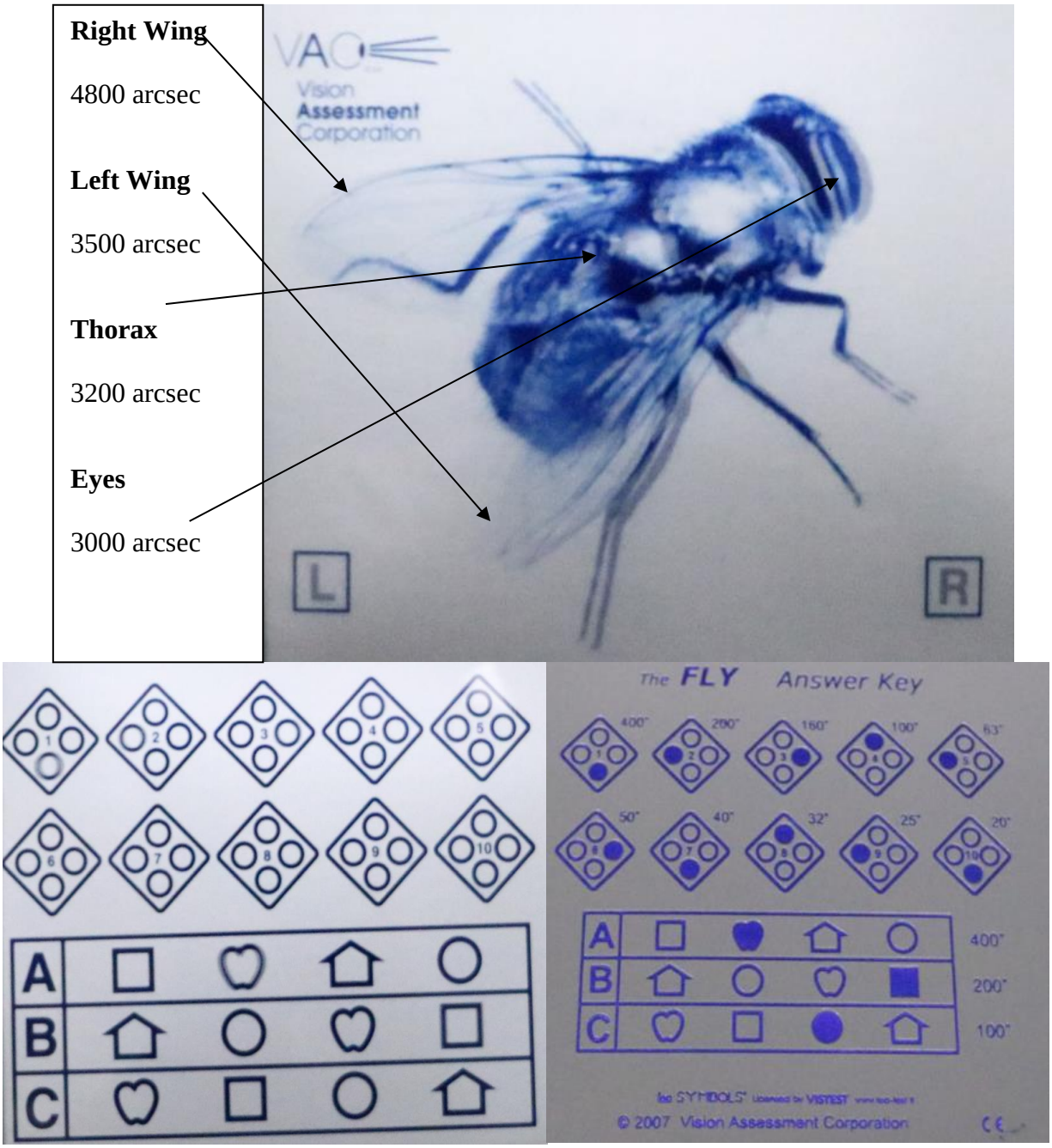

Figure 2.7: Images from the Stereofly stereovision acuity test. Top shows screening test with the L and R polarised letters matching the lenses of the glasses that the subject wears. Gross stereoacuity is gauged by components of the fly. Bottom left shows the test regions, with bottom right the answer key with arcsec thresholds.

2.4.1.2. Randot test

Random dot stereograms were invented by Béla Julesz and stemmed from work on depth perception. The stereogram does not have familiar cues or visible offsets when viewed monocularly (Julesz, 1964, 1965) and were developed from computer-generated patterns (Julesz, 1960) that form the basis of the modern Random Dot 3 (Randot) booklet. The Randot test is similar in principle to the Stereofly test, and also contains three sections, with images for each eye being offset to generate a 3D effect (see Figure 2.8). The difference is that the background is comprised of random dot noise, which encode the offset when polarised glasses are worn. This was designed to address a potential flaw in the Stereofly test, which is that the visual offset of the images can be seen by those with good acuity without wearing the glasses, and hence without using stereoscopic vision at all.

The random dots mask this offset, so one cannot clearly make out images within the background without wearing the polarised glasses, although the trade-off is that these shapes may be harder to visualise. On the first screening page are four basic shapes ranging from 900 to 300 arcsec and subjects must identify which shape is present within each, the first of which has more obvious contrast and can be seen without glasses. In the second section there are three rows, each with four basic shapes within them ranging from 300 to 100 arcsec. To answer a line correctly, subjects must get at least three of the four shapes correct. In the final section, there are ten diamond shapes each with four circles (top, bottom, left, and right), three of which appear to go into the page and one which comes out of the page. Many subjects had difficulty seeing the circles at all, and so were asked to mention if they noticed anything that appeared different in any of the four directions. This tested stereoacuity in the range 160–12.5 arcsec, covering finer resolution than Stereofly. The same rules as for the Stereofly were applied: after getting two incorrect, the last correct answer was taken as threshold. If two correct answers are made after an incorrect one, it is ignored, and they are allowed to continue.

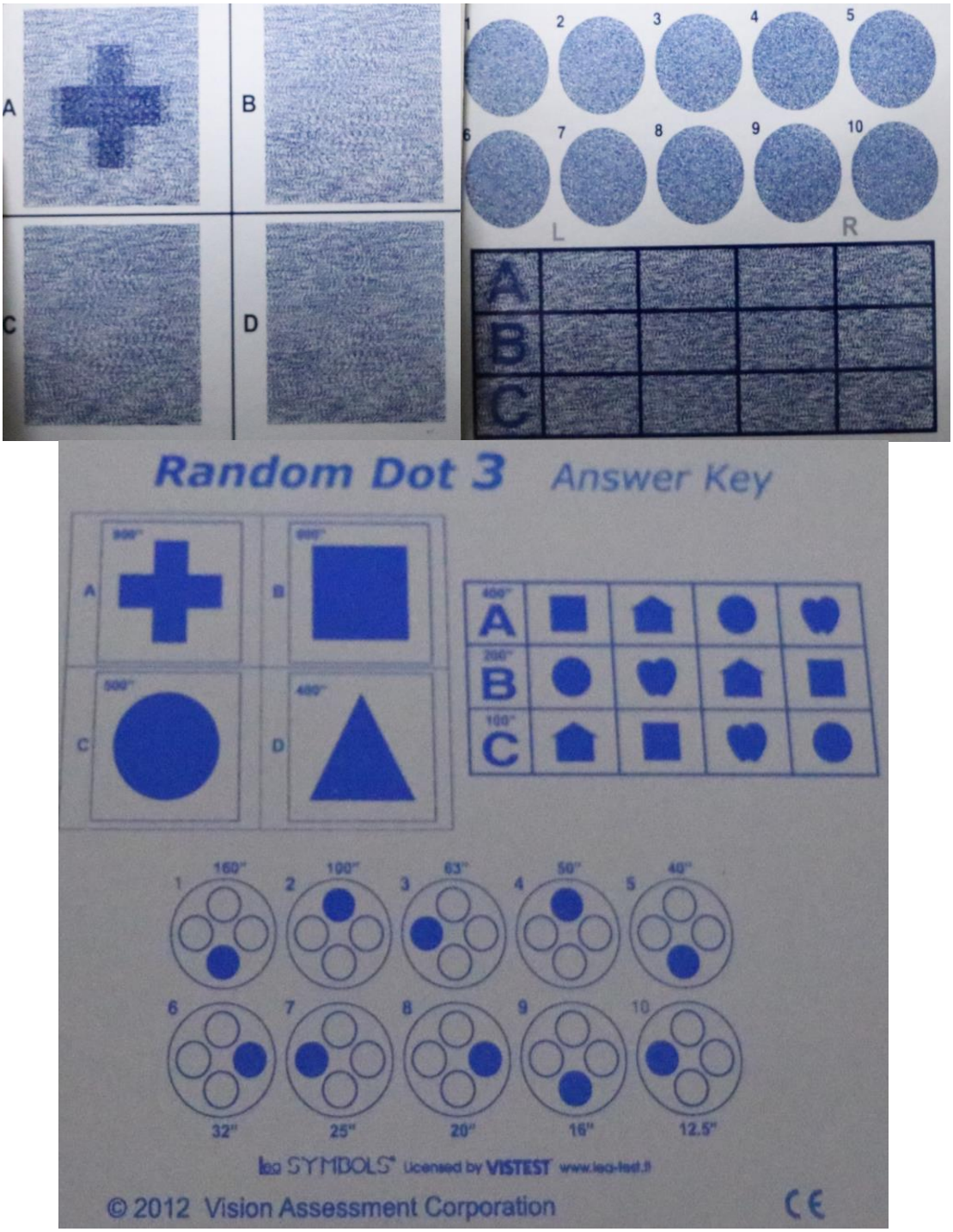

Figure 2.8: Images of the Random Dot 3 (Randot) stereovision acuity test. Top left shows gross stereoacuity by shape identification. Top right shows intermediate (shape) and fine stereoacuity (direction) tests. Bottom shows the test regions and answer key with arcsec thresholds.

2.4.2. Colour vision

Colour vision is determined by the three types of cone photoreceptor in the retina, which have photopigments sensitive to long (red), medium (green), and short (blue) wavelength light. Defects in these pigments can either originate from complete knockout of one the pigments (red = protanope, green = deuteranope, and blue = tritanope) and therefore the person is dichromatic, or from a shift in the absorbance spectrum for a pigment (red = protanomaly, green = deuteranomaly, and blue = tritanomaly) and the person is anomalously trichromatic, with reduced capacity to distinguish between overlapping spectra (see Figure 2.9**Error! Reference source not found.**).

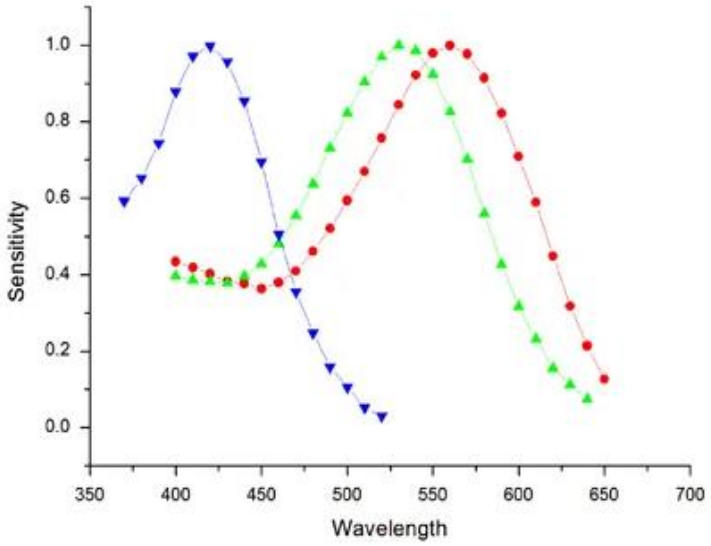

Figure 2.9: Extract from *"Colour vision deficiency"* by Simunovic (2010) showing spectra for red, green, and blue photopigments according to their relative sensitivity. Note the relatively close spectra for red and green, while blue is more distant with reduced overlap (Simunovic, 2010).

The most common colour deficiencies affect the long-wavelength sensitive (red) or medium-wavelength sensitive (green) photopigments, often described as red–green colour deficiency, which is congenitally X-linked. Reports suggest that, in European Caucasians, 8% of males and 0.4% of females are affected, with slightly lower rates in Asian populations (Birch, 2012).

In an older Australia optometric population of 7000 sequential patients screened with Ishihara plates, 6.32% of males and 0.28% of females showed congenital red–green defects (Steward & Cole, 1989). These rates are further broken down into their component disorders in Table 2.3.

Given how common red–green deficiencies are, it was important to include a measure that specifically tested for these disorders, the Ishihara (Ishihara, 1918) being one of the more commonly used tools. More generally, for detecting any kind of colour deficiency the Farnsworth–Munsell test (Farnsworth, 1943) is a very popular tool. The classic version of the Farnsworth–Munsell is the 100-hue, having 100 wells containing coloured tiles which must be ordered according to colour gradient. While the 100-hue is very accurate, with wells approaching the minimum that a normal observer can distinguish, its limitation is that it is time consuming and fatiguing, making it impractical for routine clinical use (Neitz *et al.*, 2008), especially in those who are elderly or have difficulty concentrating such as stroke patients. The smaller Farnsworth–Munsell D15 is a much quicker and convenient test designed for routine clinical use, as the subject need only order 15 wells, the trade-off being it is relatively insensitive to mild colour deficiencies (Neitz *et al.*, 2008). As we are focused on acquired cerebral colour deficiencies as a result of cortical damage from stroke, damage would typically be substantial if not complete (Zeki, 1990; Zhou *et al.*, 2018), although selective losses have also been reported (Wooten, 1981). The D15 set was chosen, as it can pick up moderate–severe colour deficiencies and is conducive to clinical application.

It should be noted that there are also reports of hemiachromatopsia (Kolmel, 1988; Paulson *et al.*, 1994; Short & Graff-Radford, 2001; Bouvier & Engel, 2006), where only half of the visual field is affected, and as Ishihara and Farnsworth-Munsell tests use both hemifields, they may

be insensitive to this group. That being said, Ishihara and Farnsworth-Munsell are two of the most commonly used tests to assess achromatopsia (Bouvier & Engel, 2006), while also providing rapid and easy testing that might be applied to a clinical environment.

2.4.2.1. Ishihara

The Ishihara test is comprised of 17 plates (images), each with a number formed by dots of a similar hue (such as red/pink/orange) on a background of distractor colours which have dissimilar hues. While those with normal trichromatic vision clearly see the outline of the numbers, those with colour defects (especially red–green) can find it difficult to demarcate between target and background. In addition, some frames encode a second number with less-overtly related colours, which may add to the uncertainty of those without normal colour vision. This makes the test very sensitive to shifts in red (protanope) and green (deuteranope), with only minimal testing of the less common blue (tritanope) deficiencies. The first frame is a control and should be detected even by those with no colour vision, and two frames throughout the test show numbers that are not identified by those with normal vision but may be detected by those with red–green defects. When marking this test, subject answers are compared against the correct number for a normal-vision respondent, and any answer other than the correct one (or the absence of a number) is taken as incorrect. While testing in this thesis focuses on continuous measures for making a categorisation between normal and abnormal, a threshold for Ishihara of >3 errors is typically treated as abnormal, with a 98.4% sensitivity reported (Birch, 2010).

2.4.2.2. Farnsworth–Munsell D15

The D15 is comprised of a base reference well and 15 wells that are spaced across the colour spectrum. When completing the test, the reference well is place in the container, and all the other colour wells are randomly arranged outside the container (see Figure 2.10). The subject

must choose the colour they believe is closest to the reference well and place it next to it, then sequentially repeat this process until all the wells have been placed. Subjects are free to remove or rearrange the well order within they container as they see fit. Subjects were notified that they would be timed for the test, but they should prioritise making sure the well order is correct over completing quickly. Once the subject completed the test, they were asked to have a final look at the order they had chosen to ensure they were happy with it. Once confirmed, the wells were turned upside down to reveal the numbers on their bases and the well order was noted. To assess the extent of colour vision deficiency associated with this test, the methods described by (Bowman, 1982) were used. In this method, each well is assigned a colour value according to the CIELAB colour space using the measures L* as lightness (black to white), a* as green to red, and b* as blue to yellow, matching the colour encoding pathways of the visual system. The difference between wells was then calculated using the formula

$$\Delta E^*_{ab} = \sqrt{(\Delta L^*)^2 + (\Delta a^*)^2 + (\Delta b^*)^2}\,.$$

Values for each difference between wells were recorded from this paper and the sum of the differences between wells was calculated (see Table 2.4). The correct order minimises the total colour difference score between wells (minimum is 117). From this a colour confusion index (CCI) was created by the ratio of the total colour difference score over the minimum score, making a perfect well order (normal) 1.00. The larger the number, the larger the abnormality up to a maximum of 5.33 if the wells are maximally different.

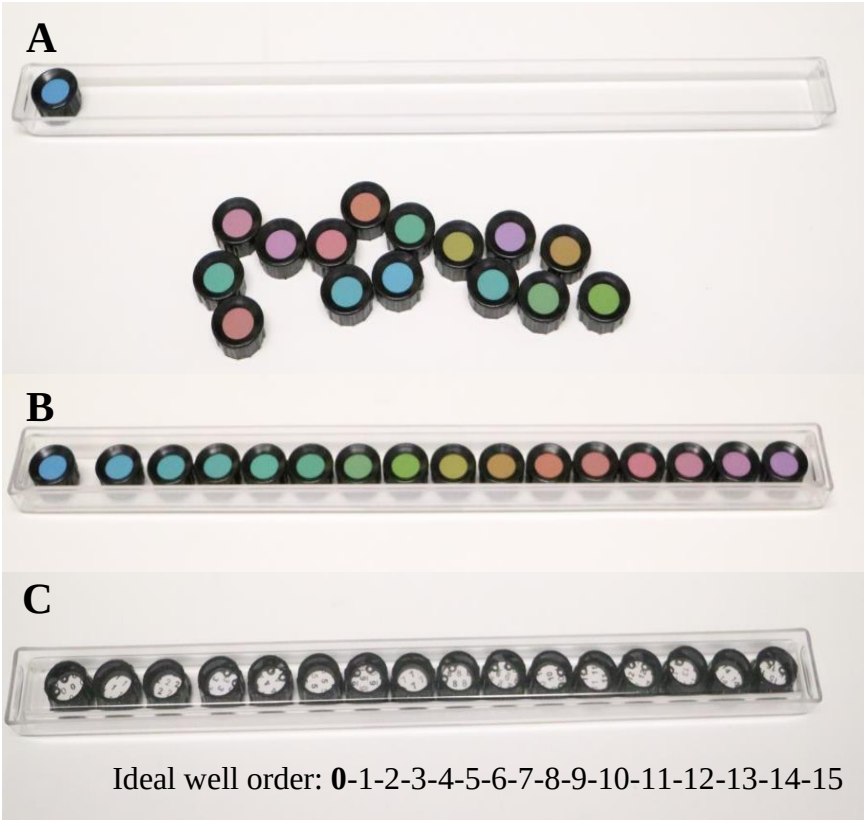

Figure 2.10: (A) shows what the subject is presented with at the beginning of the test. They must enter wells in an order that minimise differences between adjacent wells, as done in (B). The order of the wells is noted to allow a Total Color Difference Score (TCDS) to be calculated.

Minimum Order		Intermediate		Maximum Order	
Order	Difference	Order	Difference	Order	Difference
0		0		0	
1	9.4	1	9.4	8	51.1
2	6.7	2	6.7	1	44.9
3	5.9	4	11.7	9	44.4
4	5.9	7	23.2	2	40
5	4.5	3	28.1	10	38.8
6	9.4	6	18.8	3	38.3
7	10.5	5	9.4	11	37.5
8	12.1	8	29.9	4	37.6
9	7.9	9	7.9	12	38
10	12.2	10	12.2	5	38.9
11	6.3	11	6.3	13	40.5
12	5.2	12	5.2	6	40.3
13	7	13	7	14	43.9
14	6.5	14	6.5	7	44.6
15	7.5	15	7.5	15	44.3

TCDS:	117		189.8		623.1
CCI	1.00		1.62		5.33

Table 2.3: (Left) Shows perfect order with minimal well difference scores, which sums to a Total Colour Difference Score (TCDS) of 117, and a Colour Confusion Index (CCI) of 1. Intermediate (middle) confuses a couple of adjacent wells and scores a CCI of 1.62, and the worst order with maximum score CCI (right) of 5.33.

2.4.3. Global motion detection

The perception of global motion involves integrating cohesive motion within a background of noise. The random dot kinematogram (RDK) presents an image where some or all the dots move in a cohesive direction from frame to frame, while other distractor dots may move in random directions. Initial studies demonstrated that sudden dot movements are perceived as smooth coherent motion (Anstis, 1970; Julesz, 1971), and that this depends on the degree of spatial displacement (Braddick, 1974). An upper limit exists beyond which motion is no longer reliably perceived. It was later shown that detection of movement depends on the size of the stimulus patch in terms of retinal angle rather than discrete size in pixels, with inclusion of greater eccentricities increasing this displacement limit (Baker & Braddick, 1982). Displacement measured in terms of minutes of arc showed high error rates when very small (<5 arcmin, 0.083 deg) or very large (>20 arcmin, 0.333 deg) displacements were used (Cleary & Braddick, 1990). Direction of movement was assessed both foveally and peripherally in cardinal horizontal (left–right) and vertical (up–down) directions, showing isotropy between directional pairs centrally (although with greater sensitivity to vertical motion), while peripherally there was increasing anisotropy with a centripetal bias (Raymond, 1994). It was determined that this arc threshold is limited by density of the dots when tracking discrete movement, not hardwired spatial frequency (Eagle & Rogers, 1996), suggesting that less densely packed stimuli which are clear of their immediate surrounds allows better tracking and results in greater sensitivity. More recent versions have focused less on arc threshold and more on detection of coherence within noise (Schutz *et al.*, 2010). These factors informed the design of the RDK used in these experiments: limited retinal angle, moderate displacement at diagonals, both horizontal and vertical components, small dot density, and coherence on a background of noise (details in 2.4.3.1 below).

While global dot motion remains an interesting measure, before including it in our testing regimen it was important to demonstrate that such a stimulus can target motion processing at the cortical level and that it may be impaired in stroke. Nakamura et al. used magnetoencephalography to localise responses to increasing coherence on RDK displays, highlighting the posterior inferior temporal and lateral occipital sulci (human V5), with a positive association between coherence and amplitude, but not with latency (Nakamura *et al.*, 2003). This confirms that stimuli for this type of RDK target the motion-dominant area V5 in humans, and that graded stimuli result in graded responses. RDK was also recently assessed in an akinetopsic patient with bilateral lesions of V5 following stroke, revealing there was impaired perception to motion (Heutink *et al.*, 2019). We therefore conclude that RDK would be an appropriate measure to use in detecting stroke-related motion deficits.

2.4.3.1. Random dot kinematogram (RDK)

Stimulus dots were sized 8 minutes (0.13°) on screen with a Gaussian blur of the form:

$$f(x) = ae^{-\frac{x^2}{2b^2}}$$

where *a* is amplitude, here the maximal contrast brightness; *b* is the standard deviation, here 1.2 minutes such that contrast reaches 0 at a total width of 8 minutes; and *x* is the angle offset from the centre of the dot (see Figure 2.11).

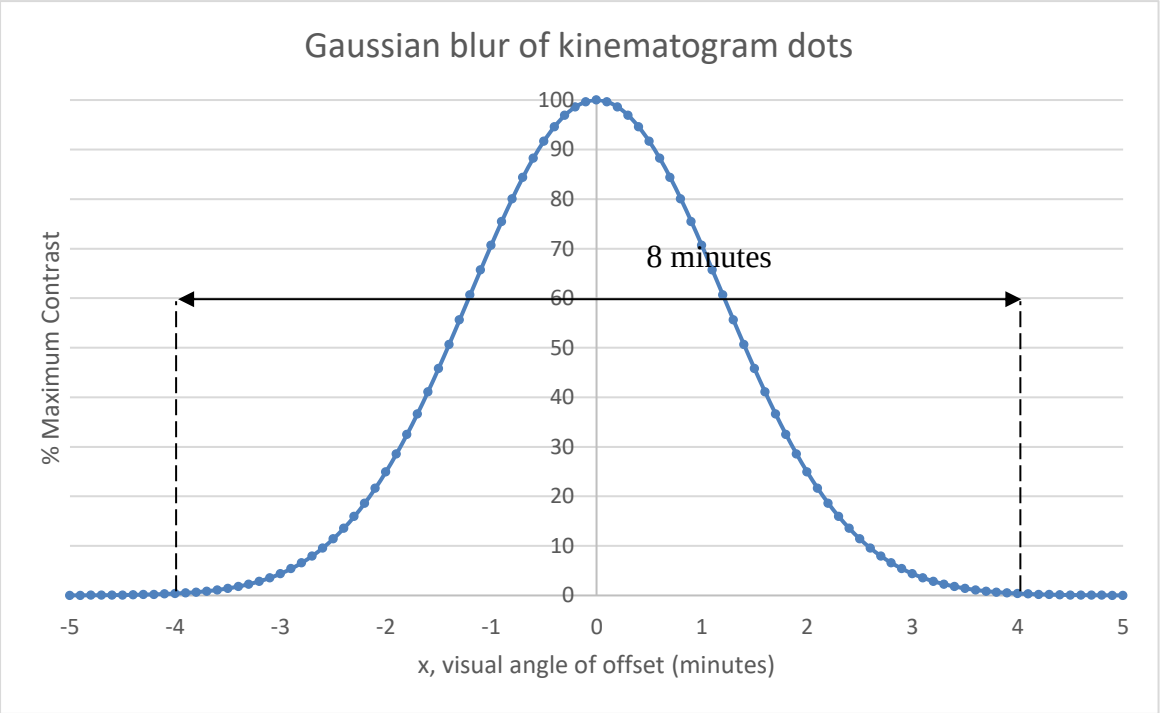

Figure 2.11: Gaussian blur of kinematogram dots showing % contrast from background against visual angle from centre of dot, using a standard deviation of 1.2 to create an effective width of 8 minutes of visual angle for each dot, equivalent to 0.133 degrees.

The RDK test comprised of 40 dots scattered across a circular grey stimulus with a fixation cross centrally. Dots are assigned as either part of cohesive movement in a single direction (left diagonal or right diagonal), or pseudo-randomly such that their net direction is 0. During a stimulus, a frame with pseudorandomly placed dots is created with a clear space surrounding each; it is displayed for 60 ms, followed by a frame with points offset by 0.16 degrees in their respective directions for another 60 ms. This process repeats continuously with new start coordinates during each iteration for a total of 2 seconds, equivalent to 16 iterations and an effective movement speed of 1.3 degrees per second.

Initially, all dots move cohesively for three test screens and the subject is told which way the stimulus is moving, in order to demonstrate the task. Then their responses are recorded, and for each correct answer the cohesive motion is progressively reduced. A two-down/one-up staircase thresholding approach was used so that every incorrect answer raised the threshold (easier), while after a mistake, two correct answers are required before lowering the threshold

(harder). This means random answers lead to steps up towards complete cohesive motion, making it statistically improbable to progress very far without having the capacity to recognise the stimulus direction. A reversal is said to occur each time there is a change from a series of steps down to a step up, or steps up to a step down (see Figure 2.12). In total, the test comprises the lesser of 10 reversals or 45 responses, after which the last 4 reversals are taken and averaged as the subject's threshold.

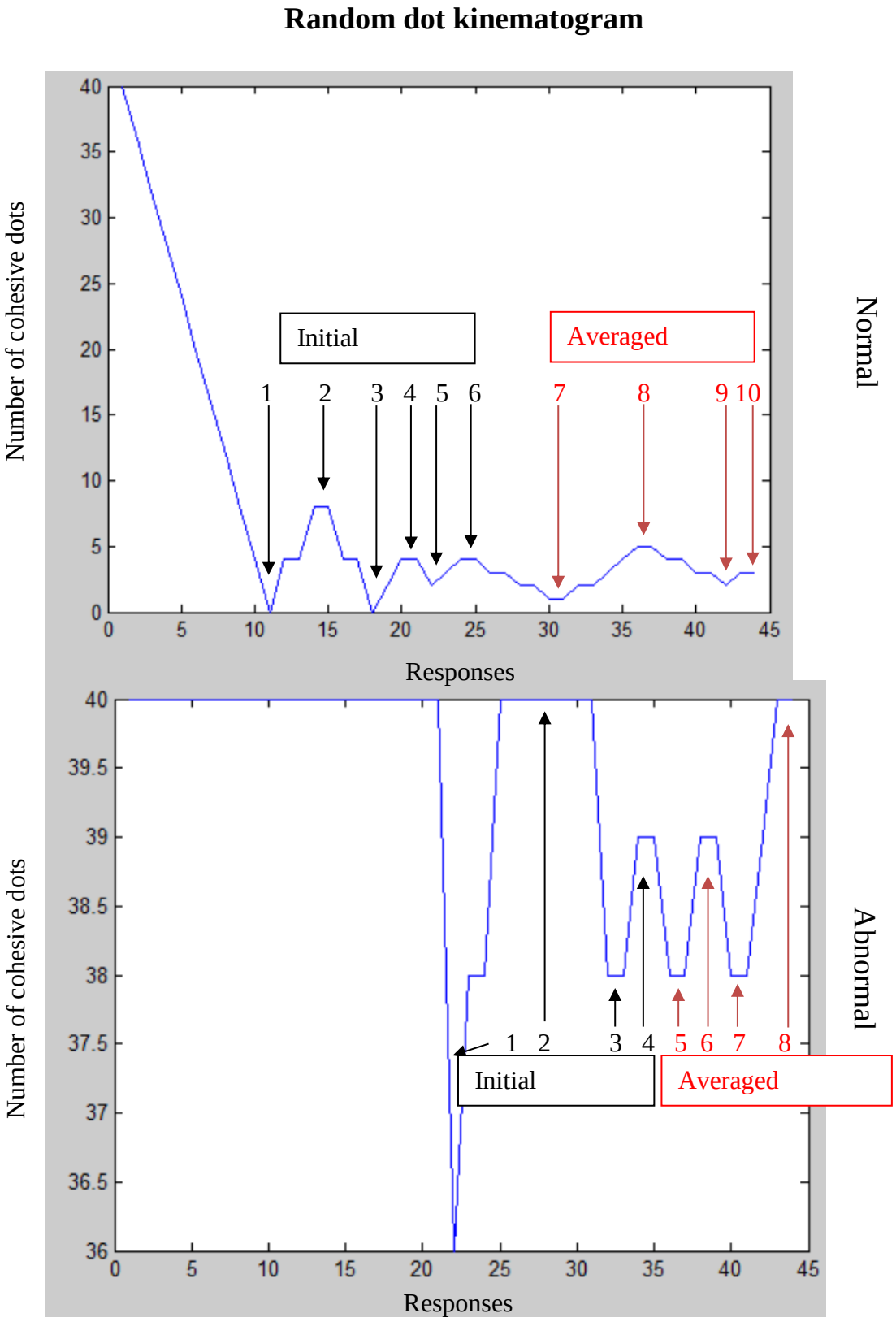

Figure 2.12: Example of random dot kinematogram (RDK) responses for normal (top) and abnormal (bottom) subjects. For both, all 40 dots cohesively move in a single direction initially, thereafter progressively decreasing in cohesive motion and adding random directional movement (noise). When a response is first incorrect after being correct, or first correct after being incorrect, this is called a reversal. Initial reversals are ignored to allow time to approach threshold and are so insensitive to early mistakes, while only the final four reversals are averaged to produce the result. This either occurs after 10 reversals (top) or after reaching 45 responses (bottom).

2.4.4. Facial recognition

Facial recognition is an important part of everyday living that is often overlooked. It allows us to recognise friends and family from strangers and to interact with people. Practically, it is not only the ability to recognise a face that matters, but the ability to remember and recall that face, which has guided the production of standardised tests. Two of the standardised tests, the Benton Facial Recognition Test (BFRT) (Benton & Van Allen, 1968) and the Recognition Memory Test for Faces (RMF) (Warrington, 1984) have shown serious shortcomings, largely to do with facial matching being possible without facial identification. BFRT presents target and test faces simultaneously with unlimited duration, allowing a feature-matching strategy, while RMF images include substantial non-face information such as hair and clothes. In both tests, a substantial proportion of normal subjects are able to score in the normal range even when the face is occluded (Duchaine & Weidenfeld, 2003). It also appears insensitive to prosopagnosia detection, with many such patients scoring normally on BFRT (Nunn *et al.*, 2001; Duchaine & Nakayama, 2004). In response, a test with only facial information and with images presented separately was developed, the Cambridge Facial Memory Test (CFMT). The CFMT appears to have higher detection rates when the standard psychophysical threshold (2-standard deviations below the mean, or the lowest 5 percentile) is used (Duchaine & Nakayama, 2006). We have therefore chosen CFMT as one of the more widely used modern variants (McKone *et al.*, 2011; Croydon *et al.*, 2014; Cho *et al.*, 2015; Albonico *et al.*, 2017; Gray *et al.*, 2017; McKone *et al.*, 2017).

2.4.4.1. Cambridge Facial Memory Test (CFMT)

The CFMT was designed to assess the ability to recognise and remember a person's face. Those with impaired facial recognition are unable to detect those unique features of a person's face which make them recognisable and so they perform poorly on the test. However there is also a memory component, which means that elderly people tend to get lower scores and there is a

substantial trend of declining score with age (Bowles *et al.*, 2009). To address this issue, the same group assessed a range of age groups, developed a formula that adjusts for age, and calculated a figure according to which those below the 5th percentile had prosopagnosia, i.e. impaired facial recognition (Bowles *et al.*, 2009). With a commonly accepted threshold of the 5th percentile, 5% percent of the general population will fall into this range. Within this group are those who have congenital deficiencies, suggested to be as high as ~2.5% (Kennerknecht *et al.*, 2006), which appear to run in families (Kennerknecht *et al.*, 2007). It remains unknown how many of these people have cerebral deficiencies.

It has been demonstrated that CFMT reveals small differences depending on ethnicity, age, and sex (Bowles *et al.*, 2009), which is perhaps not surprising given that the test exclusively uses faces of young males from the Boston region. While there is some suggestion that gender bias is minimal (Scherf *et al.*, 2017), the ethnicity difference is notable, with newer versions including Australian-specific (McKone *et al.*, 2011) and East Asian-specific (McKone *et al.*, 2017) versions. It was a limitation of our design that the Australian-specific version was not available at the time of testing, although we highly recommend that location-specific versions be used in future.

In terms of practical implementation of the test, procedures were explained to the subjects beforehand. Each section of the test comprises a presentation section where subjects are asked to learn the face(s), and a testing section where they must recall the face(s) from a three-option forced choice (details in Figures 2.13 –2.14). The practice section using cartoons was not scored and was only used to demonstrate how to complete the tasks. Section one presents a single face from three angles in sequence, and then has three sets of three-way forced choice selections, with each answer being an exact matching photo to one angle of the presented face. This process is then repeated with new faces, until in total six faces are presented with 18 responses. Section two consists of simultaneous presentation of the same six faces used in

section one, followed by 30 sets of thee-way forced choice selections, with each answer being a similar but novel image of *any* of the six presented faces (totalling five from each face). Section three consists of the same simultaneous presentation of six faces used in section two, followed by 24 sets of three-way force choice selections, with each answer being a similar but novel image with added noise from any of the six presented faces (totalling four from each face). The test comprises a total of 72 responses (section one, 18; section two, 30; section three, 24), with six target faces and 50 distractor faces.

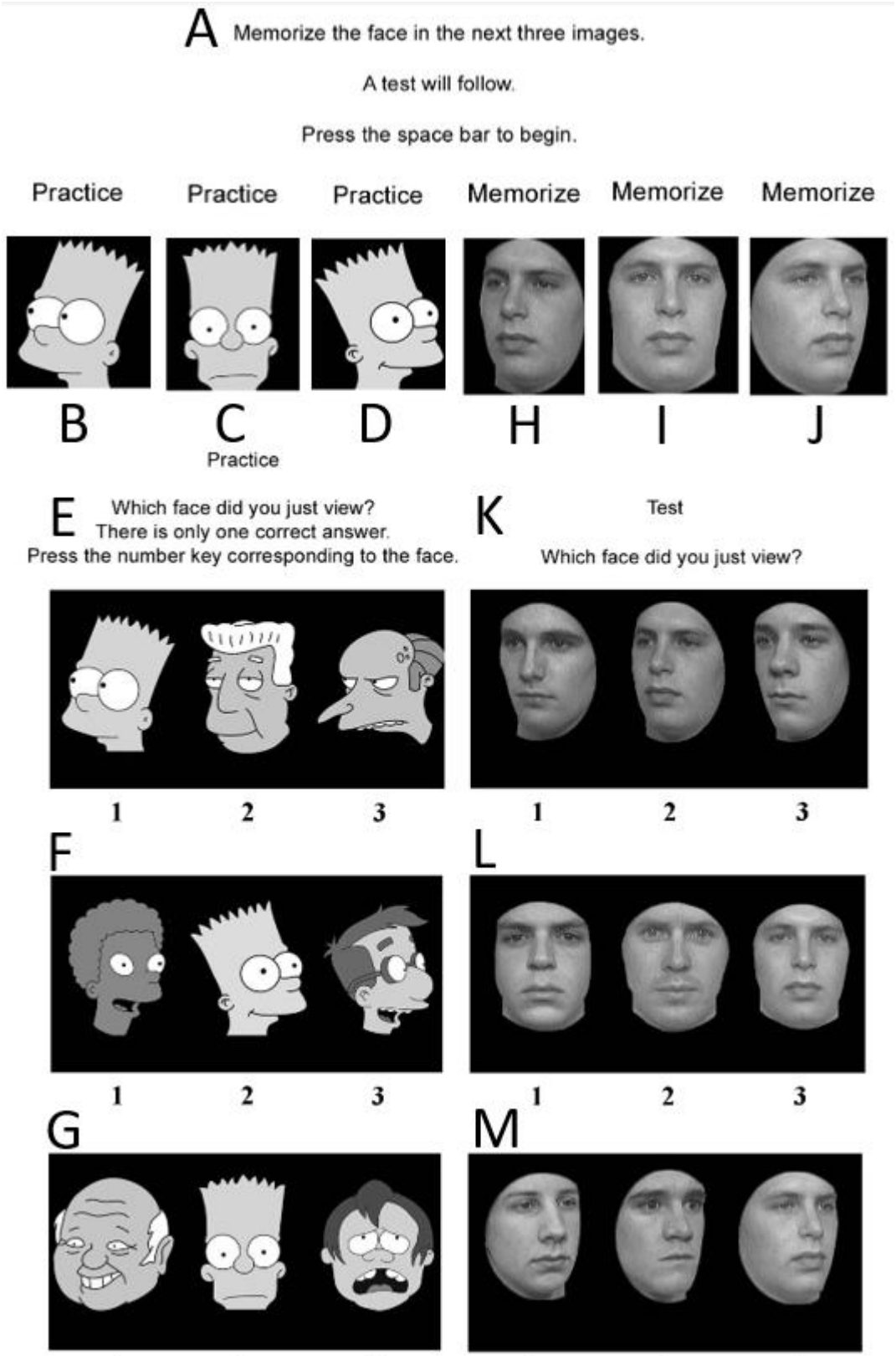

Figure 2.13: CFMT practice and section one test sequences. Left (A–G): the practice sequence outlining how to complete tasks, while the the same instructions (A) are then shown for the actual test sequence (H–M) for section one (of three). Subjects are shown a single face from three angles sequentially, then given sets of three faces containing an idental image from that set and two distractors, they are asked to identify which face was the one initially shown. Section 1 repeats this process with a total of six faces, comprising 18 results.

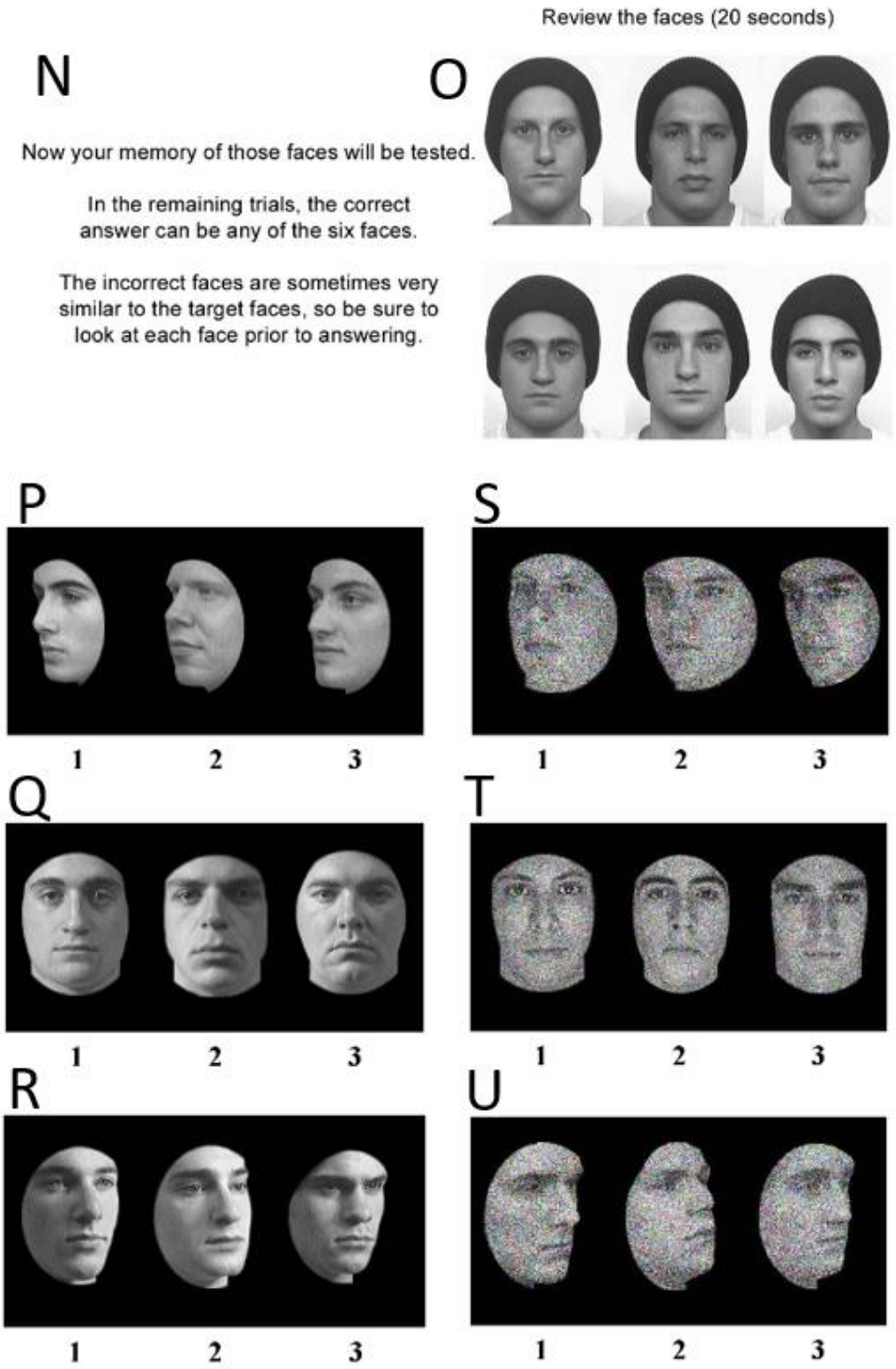

Figure 2.14: CFMT sections 2 and 3 test sequences. In both sections the instructions are the same (N) and the six faces individually tested in section 1 are used, being presented together for 20 seconds (O). Section 2 then provides sets of three faces with one face being a novel image of a person from one of the six faces which were initially asked to be memorised, with two being distractors. (P–R) In total, five versions of each of the six faces are presented, comprising 30 answers. Section 3 repeats the same 20-second review (O) and then asks for performance of the same task, which are now novel images with static noise added for added difficulty. Each of the six faces are presented four times, comprising 24 results. In total, 72 tasks are completed: section 1, identical images (18); section 2, novel images (30); and section 3, novel images with noise (24); collectively using six target faces and 50 control faces.

2.5. Perimetry

The multifocal pupillographic objective perimetry (mfPOP) device objectiveFIELD analyser (Konan Medical USA Inc, Irvine CA) presents a novel approach to using rapid light stimuli to measure pupil diameter responses. It shows promise in retinal disorders but there has only been limited testing with neurological disorders. For a full discussion of the history or perimeters and their comparison, see the introduction section *'Automated Perimetry'*. Here only the selected devices will be discussed and will cover stimuli, test procedures, and output measures.

2.5.1. Humphrey Field Analyser (HFA)

Humphrey Field Analyser II (HFA) (Carl Zeiss Meditech AG, Jena, Germany) is the most commonly used device for field testing in neurological disease (Hepworth & Rowe, 2018), using small light stimuli (Goldmann Size 3). For this study testing was done with the achromatic 24-2 SITA threshold values (see next section).

2.5.1.1. Stimuli

With the invention of the HFA II device, the common approach was to use the 30-2 pattern of grid points. This same grid format could be used for the wide field of 30-2, covering 3–33 degrees eccentricity, or the smaller but faster 24-2, covering 3–27 degrees. In comparing these approaches in neurological diseases, 24-2 has greater reliability than 30-2 (Wild *et al.*, 1991; Khoury *et al.*, 1999) and is quicker and so was selected for this study. There are 54 regions in the 24-2 test grid 6 degrees apart with 3 degree offset from the meridians, extending to 21 degrees in each of the superior, inferior, temporal regions and two points at 27 degrees nasally (Figure 2.15).

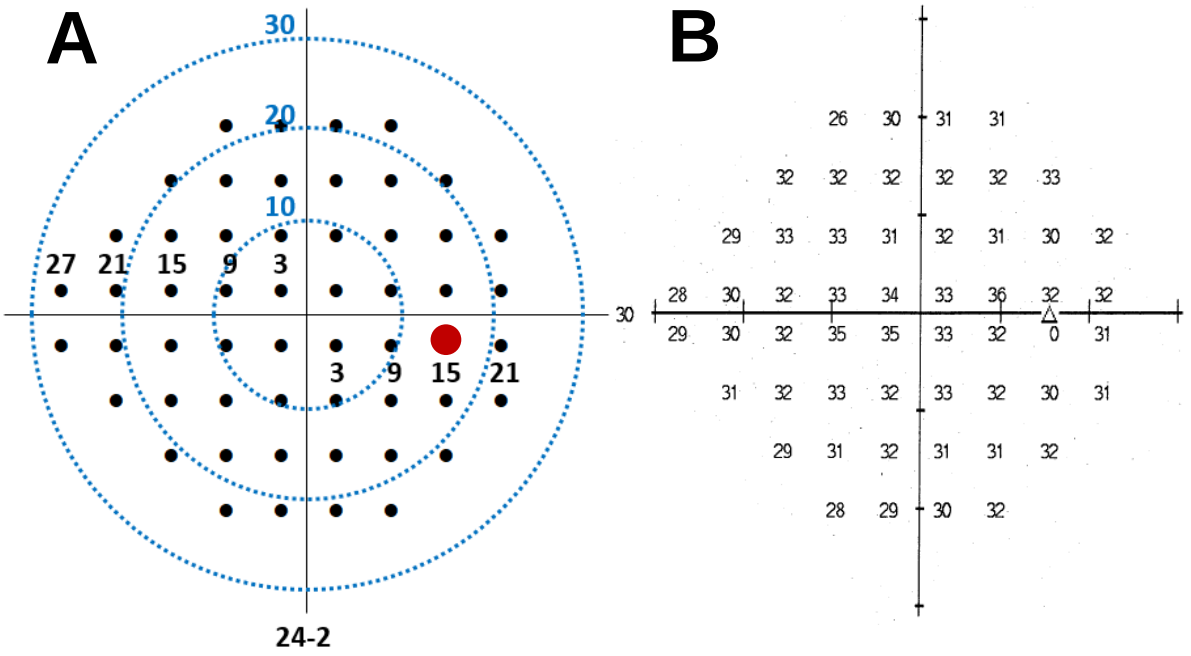

Figure 2.15: (A) Humphrey 24-2 stimuli grid for right eye with points offset from vertical and horizontal meridians by 3°, extending to 21° in each direction except nasally where there are two additional points extending to 27°. The red dot represents the blind spot (optic nerve head). (B) Shows results for a Humphrey 24-2 test for the right eye with threshold values in dB contrast, matching coordinates in A. Note that the blind spot was unresponsive, recording 0 dB, and is excluded from calculations.

HFA uses a Goldmann size 3 (0.43^{o} diameter, much smaller than the black dots in Figure 2.15) white light (achromatic) stimulus which varies in luminance throughout testing in order to calculate the threshold at which subjects can detect the stimuli in that part of the visual field. The Swedish Interactive Threshold Algorithm (SITA) was used to determine the order and luminance of test regions, being faster that the original full threshold method (Bengtsson *et al.*, 1998) while performing at least as well in hemianopias typical of stroke, chiasmal compression, and optic neuropathies (Wall *et al.*, 2001).

2.5.1.2. Testing procedures

Subjects were brought into a dimly lit room and allowed to adapt to the dim ambient illumination while information was entered into the device. Prior to testing, subjects had their ocular prescription measured via a vertometer, and this refraction was entered into the HFA

device, which then suggests a set of trial lenses. Subjects were instructed to place their chin on the chinrest and lean forwards to touch the headrest, then focus on the central fixation dot throughout testing. It was explained that they should press the button whenever they can see a dot appear on the screen, and that they could blink freely. At the beginning of testing, gaze tracking was turned on for all subjects (where tracking was possible), and the pupil was centred on a reference marker. The right eye was always tested first. During testing, small alterations in position were corrected periodically by small alterations in the chinrest to keep the reference marker centred on the pupil. If there were large deviations from the reference marker, slumping away from the headrest, repeated saccades off centre, significant drooping of the eyes, or severe fatigue, the test was paused, corrected, and recommenced if possible. Alternatively, if it was thought that the problem had caused a significant effect, testing was stopped and repeated. Any test with poor validity markers (according to device parameters of fixation loss >20% or false positive values of >33%) meant that the test for that eye was repeated following instruction to the subject.

2.5.1.3. Output measures

Threshold values were calculated from contrast according to the Weber formula $((L_{max} - L_{back}) / (L_{back}))$, where the background luminance is 10 cd/m^2 and the maximum luminance is as large as 3178 cd/m^2 which are then converted into dB as $10*\log_{10}(L_{max} - L_{threshold})$ (Fredette *et al.*, 2015). Thus, the poorest response is where a person does not detect the stimulus at L_{max} resulting in a 0 dB score, and the best response is where a person detects minimal background change, resulting in a 35 dB score. While other measures, including total deviation, pattern deviation, and probability maps, were collected, they were not used in this analysis and are not discussed here.

2.5.2. Matrix Field Analyser (MFA)

The Humphrey-Matrix (Carl Zeiss Meditec, Dublin CA) or Matrix field analyser (MFA) is another perimetry device which is less commonly used (Hepworth & Rowe, 2018), but has larger test regions and uses contrast-reversing grating stimuli. It was selected due to the larger test regions being a closer approximation to mfPOP stimuli, and so may provide a more suitable comparison.

2.5.2.1. Stimuli

The Matrix visual field test is based upon frequency doubling technology (FDT) perimetry. This relies on the spatial frequency doubling effect – when a low spatial frequency sinusoidal grating (<2 cycles/degree) is counter-phase flickered at a high temporal frequency (>15 Hz), the grating appears to have a spatial frequency twice that of its actual frequency (Taravati *et al.*, 2008). The effect is also seen well for transient onset stimuli (Maddess & Kulikowski, 1999). FDT reportedly preferentially stimulate the magnocellular pathway, targeting a cell type with less redundancy, and so greater sensitivity to early loss (originally designed for glaucoma fields) – for further discussion see Introduction section 1.6.3.2 Matrix.

In order to allow direct comparison, a similar 24-2 field map was used as for HFA, with stimuli still spaced 6 degrees apart, but with much larger stimuli 5° in diameter such that the majority of the gap is filled by stimuli but without any overlap. In addition, there is a single central test region where meridians meet, which was discarded for the purposes of comparisons as there is no analogous region in either of the two other devices. Stimuli are presented as a contrast sinusoidal grating eliciting the frequency doubling illusion (Anderson & Johnson, 2002).

Similar to HFA, stimulus contrast is varied to calculate the threshold at which a subject can detect it and a thresholding algorithm is used. In this case the Zippy Estimation by Sequential Testing (ZEST) thresholding strategy is used, which showed promised in early testing

(Anderson & Johnson, 2006), although it has been shown to converge on only 15 unevenly spaced values (Fredette *et al.*, 2015). Despite this, MFA has been compared to HFA in hemianopias and has shown similar performance (Taravati *et al.*, 2008).

2.5.2.2. Testing procedures

MFA subjects with ocular prescriptions < ±3 dioptres could be assessed without glasses, while anyone else was asked to wear their glasses for testing. This is consistent with manufacturer recommendations and is supported by the apparent tolerance to blur of the frequency doubling technology (Campbell & Green, 1965; Legge *et al.*, 1987). Prior to testing subjects were instructed to place their chin on the chinrest and lean forwards to touch the headrest, focus on a central cross during testing, and press the button when they saw a modulating grating on the screen; they could blink whenever necessary. A short demonstration was completed for <30 seconds at the beginning to confirm understanding of expectations. The right eye was always tested first. During testing, small subject movements off-centre were tolerated provided the pupil remained within the 3 mm reference marker originally centred on the pupil, and if this was exceeded the test was paused and the subject repositioned before recommencing. Where there was slumping away from the headrest, repeated saccades off-centre, significant eyelid droop, or severe fatigue, the test was paused and the subject re-instructed and the test recommenced if possible. If problems were thought to have caused a significant impact on testing, the test was stopped and redone. Any test with poor validity markers (with fixation loss >20% or false positive values of >33%, as per manufacturer guidelines) was repeated for that eye.

2.5.2.3. Output measures

Threshold stimuli for MFA uses a different methods for calculation of contrast to the HFA. Contrast is calculated according to the Michaelson formula $((L_{max} – L_{min}) / (L_{max} + L_{min}))$ for a

background L_{back} (100 cd/m^2) of the average of L_{max} (200 cd/m^2) and L_{min} (0 cd/m^2); dB values are calculated as –20*log(contrast) (Fredette *et al.*, 2015). Thus, the poorest response is where a person does not detect a maximal contrast of 0 contrasted with 200 cd/m^2 (100% contrast) resulting is 0 dB score, and the best response is where a person detects minimal change of 0 contrasted with 5 cd/m^2 (1.27% contrast) resulting in a score of 38 dB. In principle, this means HFA and MFA are equivalent at ~35–38 dB and a 1 dB loss in HFA is equivalent to a 2 dB loss in MFA (Fredette *et al.*, 2015). Despite the range extending to 38 dB, because of the ZEST testing algorithm making only 15 results accessible, and those results being unevenly distributed, there are often large gaps between values. Similar to HFA, other measures were collected including total deviation, pattern deviation, and probability maps, but they were not used in this analysis and are not discussed here.

2.5.3. Multifocal pupillographic objective perimetry (mfPOP)

Multifocal pupillographic objective perimetry (mfPOP) provides a new approach compared to previous automated perimetry. It presents multiple stimuli and measures the response via the autonomic system, bypassing the need for a subjective response.

2.5.3.1. Stimuli

Two sorts of stimuli were used: bright yellow stimuli on a dim yellow background (Y/Y), (C.I.E x,y coordinates 0.377, 0.464 bright yellow on 0.408, 0.515 dim yellow background) termed *luminance only*, and bright green stimuli on a dim red background (G/R) (x,y 0.291, 0.612 bright green on 0.551, 0.343 dim red), termed *colour exchange* (including colour and luminance components). In all other respects, these protocols are identical. As the G/R protocol is only used for chapter 6, the methods specific to that protocol will be presented there, while all general methods applicable to both protocols are presented here.

Both eyes were stimulated with independent stimuli (dichoptic) displayed at 60 frames/s using two LCD displays (see Figure 2.16) with pupil measurements recorded at a rate of 60 frames/s. Those records were sub-sampled following interpolation to 30 frames/s to enhance reliability.

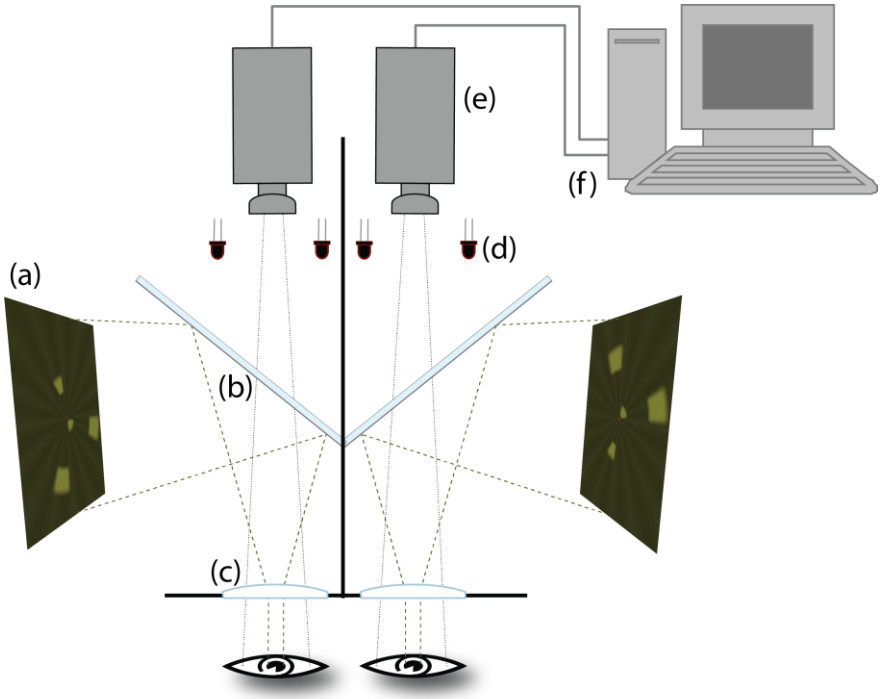

Figure 2.16: Demonstrates measurement of pupillary responses using the nuCoria device. Stimuli are presented separately on two LCD displays (a) and reflected off two cold dichroic mirrors (b) which reflect these short (visible) wavelengths while transmitting infrared light. Viewing distance was set to optical infinity by plano-convex lenses (c). Infrared illumination (d) passes through the dichroic mirrors and reflects off the irides to facilitate monitoring of each pupil by infrared video cameras (e) and recorded in real time onto a computer (f). Image reproduced with permission via personal communication from the author C. Carle.

There were 44 test-regions/eye, split across the vertical meridian in the shape of several segmented and overlapping annuli with larger regions peripherally and smaller regions centrally (see Figure 2.17). These regions were subdivided into 8 subsets by left and right eye, left and right hemisphere, and even or odd rings. Stimuli were presented in temporally sparse clustered volleys (Sabeti *et al.*, 2014) as outlined in Figure 2.18. Each volley activates an average of 50% of regions within the presented hemifield for 33 ms with a 250 ms delay

between onsets of each volley, sequentially rotating through presentations in each of the 8 subsets. Stimuli in each test region were presented on average every 4 seconds for a total of approximately 90 presentations per region throughout the test period of 360 seconds.

The two protocols (Y/Y and G/R) were completed on each visit for two visits (2 repeats of each protocol), with random allocation as to order of testing on the first occasion and the reverse order on repeat. Both protocols had a background luminance of 10 cd/m^2 and stimuli of maximum luminance of 150 cd/m^2. Due to intrinsic differences in sensitivity across the retina, both protocols employed luminance balancing across the field to maximise total signal to noise ratio, as described elsewhere (Maddess *et al.*, 2009).

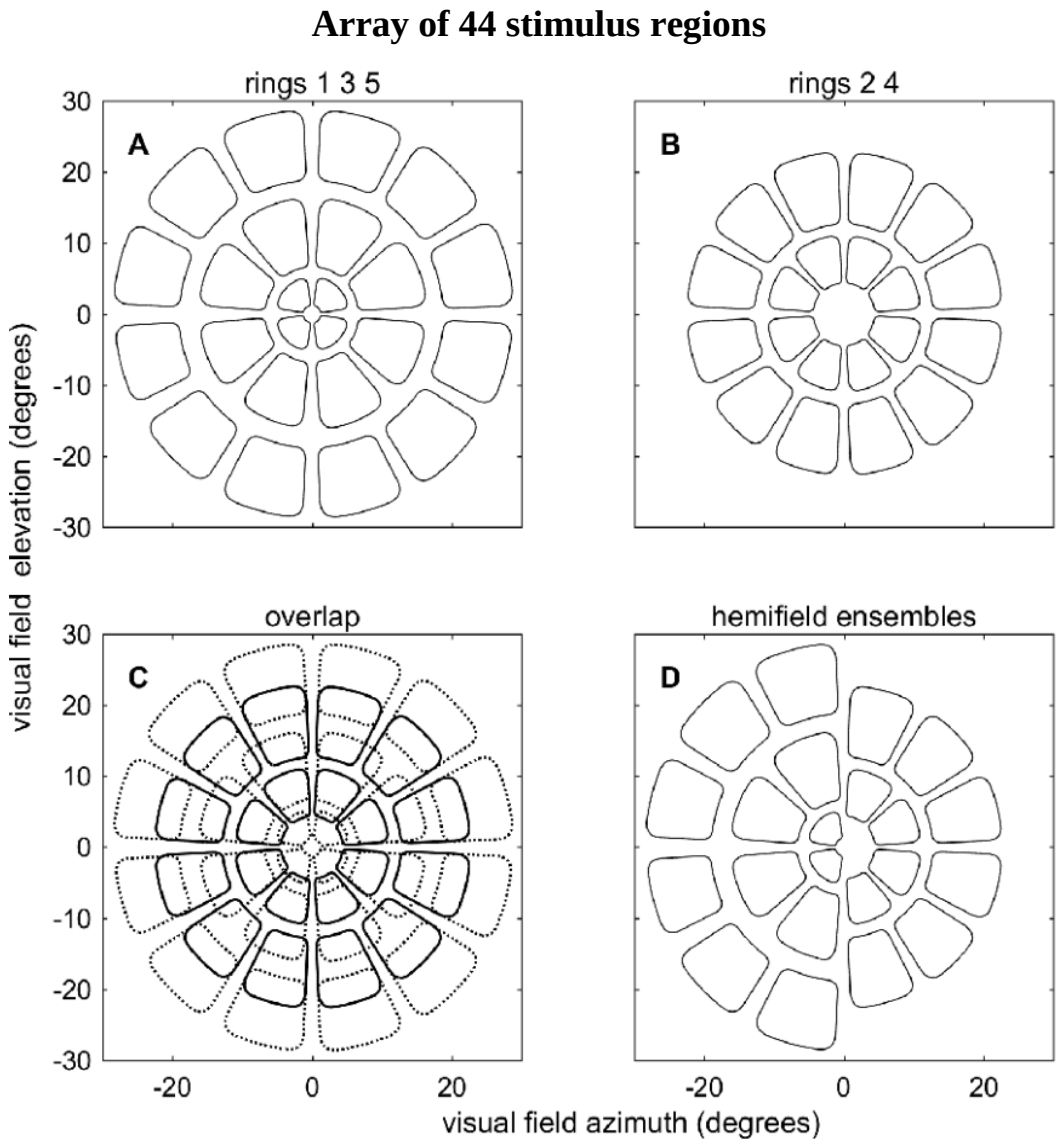

Figure 2.17: Illustration of the stimulus regions used in mfPOP protocols made up of five layers of rings totally 44 regions. (A) shows odd rings (1,3,5) which include the innermost and outermost layers. (B) show even rings (2,4) which partially overlap the odd rings. (C) presents all rings together with odd in bold, and (D) with odd (left) and even (right) adjacent to each other. This format is basic practice in mfPOP testing. Image reproduced with permission via personal communication from the author T. Maddess.

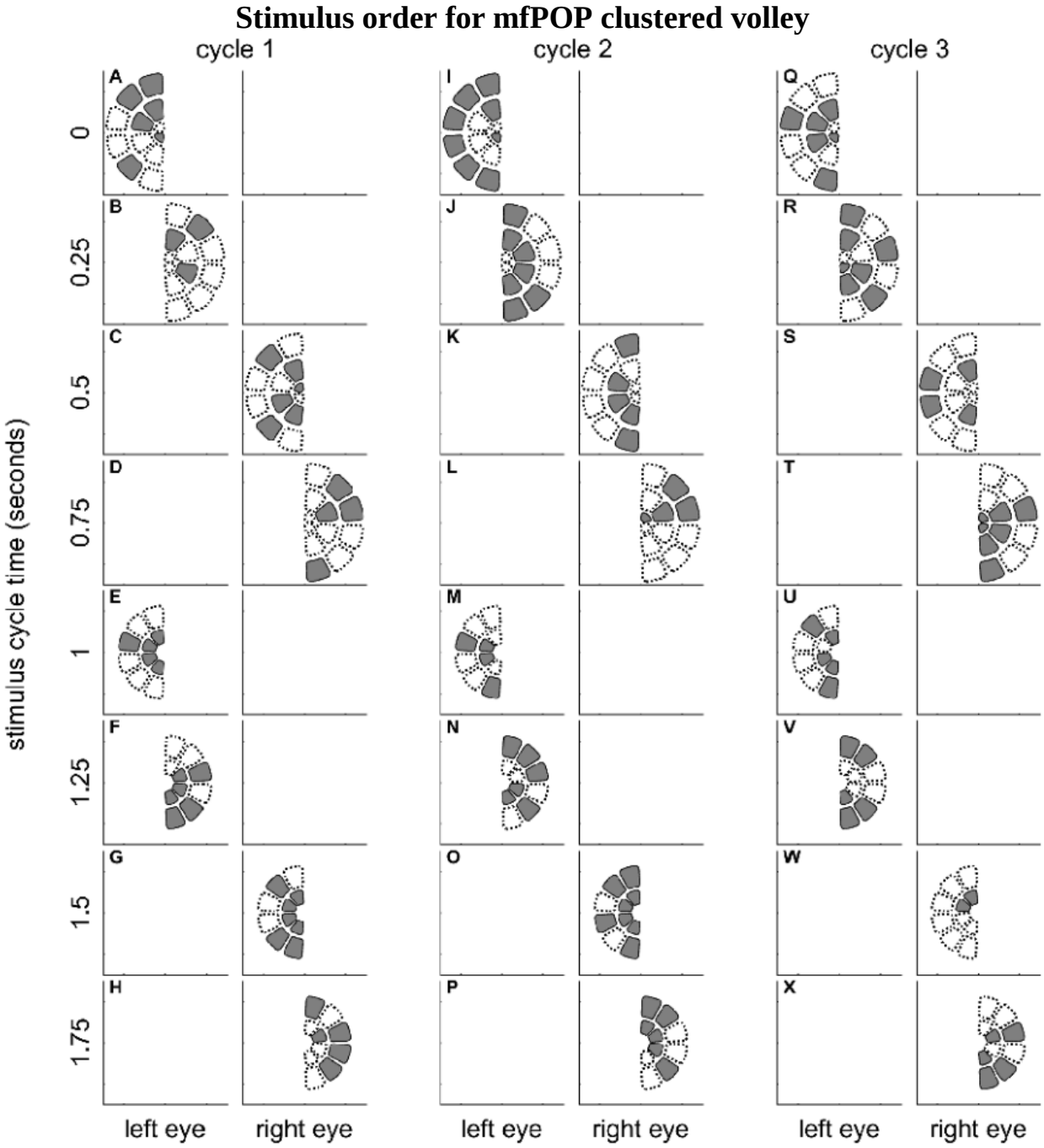

Figure 2.18: Schematic example of mfPOP clustered volley stimulus order. Stimuli are made temporally sparse by stimulating in order: (A) left eye, left hemifield, (B) left eye, right hemifield, (C) right eye, left hemifield, and (D) right eye, right hemifield. This order is first completed with odd rings (A–D) then even rings (E–H) before repeating each cycle. In each set of stimuli a cluster of pseudorandom regions are selected, with 50% of regions being activated on average, such that over the full duration of the test each region has a similar number of test-repeats. There is 250 ms between each set of stimuli, meaning there is a minimum of 2 seconds between activation of the same region, and on average 4 seconds due to pseudorandom selection. Image reproduced with permission via personal communication from the author T. Maddess.

2.5.3.2. Testing procedures

While mfPOP is insensitive to blur, its software includes an algorithm to keep trial lenses as similar as possible to reduce the effects of excessive blur. This is required as the trial lenses are not exactly at the spectacle distance. Ocular prescription was entered, automatically converted to spherical equivalent, and rounded to the nearest available lens: –9, –6, –3, 0, +3, +6, or +9 spherical dioptres. The stimuli had no spatial frequencies above 2 cycle/deg and so were little demodulated by refractive errors < 2 D (Phillips & Stark, 1977; Sabeti *et al.*, 2015). Prior to testing, subjects had their horizontal vergence aligned by presenting a large X in one eye and a plus-sign in the other; the horizontal alignment of the displays was then adjusted until these objects were fused at optical infinity. Subjects were instructed to fixate a smaller central plus-sign sustained throughout testing, and informed that they could blink as necessary but should attempt to keep this to a minimum except during breaks. In a routine test there were 9 segments each comprising ~40 seconds of test time with ~7 second breaks between each segment. The ambient light level of the test-room was recorded, and lights adjusted when necessary to keep constant at ~450 lux measured next to the mfPOP eye-pieces with a light-adaptation period of 3–5 minutes allowed prior to testing. Both eyes were tested simultaneously. Where subjects had drooping eye-lids affecting pupil diameter measures, teary eyes, or requested to stop, that segment was paused, and the duration of the break was noted before recommencement. Where there was substantial eye movement, or poor-quality signal due to excess blinking or drooping lids obscuring pupil measurement and causing data acquisition to fall below 85%, that segment was repeated. Where a second testing protocol was to follow, a minimum rest period of 3 minutes was allowed before commencing.

2.5.3.3. Output measures

Raw pupillary measures were divided by the average pre-stimulus pupil diameter through all segments and multiplied by the average diameter of 3.5 mm to produce magnitudes

standardised to 3.5 mm as reported elsewhere (James *et al.*, 2012). Response waveforms for each of the 44 test regions, each eye (left and right), and each component (direct and consensual) were extracted from the normalised pupillary responses using iterative non-linear regression as previously described (James *et al.*, 2005). From these waveforms the amplitude and latency could both be measured. Latency is further described in Chapter 6, while only amplitude is used for all other chapters, defined as the minimum height of the waveform corresponding to maximal pupillary constriction (µm).

Standardised amplitudes (µm) were converted into dB units using a generalised logarithm. The generalised log is suitable when a small amount of additive noise is present with multiplicative noise. This means it also accounts for noisy small dilations which can result in small negative values preventing typical transformation. The generalised log was of form:

$$\mathrm{Glog}(y, \lambda) = \log\left(\frac{y + \sqrt{y^2 + \lambda^2}}{2}\right),$$

with input value y and function operator λ which describes the point at which multiplicative noise begins to dominate linear noise. A λ value of 9 was selected by Prof. Ted Maddess as most appropriate for the dataset, by means of creating the most linear distribution of variance across the range. Practically, this means small values are taken as near-linear to accommodate the negative values while larger values having typical $\log_{10}$ decibel values. Values were then scaled for convenience to approximate the range of HFA and MFA devices by Prof. Ted Maddess, in order that values can be more easily compared, remembering that all devices have different physical measures and calculations of dB scales.

Response estimates for a given region had their standard error (SE) calculated by the regressive response estimation process, and a signal to noise ratio (SNR) calculated from the amplitude response divided by estimated SE (t-statistic). This allowed combination of direct and

consensual components to be combined into a single measure by weighting according to their SNR (reasoning and details in Chapter 4). Recall that since both eyes are stimulated and both pupils recorded there are 44 responses per eye and per pupil.

Finally, conversion from the 44-test region mfPOP map to the 54-region 24-2 format was done by weighted averages according to the relative contribution of the overlapping areas (Ruseckaite *et al.*, 2006). This allowed direct point-to-point comparison of the three devices all in dB, even though all three dB scales and input measures are entirely different.

2.6. MRI

In the TCH Neurology Department, it is standard practice to have a CT done on suspected stroke patients to confirm stroke and determine whether is it ischemic or haemorrhagic. While this may be effective at highlighting any bleeding, it is not particularly effective at highlighting ischemic damage or localising the damaged region. Consequently, some patients never have an MRI scan and diagnosis must rely solely on the CT for positional information of the lesion. As the penumbra region may show up on CT/MRI scans acutely, the final damaged post-stroke region may be smaller and of a different size/shape than originally demonstrated. Even with MRI, scan protocols vary in how effective they are at detecting new or old infarcts. For these reasons, an MRI was acquired for all stroke patients willing and able to do so in order to provide a more accurate description of their stroke infarct region. The protocol decided on was 3D fluid attenuated inversion recovery (FLAIR) scan, which is effective at highlighting post-stroke damage after the initial acute damage has dissipated. In addition, diffusion tensor imaging (DTI) was done with the aim of measuring tract damage. While this data was collected as part of these experiments, they were not able to be analysed due to specialist staff and time constraints, but may be reviewed for future publications.

References

Albonico A, Malaspina M & Daini R. (2017). Italian normative data and validation of two neuropsychological tests of face recognition: Benton facial recognition test and cambridge face memory test. *Neurol Sci* **38,** 1637-1643.

Ali EN, Maddess TL, Martin K, Borbelj A & Lueck CJ. (2015). Pupillary response to sparse multifocal stimuli in epilepsy patients. In *4th annual saudi epilepsy society conference*, ed. Al-Baradie RS, pp. 74-78. Neurosciences, Riyadh.

Altay Y, Altay MM, Demirok G, Balta O & Bolu H. (2016). Measurements of pupillary diameter and wavefront aberrations in pregnant women. *Scientifica (Cairo)* **2016,** 4129524.

Anderson AJ & Johnson CA. (2002). Mechanisms isolated by frequency-doubling technology perimetry. *Invest Ophthalmol Vis Sci* **43,** 398-401.

Anderson AJ & Johnson CA. (2006). Comparison of the asa, mobs, and zest threshold methods. *Vision Res* **46,** 2403-2411.

Anstis SM. (1970). Phi movement as a subtraction process. *Vision Res* **10,** 1411-1430.

Bailey MJ, Riddoch MJ & Crome P. (2004). Test-retest stability of three tests for unilateral visual neglect in patients with stroke: Star cancellation, line bisection, and the baking tray task. *Neuropsychol Rehabil* **14,** 403-419.

Baker CL, Jr. & Braddick OJ. (1982). The basis of area and dot number effects in random dot motion perception. *Vision Res* **22,** 1253-1259.

Bengtsson B, Heijl A & Olsson J. (1998). Evaluation of a new threshold visual field strategy, sita, in normal subjects. Swedish interactive thresholding algorithm. *Acta Ophthalmol Scand* **76,** 165-169.

Benton AL & Van Allen MW. (1968). Impairment in facial recognition in patients with cerebral disease. *Trans Am Neurol Assoc* **93,** 38-42.

Bhan A, Browning AC, Shah S, Hamilton R, Dave D & Dua HS. (2002). Effect of corneal thickness on intraocular pressure measurements with the pneumotonometer,

goldmann applanation tonometer, and tono-pen. *Invest Ophthalmol Vis Sci* **43,** 1389-1392.

Birch J. (2010). Identification of red-green colour deficiency: Sensitivity of the ishihara and american optical company (hard, rand and rittler) pseudo-isochromatic plates to identify slight anomalous trichromatism. *Ophthalmic Physiol Opt* **30,** 667-671.

Birch J. (2012). Worldwide prevalence of red-green color deficiency. *Journal of the Optical Society of America A, Optics, image science, and vision* **29,** 313-320.

Bouvier SE & Engel SA. (2006). Behavioral deficits and cortical damage loci in cerebral achromatopsia. *Cereb Cortex* **16,** 183-191.

Bowles DC, McKone E, Dawel A, Duchaine B, Palermo R, Schmalzl L, Rivolta D, Wilson CE & Yovel G. (2009). Diagnosing prosopagnosia: Effects of ageing, sex, and participant-stimulus ethnic match on the cambridge face memory test and cambridge face perception test. *Cogn Neuropsychol* **26,** 423-455.

Bowman KJ. (1982). A method for quantitative scoring of the farnsworth panel d-15. *Acta Ophthalmol* **60,** 907-916.

Braddick O. (1974). A short-range process in apparent motion. *Vision Res* **14,** 519-527.

Campbell FW & Green DG. (1965). Optical and retinal factors affecting visual resolution. *J Physiol* **181,** 576-593.

Cho SJ, Wilmer J, Herzmann G, McGugin RW, Fiset D, Van Gulick AE, Ryan KF & Gauthier I. (2015). Item response theory analyses of the cambridge face memory test (cfmt). *Psychol Assess* **27,** 552-566.

Chougule PS, Najjar RP, Finkelstein MT, Kandiah N & Milea D. (2019). Light-induced pupillary responses in alzheimer's disease. *Frontiers in neurology* **10,** 360-360.

Cleary R & Braddick OJ. (1990). Direction discrimination for band-pass filtered random dot kinematograms. *Vision Res* **30,** 303-316.

Croydon A, Pimperton H, Ewing L, Duchaine BC & Pellicano E. (2014). The cambridge face memory test for children (cfmt-c): A new tool for measuring face recognition skills in childhood. *Neuropsychologia* **62,** 60-67.

Duchaine B & Nakayama K. (2006). The cambridge face memory test: Results for neurologically intact individuals and an investigation of its validity using inverted face stimuli and prosopagnosic participants. *Neuropsychologia* **44,** 576-585.

Duchaine BC & Nakayama K. (2004). Developmental prosopagnosia and the benton facial recognition test. *Neurology* **62,** 1219-1220.

Duchaine BC & Weidenfeld A. (2003). An evaluation of two commonly used tests of unfamiliar face recognition. *Neuropsychologia* **41,** 713-720.

Eagle RA & Rogers BJ. (1996). Motion detection is limited by element density not spatial frequency. *Vision Res* **36,** 545-558.

Farnsworth D. (1943). The farnsworth-munsell 100-hue and dichotomous tests for color vision. *J Opt Soc Am* **33,** 568-578.

Ferber S & Karnath HO. (2001). How to assess spatial neglect--line bisection or cancellation tasks? *J Clin Exp Neuropsychol* **23,** 599-607.

Fredette MJ, Giguere A, Anderson DR, Budenz DL & McSoley J. (2015). Comparison of matrix with humphrey field analyzer ii with sita. *Optometry and vision science : official publication of the American Academy of Optometry* **92,** 527-536.

Furlan M & Smith AT. (2016). Global motion processing in human visual cortical areas v2 and v3. *J Neurosci* **36,** 7314-7324.

Gray KL, Bird G & Cook R. (2017). Robust associations between the 20-item prosopagnosia index and the cambridge face memory test in the general population. *R Soc Open Sci* **4,** 160923.

Halligan PW, Marshall JC & Wade DT. (1989). Visuospatial neglect: Underlying factors and test sensitivity. *Lancet* **2,** 908-911.

Halligan PW, Marshall JC & Wade DT. (1990). Do visual field deficits exacerbate visuo-spatial neglect? *J Neurol Neurosurg Psychiatry* **53,** 487-491.

Hawkins AS, Szlyk JP, Ardickas Z, Alexander KR & Wilensky JT. (2003). Comparison of contrast sensitivity, visual acuity, and humphrey visual field testing in patients with glaucoma. *J Glaucoma* **12,** 134-138.

Hepworth LR & Rowe FJ. (2018). Programme choice for perimetry in neurological conditions (popin): A systematic review of perimetry options and patterns of visual field loss. *Bmc Ophthalmol* **18,** 241.

Heutink J, de Haan G, Marsman JB, van Dijk M & Cordes C. (2019). The effect of target speed on perception of visual motion direction in a patient with akinetopsia. *Cortex* **119,** 511-518.

Humphreys GW, Quinlan PT & Riddoch MJ. (1989). Grouping processes in visual search: Effects with single- and combined-feature targets. *J Exp Psychol Gen* **118,** 258-279.

Ishihara S. (1918). Tests for color blindness. *Am J Ophthalmol* **1,** 457.

James AC, Kolic M, Bedford SM & Maddess T. (2012). Stimulus parameters for multifocal pupillographic objective perimetry. *J Glaucoma* **21,** 571-578.

James AC, Ruseckaite R & Maddess T. (2005). Effect of temporal sparseness and dichoptic presentation on multifocal visual evoked potentials. *Visual Neurosci* **22,** 45-54.

Julesz B. (1960). Binocular depth perception of computer-generated patterns. *Bell system technical journal* **39,** 1125-1162.

Julesz B. (1964). Binocular depth perception without familiarity cues. *Science* **145,** 356-362.

Julesz B. (1965). Texture and visual perception. *Sci Am* **212,** 38-48.

Julesz B. (1971). *Foundations of cyclopean perception*. The University of Chicago Press, Chicago.

Kaiser PK. (2008). Comparison of snellen versus etdrs protocol visual acuities performed by certified vision examiners. In *Association for Research in Vision and Ophthalmology*. Investigative Ophthalmology & Visual Science.

Kalloniatis M & Luu C. (2005). The perception of color. In *The organisation of the retina and the visual system*, ed. Kolb H, Fernandez E & Nelson R. University of Utah Health Science Center, Salt Lake City, Utah.

Kennerknecht I, Grueter T, Welling B, Wentzek S, Horst J, Edwards S & Grueter M. (2006). First report of prevalence of non-syndromic hereditary prosopagnosia (hpa). *Am J Med Genet A* **140,** 1617-1622.

Kennerknecht I, Plumpe N, Edwards S & Raman R. (2007). Hereditary prosopagnosia (hpa): The first report outside the caucasian population. *J Hum Genet* **52,** 230-236.

Khoury JM, Donahue SP, Lavin PJ & Tsai JC. (1999). Comparison of 24-2 and 30-2 perimetry in glaucomatous and nonglaucomatous optic neuropathies. *Journal of neuro-ophthalmology : the official journal of the North American Neuro-Ophthalmology Society* **19,** 100-108.

Kinyoun J, Barton F, Fisher M, Hubbard L, Aiello L & Ferris F, 3rd. (1989). Detection of diabetic macular edema. Ophthalmoscopy versus photography--early treatment diabetic retinopathy study report number 5. The etdrs research group. *Ophthalmology* **96,** 746-750; discussion 750-741.

Kolmel HW. (1988). Pure homonymous hemiachromatopsia. Findings with neuro-ophthalmologic examination and imaging procedures. *Eur Arch Psychiatry Neurol Sci* **237,** 237-243.

Kooistra CA & Heilman KM. (1989). Hemispatial visual inattention masquerading as hemianopia. *Neurology* **39,** 1125-1127.

Kruger PB & Pola J. (1986). Stimuli for accommodation: Blur, chromatic aberration and size. *Vision Res* **26,** 957-971.

Lam BL, Alward WL & Kolder HE. (1991). Effect of cataract on automated perimetry. *Ophthalmology* **98,** 1066-1070.

Legge GE, Mullen KT, Woo GC & Campbell FW. (1987). Tolerance to visual defocus. *J Opt Soc Am A* **4,** 851-863.

Li K & Malhotra PA. (2015). Spatial neglect. *Pract Neurol* **15,** 333-339.

Maddess T & Kulikowski JJ. (1999). Apparent fineness of stationary compound gratings. *Vision Res* **39,** 3404-3416.

Maddess TL, Kolic M, Essex RW & James AC. (2009). Balanced luminance multifocal pupillographic perimetry. In *Invest Ophthalmol Vis Sci*, pp. 5281.

Matsuura M, Hirasawa K, Murata H & Asaoka R. (2015). The relationship between visual acuity and the reproducibility of visual field measurements in glaucoma patients. *Invest Ophthalmol Vis Sci* **56,** 5630-5635.

McCourt ME & Jewell G. (1999). Visuospatial attention in line bisection: Stimulus modulation of pseudoneglect. *Neuropsychologia* **37,** 843-855.

McCourt ME & Olafson C. (1997). Cognitive and perceptual influences on visual line bisection: Psychophysical and chronometric analyses of pseudoneglect. *Neuropsychologia* **35,** 369-380.

McKeefry DJ, Watson JDG, Frackowiak RSJ, Fong K & Zeki S. (1997). The activity in human areas v1/v2, v3, and v5 during the perception of coherent and incoherent motion. *Neuroimage* **5,** 1-12.

McKone E, Hall A, Pidcock M, Palermo R, Wilkinson RB, Rivolta D, Yovel G, Davis JM & O'Connor KB. (2011). Face ethnicity and measurement reliability affect face recognition performance in developmental prosopagnosia: Evidence from the cambridge face memory test-australian. *Cogn Neuropsychol* **28,** 109-146.

McKone E, Wan L, Robbins R, Crookes K & Liu J. (2017). Diagnosing prosopagnosia in east asian individuals: Norms for the cambridge face memory test-chinese. *Cogn Neuropsychol* **34,** 253-268.

Micieli G, Tassorelli C, Martignoni E, Pacchetti C, Bruggi P, Magri M & Nappi G. (1991). Disordered pupil reactivity in parkinson's disease. *Clin Auton Res* **1,** 55-58.

Miller LJ, Mittenberg W, Carey VM, McMorrow MA, Kushner TE & Weinstein JM. (1999). Astereopsis caused by traumatic brain injury. *Arch Clin Neuropsych* **14,** 537-543.

Nakamura H, Kashii S, Nagamine T, Matsui Y, Hashimoto T, Honda Y & Shibasaki H. (2003). Human v5 demonstrated by magnetoencephalography using random dot kinematograms of different coherence levels. *Neurosci Res* **46,** 423-433.

Neitz M, G. GD & Neitz J. (2008). Visual acuity, color vision, and adaptation. In *Albert & jakobiec's principles and practice of ophthalmology*, 3rd edn, ed. Albert DM, Miller JW, Azar DT & Boldi BA. Saunders, Philadelphia.

Nunn JA, Postma P & Pearson R. (2001). Developmental prosopagnosia: Should it be taken at face value? *Neurocase* **7,** 15-27.

O'Connor AR, Birch EE, Anderson S, Draper H & Grp FR. (2010). The functional significance of stereopsis. *Invest Ophth Vis Sci* **51,** 2019-2023.

Paulson HL, Galetta SL, Grossman M & Alavi A. (1994). Hemiachromatopsia of unilateral occipitotemporal infarcts. *Am J Ophthalmol* **118,** 518-523.

Phillips S & Stark L. (1977). Blur - sufficient accommodative stimulus. *Doc Ophthalmol* **43,** 65-89.

Radcliffe NM. (2014). Hysteresis: A powerful tool for glaucoma care. *Review Ophthalmology* **21,** 50-57.

Raymond JE. (1994). Directional anisotropy of motion sensitivity across the visual field. *Vision Res* **34,** 1029-1037.

Ringman JM, Saver JL, Woolson RF, Clarke WR & Adams HP. (2004). Frequency, risk factors, anatomy, and course of unilateral neglect in an acute stroke cohort. *Neurology* **63,** 468-474.

Rorden C & Karnath HO. (2010). A simple measure of neglect severity. *Neuropsychologia* **48,** 2758-2763.

Ruseckaite R, Maddess T & James AC. (2006). Monocular and binocular multifocal visual evoked potentials in normal and multiple sclerosis subjects. *Mult Scler* **12,** S166-S166.

Sabeti F, Maddess T, Essex RW, Saikal A, James AC & Carle CF. (2014). Multifocal pupillography in early age-related macular degeneration. *Optometry and vision science : official publication of the American Academy of Optometry* **91,** 904-915.

Sabeti F, Nolan CJ, James AC, Jenkins A & Maddess T. (2015). Multifocal pupillography identifies changes in visual sensitivity according to severity of diabetic retinopathy in type 2 diabetes. *Invest Ophthalmol Vis Sci* **56,** 4504-4513.

Scherf KS, Elbich DB & Motta-Mena NV. (2017). Investigating the influence of biological sex on the behavioral and neural basis of face recognition. *eNeuro* **4**.

Schutz AC, Braun DI, Movshon JA & Gegenfurtner KR. (2010). Does the noise matter? Effects of different kinematogram types on smooth pursuit eye movements and perception. *J Vision* **10**.

Shah S, Chatterjee A, Mathai M, Kelly SP, Kwartz J, Henson D & McLeod D. (1999). Relationship between corneal thickness and measured intraocular pressure in a general ophthalmology clinic. *Ophthalmology* **106,** 2154-2160.

Shamir RR, Friedman Y, Joskowicz L, Mimouni M & Blumenthal EZ. (2016). Comparison of snellen and early treatment diabetic retinopathy study charts using a computer simulation. *Int J Ophthalmol-Chi* **9,** 119-123.

Short RA & Graff-Radford NR. (2001). Localization of hemiachromatopsia. *Neurocase* **7,** 331-337.

Simunovic MP. (2010). Colour vision deficiency. *Eye (Lond)* **24,** 747-755.

Stark LR & Atchison DA. (2002). Monocular accommodation response for totally occluded objects. *Optometry and vision science : official publication of the American Academy of Optometry* **79,** 658-666.

Stark LR, Lee RS, Kruger PB, Rucker FJ & Ying Fan H. (2002). Accommodation to simulations of defocus and chromatic aberration in the presence of chromatic misalignment. *Vision Res* **42,** 1485-1498.

Steward JM & Cole BL. (1989). Incidence of congential colour vision defects in an australian optometric population. In *Colour vision deficiencies IX*, ed. Drum B & Verriest G, pp. 109-111. Springer, Dordrecht.

Stodtmeister R. (1998). Applanation tonometry and correction according to corneal thickness. *Acta Ophthalmol Scand* **76,** 319-324.

Stone SP, Halligan PW & Greenwood RJ. (1993). The incidence of neglect phenomena and related disorders in patients with an acute right or left hemisphere stroke. *Age Ageing* **22,** 46-52.

Sunderland A, Wade DT & Langton Hewer R. (1987). The natural history of visual neglect after stroke. Indications from two methods of assessment. *Int Disabil Stud* **9,** 55-59.

Taravati P, Woodward KR, Keltner JL, Johnson CA, Redline D, Carolan J, Huang CQ & Wall M. (2008). Sensitivity and specificity of the humphrey matrix to detect homonymous hemianopias. *Invest Ophth Vis Sci* **49,** 924-928.

Vaina LM. (1995). Akinetopsia, achromatopsia and blindsight: Recent studies on perception without awareness. *Synthese* **105,** 253-271.

Wall M, Punke SG, Stickney TL, Brito CF, Withrow KR & Kardon RH. (2001). Sita standard in optic neuropathies and hemianopias: A comparison with full threshold testing. *Invest Ophthalmol Vis Sci* **42,** 528-537.

Warrington EK. (1984). *Recognition memory test: Manual*. NFER-Nelson, Berkshire, UK.

Whitacre MM, Stein RA & Hassanein K. (1993). The effect of corneal thickness on applanation tonometry. *Am J Ophthalmol* **115,** 592-596.

Wild JM, Searle AE, Dengler-Harles M & O'Neill EC. (1991). Long-term follow-up of baseline learning and fatigue effects in the automated perimetry of glaucoma and ocular hypertensive patients. *Acta Ophthalmol (Copenh)* **69,** 210-216.

Wolfs RC, Klaver CC, Vingerling JR, Grobbee DE, Hofman A & de Jong PT. (1997). Distribution of central corneal thickness and its association with intraocular pressure: The rotterdam study. *Am J Ophthalmol* **123,** 767-772.

Wooten BR. (1981). Partial cerebral achromatopsia with selective hue loss. In *International research group on colour vision deficiencies symposium*, ed. Verriest G. Dr W. Junk Publishers, Berlin.

Zeki S. (1990). A century of cerebral-achromatopsia. *Brain* **113,** 1721-1777.

Zhang Q, Shi J, Luo Y, Liu S, Yang J & Shen M. (2007). Effect of task complexity on intelligence and neural efficiency in children: An event-related potential study. *Neuroreport* **18,** 1599-1602.

Zhou C, He Y & Li X. (2018). Cerebral achromatopsia secondary to ischemic stroke. *Neurol India* **66,** 573-575.

Appendix A: Line Bisection Test

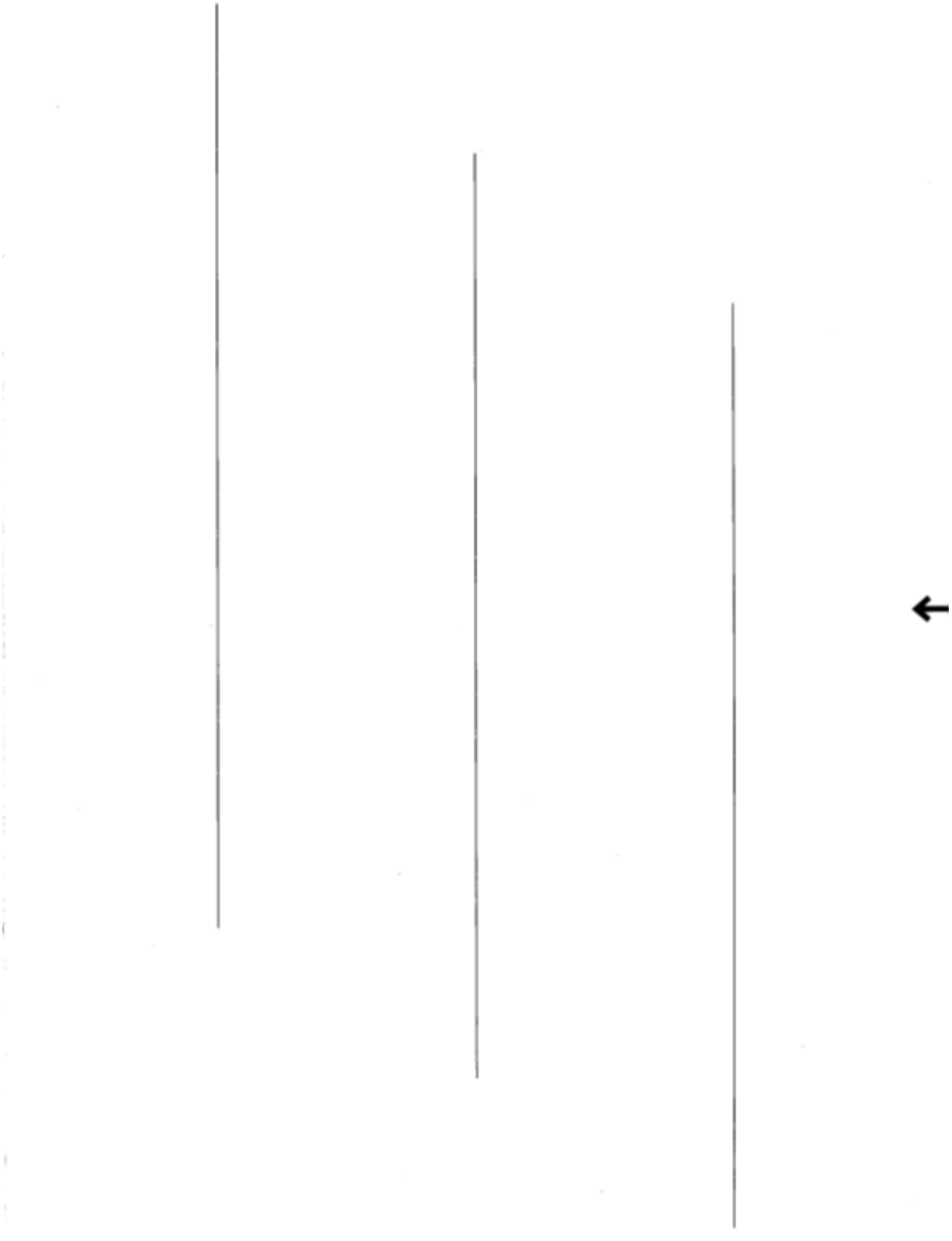

Appendix B: Star Cancellation Test

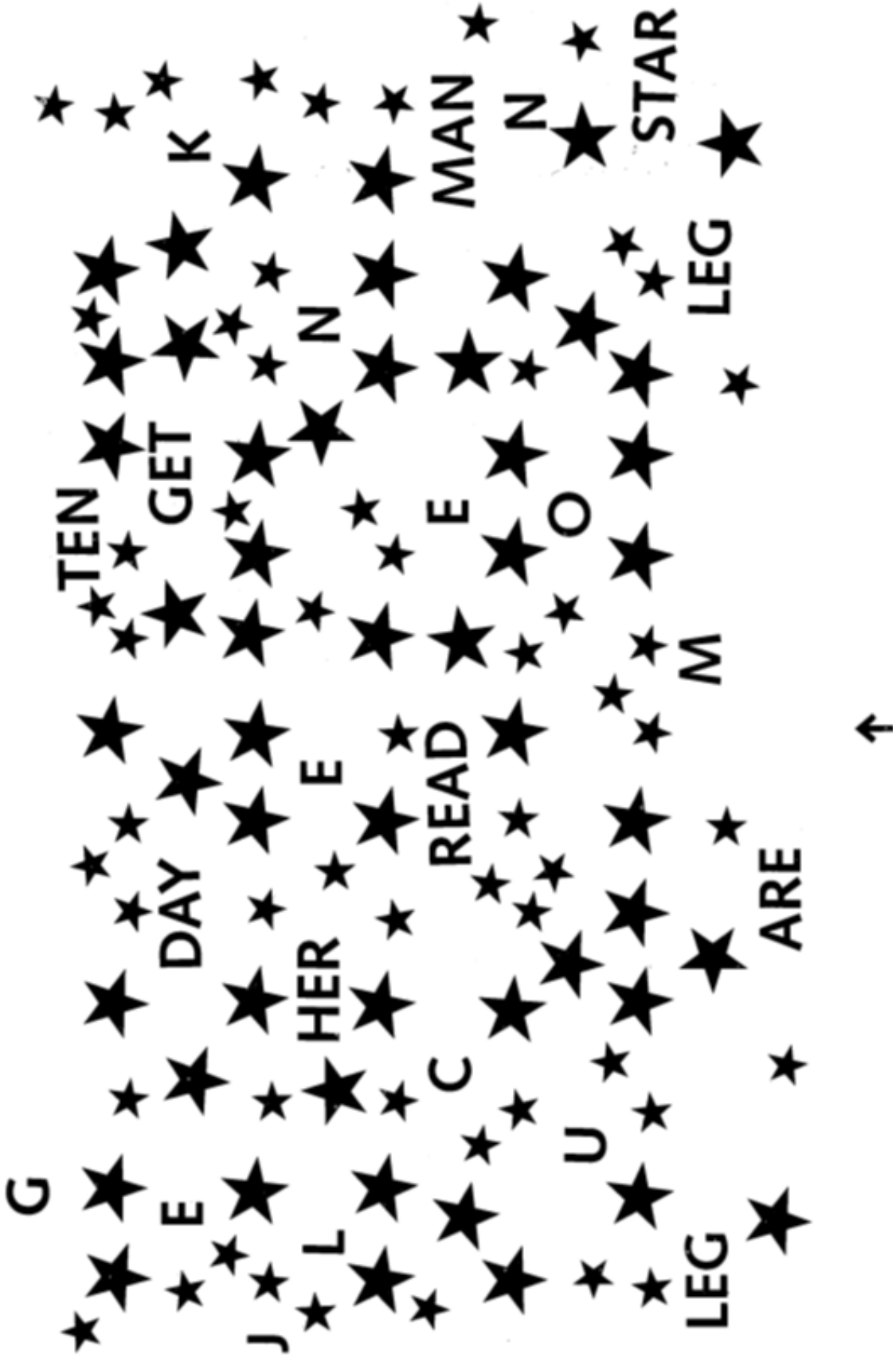

Chapter 3: Higher visual function loss and its assessment in stroke

3.1. Abstract

3.1.1. Purpose

This study investigated higher visual function deficits in perception of colour, facial recognition, stereopsis, and coherent global motion, as a pilot to determine if subtle deficits are common in stroke patients and which methods are most effective in detecting them.

3.1.2. Methods

Stroke patients (n = 24) and controls (n = 26) were tested using a test battery of Ishihara, Farnsworth–Munsell D15, Cambridge Facial Memory Test, stereofly, randot, and random dot kinematogram as outlined in the general methods section. Receiver operator characteristics with bootstrap were produced to calculate appropriate threshold values, their rates of presentation, and area under curve (AUC) was calculated to indicate which tests were most valuable. Principal component and mean likelihood analysis with scree plots were also used to indicate tests which account for the most variability in responses, providing other measures of test diagnostic value and indicating which tests groups measure the same component.

3.1.3. Results

Stereofly, randot and Ishihara reached significance ($p < 0.01$) for AUC with means and SD of 0.79 ± 0.08, 0.76 ± 0.09, and 0.73 ± 0.08 respectively. No other variables reached significance. At false positive ratios (FPRs) of 5%, 10%, and 20%, stereofly, Ishihara, and randot had the highest sensitivities with values of 20–30%, 35–40%, and 60%. At very low FPRs of 2% and 5%, Farnsworth–Munsell performed equal or better to these test variables. Principal component scree plots suggested two or three components, representing 48% and 63% variance. Both were

examined, revealing that the primary component was predominantly stereofly and randot, while the secondary component was CFMT with Farnsworth–Munsell.

3.1.4. Conclusions

Stereovision as measured by stereofly or randot shows significant deficits in stroke patients compared to controls, with stereofly having marginally better sensitivities across the useful range. Combining tests would be of limited usefulness given they both load onto the same factor. Colour vision as measured by Ishihara also shows significant deficits. While the other colour vision test (Farnsworth–Munsell) provides some utility, it did not reach significance alone. Given that colour vision does appear to be affected, and that Farnsworth–Munsell D15 approached significance, there may be some utility in using the larger more robust FM100. Combination of CFMT with FM appears likely to be due to close localisation anatomically, in contrast to SF and RD which are functionally similar.

3.2. Introduction

Based on many case reports following stroke, it is well established that deficits in higher visual function occur – such as visual neglect[11] (Cherney & Halper, 2001; Pollock *et al.*, 2011), achromatopsia[12] (Setala & Vesti, 1994; Bartolomeo *et al.*, 1997; Duvelleroy-Hommet *et al.*, 1997; Cowey *et al.*, 2008; von Arx *et al.*, 2010; Pagani *et al.*, 2012; Carota & Calabrese, 2013; Bartolomeo *et al.*, 2014; Zhou *et al.*, 2018), prosopagnosia[13] (Lander *et al.*, 2004; Lu *et al.*, 2005; Lang *et al.*, 2006; Fox *et al.*, 2011; Heutink *et al.*, 2012), akinetopsia[14] (Vaina, 1994; Rizzo *et al.*, 1995; Barton *et al.*, 1996; Vaina *et al.*, 2001; Cooper *et al.*, 2012), and astereopsis[15] (Ross, 1983; Schaadt *et al.*, 2014; Schaadt *et al.*, 2015; Schow *et al.*, 2016). However, little work has been done in identifying less overt deficits and the relative frequency of these conditions in the stroke population.

This study investigated higher visual function deficits in perception of colour (using Ishihara and Farnsworth–Munsell), facial recognition (using the Cambridge Face Memory Test [CFMT]), stereopsis (using stereofly & randot), cohesive motion (kinematogram) and visual neglect (line bisection and star cancellation). We used them to identify whether any deficits are common in stroke patients and to determine which methods are most effective in detecting impairment. Given the heterogeneity of stroke presentation, and the relatively small sample size of 24 (against 26 controls), this was only intended as a pilot to test a broad range of methods

[11] Visual pathway remains intake, but does not conciously acknowledge items on side contralateral to lesion.
[12] Inability to recognise colours, seeing the world in grey, following a cortical lesion. More subtle defects may diminish colour sensitivity without being blind to colour.
[13] Inability to recognise faces and unique features of faces, following a cortical lesion. In the most severe cases, they cannot recognise their own face, while more subtle defects may make discerning between faces difficult.
[14] Inability to decern motion either generally (seeing all motion as series of static images) or in motion coherence (cannot detect cohesive motion from noise).
[15] Inability to use binocular vision to produce three-dimensional percept. May reply on other feautres or in severe cases perceive the world as flat.

which might then be refined in a larger study, one less demanding of subject test-time and having more definitive outcomes.

3.3. Methods

Full methods, including recruitment, reasoning for test selection, and their administration can be found in General Methods (Chapter 2). Only a summary is provided here for convenience. As outlined in General Methods 2.1, there is evidence for both the functional specialisation of cortical processing based on isolated deficits, although rare (Vaina, 1995), and distributive model of cortical processing, based on selective stimuli activating many cortical areas (McKeefry *et al.*, 1997; Furlan & Smith, 2016). This study recruited stroke subjects without consideration of cortical location, because we already know that isolated deficits are rare, but do not know the extent of more subtle deficits, which do not have established locations.

A total of 24 stroke subjects (non-selective to location) were recruited, along with 26 control subjects. Both groups were screened for visual impairment due to retinal disorders using both a questionnaire and ophthalmic equipment, and they met the acuity criteria of best-corrected visual acuity of logMAR >0.5 (6/19). All subjects then completed a series of higher visual function tests outlined below.

3.3.1. Higher visual function tests

The HVF tests are listed below. In order to complete a principal component analysis (PCA), a single measure is required for each test, and so summary variables were made for tests with multiple measures – these are summarised in Table 3.1**Error! Not a valid bookmark self-reference.** along with the abbreviation code used in graphing.

Table 3.1: Higher visual function tests, summary variables, and short-codes.

Short code	Test	Summary variable
LB	Line bisection: 3 × 19 cm lines from behavioural inattention test (Wilson *et al.*, 1987)	Average error from 3 lines (mm)
Ishi	Ishihara 24-plate set (Ishihara, 1918)	Sum of correct answers (both eyes)
FM	Farnsworth-Munsell D-15 dichotomous test (Farnsworth, 1947)	Colour confusion index: sum of the hue difference of selected well order over ideal well order (Bowman, 1982).
CFMT	Cambridge Facial Memory Test (Duchaine & Nakayama, 2006)	Sum of correct answers (all 3 sections)
RD	Randot dot 3 with Lea symbols (Vision Assessment Corporation, 2012, Illinois USA)	Minimum threshold achieved in test
SF	The fly stereo acuity test with Lea symbols (Vision Assessment Corporation, 2007, Illinois USA)	Minimum threshold achieved in test
Km	Kinematogram (custom design)	Minimum threshold achieved in test

3.3.1.1. Reliability of higher visual function tests

The sensitivities of these tests are unknown in the stroke population, which is the purpose in comparing with controls in this study. While sensitivity may be unknown, the reliability of many of these tests has been previously reported, which may inform if they are likely to be internally consistent.

Line bisection in terms of the Schenkenberg line bisection test showed intraclass correlation coefficients for intra-rater reliability between 0.82-1 (Stone *et al.*, 2019), although it should be acknowledged that the standard line bisection test used for this study has fewer lines to bisect.

A report of the quantitative reliability of the Ishihara for normal controls could not be found, although it has been qualitatively reported as having high test-retest reliability with 102 normal subjects scoring ≤3 errors on both of two attempts (Johnson, 1992). The Farnsworth-Munsell D15 assessed using the same colour-confusion index (CCI) as this study, showed the mean difference between test and retest of -0.02 ± 0.128 which is a small difference but with substantial variability. The resulting intraclass correlation coefficient was 0.56 (95% confidence interval 0.43-0.67) which shows questionable reliability (Good *et al.*, 2005). Various groups report a CFMT Cronbach's alpha reliability between 0.83-0.88 (Herzmann *et al.*, 2008; Bowles *et al.*, 2009; Wilmer *et al.*, 2010), considered high by the standard of cognitive tasks. The randot stereovision test is more commonly administered in children, with reliability in those aged 4-10 years showing within-subject variation of 1.57 (95% CI 1.44-1.71) randot plates (Adler *et al.*, 2012), with those in the older age groups showing greater stability between testing. In adults with stable strabismus, stereoacuity measured on consecutive visits showed differences of 0.59 log arcsec equating to 1.95 octave steps of difference (Adams *et al.*, 2009). Together these suggest that the randot stereovision test is moderately stable in those without visual impairment, but likely has greater test-retest variability in those with impaired stereopsis. Similar results were demonstrated in stereofly stereo acuity test, suggesting those with impaired stereopsis (>160 arcsec) become increasingly variable in their responses (Fawcett & Birch, 2003). As the random dot kinematogram is an original test, there is no reported reliability measure, although anecdotally unaffected staff members showed similar results on repeats prior to study commencing, while during the study it was noted a few subjects scored substantially differently on repeat, leaving reliability uncertain.

3.3.2. Receiver operator characteristics and thresholds

In clinical practice, tests routinely require a 'normal range' or 'threshold' to allow categorisation into normal or abnormal for diagnosis and treatment purposes. The aim is to distinguish between two distributions: 'normal' patients who do not have the disease, and 'abnormal' patients who do (Nettleman, 1988; Junge & Dettori, 2018).

In this study, the equivalent groups are 'control' and 'stroke', where their diagnostic status is already known, while the sensitivity and specificity of the psychophysical tests we are trialling are not. Naturally, sensitivity and specificity depend on what threshold is used to demarcate between normal and abnormal, and one way of measuring how well a test performs at all possible thresholds is using a receiver operator characteristic (ROC) plot, with its overall quantitative performance being reflected in its area under the curve (AUC) (Nettleman, 1988; Junge & Dettori, 2018). This study is not interested in the diagnostic capacity of HVF tests to detect stroke, but rather whether HVF deficits exist in the stroke population (as compared to controls). As the threshold for demarcating between a 'normal' and an 'abnormal' is not well established, ROC plots provide a means to assess relative diagnostic power.

To illustrate this, Figure 3.1 shows a range of possible distributions, from perfect score for AUC of 1, to a minimal (chance) score of 0.5. A perfect test has a sensitivity of 100% (all stroke patients have abnormal result) with a false-positive ratio (FPR) of 0% (no controls have abnormal result). In comparison, a test which had no power to discern between groups (chance level) would have a sensitivity of 50% and a FPR of 50%, indicating a person from either group would be equally likely to be classified as having an abnormal result. The beauty of this technique is that all potential thresholds are attempted, allowing the user to select an appropriate sensitivity or specificity which is appropriate to the context.

In practice where the result may prompt an invasive clinical decision, there is generally a low threshold for false positives, while in screening where follow-up is not invasive, keeping sensitivity high may be more important. The context often determines what an appropriate value is, and for these purposes the ROC provides information about all possible values across every possible threshold, while also providing a quantitative measure of overall diagnostic performance.

In this study, it is not known how common a deficit is in the stroke population or in the normal population; however it would be fair to assume that to identify a deficit due to stroke, it would have to be sufficiently different to the normal population. In psychophysical tests like this, a threshold which categorises the lowest scoring 5% of the population as abnormal is commonly used, and will be presented alongside the recommended threshold. On a ROC curve, this corresponds to a FPR of 5%, and the sensitivity at this threshold represents how common a deficit is in the stroke population.

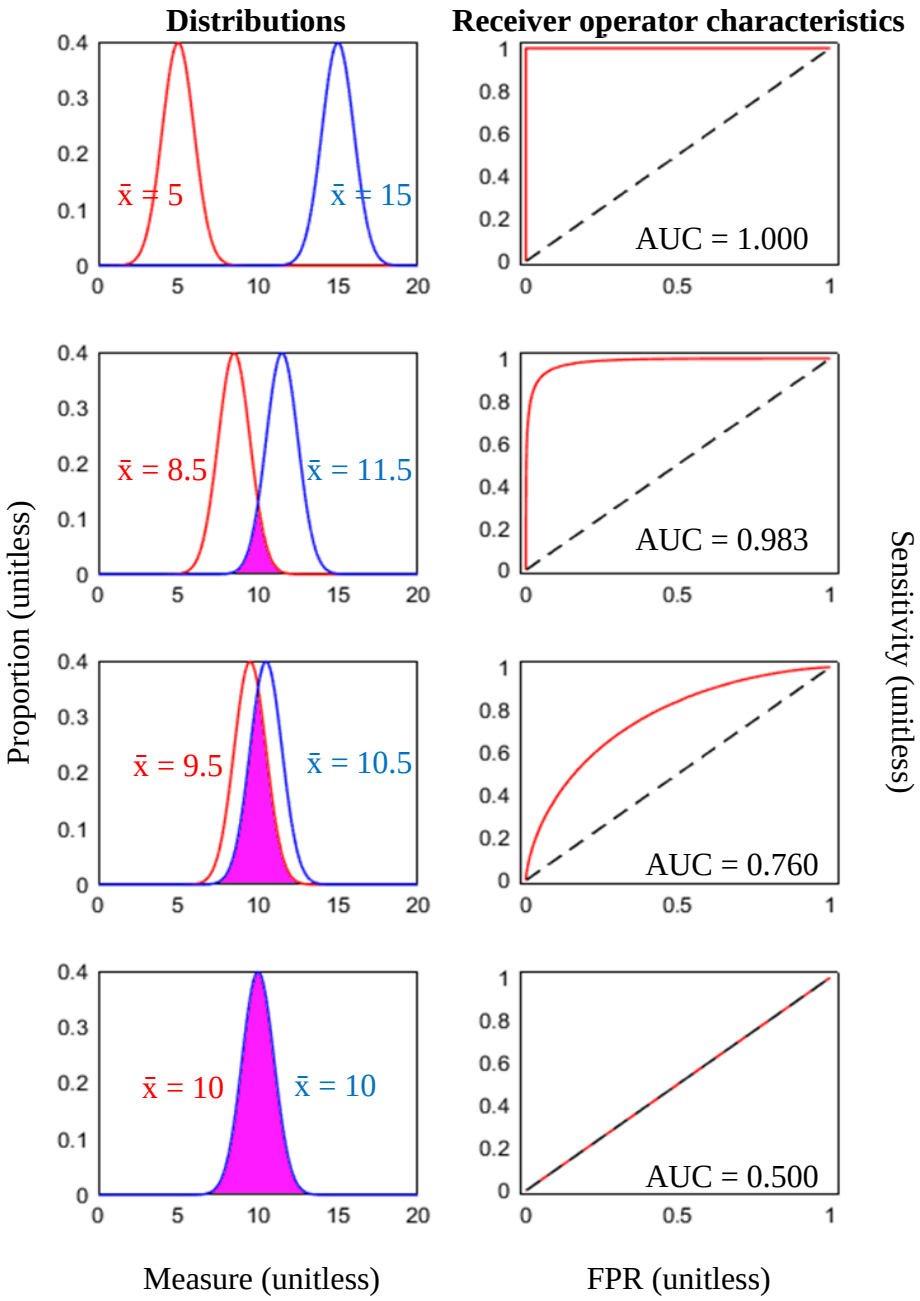

Figure 3.1: Comparison of different distributions with their receiver operator characteristics (ROC) plots for hypothetical distributions of a test measure.

Left: Hypothetical distributions for normal (blue) and disease (red) with increasingly overlapping distributions highlighted in pink. Distributions are evenly spaced either side of 10 with SD of 1, and progressively made closer until they completely overlap.

Right: Associated ROC plots showing sensitivity against false-positive ratio (FPR) plotted in red, chance line (black dashed), and their area under the curve (AUC). When distributions are independent, the AUC is 1.000 and where they completely overlap, the AUC is 0.500.

3.3.3. Principal component analysis and mean likelihood ratios

Principal component analysis (PCA) is a statistical operation on a dataset with multiple variables, which may or may not be correlated, with the aim of achieving data reduction and highlighting those variables which provide the most information. It determines orthogonal (independent) vectors, called factors, which explain the greatest variance in the dataset. These factors are the principal components, with the first explaining the most variance and each subsequent factor explaining large fractions of the remaining variance. Collectively, there are the same number of factors as there are variables, and the sum of their weighting or factor scores is 1 (Wold et al., 1987; Jolliffe & Cadima, 2016; Lever et al., 2017). An example is provided in Figure 3.2, using 2-dimensional data for ease of visualisation. It highlights that components may orient to any direction, that each subsequent component must explain equal or less variance than the one before, and that factor scores always sum to 1. While in 2-dimensional data there are only two components, restricting the second to a single plane, in data sets with more dimensions there may be many orthogonal planes a component may take, with the total number of components equal to the number of variables used.

When there are many variables it is impractical to consider all the factors, and so in determining which of the factors should be included, it is useful to know the sum-total amount of variance explained by the preceding factors, which can be demonstrated in a scree plot. It may also be useful to look at how much each variable contributes to a given component, also known as its *loading*. If a factor score is high and only a few variables predominate with high loadings, then these are the variables with the most value (while others just correlate with these and contribute little additional information). While each component has a loading value for all its variables, when including multiple components in the model, the variable *communalities* may be more useful, as it describes the total amount of variance in that variable accounted for by all the included components (defined as the sum of square factor of loadings for that variable).

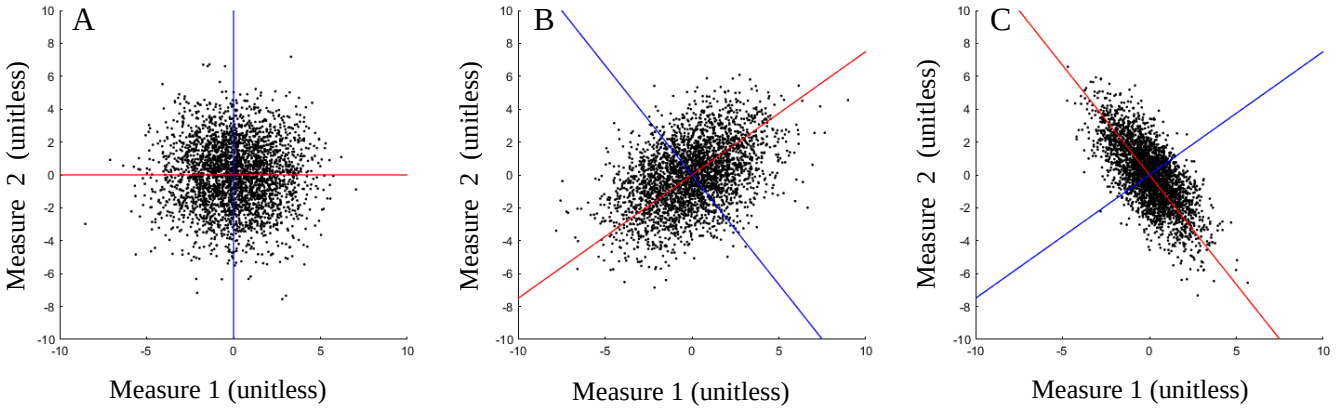

Figure 3.2: Examples of 2-dimensional data with its primary (red) and secondary (blue) principal components.

(A) Equal variance in all directions – so the primary principal component may be in any direction; however its secondary component must be orthogonal. Due to equal variance throughout, both components will explain the same amount of variance and their loadings with be equal (i.e. 1^{o} = 0.5 and 2^{o} = 0.5).

(B) Greater variance diagonally – so the direction of the primary principal component aligns with greatest variability (angled upwards) and explains almost twice the variance, so it will have a weighting twice as large as the second component (i.e. 1^{o} = 0.66 and 2^{o} = 0.33).

(C) Larger variability diagonally – again the direction of the primary component aligns with greatest variability (angled downwards). This that highlights the component may be in any direction. Here the primary component explains markedly more variability than the second and will be many times larger (i.e. 1^{o} = 0.8 and 2^{o} = 0.2).

Maximum likelihood analysis (MLA) is an alternative form of principal component analysis with less restrictive criteria as to the orthogonal nature of sequential components, and which may uncover factors that are more natural. It uses a different approach to optimisation but provides similar output measures. In considering which better explains the data, both PCA and MLA can be compared, using their mean communalities for an equal number of components.

3.4. Results

3.4.1. Receiver operator characteristics

Below are separately presented results for all seven test variables using ROC and Thresholds for stroke patients, compared to controls. In each graph the bootstrap randomly sampled (with

replacement) from the 24 stroke subjects 24 times (and the 26 control subjects 26 times) to generate a new population each time, producing subtly different ROC plots, allowing the possibility that the same sample might be selected multiple times and create a more varied ROC plot. When repeated many times, and all varied ROC plots are combined, it generates a distribution of values allowing an unbiased measure of mean and standard deviation across the entire range, providing a smooth curve and a measure of error. The larger the number of bootstrap repeats, the more stable the final mean values. Repeated trials showed bootstrap values of 100,000 were sufficient for the area under curve (AUC) to be accurate to the nearest two decimal places, but due to ease of calculation 1,000,000 repeats better pictorially demonstrated the method with smoother curves, and so was used in the final calculations. All graphs have been standardised in this presentation:

Top Left: Shows a 2D histogram heatmap of all bootstrapped ROC plots with logarithmic scales such that bright values show areas of relative density and darker areas low density. Due to there being 24 patients and 26 controls, there are 24 possible changes in the sensitivity and 26 in the FPR, resulting in a pixilation effect. This shows the full range and relative count of how common each ROC bootstrap was with a calculation of the mean and standard deviation of the data set.

Bottom Left: Shows the mean (full line), ± 1 standard deviation (dotted lines) based on the ROC heatmap. The dashed diagonal line represents chance. Values for the area under the curve (AUC) for each test are presented in a table following the ROC plots.

Top Right: Shows a 2D histogram heatmap of all bootstrapped threshold plots on a logarithmic scale. While threshold should be a continuous measure, due to the sample size or test construction, there are values for which there is no response, resulting in some of the binned

values showing up as horizontal gaps in the data. Where this occurs, data is extrapolated to the next valid data point.

Bottom Right: Shows the mean (full line) ± 1 standard deviation (dotted lines) based on the threshold heatmap. This can be directly compared with ROC maps at areas with the same FPR value and outlines what the reference threshold is for each ROC value. It also indicates the relative distribution of respondents, with a shallow slope representing many respondents and a steep slope representing relatively few.

Line bisection (Figure 3.3) and kinematogram (Figure 3.6) both performed below chance, suggesting stroke subjects marginally outperformed controls. This suggests damage in these visual functions is either very minimal, or that the tests used are not effective in detecting visual deficits. Line bisection and kinematogram also both has evening distributed results over their lower range (normal scores), with relatively few results in the upper range (abnormal scores).

Farnsworth-Munsell (FM; Figure 3.8) and Cambridge Facial Memory Test (CFMT; Figure 3.9) both scored marginally above chance, although for very different reasons. FM had a large number of subjects with perfect scores (CCI 1.0), including 81% of controls and 64% of stroke subjects, meaning there is no data for high FPR scores, as it is not possible to differentiate between identical scores. The result was FM did not have much power to resolve difference between stroke and control subjects. A more challenging test with greater well number and finer colour differences may improve ability to demarcate between groups. CFMT, on the other hand, suffered from many controls having poor scores, therefore not being able to clearly differentiate between low scoring individuals. This is somewhat surprising, but with an elderly population having reduced working memory, this may explain why results are below expectations. The test may be improved by either making the test easier or lowering the minimum chance score. Using the newer Australian CFMT, rather than the version used here

(faces from Boston residents), may improve scores as Australian test subjects have been shown to score better on Australian faces (McKone *et al.*, 2011). Likewise, the minimum chance score could be reduced by including more distractor faces, such that rather than a force 3-person forced choice (33% chance), there is a 5-person forced choice (20% chance).

Randot (Figure 3.4), stereofly (Figure 3.5), and Ishihara (Figure 3.7) all performed well above chance. Interestingly, both measure of stereovision (randot and stereofly) have very similar ROC plots and threshold shapes, although subjects scored much lower thresholds on stereofly than randot, suggesting stereofly is an easier test of stereovision. Ishihara also suffered from some similar effects to that of FM, in that many subjects scored very highly, so reducing the dynamic range of the test. However, Ishihara still performed well in differentiating stroke and control subjects, with subtle but consistently lower scores in the stroke group.

Overall, the best shaped plots were randot, stereofly, and Ishihara. FM and CFMT tests showed some potential but need modification to test closer to the middle of their range. Line bisection and kinematogram show little utility. To better summarise and compare results, a table summary is provided with calculation of the AUC, SD, and *p*-values (Table 3.2).

Line Bisection Receiver Operator Characteristics with Thresholds for Bootstrap (*n*=1,000,000)

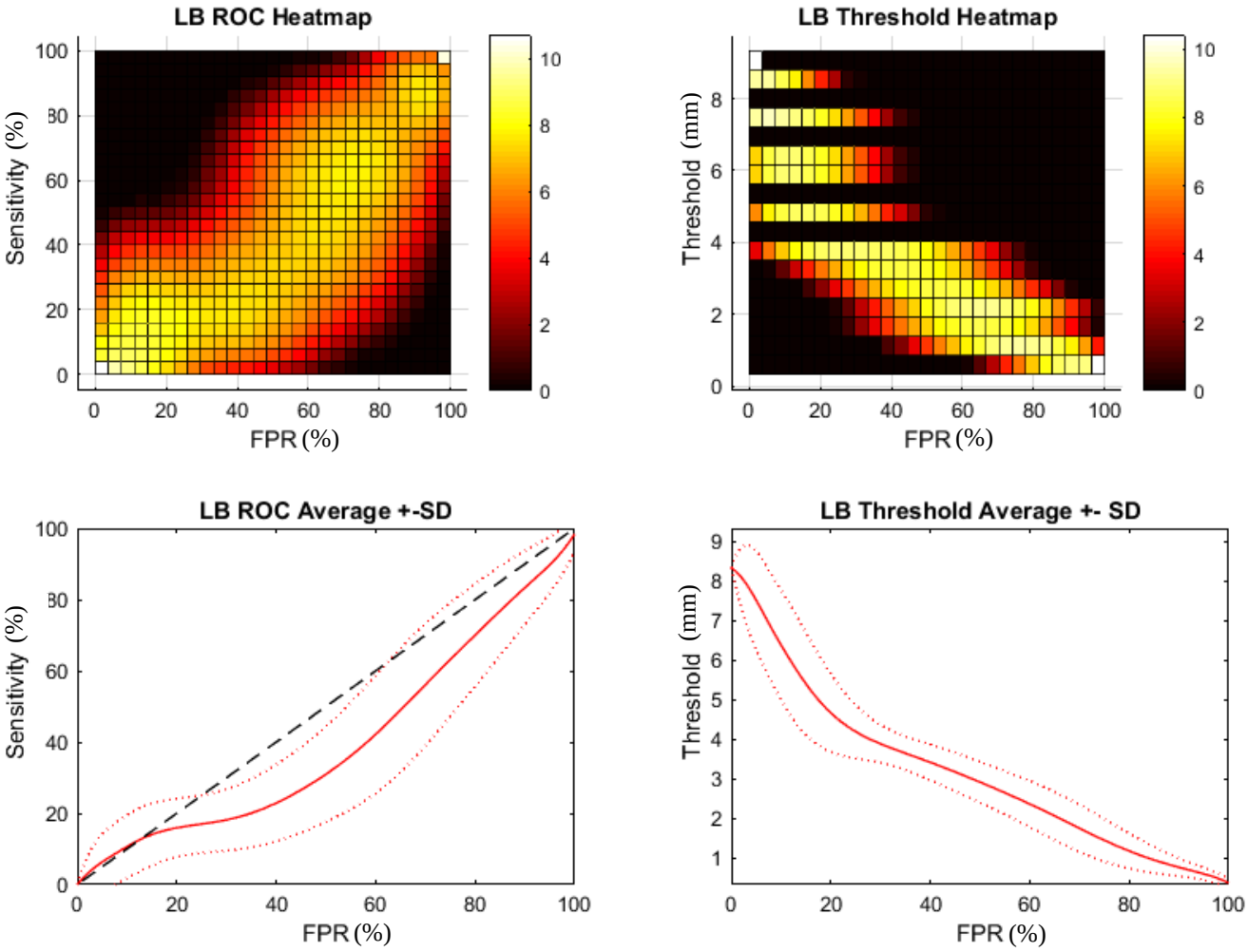

Figure 3.3: Line bisection ROC plots.

Top Left: There is a higher degree of variability throughout the entire range. Shallow initially, and steeper towards higher sensitivities.

Bottom left: Line is modestly below chance through the majority of the graph. On average control subjects performed marginally worse than the stroke subjects.

Top Right: The minimum score is 0 mm (perfect score) and the maximum 9 mm (worst score). Horizontal gaps are visible where no response was recorded at that threshold across the range 4-8 mm.

Bottom Right: Response is mostly linear in the range 0-4 mm, indicating responses are relatively evenly distributed this range, while at 4-8 mm the gradient is steeper reflecting fewer responses.

Randot Receiver Operator Characteristics with Thresholds for Bootstrap (*n*=1,000,000)

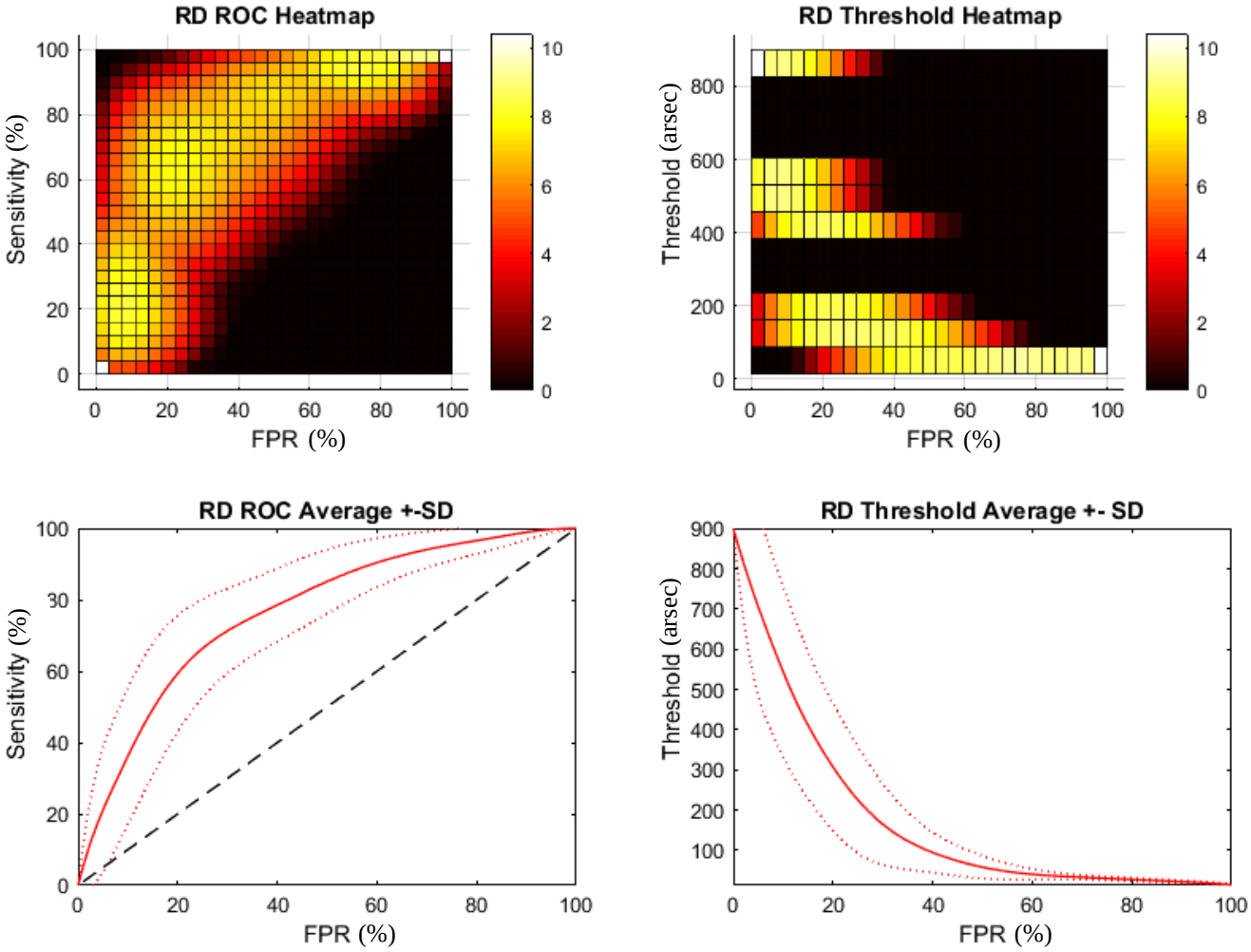

Figure 3.4: Randot stereovision ROC plots.

Top Left: Less variable at low sensitivity (0-40%) and high FPR (80-100%), with increased variability at intermediate values. There is a prominent curve, with the flexion point at about 65% sensitivity and 25% FPR.

Bottom Left: Both mean and SD exceed chance over most of the range, with a favourable AUC. Suggests test will be effective in demarcating stroke.

Top Right: The minimum score is 12.5 arcsec (perfect score) and the maximum 900 arcsec (worst score). Large horizontal gaps exist between 200-400 arsec and 600-900 arcsec as it was not possible to score values in this range using the randot test.

Bottom Right: Responses shows a steep initial curve with relatively few respondents until 100-200 arcsec, where the gradient becomes shallow, with many respondents in the remaining range.

Stereofly Receiver Operator Characteristics with Thresholds for Bootstrap (*n*=1,000,000)

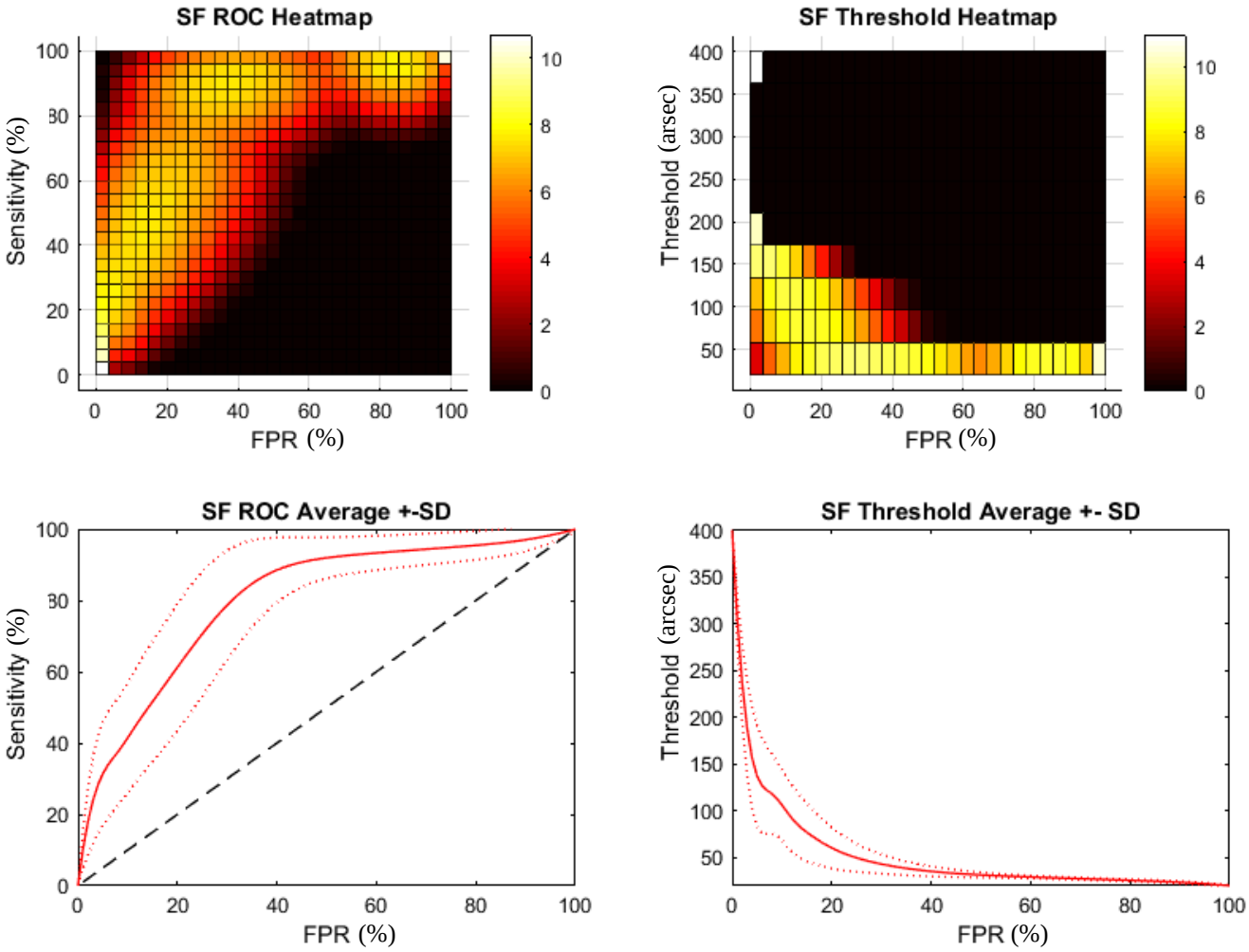

Figure 3.5: Stereofly stereovision ROC plots.

Top Left: Reduced variability at high FPR values (50-100%), with increased varaibility as intermediate values. Prominanet curve, similar to randot, with a higher flexion point at about 90% sensitivity and 40% FPR.

Bottom Left: Line and SD exceed chance over the entire range, with a very favourable AUC. Suggests test will be effective in demarcating stroke.

Top Right: The minimum score is 20 arcsec (perfect score) and the maximum 400 arcsec (worst score), less than half that of randot. This is because the more crude tests using the fly wings and body had very large values (3000 – 4800 arsec) and no subjects failed this component of the test. Similar to randot no result was possible in the range 200-400 arsec, resulting in a horizontal gap in data.

Bottom Right: A similar but more extreme version of randot, with very few responses at larger thresholds (<10% above 150 arsec), and the majority of responses < 50 arcsec, suggesting large deficits were uncommon.

Kinematogram Receiver Operator Characteristics with Thresholds for Bootstrap (*n*=1,000,000)

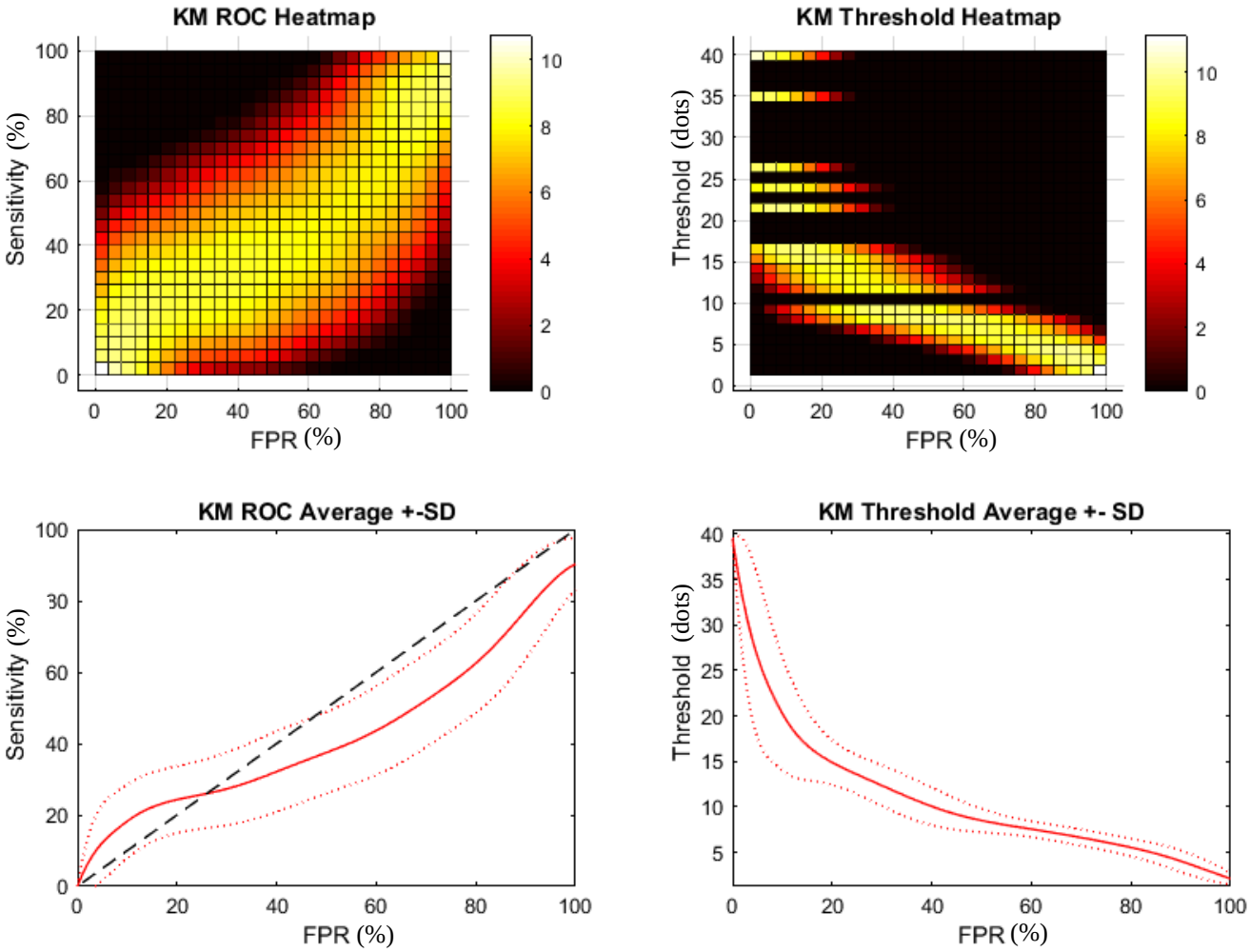

Figure 3.6: Random dot kinematogram (RDK) cohesive motion ROC plots.

Top Left: The RDK has the largest variation of all plots presented, extending acrorss the full range. The mean appears roughly linear, with only a slight curvature.

Bottom Left: Mean briefly exceeds chance for FPR <20%, then falls below chance for the rest of its range. It appears similar to line bisection, and performs equally poorly.

Top Right: Threshold units are the number of dots (of 40) and responses cover the full range, including values at both extremes (complete cohesion and minimal cohesion). Due to many possible values, there are some gaps where no result was recorded at that threshold, most prominently in the larger range (more than 50% cohesion).

Bottom Right: Similar shape to line bisection. There are relatively few responses, with a steep gradient at thresholds >15 dots, and then a fairly even distribution of responses over the remaining range.

Ishihara Receiver Operator Characteristics with Thresholds for Bootstrap (*n*=1,000,000)

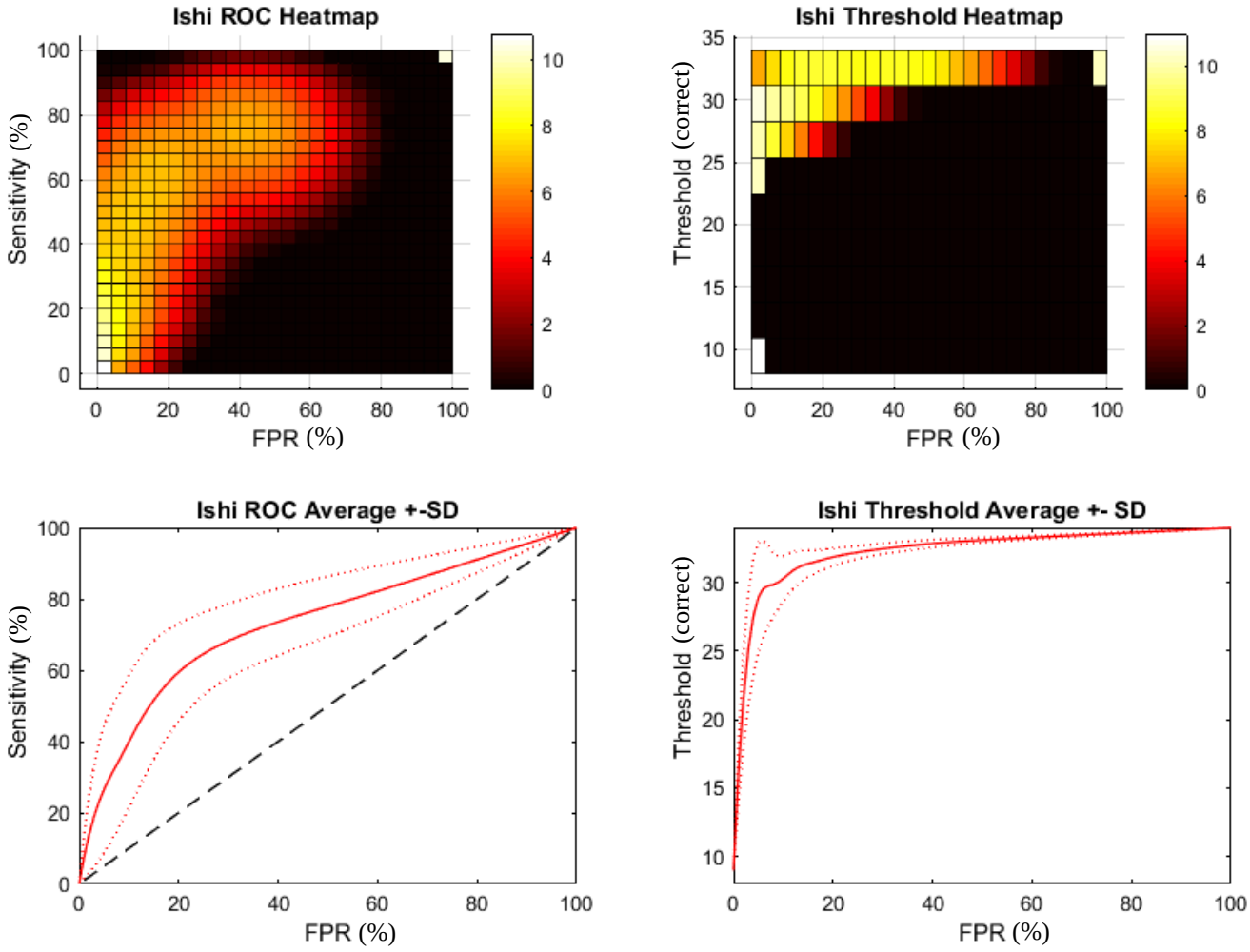

Figure 3.7: Ishihara - sum of correct values for both eyes ROC plots.

Top Left: Simlar variability and form to randot and stereofly plots, except no data exists for the upper FPR (80-100%), with values largely nested in the low FPR range (<10%). This likely reflects that 57% of controls scored a perfect 34/34 such that it is not possible to score a high FPR, instead suddenly jumping to 100% FPR and 100% sensitivity.

Bottom Left: Mean and SD exceed chance over the entire range, with a favourable AUC, although not quite as favourable as randot or stereofly. Beyond apex at ~60% sensitivity and 20% FPR, line is very linear due to a lack of data points.

Top Right: The maximum (perfect score) is 34 and the minimum (worst score) 9. One respondent scored 9, and the rest all exceeded 24, so a large gap exists between these values.

Bottom Right: Note the plot is inverted compared to previous plots, as high scores represent higher performance in this test. This plot shows a particularly steep curve, reflecting that the large majority (>90%) scored above 30.

Farnsworth-Munsell Receiver Operator Characteristics with Thresholds for Bootstrap (*n*=1,000,000)

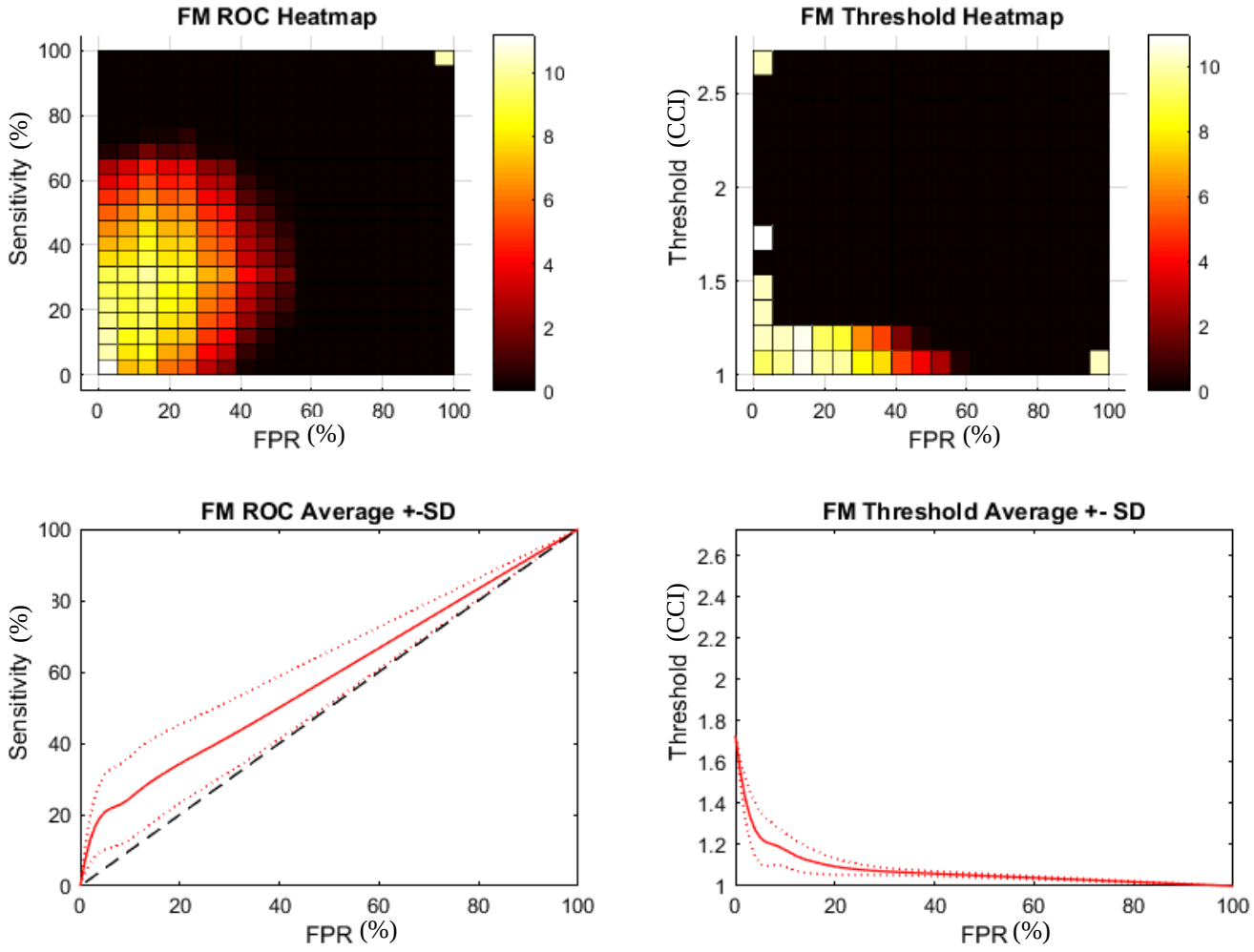

Figure 3.8: Farnsworth-Munsell D15 Colour Confusion Index (CCI) ROC plots

Top Left: It is difficult to judge variation when there is such a substantial gap in data points in the range 40-100% FPR. This is due to a similar effect to that of Ishihara, where 81% of controls (all but 4) scored a perfect 1.0 CCI, and so any score with a FPR >19% also jumps to 100% FPR and 100% sensitivity (other than via bootstrap resampling).

Bottom Left: ROC plot marginally exceeds chance through the full range, although artificial linearity is noted beyond the 20% mark due to limited data points. The 1 SD line aligns with the edge of chance throughout, suggesting test is unlikely to meet significance.

Top Right: There are gaps in threshold due to only 1 subject scoring above 1.5 CCI, and gaps in the FPR due to so many perfect scores in controls. This makes interpretation difficult. Point at 1.73 is the maximum score, with all data points passing though this point (white), while the marker at 2.72 is an artefact of graph construction and is not meaningful.

Bottom Right: As noted the peak value is 1.73 with a steep gradient demonstrating relatively few results with a CCI of >1.2, and the vast majority being very near to or exactly 1.0.

CFMT Receiver Operator Characteristics with Thresholds for Bootstrap (*n*=1,000,000)

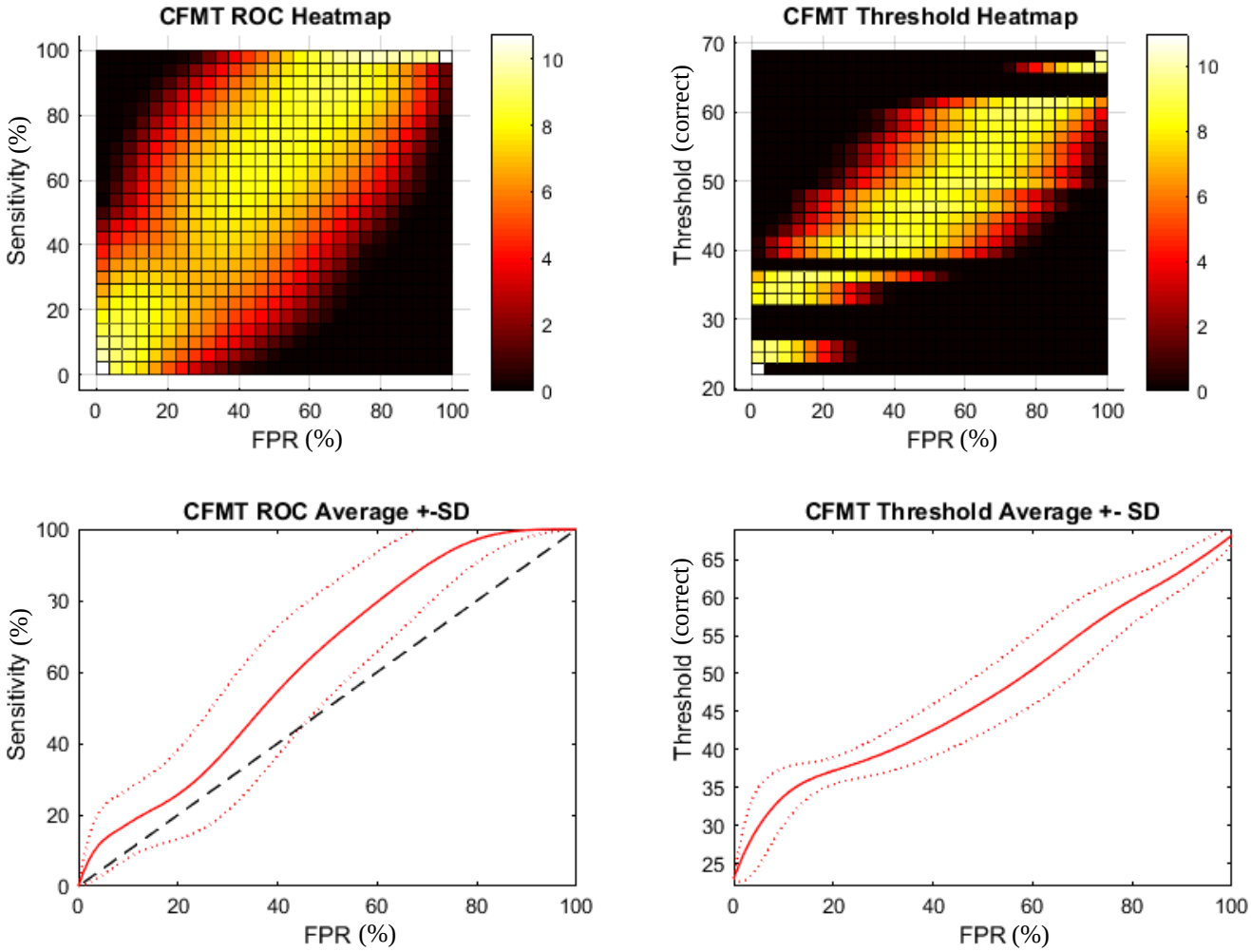

Figure 3.9: Cambridge Facial Memory Test (CFMT) total score

Top Left: Substantial variation exists though the full range, almost as prominently as RDK. Response is roughly linear, also similar to RDK, but with a marginally more favourable mean.

Bottom Left: Mean exceeds chance through the full range, but SD range does not until ~45% FPR, suggesting it is unlikely to meet significance, but shows some promise.

Top Right: A perfect score (72) was not achieved by any subject, with the maximum score (69) and the minimum expected score through random guessing would be 24 (33% correct) with several subjects scoring 23 or 24. Small gaps exist in the data given the large range of values possible, more prominently at extremes (<40 and >65 correct).

Bottom Right: There are relatively few scoring <35 (2 in control and 4 in stroke), with a fairly even distribution of results for scores 35 and above.

Line Bisection				
FPR	Sens	SD	Thresh	SD
2%	3.00	4.65	8.10	0.76
5%	6.34	7.85	7.52	1.25
10%	10.66	8.87	6.38	1.38
20%	15.93	8.19	4.67	0.99
AUC				
-SD	Mean	+SD	Z-score	Sig
0.29	0.40	0.51	-0.91007	0.71859
25%ile	Median	75%ile		Not Sig
0.32	0.40	0.47		

Ishihara				
FPR	Sens	SD	Thresh	SD
2%	13.88	10.87	21.50	3.48
5%	26.53	17.78	28.92	4.01
10%	39.92	18.59	30.29	1.66
20%	59.45	13.72	31.86	0.64
AUC				
-SD	Mean	+SD	Z-score	Sig
0.65	0.73	0.81	2.81398	0.00245
25%ile	Median	75%ile		Sig
0.67	0.73	0.78		

Randot				
FPR	Sens	SD	Thresh	SD
2%	9.81	10.58	816.50	138.41
5%	21.12	17.47	705.56	220.65
10%	36.19	19.11	543.54	212.29
20%	59.35	16.23	306.86	158.22
AUC				
-SD	Mean	+SD	Z-score	Sig
0.68	0.76	0.85	3.04522	0.00116
25%ile	Median	75%ile		Sig
0.71	0.77	0.82		

Farnsworth-Munsell				
FPR	Sens	SD	Thresh	SD
2%	12.62	6.46	1.42	0.10
5%	20.80	10.52	1.23	0.13
10%	24.63	11.59	1.18	0.08
20%	34.24	11.00	1.09	0.04
AUC				
-SD	Mean	+SD	Z-score	Sig
0.51	0.58	0.64	1.19516	0.11600
25%ile	Median	41.00		Not Sig
0.53	0.58	0.62		

Stereofly				
FPR	Sens	SD	Thresh	SD
2%	17.85	9.28	237.22	41.50
5%	31.39	14.52	137.09	54.17
10%	41.44	15.38	106.22	37.91
20%	61.26	17.76	60.26	21.91
AUC				
-SD	Mean	+SD	Z-score	Sig
0.71	0.79	0.88	3.59598	0.00162
25%ile	Median	75%ile		Sig
0.74	0.80	0.85		

CFMT				
FPR	Sens	SD	Thresh	SD
2%	7.05	6.16	26.21	3.60
5%	12.85	9.58	29.86	5.21
10%	17.55	9.62	33.80	3.76
20%	25.73	12.48	37.19	1.78
AUC				
-SD	Mean	+SD	Z-score	Sig
0.51	0.62	0.73	1.12811	0.12964
25%ile	Median	75%ile		Not Sig
0.56	0.63	0.70		

Kinematogram				
FPR	Sens	SD	Thresh	SD
2%	6.17	6.99	33.04	6.47
5%	12.22	10.74	26.50	9.02
10%	18.24	10.27	20.24	6.21
20%	24.30	9.35	14.88	2.45
AUC				
-SD	Mean	+SD	Z-score	Sig
0.31	0.42	0.53	-0.71762	0.76350
25%ile	Median	75%ile		Not Sig
0.35	0.42	0.50		

Table 3.2: Tables outlining sensitivities and thresholds at FPRs of 2, 5, 10, and 20% and the total AUC for the mean and ± 1 SD curves with associated *Z*-scores and *p*-values.

Randot, stereofly, and Ishihara are all highly significant with $p<0.01$. Farnsworth–Munsell and CFMT both have a mean AUC above chance, but they do not reach significance. Line bisection mean is at chance level and kinematogram scored below chance.

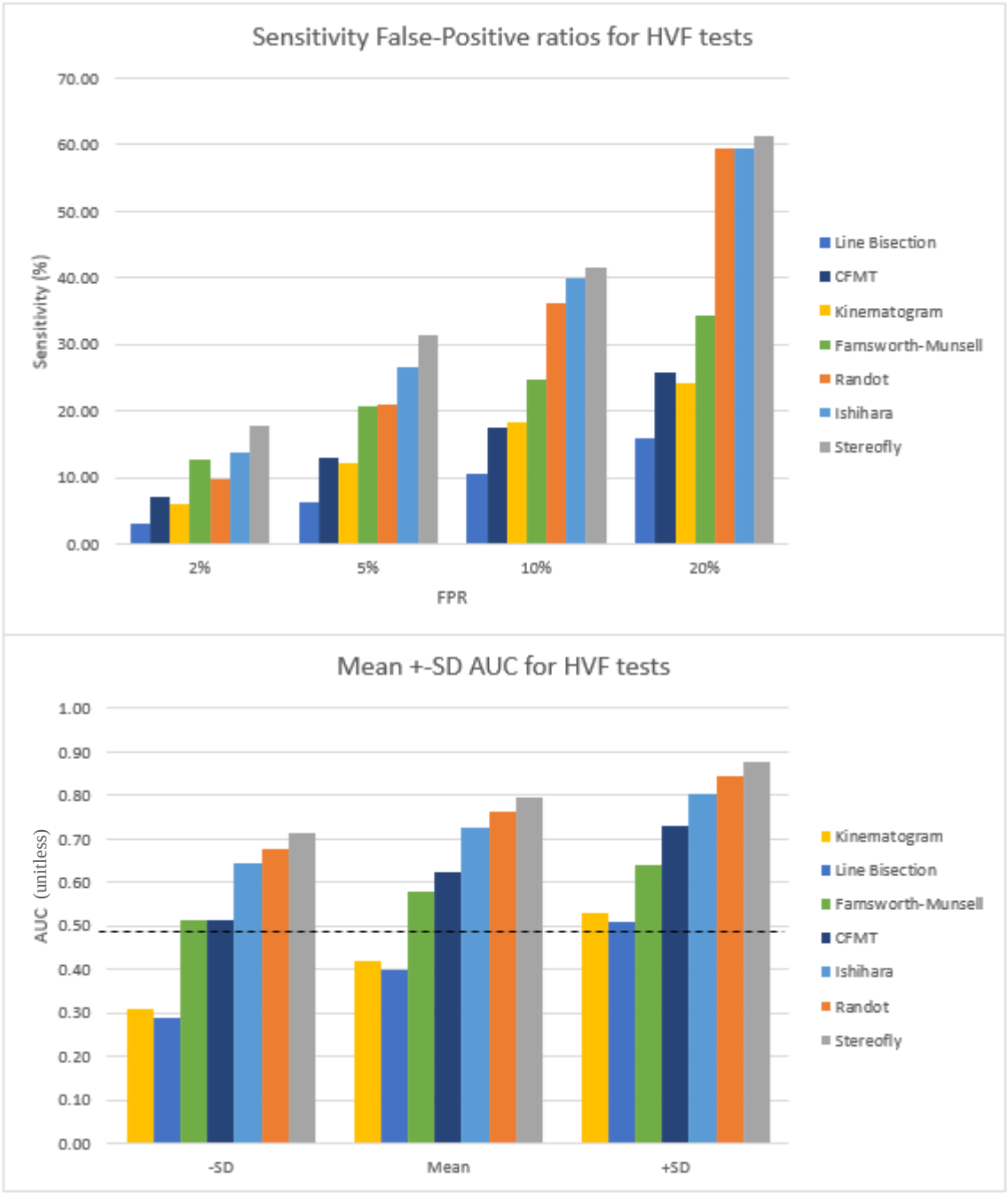

Figure 3.10: (Top) Sensitivity at FPRs of 2, 5, 10, and 20%, ordered smallest to largest by values at 10% FPR. FPRs of 5, 10, and 20% show very similar trends with stereofly, Ishihara, and randot leading, and Farnsworth–Munsell marginally better than the remaining 3 tests. There is a very linear increase in sensitivity at these low FPR percentages.

(Base) Mean area under curve (AUC) for each test variable ordered by mean. The dashed line represents chance level AUC at 0.5. Stereofly, randot, and Ishihara are again the 3 with notably high means which exceed chance (including at their SD values, consistent with them reaching significance).

The tests with the largest AUC were randot, stereofly, and Ishihara, which show clearly significant responses, while FM and CFMT approach significance, and LB and KM appear at or below chance (see Table 3.2). To confirm significance of indeterminate variables, the mean and SD for AUC were calculated to provide *Z*-scores and *p*-values in Table 3.2 and were graphed in Figure 3.10, highlighting that the lower SD for CFMT and FM was marginally above chance, but that they were not significant at the 5% level.

In order to better compare these tests over a clinically useful range, the sensitivities and thresholds for FPR values of 2%, 5%, 10% and 20% were also produced in Table 3.2 and graphed in Figure 3.10. While overall the same three tests are highlighted as most effective – SF, RD, and Is – at 2–5% FPR levels FM performs equal to or better than RD. This is important given that 5% is a commonly used threshold for FPR in psychophysical testing, so FM should therefore also be considered a useful measure. This then highlights that the two stereoscopic measures (SF and RD) and the two colour measures (Is and FM) appear to be the most useful tests and that stereopsis and colour are the domains most worth testing post-stroke.

3.4.2. Principal components

Having produced ROC plots which highlight which tests appear effective in detecting stroke, we wanted to determine if these are independent measures or if some of these tests correlate and are measuring only a single underlying measure. In order to clarify this, a principal component analysis (PCA) was done on the seven summary variables generated from the testing panel, with the following abbreviations: line bisection (LB), Ishihara (Is), Farnsworth–Munsell (FM), CFMT (Ct), randot (RD), stereofly (SF), and kinematogram (Km). Principal curves were generated from data from stroke and control subjects only.

3.4.2.1. Scree plot: selecting number of factors

The first step in this analysis was to determine how many components should be considered, which may be observed from the scree plot in Figure 3.11. This shows how much of the total variance is accounted for by each variable, ordered from most to least (red), and their cumulative variance (green). In PCA, three common practices are used in determining the number of components to include (Tabachnick, 1996):

1. The total number of variables ≥1 [in this case three];
2. The point at which a curve begins to level off [in this case two];
3. When a suitable amount of total variance has been explained [unclear].

We therefore conclude that two or three components was an appropriate number and completed the analysis with both two factors and three factors, with the three-factor analysis figures omitted due to gross similarity to the two-factor analysis.

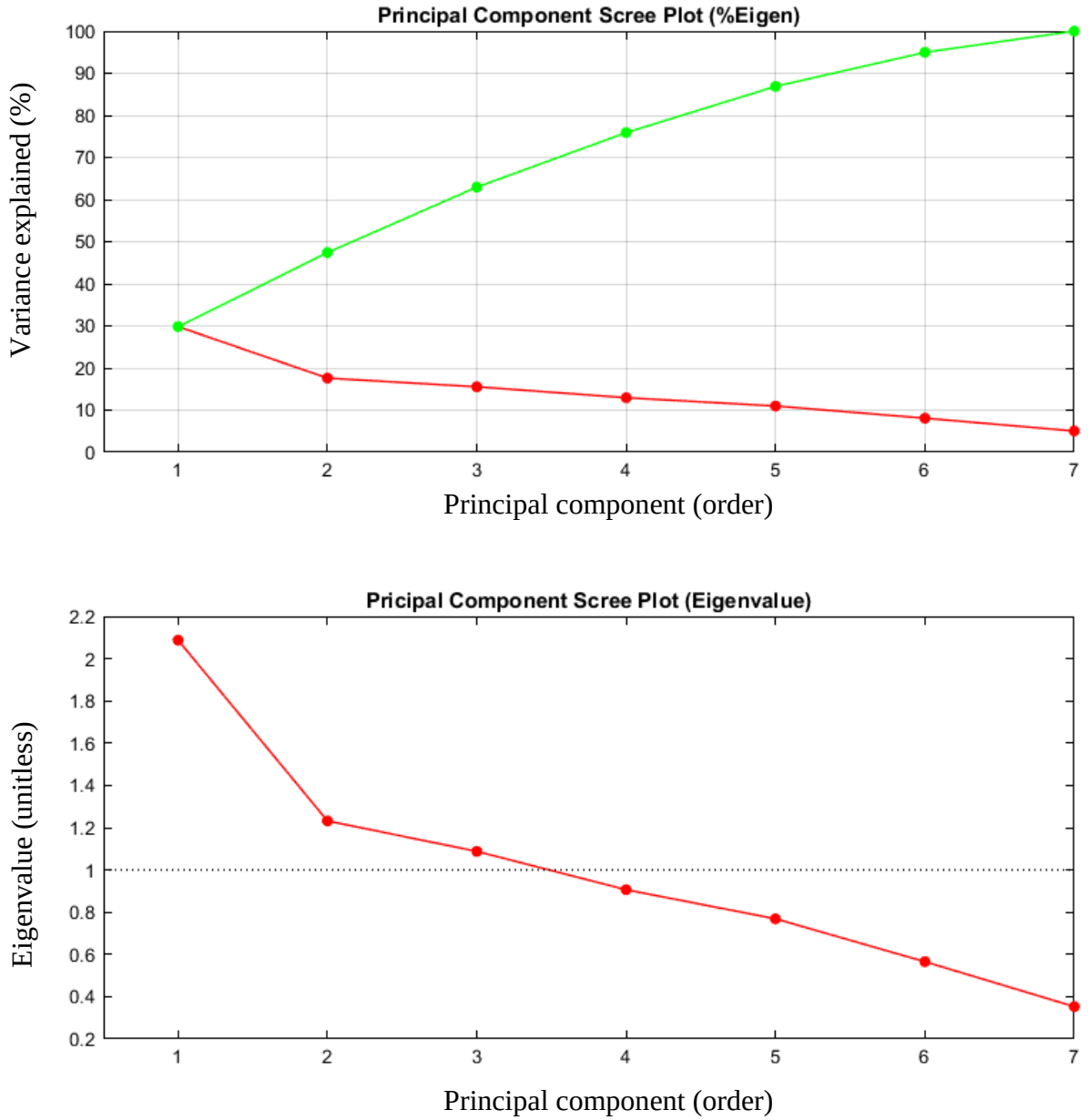

Figure 3.11: Scree plot for principal component analysis of 7 test variables.

(Top) Percentage of variance explained by each component (red) and cumulatively (green). The first 3 components contribute 30%, 18%, and 16% respectively, cumulatively totalling 63% of variance.

(Bottom) Eigenvalues for each of the 7 components. A dotted line marks the threshold for which a component accounts for the same variance as a single variable would.

3.4.2.2. Factor loadings

Both principal component (PC) and mean likelihood (ML) factor loadings were produced for two-factors which can be seen in Table 3.12. These factor loadings represent how much each variable contributed to the first and second components. When multiple variables are grouped into the same component, it implies they are assessing the same underlying measure.

Principal component loadings

The raw principal component loadings (Table 3.12: Left rows 1–2) show that the first component is largely comprised of RD, SF, and LA, with Km to a lesser extent. All these factors are negatively loaded – which is consistent with lower scores being better performing in these tests. The second principle component is largely comprised of FM and Ct with a negative and positive loading respectively, again consistent with low scores being better performing for FM while high scores for Ct.

Mean likelihood loadings

The raw mean likelihood loadings (Table 3.12: Left rows 3–4) show that the first component is predominantly Ct and to a lesser extent FM, highlighting the same variables as the PC second component. In the ML second component,t RD and SF are the main contributors, highlighting the same key variables as the PC first component.

Integration of PC and ML loadings

Considering first and second components together – if one looks across the rows the key factors in both PC and ML are SF and RD as a group, and FM and Ct as a group. This equates to the key components being (1) a measure of depth perception, and (2) a mixture of seemingly unrelated facial recognition and colour. Notably absent is the other colour measure Is, which does not score highly throughout.

Principal Component (PC) and Mean Likelihood (ML) rotated loandings

	Raw Loadings				Absolute Loadings			
	Principal Component		Mean Likelihood		Principal Component		Mean Likelihood	
	First	Second	First	Second	First	Second	First	Second
FM	-0.04	0.77	-0.41	-0.09	0.04	0.77	0.41	0.09
Ct	0.16	-0.77	0.94	-0.05	0.16	0.77	0.94	0.05
Is	0.17	-0.21	0.10	0.10	0.17	0.21	0.10	0.10
Km	-0.48	0.12	-0.23	-0.19	0.48	0.12	0.23	0.19
LA	-0.62	-0.38	0.03	-0.19	0.62	0.38	0.03	0.19
SF	-0.74	0.18	-0.18	-0.64	0.74	0.18	0.18	0.64
RD	-0.75	0.38	-0.36	-0.85	0.75	0.38	0.36	0.85

Table 3.12: Principal component and mean likelihood rotated loadings for the first and second components. (Left) Raw weighted loadings; (Right) Absolute values of the weighted loadings to more clearly demonstrate magnitude of contribution. The table is colour-coded so that larger weightings are more red while smaller ones are more white. Variables are ordered descending by first principal component.

Communalities

Both principal component and mean likelihood communalities were produced for the two factors (Figure 3.13). These represent how well each variable is explained by the two-factor model.

Principal component communalities

The best explained variables with >50% communalities were RD (70%), Ct (61%), FM (59%), SF (58%), and LA (53%). Km and Is are poorly explained with scores of 25% and 7% respectively.

Mean likelihood communalities

The best explained variables with >50% communalities were RD (89%) and Ct (85%) with very high scores exceeding those in PC. However, the other variables were more poorly explained with SF (44%), FM (18%), and all other variables <10%.

Integrating PC and ML communalities

Overall, PC gives greater explanation of variables with an average of 47% communality for the 7 variables, while ML had an average of 36%. While it might initially appear that there is no added benefit to the more flexible ML over PC, when considering only the groups highlighted in the principal component (Ct/FM and RD/SF), the average communalities for these pairs are slightly higher in ML. Both PC and ML highlight these same four variables as their highest communalities, and these are consistent with the component analysis.

Principal Component (PC) and Mean Likelihood (ML) communalities

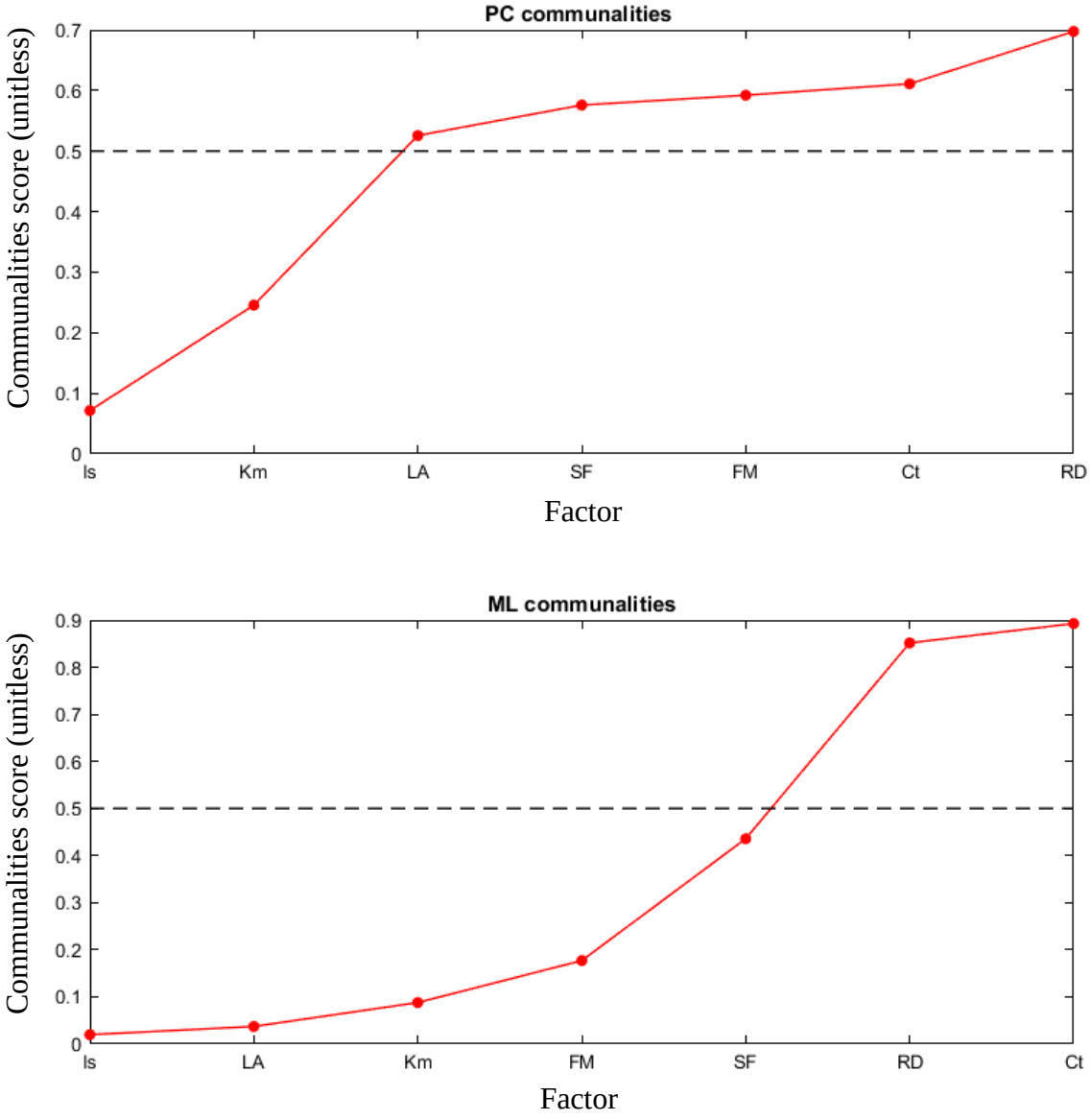

Figure 3.13: Communalities for the 2-component PC and ML versions of component analysis. Note that each is ordered by its smallest to largest variable with different orders demonstrating the large difference in communalities between versions.

3.5. Discussion

This study examined domains of higher visual function loss not routinely tested in clinical practice: stereovision (stereofly, randot), colour vision (Ishihara, Farnsworth–Munsell), facial recognition (CFMT), motion perception (kinematogram), and visual neglect (line bisection). Each test was analysed with receiver operator characteristics (ROC) plots of sensitivity (Sens) against false positive ratio (FPR), followed by principal component analysis using both principal component (PC) and mean likelihood (ML) approaches.

ROC plots suggested stereovision and colour as the more useful tests, with stereofly, randot, Ishihara, and Farnsworth–Munsell (FM) being the tests with the highest sensitivity at reasonable FPR values (2%, 5%, 10%, and 20%). When considering the entire graph, the total AUC was highly significant $p<0.01$ in stereofly, randot, and Ishihara. Although both CFMT and FM also had their AUC means modestly exceeding chance and approaching significance, they were non-significant. The worst performing tests – line bisection and kinematogram – had AUC values which were below chance. Collectively this demonstrates that stereovision and colour were the most useful measures in distinguishing between stroke and control populations.

Comparing the top scoring tests, stereofly appeared to have marginally better sensitivity and marginally larger AUC compared to its counterpart randot. While Ishihara had marginally lower AUC compared to both stereofly and randot, it did manage to out-perform randot in sensitivity at FPR <20%. This is important given that psychophysical tests typically use a FPR of 5% as an appropriate threshold to demarcate between normal and abnormal (a level which equates to the lowest scoring 5% of the general population).

For colour vision, Ishihara has consistently higher sensitivity and a larger significant AUC, while Farnsworth–Munsell did not reach significance. This is unexpected given that the Ishihara test is largely designed to identify red–green colour defects, while Farnsworth–

Munsell is considered an unbiased test of the full colour range. However, it has been demonstrated that those with cerebral achromatopsia perform randomly on the FM 100-hue test and Ishihara at normal reading distance (Cowey *et al.*, 2008). Given that the large bulk of Ishihara responses were not random, but instead were marginally decreased or normal, if a colour deficit is present it is likely to be quite subtle. Therefore using the D15 set (the smaller 15-hue subset of the 100-hue set) which is designed for very crude deficits may not have been as effective as using the larger FM100 set (Bassi *et al.*, 1993; Lopez *et al.*, 2000), with more subtle differences between wells, and so including FM100 in future testing may be worthwhile.

CFMT ROC plots were modestly above chance, but still did not achieve significance, which was surprising given that the principal component analysis highlighted it as very important in both PC and ML factors. CFMT is known to have a substantial age effect (Bowles *et al.*, 2009) and given that many of our test group were in the older range, this would have reduced the ability to demarcate between controls and stroke groups; in other words it is possible that with a younger group CFMT might achieve significance. Using the Australian version of the CFMT on our Australian subjects would eliminate racial bias demonstrated between countries (Bowles *et al.*, 2009; McKone *et al.*, 2011; McKone *et al.*, 2017), and may allow higher scores in the control group, thereby reducing false positive scores and increasing AUC. The other approach would be to expand the dynamic range by lowering the expected outcome from random guessing. Currently in a 3-way forced choice, 33% of answers are correct even when the subject is guessing. This results in many of the older population, who have lower scores, falling below chance level. If the test were modified to a 5-way force choice, then each correct answer would have more meaning, and the expected outcome would drop to 20%, perhaps providing some additional range which is needed to test elderly subjects.

Regarding the non-significance of KM, another study focusing on motion detection did provide some evidence that occipito–parietal stroke may result in reduced sensitivity to coherence,

although occipital–temporal and frontal did not (Vaina *et al.*, 2010). The lack of significance for LB was not unexpected given that the design of the study required that patients had recovered for at least 3 months and that visual neglect typically resolves within this timeframe (Ijaola & Kausar, 2009; Ali *et al.*, 2013).

Principal component scree plots were produced to help define the appropriate number of components to include. It was clear that the first component eigenvalue (2.09) was notably larger than the other components – and almost double that of the second (1.23) or third (1.09) components, which were only marginally above the threshold of 1. One approach to selecting factors is taking the first point where values begin to plateau (two values), and the other approach is eigenvalues ≥1 (three values); both were explored, although for ease of interpretation only the two-component results were presented. In the two-factor analysis, one factor appeared to be stereovision including RD and SF, while the other grouped together colour and facial recognition (FM and Ct). Addition of a third component produced similar relationships as with two components: RD and SF and FM and Ct were both grouped together with the new addition of Km and Is as the new component in PC, while Km alone in the ML components. Given the comparatively low eigenvalue for the third component – near the threshold of 1, and the below the chance AUC for the ROC plot of Km – this may be a result of over-analysis of a small data set and is unlikely to be meaningful. It is also noted that PC and ML are better used for large populations, and with a relatively small subject pool, collection of a larger data set may allow clearer results from this type of analysis.

Through all ROC and PCA plots, stereovision was a key factor. In considering potential confounders, the effectiveness of stereovision could quite reasonably be explained by there being a greater burden of blurry vision in the stroke population (Rowe *et al.*, 2009) and that blurry vision directly affects the ability to distinguish fine stereovision. This potential relationship was investigated by assessing best corrected visual acuity (BCVA) from the worst

eye – given that stereoscopic vision relies on a difference between the eyes and should therefore be limited by the eye with the lowest BCVA. A scatter plot of worst eye BCVA in both stroke and controls combined against stereofly and randot produced somewhat linear trendlines with poor to moderate *R*-values. This suggests that VA may explain a component but not all the sensitivity noted on ROC curves. Interestingly, those with cerebral achromatopsia have been demonstrated as able to discern colour differences when colours are abutting by edge detection, but not when spaced (Heywood *et al.*, 1991) so that when Ishihara is viewed at >2 m or with blur, they may become discernible (Cowey *et al.*, 2008). Given that blurry vision may not only affect stereovision, but also the effectiveness of Ishihara, it is essential that any correctable acuity be done prior to testing.

Other than stereovision, colour appeared to be affected with Ishihara being significant in ROC plots, and FM being highlighted in conjunction with CFMT in principal component analysis. It was initially surprising that the two colour measures were not grouped together, but rather that FM was paired with CFMT. While colour certainly plays a role in facial identification, the CFMT itself is achromatic and so any colour deficit would not put them at disadvantage in facial recognition. However, in a study looking at acquired prosopagnosia, 6 of the 12 subjects also had dyschromatopsia (Moroz *et al.*, 2016), with a suggestion that this relates to damage to the fusiform gyri, consistent with PET and MRI imaging of achromatopsic patients (Lueck *et al.*, 1989; Heywood *et al.*, 1991; Bartolomeo *et al.*, 2014). In other words, facial recognition and colour perception may not be functionally related, but rather in structurally adjacent regions on the ventral surface of the brain, so that damage to one commonly results in damage to the other. Establishment of a plausible explanation for this linkage certain strengthens the case that these measures are true deficits arising from stroke lesions.

Overall there is good evidence that stereovision is the most useful domain measured, with stereofly being the test of choice based on AUC and sensitivities at low FPR. Stereofly was

also subjectively a better test to measure patients since instructions were more easily understood than in randot, where the image with background noise appeared to confuse some participants. Despite this, randot also performed well overall, with only marginally less AUC and sensitivities, and the principal component analysis suggests they are indeed measuring the same thing, which is reassuring. It may be appropriate in further studies to assess ocular alignment in order to ascertain whether stereoacuity is centrally or peripherally impaired, towards providing either intervention or harm minimisation. Colour vision is the other measure with potential utility, particularly the Ishihara, which performed well in AUC and sensitivities. It quite substantially beat the other colour test (Farnsworth–Munsell) and they were not grouped together highly in the principal component analysis. Using the ROC 5% FPR as representative of how common deficits might be expected to be in the stroke population, the stereovision deficit appeared to be 20–30%, depending on the test used, and colour vision deficit of 20–25%, again depending on the test used. With the short test duration of these measures, it may be possible to further expand or combine tests to provide higher sensitivities – especially in the colour domain, where tests appeared to be measuring different things (noting they were not grouped together in principal components). Deficits in colour were not substantial in most instances, and it should be carefully weighed up if testing is necessary – given there is very limited capacity to treat, and it is unlikely to cause significant morbidity. Stereovision deficits on the other hand were often relatively severe, with many participants being unable to detect the crudest stimuli. Given that there appears to be a weak relationship between BCVA and stereovision, it is hard to say how much of these deficits are blur and how much is actual stereoscopic deficit. However, whether through primary damage or through secondary effects of lowered visual acuity, it has the potential to be clinically meaningful in the context of minimising future harm (through avoiding household collisions, losing balance, or competently driving). It may be useful to develop other tests to use in combination, given

that stereofly and randot largely use the same principles and do not appear to provide much more utility when their measures are combined.

A future direction may be to include analysis of HVF loss in other forms of visual impairment, in order to ascertain if these deficits occur as a result of true cortical damage, or merely due to impaired quality of vision. Similarly, characterisation of stroke damage would be useful. While MRI data was collected for the majority of stroke patients, analysis of this data has not yet been possible. It was mentioned in the introduction that there is the potential for both functional specialisation and distributive processing of visual percepts, so imaging studies of those with subtle defects would be of interest in contributing to that discussion. Subsequent studies can analyse this MRI data, and with larger numbers, correlate abnormalities with location, towards a broader undertaking of visual processing.

3.6. Conclusion

Stereovision deficits occur relatively common in stroke patients and are associated with the potential for intervention and harm minimisation. Both stereofly and randot are useful and moderately effective for this purpose, with stereofly being the test of choice in terms of sensitivity and useability. Colour vision deficits appear commonly as well, with Ishihara being moderately effective in detecting deficits, while Farnsworth–Munsell has a limited capacity to identify them. Deficits in colour vision do not appear substantial and may not require intervention in many instances. This study had a small mixed stroke patient population and was only intended as a pilot, so a larger study with more restrictive criteria on stroke patient inclusion would be useful, with a focus on stereovision and colour likely to be most worthwhile. It is also recommended to consider the full FM100, or a set between the D15 and FM100 with more than 15 hues, which may provide the extra sensitivity required to make the Farnsworth–Munsell test competitive with Ishihara and useful in identifying colour deficits.

References

Adams WE, Leske DA, Hatt SR & Holmes JM. (2009). Defining real change in measures of stereoacuity. *Ophthalmology* **116,** 281-285.

Adler P, Scally AJ & Barrett BT. (2012). Test--retest variability of randot stereoacuity measures gathered in an unselected sample of uk primary school children. *The British journal of ophthalmology* **96,** 656-661.

Ali M, Hazelton C, Lyden P, Pollock A, Brady M & Collaboration V. (2013). Recovery from poststroke visual impairment: Evidence from a clinical trials resource. *Neurorehab Neural Re* **27,** 133-141.

Bartolomeo P, Bachoud-Levi AC & Denes G. (1997). Preserved imagery for colours in a patient with cerebral achromatopsia. *Cortex* **33,** 369-378.

Bartolomeo P, Bachoud-Levi AC & Thiebaut de Schotten M. (2014). The anatomy of cerebral achromatopsia: A reappraisal and comparison of two case reports. *Cortex* **56,** 138-144.

Barton JJS, Sharpe JA & Raymond JE. (1996). Directional defects in pursuit and motion perception in humans with unilateral cerebral lesions. *Brain* **119,** 1535-1550.

Bassi CJ, Galanis JC & Hoffman J. (1993). Comparison of the farnsworth-munsell 100-hue, the farnsworth d-15, and the lanthony d-15 desaturated color tests. *Arch Ophthalmol-Chic* **111,** 639-641.

Bowles DC, McKone E, Dawel A, Duchaine B, Palermo R, Schmalzl L, Rivolta D, Wilson CE & Yovel G. (2009). Diagnosing prosopagnosia: Effects of ageing, sex, and participant-stimulus ethnic match on the cambridge face memory test and cambridge face perception test. *Cogn Neuropsychol* **26,** 423-455.

Bowman KJ. (1982). A method for quantitative scoring of the farnsworth panel d-15. *Acta Ophthalmol* **60,** 907-916.

Carota A & Calabrese P. (2013). The achromatic 'philosophical zombie', a syndrome of cerebral achromatopsia with color anopsognosia. *Case Rep Neurol* **5,** 98-103.

Cherney LR & Halper AS. (2001). Unilateral visual neglect in right-hemisphere stroke: A longitudinal study. *Brain Injury* **15,** 585-592.

Cooper SA, Joshi AC, Seenan PJ, Hadley DM, Muir KW, Leigh RJ & Metcalfe RA. (2012). Akinetopsia: Acute presentation and evidence for persisting defects in motion vision. *J Neurol Neurosur Ps* **83,** 229-230.

Cowey A, Alexander I, Heywood C & Kentridge R. (2008). Pupillary responses to coloured and contourless displays in total cerebral achromatopsia. *Brain* **131,** 2153-2160.

Duchaine B & Nakayama K. (2006). The cambridge face memory test: Results for neurologically intact individuals and an investigation of its validity using inverted face stimuli and prosopagnosic participants. *Neuropsychologia* **44,** 576-585.

Duvelleroy-Hommet C, Gillet P, Cottier JP, de Toffol B, Saudeau D, Corcia P & Autret A. (1997). [cerebral achromatopsia without prosopagnosia, alexia, object agnosia]. *Rev Neurol (Paris)* **153,** 554-560.

Farnsworth D. (1947). Investigation on corrective training of color blindness. *Sight Sav Rev* **17,** 194-200.

Fawcett SL & Birch EE. (2003). Validity of the titmus and randot circles tasks in children with known binocular vision disorders. *J Aapos* **7,** 333-338.

Fox CJ, Hanif HM, Iaria G, Duchaine BC & Barton JJS. (2011). Perceptual and anatomic patterns of selective deficits in facial identity and expression processing. *Neuropsychologia* **49,** 3188-3200.

Furlan M & Smith AT. (2016). Global motion processing in human visual cortical areas v2 and v3. *J Neurosci* **36,** 7314-7324.

Good GW, Schepler A & Nichols JJ. (2005). The reliability of the lanthony desaturated d-15 test. *Optometry and vision science : official publication of the American Academy of Optometry* **82,** 1054-1059.

Herzmann G, Danthiir V, Schacht A, Sommer W & Wilhelm O. (2008). Toward a comprehensive test battery for face cognition: Assessment of the tasks. *Behav Res Methods* **40,** 840-857.

Heutink J, Brouwer WH, Kums E, Young A & Bouma A. (2012). When family looks strange and strangers look normal: A case of impaired face perception and recognition after stroke. *Neurocase* **18,** 39-49.

Heywood CA, Cowey A & Newcombe F. (1991). Chromatic discrimination in a cortically colour blind observer. *Eur J Neurosci* **3,** 802-812.

Ijaola FO & Kausar SA. (2009). Visual impairment following stroke: Do stroke patients require vision assessment ? *Age Ageing* **38,** 629-630.

Ishihara S. (1918). Tests for color blindness. *Am J Ophthalmol* **1,** 457.

Johnson DD. (1992). The ishihara test: On the prevention of job discrimination. *J Am Optom Assoc* **63,** 352-360.

Jolliffe IT & Cadima J. (2016). Principal component analysis: A review and recent developments. *Philos Trans A Math Phys Eng Sci* **374,** 20150202.

Junge MRJ & Dettori JR. (2018). Roc solid: Receiver operator characteristic (roc) curves as a foundation for better diagnostic tests. *Global Spine J* **8,** 424-429.

Lander K, Humphreys G & Bruce V. (2004). Exploring the role of motion in prosopagnosia: Recognizing, learning and matching faces. *Neurocase* **10,** 462-470.

Lang N, Baudewig J, Kallenberg K, Antal A, Happe S, Dechent P & Paulus W. (2006). Transient prosopagnosia after ischemic stroke. *Neurology* **66,** 916-916.

Lever J, Krzywinski M & Altman N. (2017). Principal component analysis. *Nature Methods* **14,** 641.

Lopez P, Caruso RC & Kaiser-Kupfer MI. (2000). A comparison of lanthony's desaturated 15 hue test with the farnsworth-munsell 100 hue test for the quantification of color vision deficiencies. *Invest Ophth Vis Sci* **41,** S356-S356.

Lu XS, Ye J, Zhou S, Lu BX & Chen XH. (2005). Unilateral spatial neglect, global processing deficit and prosopagnosia following right hemisphere stroke: A case report. *Chinese Med J-Peking* **118,** 1846-1848.

Lueck CJ, Zeki S, Friston KJ, Deiber MP, Cope P, Cunningham VJ, Lammertsma AA, Kennard C & Frackowiak RS. (1989). The colour centre in the cerebral cortex of man. *Nature* **340,** 386-389.

McKeefry DJ, Watson JDG, Frackowiak RSJ, Fong K & Zeki S. (1997). The activity in human areas v1/v2, v3, and v5 during the perception of coherent and incoherent motion. *Neuroimage* **5,** 1-12.

McKone E, Hall A, Pidcock M, Palermo R, Wilkinson RB, Rivolta D, Yovel G, Davis JM & O'Connor KB. (2011). Face ethnicity and measurement reliability affect face recognition performance in developmental prosopagnosia: Evidence from the cambridge face memory test-australian. *Cogn Neuropsychol* **28,** 109-146.

McKone E, Wan L, Robbins R, Crookes K & Liu J. (2017). Diagnosing prosopagnosia in east asian individuals: Norms for the cambridge face memory test-chinese. *Cogn Neuropsychol* **34,** 253-268.

Moroz D, Corrow SL, Corrow JC, Barton ARS, Duchaine B & Barton JJS. (2016). Localization and patterns of cerebral dyschromatopsia: A study of subjects with prospagnosia. *Neuropsychologia* **89,** 153-160.

Nettleman MD. (1988). Receiver operator characteristic (roc) curves. *Infect Control Hosp Epidemiol* **9,** 374-377.

Pagani R, Bosco G, Dalla Valle E, Capitani E & Laiacona M. (2012). The assessment of colour perception, naming and knowledge: A new test device with a case study. *Neurol Sci* **33,** 801-809.

Pollock A, Hazelton C & Brady M. (2011). Visual problems after stroke: A survey of current practice by occupational therapists working in uk stroke inpatient settings. *Top Stroke Rehabil* **18,** 643-651.

Rizzo M, Nawrot M & Zihl J. (1995). Motion and shape perception in cerebral akinetopsia. *Brain* **118,** 1105-1127.

Ross JE. (1983). Disturbance of stereoscopic vision in patients with unilateral stroke. *Behav Brain Res* **7,** 99-112.

Rowe F, Brand D, Jackson CA, Price A, Walker L, Harrison S, Eccleston C, Scott C, Akerman N, Dodridge C, Howard C, Shipman T, Sperring U, MacDiarmid S & Freeman C. (2009). Visual impairment following stroke: Do stroke patients require vision assessment ? *Age Ageing* **38,** 188-193.

Schaadt AK, Brandt SA, Kraft A & Kerkhoff G. (2015). Holmes and horrax (1919) revisited: Impaired binocular fusion as a cause of "flat vision" after right parietal brain damage - a case study. *Neuropsychologia* **69,** 31-38.

Schaadt AK, Schmidt L, Reinhart S, Adams M, Garbacenkaite R, Leonhardt E, Kuhn C & Kerkhoff G. (2014). Perceptual relearning of binocular fusion and stereoacuity after brain injury. *Neurorehabil Neural Repair* **28,** 462-471.

Schow T, Harris P, Teasdale TW & Rasmussen MA. (2016). Evaluation of a four month rehabilitation program for stroke patients with balance problems and binocular visual dysfunction. *Neurorehabilitation* **38,** 331-341.

Setala K & Vesti E. (1994). Acquired cerebral achromatopsia - a case-report. *Neuro-Ophthalmology* **14,** 31-36.

Stone A, Cooke D, Morton D & Steele M. (2019). Reliability of revised scoring methods for the schenkenberg line bisection test with adults following stroke: Preliminary findings. *Brit J Occup Ther* **82,** 750-758.

Tabachnick BGF, L.S. (1996). *Using multivariate statistics*. Harper Collins, New York.

Vaina LM. (1994). Functional segregation of color and motion processing in the human visual-cortex - clinical-evidence. *Cereb Cortex* **4,** 555-572.

Vaina LM. (1995). Akinetopsia, achromatopsia and blindsight: Recent studies on perception without awareness. *Synthese* **105,** 253-271.

Vaina LM, Cowey A, Eskew RT, LeMay M & Kemper T. (2001). Regional cerebral correlates of global motion perception - evidence from unilateral cerebral brain damage. *Brain* **124,** 310-321.

Vaina LM, Sikoglu EM, Soloviev S, LeMay M, Squatrito S, Pandiani G & Cowey A. (2010). Functional and anatomical profile of visual motion impairments in stroke patients correlate with fmri in normal subjects. *J Neuropsychol* **4,** 121-145.

von Arx SW, Muri RM, Heinemann D, Hess CW & Nyffeler T. (2010). Anosognosia for cerebral achromatopsia-a longitudinal case study. *Neuropsychologia* **48,** 970-977.

Wilmer JB, Germine L, Chabris CF, Chatterjee G, Williams M, Loken E, Nakayama K & Duchaine B. (2010). Human face recognition ability is specific and highly heritable. *Proc Natl Acad Sci U S A* **107,** 5238-5241.

Wilson B, Cockburn J & Halligan P. (1987). Development of a behavioral-test of visuospatial neglect. *Arch Phys Med Rehab* **68,** 98-102.

Wold S, Esbensen K & Geladi P. (1987). Principal component analysis. *Chemometr Intell Lab* **2,** 37-52.

Zhou C, He Y & Li X. (2018). Cerebral achromatopsia secondary to ischemic stroke. *Neurol India* **66,** 573-575.

Chapter 4: Pupillometry – direct and consensual responses in stroke, chiasmal compression, and AION

4.1. Abstract

4.1.1. Purpose

mfPOP records both direct and consensual responses to stimuli presented concurrently to either eye. Pictorial perimetry reports may use direct responses, consensual responses, or a combination of the two. In order to determine which method is most appropriate, the relationship between direct and consensual needs to be explored.

4.1.2. Methods

Scatter plots of each visual field region's direct and consensual response amplitude were plotted for each of the groups (stroke n = 25, pituitary n = 11, and AION n = 10) split by nasal/temporal region with trendline and correlation coefficient (r-scores) for each to demonstrate their relationship. Bland–Altman plots of the same were produced to highlight their differences. Fields for each subject were produced for: direct, consensual, their difference (Dir – Con) and their ratio (Dir / Con) the group averages are presented here to test whether there are any spatial differences in pupillary response. Signal-to-noise ratio (SNR) plots for direct and consensual were used for appropriate amalgamation into a single measure for production of reports.

4.1.3. Results

Scatterplots demonstrate a high degree of correlation between direct and consensual response in stroke, pituitary, and AION, both nasally (r-scores of 0.93, 0.88, and 0.95 respectively) and

temporally (*r*-scores of 0.94, 0.89, and 0.94 respectively). Bland–Altman plots demonstrate that, on average, direct is marginally larger (<1 dB) than consensual in all groups and highlight the heteroscedasticity, with larger responses having greater variability. Visual field plots for direct and consensual responses show crude agreement with each other, although there is substantial noise. Visual field plots for direct and consensual difference and their ratios highlight that their relationship varies in space, with direct larger than consensual in temporal regions, while they are proportionate or marginally larger in nasal regions (in all groups).

4.1.4. Conclusions

Direct and consensual are highly related, but vary across the field consistently in all diseases, suggesting this is independent of disease state. A plausible explanation for this is greater decussational input from pretectal olivary nucleus (PON) to Edinger–Westphal nucleus (EWN), combined with a greater number of nasal retina inputs. Variation in SNR is similar to that of the signal alone, indicating that the increase in signal for direct responses temporally is not accompanied by much increase in noise, and that direct and consensual are not equivalent. Selecting only direct or consensual could produce naso-temoporal variation, which is not reflective of any true field difference and a SNR-weighted average is recommended to temper this response without biasing the result.

4.2. Introduction

The Multifocal Pupillographic Objective Perimetry (mfPOP) method concurrently measures both direct and consensual pupillary responses to stimuli presented either nasally or temporally to each eye. It also derives estimates of the response for each of its 44 regions with a measure of their variance. This provides a substantial amount of information, which must then be condensed to produce plots for clinical interpretation and for comparison with other visual field devices. Practically, this means deriving a single measure of sensitivity using direct or

consensual responses, or a combination of the two. While it is well established in control groups that the direct response to whole-field stimulation is consistently marginally larger than consensual (Lowenstein, 1954; Smith *et al.*, 1979; Fan *et al.*, 2009), it has not been established that this remains true in neurological disease such as stroke, chiasmal compression, and anterior ischemic optic neuropathy (AION), which respectively classically show homonymous defects, bitemporal defects, and altitudinal defects. There are also studies outlining that direct and consensual responses differ (contraction anisocoria) according to visual hemifield, with temporal fields showing greater direct than consensual responses, while nasal field results are mixed - some studies stating consensual may marginally exceed direct (Cox & Drewes, 1984; Martin *et al.*, 1991), while others present evidence of equivalence (Smith & Smith, 1980; Wyatt & Musselman, 1981; Schmid *et al.*, 2000; Carle *et al.*, 2011). This apparent discrepancy was addressed by Carle et al. by concluding that stimulus intensity affects anisocoria in nasal regions, with stimuli typically used in mfPOP having intensities that result in near-equivalence of direct and consensual responses, whereas stimuli that are either more or less intense tend to give consensual responses that modestly exceed direct (Carle *et al.*, 2011). It was also demonstrated that although response size varied across the visual field, the relationship between direct and consensual responses in nasal regions of controls was roughly homogenous, in addition to being near-equivalent for this level of intensity. Given that this chapter uses the same mfPOP device and similar protocols to the Carle et al. study (although in neurological disease rather than in controls), an extract from this paper is included for comparison (Figure 4.1). Both anisocoria patterns in these studies and anatomical evidence in primates (Tigges & O'Steen, 1974; Hutchins & Weber, 1985; Gamlin & Clarke, 1995; Clarke *et al.*, 2003) are consistent with a stronger input from the pretectal olivary nucleus (PON) to the contralateral

(decussational) Edinger–Westphal Nucleus (EWN) as compared to ipsilateral (linear) connections.

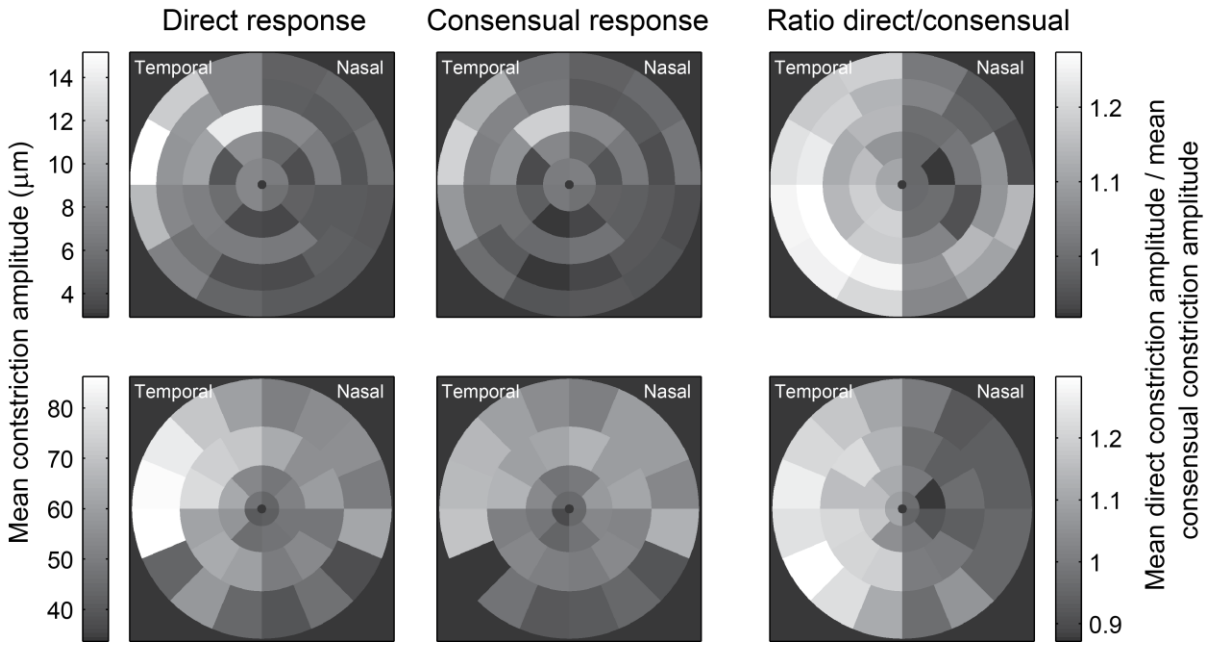

Figure 4.1: Left and right eyes are both presented as left-equivalent to allow them to be combined. (A) shows average responses for 32 eyes from patients with dense sampling of visual fields. Direct and consensual responses have similar retinotopy but their ratio reveals naso-temporal differences: temporal having a high direct/consensual ratio of ~1.2 while the nasal direct/consensual ratio remains proportionate at near 1. (B) shows average response for 84 eyes from control patients with less-dense sampling of fields. Despite the pattern of direct and consensual plots being different to A, their ratios appear almost identical. Data from *'Contraction anisocoria: segregation, summation, and saturation in the pupillary pathway'* by Carle et al, 2011, image reproduced with permission from personal commication with author C. Carle.

Since pupillometry is being investigated as a way of characterising visual field damage in neurological diseases, it would of course be of interest to see how these pupillary principles and patterns alter as neurological diseases progress. If the intent is to then go on and make a comparison between mfPOP readings and other visual field devices, we must first consider how responses can be amalgamated or condensed into a single indicative measure.

4.3. Methods

4.3.1. Subjects and screening

A history of mfPOP and the reasoning for the test parameters used can be found in the Introduction chapter (1.6.4. Multifocal methods). Full descriptions are presented in the General Methods, including recruitment (section 2.1), screening (section 2.2), mfPOP stimuli, procedures, and output measures (section 2.5.3). For brevity, here an overview is presented.

Subjects were recruited from multiple hospital and eye clinic sources and informed consent was obtained. Subjects were screened for pre-existing ocular conditions, both via questionnaire and clinical assessment and included: best corrected visual acuity of 6/24 or better, cataract screening, intraocular pressure measurement, fundus photo, and OCT scan of posterior pole and optic nerve head. Groups consisted of stroke (heterogenous cortical lesions) (n = 25), chiasmal compression (n = 11), and AION (n = 10).

4.3.2. Multifocal Pupillographic Objective Perimetry (mfPOP)

Pupil diameter was assessed using mfPOP objectiveFIELD analyser (Konan Medical USA Inc, Irvine CA) which uses rapidly presented stimuli with a fixed luminance and measures the pupil response, obtaining data for 44 test regions extending out to 20° eccentricity in each direction. A total of four tests were completed using mfPOP.

4.3.2.1. Testing protocol and settings

Ambient light was kept constant and the device hood acted to minimise effects of background luminance. Lenses nearest the subject's prescription glasses were used rounded to the nearest 3 spherical dioptres, since mfPOP is insensitive to moderate blur. Vergence was aligned at optical infinity. Patients were instructed to maintain focus on a central marker, that they can blink at any time but should minimise it during testing (9 × 45 s segments), instead utilising the breaks (7 s between segments).

The mfPOP design (Figure 2.16) allows both eyes to be tested and recorded simultaneously, using independent stimuli (dichoptic) displayed and recorded at 60 frames/s and interpolated to 30 frames/s. Pupil diameter was measured from an average circular fit of the pupil, with data automatically removed if there was a poor quality signal (perhaps from blinking or obscuration from eyelashes), with a segment being repeated if data acquisition fell below 85%.

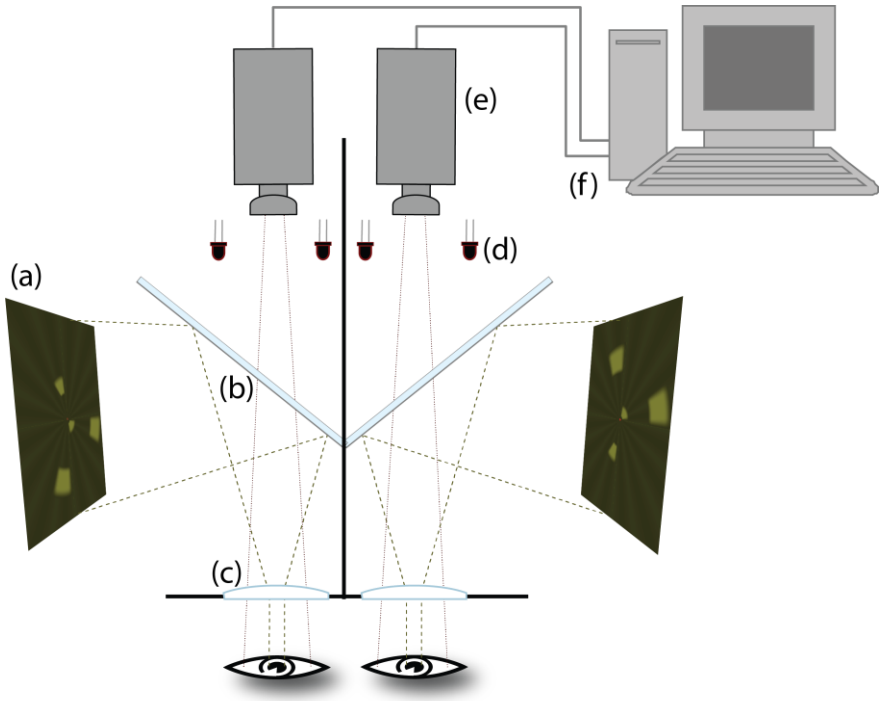

Figure 4.2: Demonstrates measurement of pupillary responses using mfPOP. Stimuli are presented separately on two LCDs (a) and reflected off two cold dichroic mirrors (b) which reflect these shorter wavelengths while transmitting near-infrared. Viewing distance is increased to optical infinity by plano-convex lenses (c). Infrared illumination (d) passes through the dichroic mirror and reflects off the eyes to facilitate monitoring of each pupil by an infrared video camera (e) and recorded in real time onto a computer (f). Image reproduced with permission via personal communication from the author C. Carle.

The stimulus background was yellow with an average luminance of 10 cd/m^2, and stimuli were yellow with an average luminance of 150 cd/m^2 (Y/Y). The stimulus layout comprised 44 regions split across the vertical meridian in the shape of several segmented annuli which partially overlap, with larger peripheral stimuli (see Methods Figure 2-21). The 44 regions were

divided into 8 sections comprising left and right eye, left and right hemifield, and odd or even rings. Presentations were in clustered volleys (Sabeti *et al.*, 2014), which were temporally sparse but could be spatially near (see Methods Figure 2-22). Each volley consists of activation of, on average, 50% of regions within a subset for 33 ms, with a 250 ms delay between the onsets of each volley, sequentially rotating through presentations in each of 8 subsets. This means that, in total, each region is presented on average every 4 seconds for a total of around 90 presentations throughout the total test duration of 360 seconds.

4.3.2.2. Signal extraction and processing

Following continuous collection of data during the testing period, all data was processed. The output signal was converted into response amplitudes using a multiple linear regression method described elsewhere (James, 2003; James *et al.*, 2005; Ruseckaite *et al.*, 2005). Responses were normalised to an average diameter of 3.5 mm to account for differences in resting pupil diameter between subjects (James *et al.*, 2012).

Amplitudes (μm) were converted into dB units using a generalised logarithmic transform which stabilises the variance and removes small dilations that would result in negative values preventing dB transformation. The generalised logarithmic transform was of the form:

$$\mathrm{Glog}(y,\lambda) = \log\left(\frac{y+\sqrt{y^2+\lambda^2}}{2}\right)$$

with λ set to 9 based on appropriateness to the dataset. Data was then linearly scaled to conveniently match the HFA range. Conversion from the 44 region map of the mfPOP stimuli to the 54-region HFA 24-2 format was done by weighting averages in accordance with their overlap.

In this chapter both direct and consensual responses are set out separately; how they might be combined most effectively is considered below. Testing of the Y/Y protocol was done on two

visits by each subject, and analysis of differences between visits is addressed in Chapter 6. As it is expected that clinicians would only test a subject on a single occasion, it is important that any method used to combine direct and consensual is appropriate to the variability present in a single unaveraged test. For this reason, only the first test is considered in this chapter, while other chapters average over repeats.

To investigate the relationship and similarities between direct and consensual pupillary response for the 3 neurological diseases, simple scatter plots of direct and consensual responses of all visual field locations from subjects within a patient-group were produced, with a correlation coefficient (Pearson's *r*) to show the trend and relationship.

Bland–Altman plots were produced to display means across direct and consensual responses against differences between direct and consensual responses, a way of highlighting and quantifying differences (Bland & Altman, 1999; Zaki *et al.*, 2012; Giavarina, 2015). The overall mean and 95% confidence intervals (defined by 1.96 SD from the mean) were used to describe the variability between direct and consensual (on the ordinate) with respect to the base signal (the average of direct and consensual, abscissa).

Visual field plots of pupil responses for both eyes using the 24-2 format are presented in greyscale. Using the generalised log-transform, 0 dB represents no response (black) and maximum response amplitudes (in the 25–30 dB range) are shown in white. Average visual fields for each patient group were produced by taking the mean of each visual field location across all patients for each eye. Plots of direct, consensual, their difference (Dir – Con), and their ratio (Dir / Con) were used to investigate naso-temporal differences, with a colour scale used such that no difference (0) is shown as white, direct exceeding consensual as increasingly more red, and as consensual exceeding direct as increasingly more blue.

Signal-to-noise ratio (SNR) was investigated with signal represented by response amplitude and noise by the SE of the raw amplitude. The multifocal analysis method used multiple recorded responses (effectively one for each stimulus presentation) to measure each test point, allowing calculation of an estimated SE for that response.

In combining SNR for each point, signal was averaged prior to dB conversion in order to allow linear summing, while noise was averaged as the root mean square (RMS) due to conversion of SE into variance before linear summing is possible.

All calculations and graphs were produced using Matlab version 2016B (The MathWorks, Inc., Natick, USA) and Microsoft Excel 2016.

4.4. Results

Figures 4.3– 4.5 show that patient groups in all three neurological groups showed highly linear relationships between direct and consensual responses, with a high degree of correlation and near-zero *y*-intercepts. In the larger range, all three also appear to have trendlines shallower than perfect linear correlations (greater direct than consensual responses). This effect appears most prominently in the temporal visual field test regions, while nasal test regions are closer to the line of equivalence, especially in chiasmal compression and AION, and which become slightly above equivalence before the majority of the data points (greater consensual than direct). In stroke, there does not appear to be any heteroscedasticity, while in the pituitary and AION groups there is quite definitely an increase in variability at larger responses.

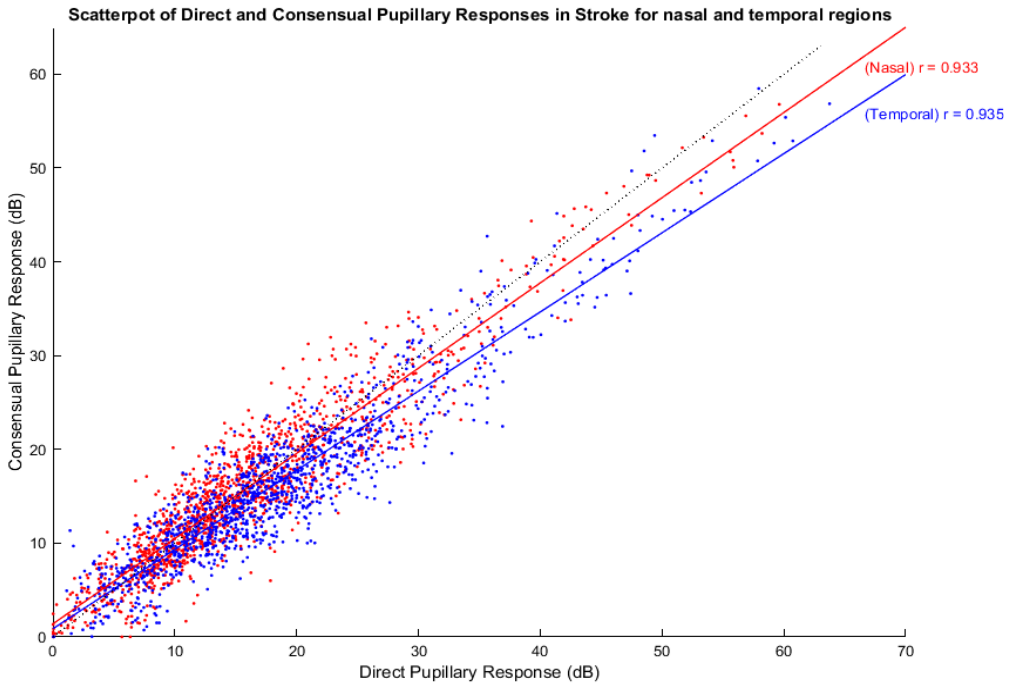

Figure 4.3: Scatter plot of direct and consensual responses for all 44 regions in the stroke cohort with nasal regions shown in red and temporal regions in blue. The dotted line represents a perfect linear correlation and solid lines are least squares trendlines for each data set. There is a highly linear correlation in both, with high *r*-values and near-zero *y*-intercept, suggesting that direct and consensual are highly related. There is a slightly shallower trend than linear correlation suggesting that direct marginally exceeds consensual at high values, which appears more prominent in the temporal plot. A combined plot was also computed but not presented and had an *r*-value of 0.93.

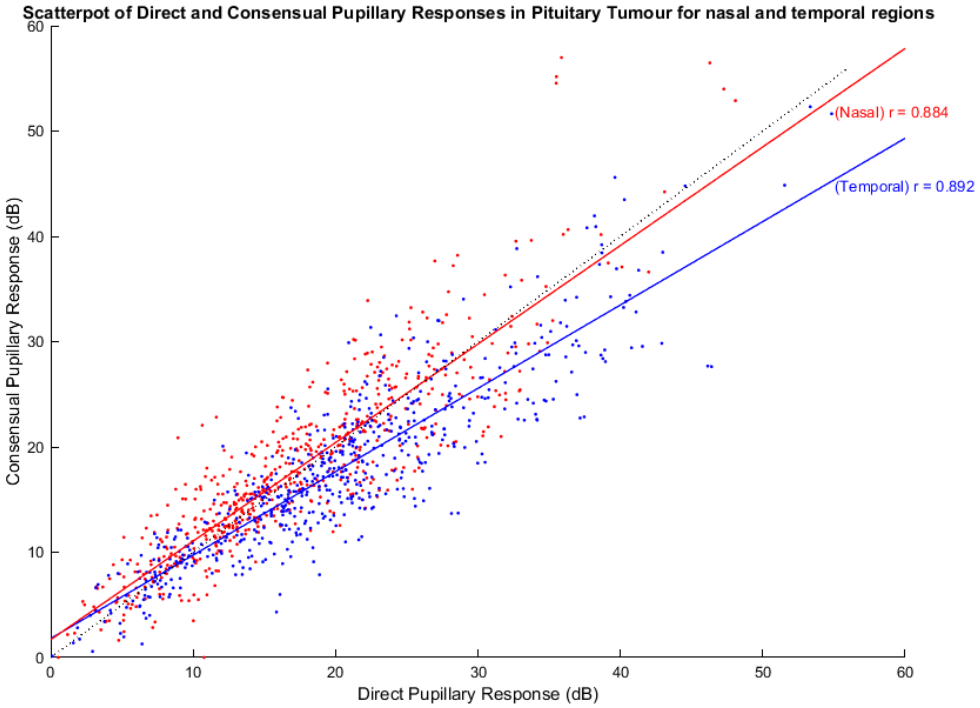

Figure 4.4: Scatter plot of direct and consensual responses for all 44 regions in chiasmal compression cohort as per Figure 4.3. There is a highly linear correlation in both, with moderately high *r*-values and near-zero *y*-intercept, suggesting that direct and consensual are highly related. Nasal has a trendline almost exactly matching perfect linear correlation (dotted line), while temporal shows a shallower curve indicating that direct may exceed consensual. A combined plot was also computed but not presented with an *r*-value of 0.87. There appears to be some heteroscedasticity as values increase.

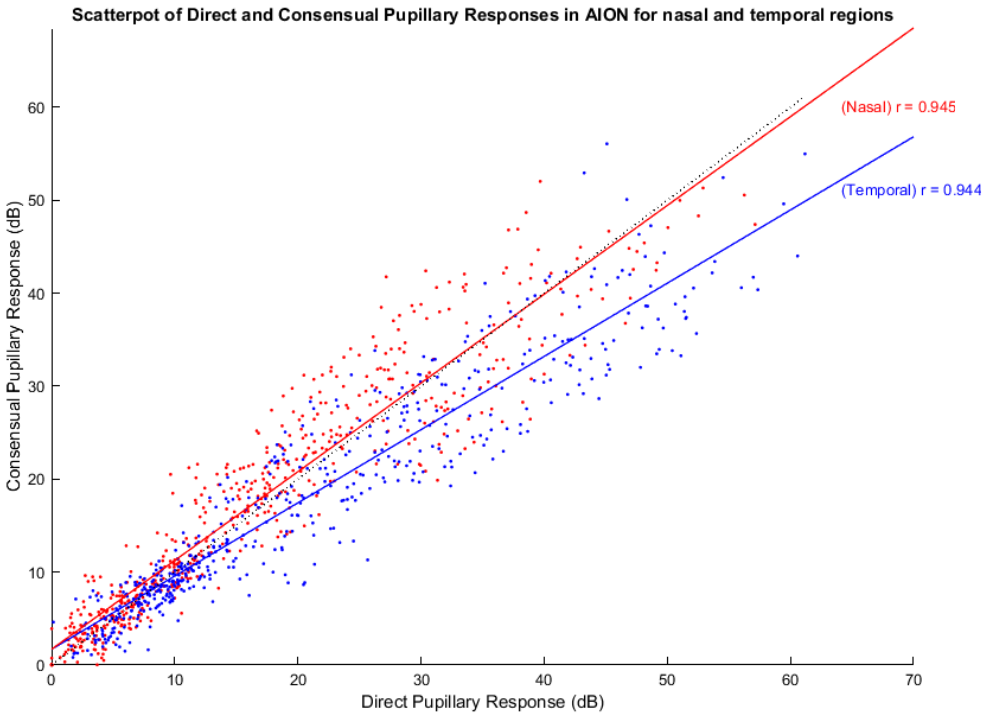

Figure 4.5: Scatter plot of direct and consensual responses for all 44 regions in the AION cohort as per Figure 4.3. There is a highly linear correlation in both, with high *r*-values and near-zero *y*-intercept, suggesting that direct and consensual are highly related. Nasal has a trendline almost exactly matching perfect linear correlation (dotted line), while temporal shows a shallower curve indicating that direct may exceed consensual. A combined plot was also computed but not presented with an *r*-value of 0.93. There appears to be some heteroscedasticity as values increase.

To better examine the differences between the results and more accurately calculate how much larger direct is than consensual in each group, Bland–Altman plots of the same datasets were produced. Figures 4.6 – 4.8 represent stroke, pituitary, and AION direct vs consensual responses. Common features of the graphs are the mean (solid line), 95% confidence interval (dotted lines), and 95th percentile (dashed lines).

Figures 4.6 – 4.8 demonstrate that the mean direct response is significantly larger than the mean consensual in temporal regions of all groups by a margin of ~2 dB, while the consensual significantly exceeded temporal in chiasmal compression and AION by <1 dB, with stroke having a non-significant difference. There is heteroscedasticity in the AION and pituitary groups which was notably absent in the stroke group, likely explaining why stroke has the smallest range (maximum difference between direct and consensual). The large density of responses in all groups were those with means <25 dB, which were most dense near zero difference and only rarely extend beyond a 10 dB difference. With means below 25 dB, differences of 10 dB represent a substantial amount of variation, nearly 50% of their average. While there are certainly average linear trends in the scatter plots, the variability in Bland–Altman analyses suggests that substantial differences remain between direct and consensual responses, particularly at large amplitudes, which warrants further investigation. Given that direct and consensual responses have been noted to differ systematically throughout the visual field in control patients, that this may also be true in these conditions. To investigate this, average visual field responses for each visual field point in each condition were generated for direct only, consensual only, direct – consensual difference, and direct / consensual ratios, pictorially displaying the average fields as if they were a single person's responses. This allows similarities and differences to be organised according to spatial location.

Graphs are displayed in 24-2 format with direct and consensual responses being in greyscale (with the smallest average responses in black and the largest in white). Differences and ratios are presented in a colour-scale, with no-difference or ratio of 1 being white, direct exceeding consensual in red, and the reverse in blue. To allow comparison, direct and consensual are presented on the same scale. Units for direct, consensual, and their difference are in dB, while ratios are unitless. On the axes, degrees of eccentricity are displayed as a guide to relative extent of the visual field range.

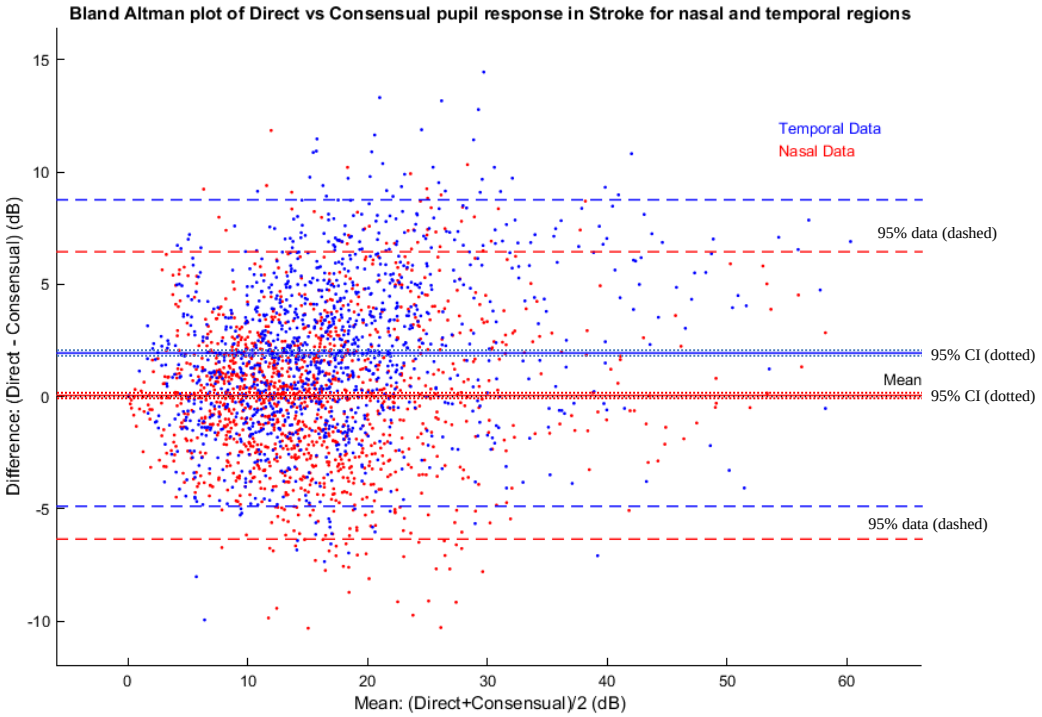

Figure 4.6: Bland–Altman plot of direct and consensual pupillary response in the stroke group, with temporal field in blue and nasal in red. Consistent with the interpretation of the scatter plots, the mean of direct responses is greater than those of consensual in the temporal regions by 1.94 dB (p<0.0001), with 95% confidence interval of 1.81 - 2.07 dB. In nasal regions, direct and consensual are equal on average, with mean of 0.05 dB (p<0.4314) and 95% confidence interval of –0.07 - 0.17 dB. There is a similar degee of variability, with temporal and nasal SD of 3.48 and 3.26 dB respectively, with the largest differences approaching 15 dB and –10 dB at mid-range means of ~25 dB.

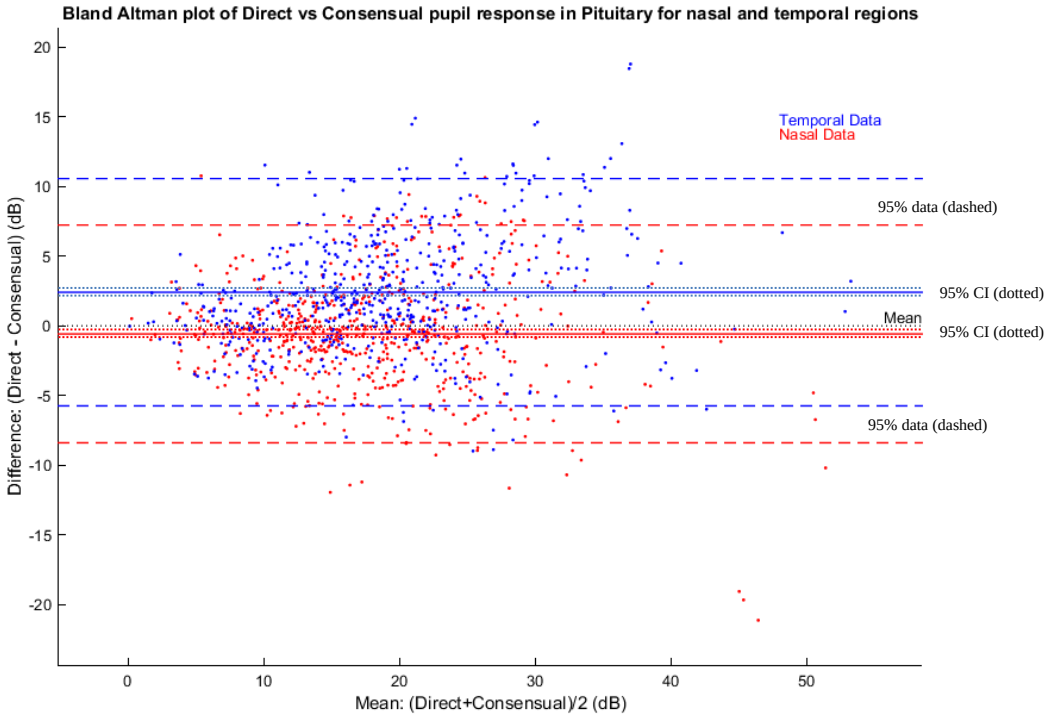

Figure 4.7: Bland–Altman plot of direct and consensual pupillary response in the chiasmal compression group, with temporal field in blue and nasal in red. Consistent with the scatter plots, direct is greater than consensual in the temporal region by 2.41 dB (p<0.0001), 95% confidence interval of 2.16 - 2.66 dB. In nasal regions, consensual marginally exceeds direct, with a mean of –0.58 dB (p<0.0001) and 95% confidence interval of –0.82 - –0.34 dB. There is a similar degree of variability with temporal and nasal SD of 4.16 and 3.98 dB respectively, with the largest differences approaching 20 dB and –20 dB at high means of 35–55 dB.

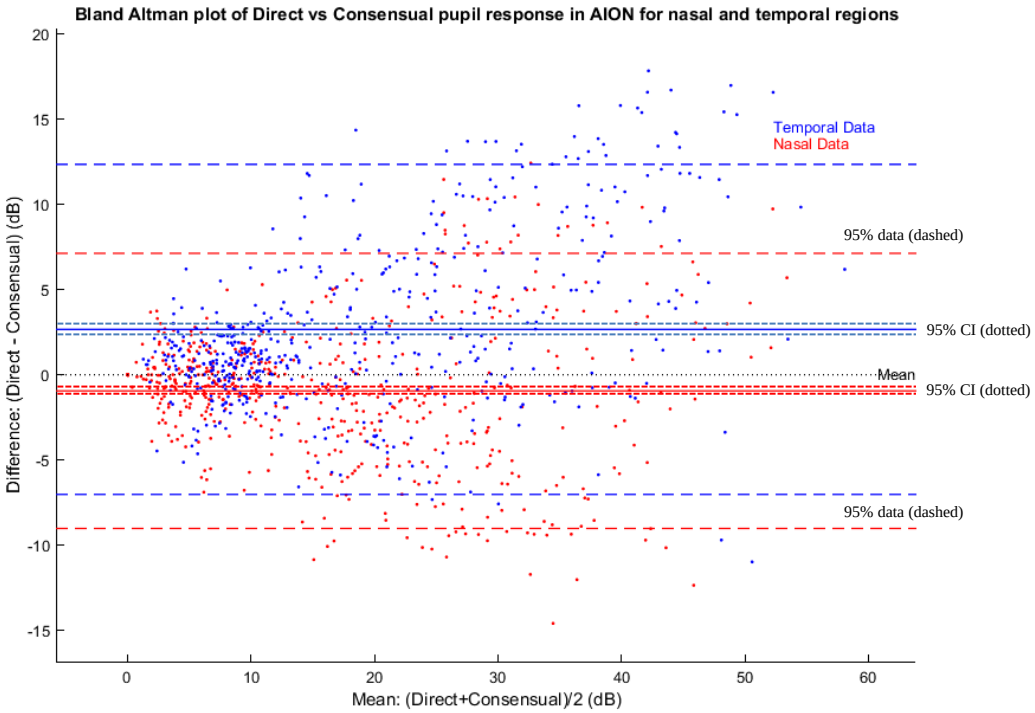

Figure 4.8: Bland–Altman plot of direct and consensual pupillary response in the AION group with temporal field in blue and nasal in red. Consistent with scatter plots, direct is greater than consensual in the temporal region by 2.66 dB (p<0.0001), with 95% confidence interval of 2.37 – 2.95 dB. In nasal regions, consensual modestly exceeds direct with a mean of –0.95 dB (p<0.0001) and 95% confidence intervals of –1.19 - –0.71 dB. There is modestly more variation in temporal than nasal data with SD of 4.94 and 4.11 dB respectively, with the largest differences approaching 18 and –15 dB at high means of 35–55 dB.

Figure 4.9 shows a comparison of direct and consensual for the stroke group. Visual inspection reveals direct and consensual are well aligned, but with clearly visible variation. There is a notable hemifield difference approximating a modest right-sided hemianopia, which is more prominent in the left eye and persists in both direct and consensual responses. While this could be caused by a greater number of right-sided hemianopias in the stroke group, there is actually more left-sided hemianopias, and the effect persisted in the pituitary and AION groups. This is most likely an artefact due to gain control, being based on order of stimulation, an issue which is covered in the Discussion below.

In reviewing the mean difference, there are modest differences of –2 to 4 dB, highlighting that there are a few regions nasally where consensual exceeds direct, while in most temporal regions, direct exceeds consensual. Ratios reflect a similar response, with most temporal regions showing a 10–20% larger direct response, while nasally the responses average out as nearly the same. Figure 4.10 shows a comparison of direct and consensual for the chiasmal compression group. Results are remarkably similar to the stroke group, with moderate alignment of direct and consensual, temporal regions with greater direct responses, and nasal regions with some consensual responses exceeding direct. The main difference appears to be that the temporal bias towards the direct component is less pronounced and the nasal bias is a little more pronounced, with the net difference now showing that consensual modestly exceeds temporal nasally.

Figure 4.11 shows a comparison of direct and consensual for the AION group and is much the same as with the stroke and chiasmal compression groups. There is perhaps better alignment with the chiasmal compression group than the stroke group, in that there is quite definitively a nasal bias towards consensual exceeding direct, while the temporal region appears consistent in all diseases. The key difference in this group is a notably larger difference in the left eye temporal region than in the right.

Overall, Figures 4.9 – 4.11 demonstrate that direct and consensual responses by region grossly match, but with significant noise, consistent with the Bland–Altman plots. But perhaps more interestingly, while not clearly evident in visual inspection of direct and consensual responses, there are consistent small differences naso-temporally. In all conditions, direct exceeded consensual in temporal regions, while in nasal regions they were either equivalent or had consensual modestly exceed direct. Temporal differences were more pronounced than nasal, and this might explain why larger responses were more variable and why direct has an average response greater than consensual in Bland–Altman.

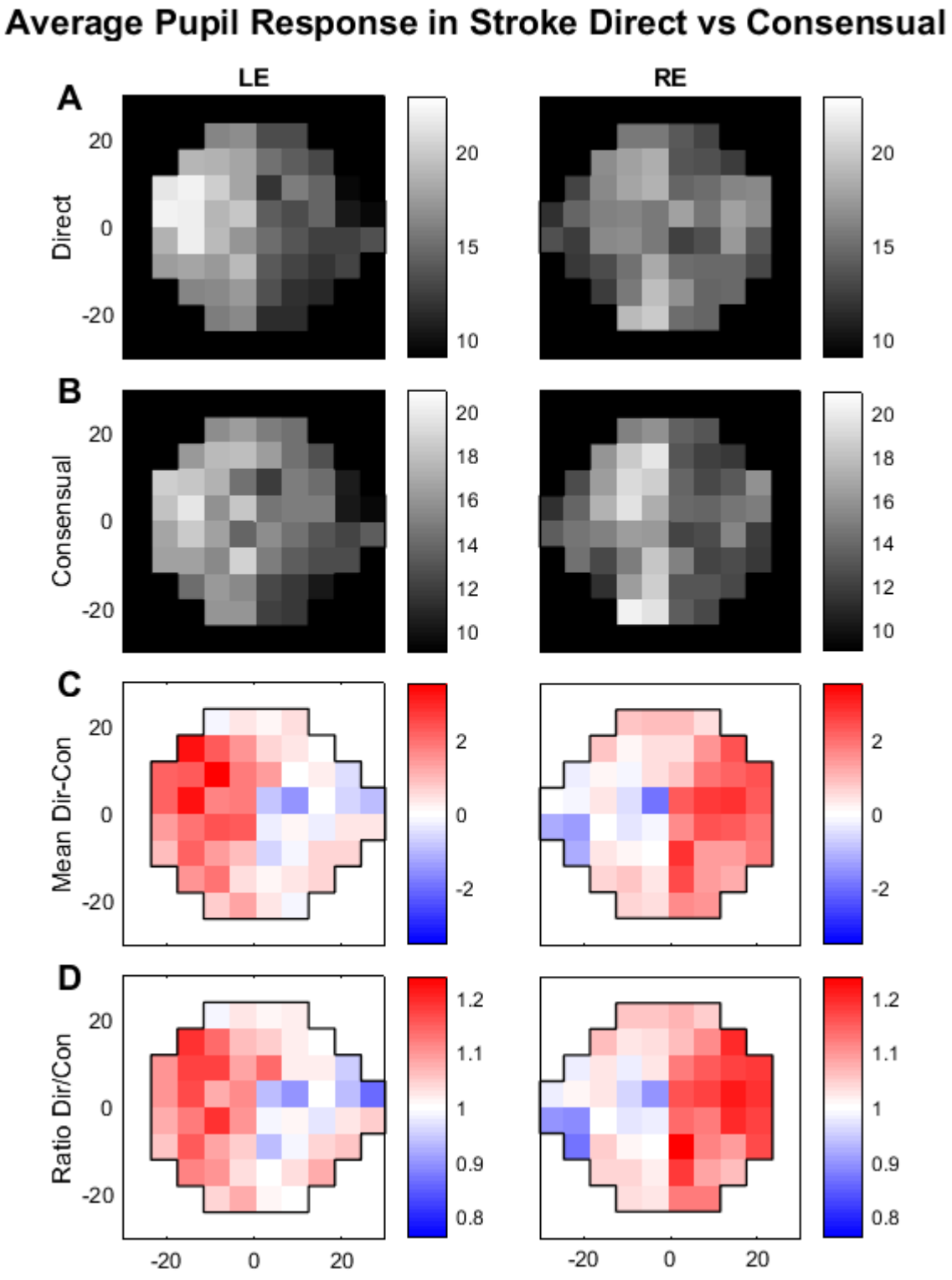

Figure 4.9: Visual field plots for the stroke group showing average subject responses for (A) direct, (B) consensual, (C) difference (Dir – Con), and (D) ratio (Dir / Con). Direct and consensual appear similar, with their difference and ratios revealing that temporal regions tend to have direct responses exceeding consensual, while nasal regions are more equal.

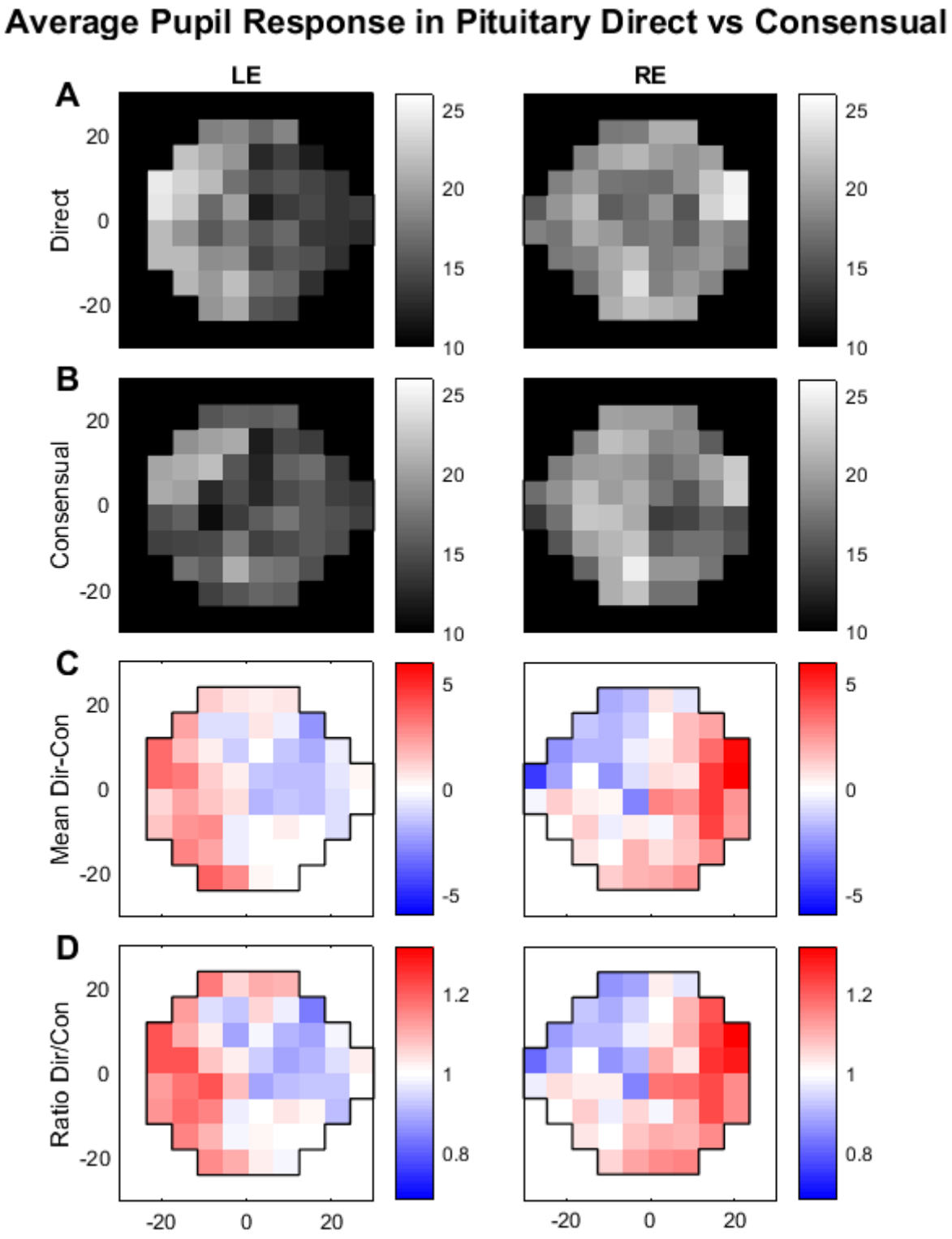

Figure 4.10: Visual field plots for the chiasmal compression group showing average subject responses for (A) direct, (B) consensual, (C) difference (Dir – Con), and (D) ratio (Dir / Con). Direct and consensual appear similar, with their difference and ratios revealing that temporal regions tend to have direct responses exceeding consensual, while nasal regions have consensual modestly exceeding direct.

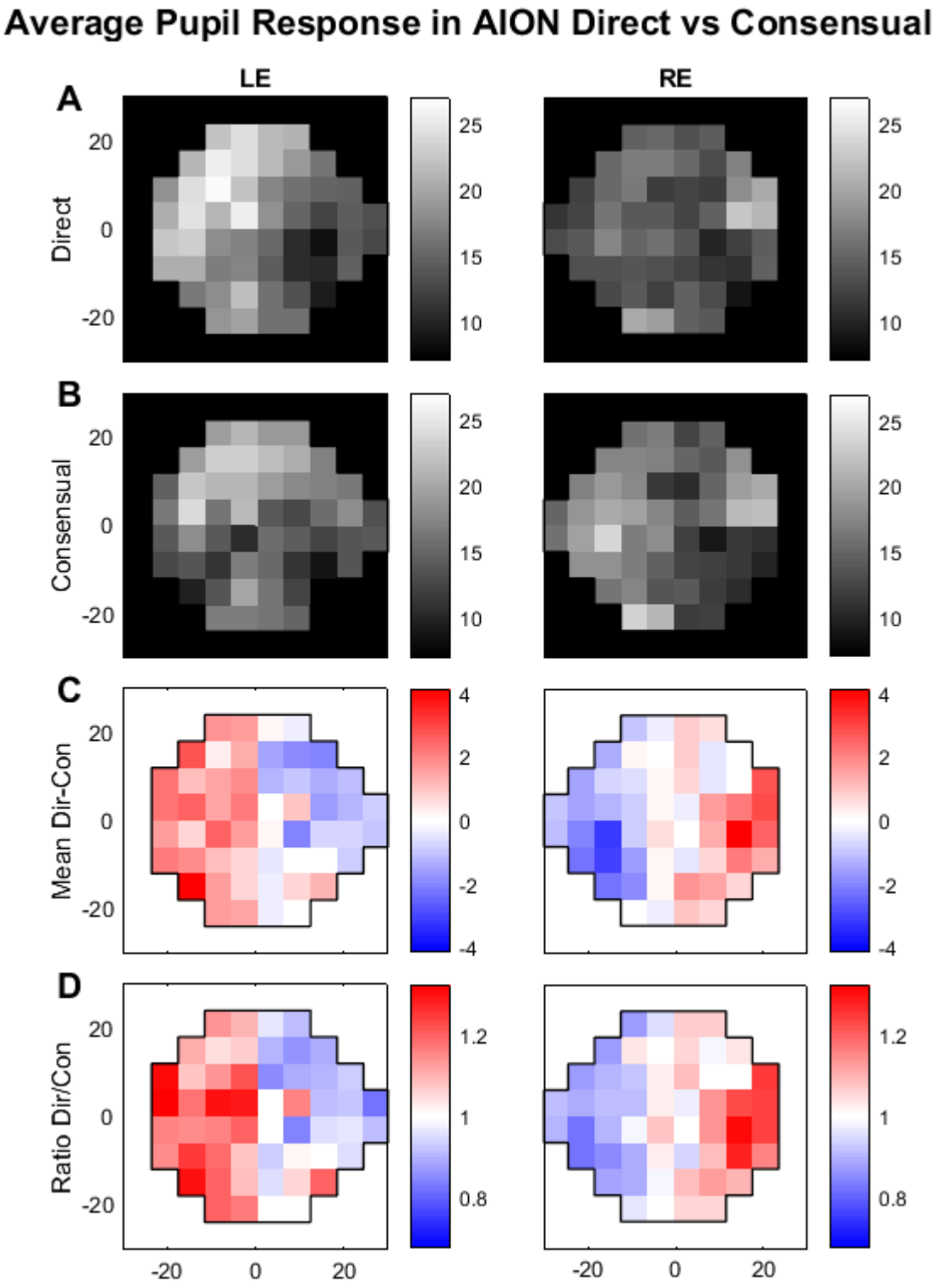

Figure 4.11: Visual field plots for the stroke group showing average subject responses for (A) direct, (B) consensual, (C) difference (Dir – Con), and (D) ratio (Dir / Con). Direct and consensual appear similar, with their difference and ratios revealing that temporal regions tend to have direct responses exceeding consensual, while nasal regions have consensual exceeding direct. The left eye appears to have more pronounced differences than the right.

With larger direct / consensual ratios occurring temporally, it follows that the direct signal is larger than consensual in the temporal visual field, but this does not consider the noise component, and this component may also be larger based on the apparent heteroscedasticity in the scatter plots. A larger signal is not a necessarily a better signal unless its noise is proportionally smaller, and so SNR is a measure of how confident one is that a signal is noticeably different to background noise. To explore whether the SNR for direct and consensual responses also vary naso-temporally and to quantify this difference, Bland–Altman plots of direct and consensual for nasal and temporal regions were produced separately. Averages were taken of the entire nasal region amplitudes (signal) and standard deviations for each point (noise) were averaged by calculating the root mean square (RMS). To gauge the variability in direct and consensual SNR generally, a plot of non-averaged points for nasal and temporal together was also produced.

Similar plots were produced for AION and pituitary, but with very similar results - they are omitted here. Figure 4.12 highlights that the average direct and consensual SNRs are the same in nasal regions, consistent with the equivalent signal demonstrated in Figure 4.9. Also, in keeping with previous results, Figure 4.13 demonstrates that in temporal regions the average SNR for direct is greater than consensual. In contrasting the two, not only are the means different, but there are larger confidence intervals in the temporal region showing greater variation in SNR. Along the *x*-axis it can be seen that results typically have a SNR of between 2 and 7, such that with differences as large as 1.9, there is quite substantial variation among some points. When the same plot is produced without averaging the points, individual point variation along the *x*-axis was as small as 0.01 and as large as 12.2 and *y*-axis differences as large as 4.4. This demonstrates that individual variation between points is quite large and that, despite an average favouring direct overall, many of the points (particularly those in nasal regions) have higher SNR in consensual. Neither direct or consensual alone is individually

accurate enough to replace the other, and so potential ways to combine the two should be considered where the SNR is factored in and neither is discarded, such as an SNR-weighted mean.

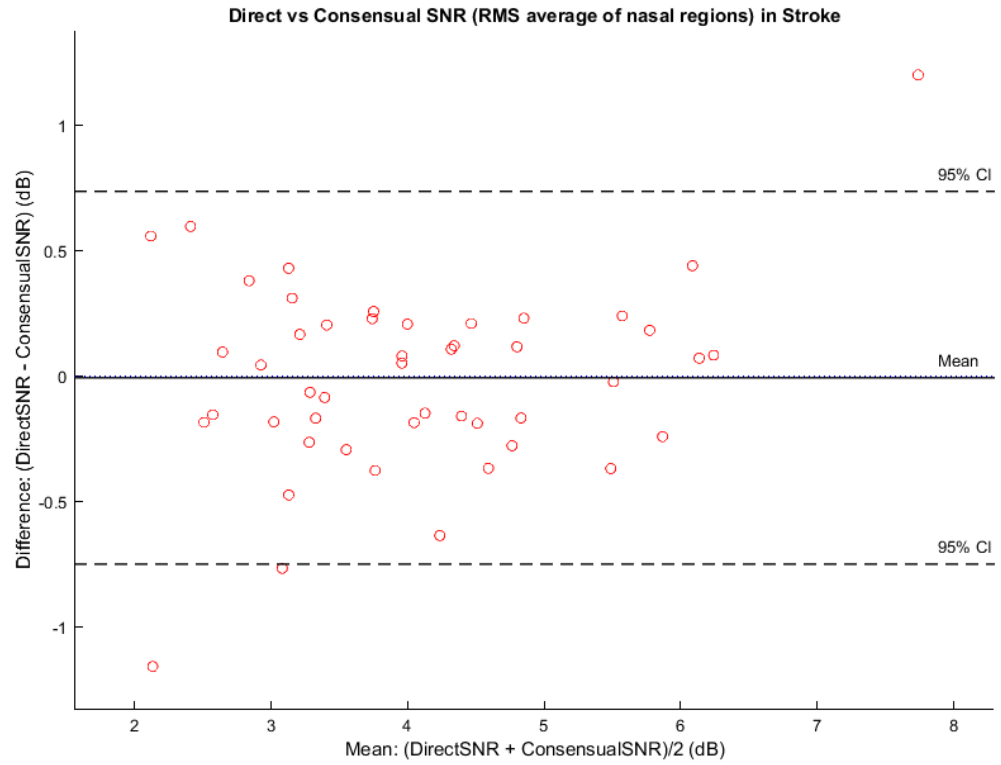

Figure 4.13: Bland–Altman plot of direct SNR against consensual SNR for averaged nasal regions in stroke subjects. The mean is –0.01 dB with a CI of ±0.74 dB and the range from 1.20 to –1.16 dB.

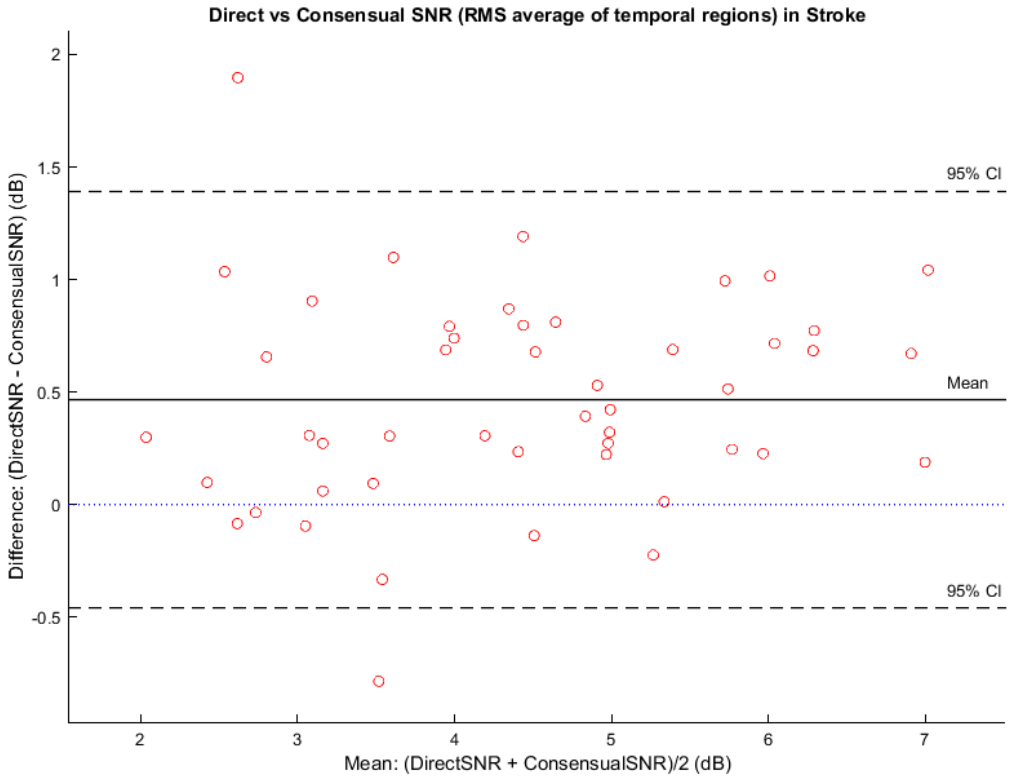

Figure 4.12: Bland–Altman plot of direct SNR against consensual SNR for averaged temporal regions in stroke subjects. The mean is 0.47 dB with a CI of ±0.93 dB and the range from 1.90 to –0.78 dB.

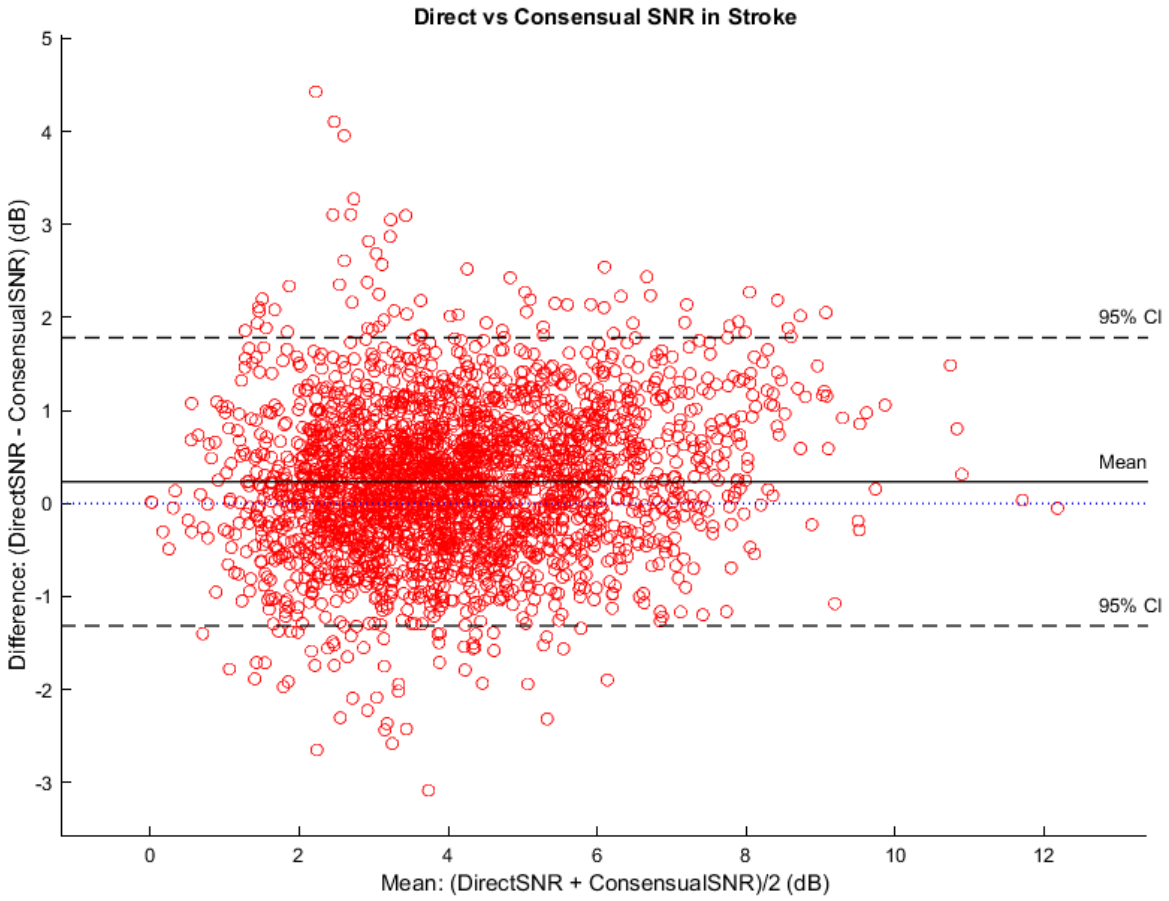

Figure 4.14: Bland–Altman plot of direct SNR against consensual SNR for all visual field regions in stroke subjects. The mean is 0.23 dB with a CI of ±1.5 dB. The *y*-axis range was –3.1 to 4.4 dB, while the *x*-axis range was 0.01 to 12.2 dB. There is marked variation.

The observed difference in direct and consensual response between nasal and temporal visual field mfPOP test regions can be explained by the preferential decussational input from the PON to the EWN. However, if this is assumed to be the only mechanism, it would predict that the temporal direct response would be equal to the nasal consensual, and also that temporal consensual would be equal to nasal direct (equal and opposing biases). To investigate this, a box and whisker plot was created (Figure 4.15). Similar graphs were produced for chiasmal compression and AION with similar results – direct temporal was always the largest with smaller differences between other components. The chiasmal compression box and whisker plot is almost identical to stroke, although without outliers, while AION shows the same overall

trend but with more variability (roughly double the interquartile range for all components). This reveals that direct temporal and consensual nasal are not equal, and that there may be a small difference between direct nasal and consensual temporal. This raises the question of whether larger decussational input from PON to EWN is the only factor at play. Given that both temporal fields appear larger than their nasal counterparts, and temporal fields represent the nasal retinal fibres that cross at the chiasm, perhaps if there were also a modestly larger input from these nasal fibres, this might account for the results. These possibilities are outlined in Figure 4.17 and their plausibility is discussed further in the Discussion.

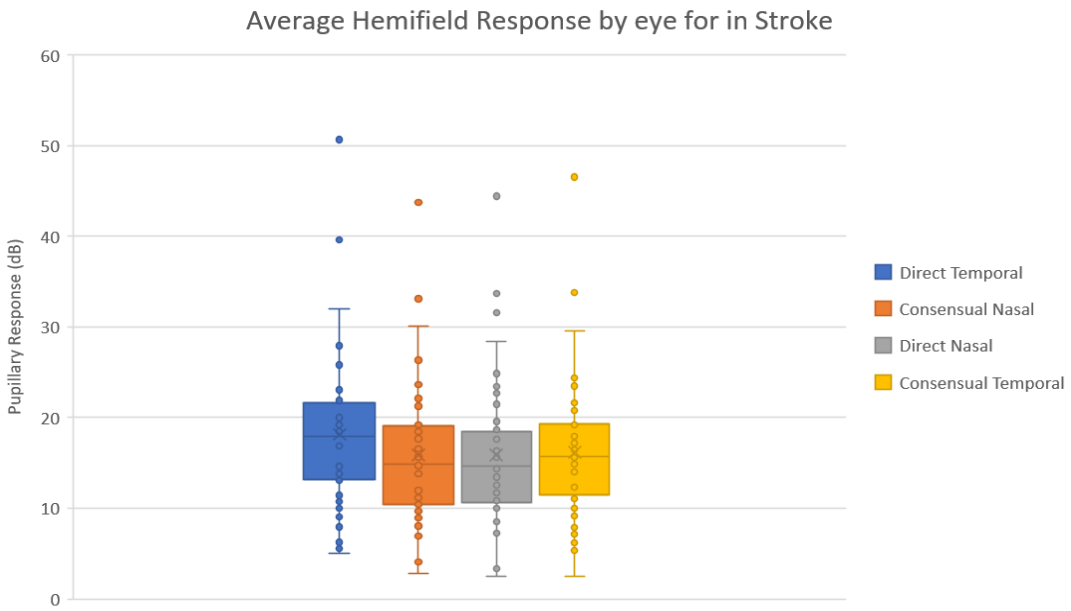

Figure 4.15: Box and whisker plot of hemifield averages by component for each eye of each stroke patient. The box shows the median, upper quartile (75-percentile), lower quartile (25 percentile), while whiskers show 1.5 x interquartile range. Cross represents the mean. Direct temporal response is largest with median, all quartiles and ranges modestly exceeding the other components. Direct nasal is very marginally smaller than consensual temporal, while other components appear equal.

4.5. Discussion

There was a highly linear correlation between direct and consensual, supporting the idea that they may be equivalent, but results from Bland–Altman suggest consistent differences. Direct was shown to be modestly greater than consensual on average in all conditions, consistent with previous studies of control patients who demonstrated the same (Lowenstein, 1954; Smith *et al.*, 1979; Fan *et al.*, 2009). This overall difference was then highlighted to be due almost entirely to nasal–temporal differences, with temporal hemifields having larger direct responses and nasal hemifields having similar or modestly greater consensual responses. As discussed in the introduction, it is a common finding that temporal hemifields have larger direct responses (more prominent), while results for nasal fields were mixed – some showing, as we did, that consensual exceeds direct (Cox & Drewes, 1984; Martin *et al.*, 1991), while other show equivalence (Smith & Smith, 1980; Wyatt & Musselman, 1981; Schmid *et al.*, 2000; Carle *et al.*, 2011).

A comparison to the closely related results from (Carle *et al.*, 2011), who used the same device with the same background luminance (10 cd/m^2) but brighter stimuli (290 cd/m^2 compared to our 150 cd/m^2), reveals that Carle et al. found near-equivalence of direct and consensual in the nasal field, whereas we found that consensual was larger. This earlier work addressed factors which may explain how these discrepant results might originate – that they may depend on stimulus intensity – such that less intense stimuli (like ours) will show a consensual bias, while more intense stimuli will plateau at equivalence for the ranges typical in testing, with a theoretical model predicting modest consensual bias for even more intense stimuli (Carle *et al.*, 2011). This model is based on equal input to the PON and greater contralateral input to the EWN, giving potential for saturation, and our results seem to support this model, although the results can only address the less intense range.

If the proposed PON bias towards contralateral input to EWN (crudely estimated at 15%) were the only factor considered, and pupillary input from nasal and temporal fibres is presumed even, then this would explain the temporal field bias (direct > consensual) and would predict that the nasal field would be equally and oppositely biased (consensual > direct) (Figure 4.17, part C). However, both our results and results from the multiple studies listed above, all report that the temporal field shows the greater bias, with small or no bias in the nasal region. In considering why this might be, it is interesting to note there are known differences in the fibres which supply the PON. There is a higher density of nasal retinal fibres extending laterally within the 30° eccentricity tested using mfPOP (see Figure 4.16), and there are also more nasal retinal fibres that decussate at the optic chiasm, compared to fibres from the temporal retina which continue uncrossed. Studies in primates based on the relative quantity of cortical layer IVc occupied by the ipsilateral and contralateral eyes suggest that 58% decussate and 42% remain uncrossed (Horton & Hocking, 1996; Horton, 1997), while in a human histology study of a single person, 53% of the fibres decussated and 47% did not (Kupfer *et al.*, 1967). If this bias between visual pathways is considered in isolation, with no effect of PON to EWN bias, this would produce stronger nasal retina (temporal field) responses, although it predicts the direct and consensual responses would be about even (Figure 4.17, part B). However, if both effects are considered together (bias towards chiasmal decussation and bias from PON to contralateral EWN), this prediction more closely matches the results, with direct exceeding consensual in the temporal field, consensual exceeding direct in the nasal field, and temporal field effects being of larger magnitude (Figure 4.17, part D).

Cone cell densities in the human retina – Curcio& Allen (1990)

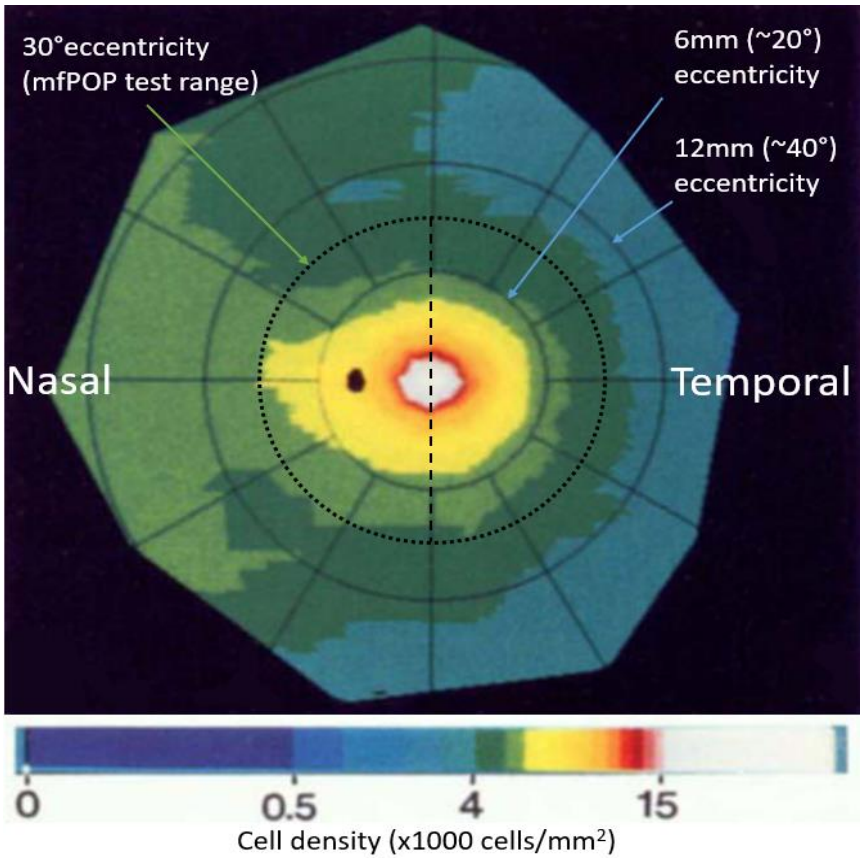

Figure 4.16: Cone cell densities of the human retina showing isodensity lines, with the colour scale bar ranging from 0–15,000 cells/mm^2 (beyond which is white). The original scale bars are labelled with blue arrows at 20° and 40° eccentricity, with a dotted circle added at 30° eccentricity (the mfPOP format width). The vertical meridian is highlighted with a dashed line to help to compare nasal and temporal differences. Note the higher density of cones on the nasal side compared with the temporal side, extending past the ONH. Reproduced with permission (Curcio & Allen, 1990).

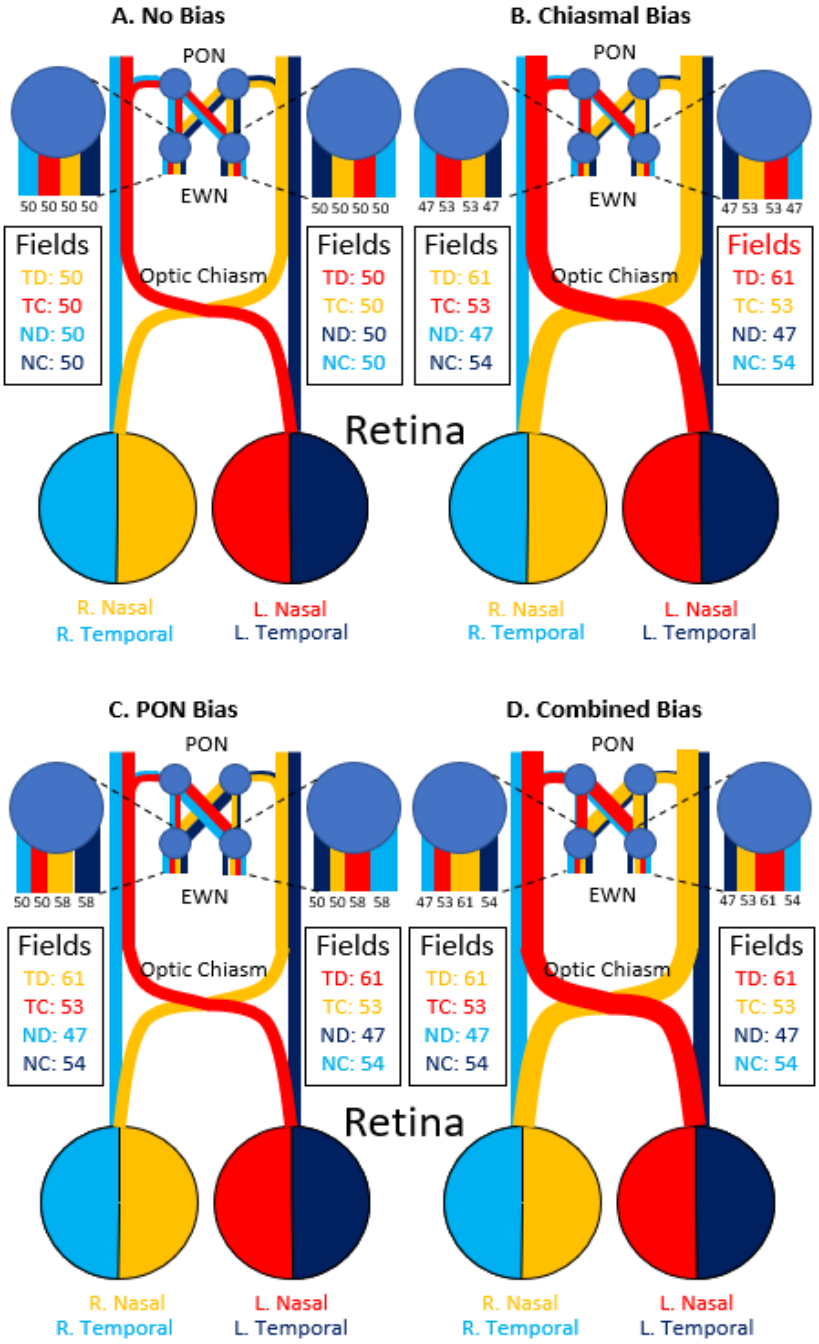

Figure 4.17: Theoretical models of the visual pathways with retinal input from right temporal (light blue), right nasal (orange), left nasal (red), and left temporal (dark blue) with their relative predicted pupil responses. For clarity, these are also presented for the visual field in the tables with key T = temporal, N = nasal, D = direct, and C = consensual. Numbers are only to indicate relative response to allow comparison based on experimental bias at the PON–EWN and nasal–temporal levels. (A) Pathway with no bias – equal input. (B) Preferential nasal/optic chiasms bias (53% of fibres). (C) PON to EWN preferential bias towards contralateral input (15% larger). (D) Combined bias of (B) and (C) including retinal and nuclei bias.

Comparing chiasmal compression direct and consensual bias to that of stroke, bias in the temporal fields was less pronounced, while bias in the nasal fields was more pronounced. Chiasmal compression typically results in bitemporal visual field lesions, and so it was considered whether this might explain the differences. However, as damage to the chiasm would affect all temporal output, and so should equally affect direct and consensual responses (as they separate at the PON), this would seem unlikely. Additionally, similar results were noted in AION, which has no grounds for these differences to have occurred.

A feature highlighted in the results for both direct and consensual across all disease states was the appearance of a mild right homonymous hemianopia, more prominent in the left eye. Given its presence in all disease types, it would appear that this is an artefact of the device itself. It is most simply explained by noting that there is gain control in the pupillary system, which has recently been suggested to be at the EWN level (Carle *et al.*, 2019). The sequence of stimuli in these experiments is to present to the left eye first (left hemifield then right hemifield), followed by the right eye (left hemifield then right hemifield). As the first presentation (left eye, left hemifield) in each segment is the most responsive, and the first presentation in the right eye (right eye, left hemifield) is also more responsive, this would explain both the notable left–right hemifield bias, and why the right eye hemifield bias is less pronounced. As integration has been suggested at the EWN, both pupillary inputs are represented at the EWN, and so it makes sense that gain control may exist between eyes as well as within eyes. While randomisation of stimuli sequence should eliminate this bias, gaps between stimuli would have to be added to maintain temporally sparse stimuli, and this would substantially lengthen test duration. Alternatively, alternating testing order between segments might also provide reduced bias, without altering test duration. This may be explored in future studies.

Variability was highlighted early in the analysis as substantial, with Bland–Altman plots of direct vs consensual revealing it was not uncommon for variation in direct and consensual

responses to be near 50% of their average. In pictorial displays of the averaged visual field, direct and consensual visual fields certainly showed some correlation, but still had marked variation between them, despite them being averages of the group. This was also maintained in SNR plots, showing similar degrees of variation to direct and consensual responses. In assessing how one should amalgamate the direct and consensual responses, this result suggests that while there is a correlation, the responses are not interchangeable, and they vary quite substantially in their SNR. While direct is marginally larger in both signal and SNR, this is only because of the temporal field and so to select only direct would discard a lot of valid data, some of which has better SNR (particularly in the nasal field). A simple average does not account for the amount of variation in SNR, or the naso–temporal differences. Using the largest SNR of the pair would certainly be worth considering, but given that the point of the test is to highlight damaged regions (which will have intrinsically low signal), this may under-represent the true amount of damage and give a positive bias. Therefore, the most appropriate combination based on this data is to complete an average of direct and consensual weighted by SNR. This approach accounts for the naso–temporal differences (since temporally wherever direct exceeds consensual it will have a greater SNR and be proportionately more weighted), while the same is true for consensual nasally. This technique does not discard any data, and should minimise any positive bias.

4.6. Conclusion

Direct and consensual pupillary response amplitudes correlate, but with substantial noise, indicating they are not entirely equivalent. On average, the direct response is greater than the consensual in temporal regions, but it is equivalent or marginally smaller in nasal regions, consistent with controls in previous studies. This effect persisted across all disease types suggesting it is an innate physiological difference. These differences may be explained by larger decussational input from PON to EWN and a greater number of nasal fibres. Similar

degrees of variability in response amplitude and SNR point to neither component being totally superior to the other. In order to combine measures, with the intention of accounting for spatial differences, but without causing positive bias, a combination using an SNR-weighted average is the most suitable.

References

Bland JM & Altman DG. (1999). Measuring agreement in method comparison studies. *Stat Methods Med Res* **8,** 135-160.

Carle CF, James AC, Rosli Y & Maddess T. (2019). Localization of neuronal gain control in the pupillary response. *Frontiers in neurology* **10,** 203.

Carle CF, Maddess T & James AC. (2011). Contraction anisocoria: Segregation, summation, and saturation in the pupillary pathway. *Invest Ophthalmol Vis Sci* **52,** 2365-2371.

Clarke RJ, Blanks RH & Giolli RA. (2003). Midbrain connections of the olivary pretectal nucleus in the marmoset (callithrix jacchus): Implications for the pupil light reflex pathway. *Anat Embryol (Berl)* **207,** 149-155.

Cox TA & Drewes CP. (1984). Contraction anisocoria resulting from half-field illumination. *Am J Ophthalmol* **97,** 577-582.

Curcio CA & Allen KA. (1990). Topography of ganglion cells in human retina. *J Comp Neurol* **300,** 5-25.

Fan X, Miles JH, Takahashi N & Yao G. (2009). Sex-specific lateralization of contraction anisocoria in transient pupillary light reflex. *Invest Ophthalmol Vis Sci* **50,** 1137-1144.

Gamlin PD & Clarke RJ. (1995). The pupillary light reflex pathway of the primate. *J Am Optom Assoc* **66,** 415-418.

Giavarina D. (2015). Understanding bland altman analysis. *Biochem Med (Zagreb)* **25,** 141-151.

Horton JC. (1997). Wilbrand's knee of the primate optic chiasm is an artefact of monocular enucleation. *Trans Am Ophthalmol Soc* **95,** 579-609.

Horton JC & Hocking DR. (1996). Intrinsic variability of ocular dominance column periodicity in normal macaque monkeys. *J Neurosci* **16,** 7228-7239.

Hutchins B & Weber JT. (1985). The pretectal complex of the monkey: A reinvestigation of the morphology and retinal terminations. *J Comp Neurol* **232,** 425-442.

James AC. (2003). The pattern-pulse multifocal visual evoked potential. *Invest Ophth Vis Sci* **44,** 879-890.

James AC, Kolic M, Bedford SM & Maddess T. (2012). Stimulus parameters for multifocal pupillographic objective perimetry. *J Glaucoma* **21,** 571-578.

James AC, Ruseckaite R & Maddess T. (2005). Effect of temporal sparseness and dichoptic presentation on multifocal visual evoked potentials. *Visual Neurosci* **22,** 45-54.

Kupfer C, Chumbley L & Downer JC. (1967). Quantitative histology of optic nerve, optic tract and lateral geniculate nucleus of man. *J Anat* **101,** 393-401.

Lowenstein O. (1954). Alternating contraction anisocoria; a pupillary syndrome of the anterior midbrain. *AMA Arch Neurol Psychiatry* **72,** 742-757.

Martin TI, Kardon RI & Thompson HS. (1991). Unequal direct and consensual pupillary responses to hemiretinal stimuli. *Invest Ophth Vis Sci* **32,** 1124.

Ruseckaite R, Maddess T, Danta G, Lueck CJ & James AC. (2005). Sparse multifocal stimuli for the detection of multiple sclerosis. *Ann Neurol* **57,** 904-913.

Sabeti F, Maddess T, Essex RW, Saikal A, James AC & Carle CF. (2014). Multifocal pupillography in early age-related macular degeneration. *Optometry and vision science : official publication of the American Academy of Optometry* **91,** 904-915.

Schmid R, Wilhelm B & Wilhelm H. (2000). Naso-temporal asymmetry and contraction anisocoria in the pupillomotor system. *Graef Arch Clin Exp* **238,** 123-128.

Smith SA, Ellis CJ & Smith SE. (1979). Inequality of the direct and consensual light reflexes in normal subjects. *The British journal of ophthalmology* **63,** 523-527.

Smith SA & Smith SE. (1980). Contraction anisocoria: Nasal versus temporal illumination. *The British journal of ophthalmology* **64,** 933-934.

Tigges J & O'Steen WK. (1974). Termination of retinofugal fibers in squirrel monkey: A re-investigation using autoradiographic methods. *Brain Res* **79,** 489-495.

Wyatt HJ & Musselman JF. (1981). Pupillary light reflex in humans: Evidence for an unbalanced pathway from nasal retina, and for signal cancellation in brainstem. *Vision Res* **21,** 513-525.

Zaki R, Bulgiba A, Ismail R & Ismail NA. (2012). Statistical methods used to test for agreement of medical instruments measuring continuous variables in method comparison studies: A systematic review. *Plos One* **7,** e37908.

Chapter 5: Visual field comparison of standard automated perimetry and pupillometry in stroke, chiasmal compression, and AION

5.1. Abstract

5.1.1. Purpose

The Humphrey and Matrix field analysers (HFA, MFA) are routinely used in clinical practice to assess visual fields. While there is a lot of research into comparisons in glaucoma, there is limited research on comparisons in stroke, pituitary tumour, and AION. Multifocal pupillographic objective perimetry (mfPOP) is a novel perimeter under development which has many potential advantages over traditional testing, including simultaneous testing of the two eyes, both response amplitude and delay, standard errors of the field data, and objectivity. While mfPOP has been shown useful in a number of retinal disorders, it has not yet been tested in neurological disorders, which are of particular interest given it utilises pupillary responses which are neurally encoded. The aims of this study are to investigate relationships between these devices and compare their diagnostic ability in order to suggest which device(s) are most effective. Of particular interest is whether post-geniculate lesions appear in mfPOP, as in standard automated perimetry.

5.1.2. Methods

There were 25 stroke, 11 pituitary tumour, and 10 AION patients who were recruited and screened for retinal disorders with a test set including OCT scan, IOP measure, and BCVA. Subjects were tested using Humphrey 24-2 SITA-Full perimetry (HFA), Matrix frequency

doubling 24-2 perimetry (MFA), and an mfPOP yellow/yellow protocol. Control data was used from a previous study using the same protocol. Threshold values in dB were used for HFA and MFA devices. The mfPOP data had pupillary response measures extracted by region using iterative nonlinear regression. Direct and consensual signals were combined by SNR-weighted means, converted in dB using the generalised logarithm, and interpolated onto a 24-2 grid. Comparisons were made with scatter plots (using principal curves with and without 0 dB points included), Bland–Altman plots, and intraclass correlation coefficients using hemifield ratios. Diagnostic ability was assessed using area under receiver operator characteristics plots (with bootstrap based upon the hemifield ratio signal).

5.1.3. Results

Principal curves for scatterplots (with 0 dB points removed) show a somewhat linear relationship between HFA and MFA and a non-linear logarithmic-like relationship with mfPOP. Bland–Altman plots demonstrated the most linear relationship between HFA and MFA over their upper range in all conditions, with small mean differences and 95% CIs when the devices were compared. Bland–Altman plots for HFA and mfPOP showed very limited agreement, with large mean difference and 95% CI; MFA and mfPOP also showed limited agreement with intermediate mean difference and large 95% CI. Hemifield ROC plots for HFA, MFA, and mfPOP showed AUC of 0.842*, 0.844*, and 0.531 for stroke (* = significant); AUC of 0.724*, 0.966*, and 0.545 for chiasmal compression; and 0.912*, 0.885*, and 0.533 for AION. The ICC for HFA vs MFA were 0.985 for stroke, 0.923 for pituitary, and 0.962 for AION (all highly significant), while correlations between HFA and mfPOP or MFA and mfPOP were all non-significant or marginally significant.

5.1.4. Conclusions

HFA and MFA correlate very well with each other in all conditions, while mfPOP did not correlate well with either HFA or MFA, but marginally better with MFA. This may be due to

mfPOP more linearly correlating with structural loss (RNFL thickness) while HFA and MFA show more logarithmic relationships to structure. HFA and MFA performed well at detection of conditions using hemifield ratios, with HFA slightly out-performing MFA in stroke and AION, while MFA substantially out-performed HFA in chiasmal compression. mfPOP was not effective at distinguishing disease state based on hemifield ratios. Visual inspection suggested that mfPOP demonstrated some correlation in complete/near-complete homonymous hemianopia, which suggests detection of post-LGN damage; a likely hypothesis is retrograde degeneration, which is only noted in hemianopia but not quadrantanopia or smaller. Further investigation is necessary using MRI data to confirm this hypothesis.

5.2. Introduction

In the assessment of visual fields, standard automated perimetry (SAP) has become the mainstay of clinical practice; it is a standardised approach that is minimally dependent upon the person administering the test. Different approaches can be used such as the Humphrey Field Analyser (HFA) which uses Goldmann size III (0.43° diameter) stimuli with varying luminance, and the Matrix Field Analyser (MFA), which uses larger contrast-reversing grating stimuli whose varying contrast produces a frequency-doubling effect. Each of these devices has its own limitations, with HFA being demonstrated in glaucomatous fields to have poor reproducibility over most of its range (Heijl *et al.*, 1989; Artes *et al.*, 2002) and greater peripheral variability (Berezina *et al.*, 2011) consistent with other similar devices (Pearce & Maddess, 2016). The small stimulus size of these devices is suggested to be a strong contributor to these effects (Wall *et al.*, 2013; Gardiner *et al.*, 2015; Numata *et al.*, 2017), as is undersampling (Weber & Dobek, 1986; Maddess, 2011b, 2014). MFA attempts to correct some of these deficits with larger stimuli, which do appear to have reduced variability (Chauhan & Johnson, 1999; Artes *et al.*, 2005; Horani *et al.*, 2007; Wall *et al.*, 2009; Wall *et al.*, 2010). A new Mean Likelihood (ML) algorithm was also used for estimation, replacing the Swedish Interactive Thresholding Algorithm (SITA) used in HFA with the Zippy Estimation of Sequential Testing (ZEST). ZEST showed promise on early testing (Anderson & Johnson, 2006) but causes all results to converge on only 15 unevenly spaced values (Fredette *et al.*, 2015), which may contribute to the reduced variability. Different contrast definitions are also used: HFA uses the Weber formula, while Matrix uses the Michelson formula. There are also different calculations of log units, with HFA using 10*log(Amplitude) and MFA using 20*log(Amplitude), meaning no direct correlation of units is possible between machines despite having a procedurally similar approach and coincidently similar values (Fredette *et al.*, 2015).

While it would seem that MFA has the edge in early glaucoma detection (Medeiros *et al.*, 2004; Kim *et al.*, 2007), in optic nerve and chiasmal damage they are reportedly similar clinically (Huang *et al.*, 2008). In detection of post-LGN lesions producing homonymous field defects (typical in stroke), HFA out performs MFA but not to statistical significance (Taravati *et al.*, 2008). In practice, HFA is by far the most commonly used device for testing of neurological conditions (Hepworth & Rowe, 2018).

Multifocal pupillographic objective perimetry (mfPOP) provides an entirely new approach to assessing field damage by removing the subjective patient response to stimuli and replacing it with an objective autonomic response of pupil constriction to light. It also takes into consideration lessons from the HFA and MFA in terms of having large stimuli to reduce test–retest variability, and increasingly larger stimuli peripherally to counter the increased peripheral variability seen in HFA and compensate to some extent for the smaller retinal magnification (Holden & Fitzke, 1988). It has veered away from both the SITA and ZEST approximations, which are both based on varying stimulus intensity with a binary response, in favour of using fixed contrast stimuli while measuring the amplitude response. By presenting multiple stimuli simultaneously (multifocally) and then extracting component signals, this also allows both eyes to be tested at once, a faster test time, and multiple tests of a single field location, allowing less variability and more consistency (Maddess *et al.*, 2009). It has been trialled and shown promise in a number of common retinal diseases including early detection of diabetic retinopathy (Bell *et al.*, 2010; Coombes *et al.*, 2012; Sabeti *et al.*, 2015), early detection of age-related macular degeneration (AMD) (Sabeti *et al.*, 2011; Sabeti *et al.*, 2013; Sabeti *et al.*, 2014; Sabeti *et al.*, 2017), and similar diagnostic accuracy to SAP in glaucoma (Maddess *et al.*, 2009; Carle *et al.*, 2011a; Maddess *et al.*, 2013; Carle *et al.*, 2015). For neurological conditions, there also appears to be some promising results in migraine (Lueck *et al.*, 2014) and epilepsy (Ali *et al.*, 2015). Testing of neurologically based conditions which

affect visual field loss is limited, with multiple sclerosis being assessed (Maddess *et al.*, 2012a; Ali *et al.*, 2014). However, conditions such as anterior ischemic optic neuropathy (AION), chiasmal compression, and stroke have been largely unexplored. Neurological testing with mfPOP is of particular interest, given it objectively measures neurological pathways via the pupillary response and that completion of complex tasks like SAP may be difficult and exhausting for those with neurological deficits. It would be interesting to identify whether any differences can be detected and whether they correlate with the locations identified in traditional field testing. AION manifests as anterior damage at the optic disc, chiasmal compression as an intermediate at the optic chiasm, and occipital stroke as a more posterior damage post-LGN, which is notably after the subcortical pupillary response branch point.

Significant cortical input from both striate and extrastriate vision areas to the pretectal olivary nucleus (PON) has been demonstrated in monkeys (Gamlin, 2006). These include input from occipital cortex (V1) (Benevento & Rezak, 1976; Benevento *et al.*, 1977; Distler & Hoffmann, 1989), visual association cortices V2-5 (Benevento & Davis, 1977; Benevento *et al.*, 1977; Dineen & Hendrickson, 1983), and the inferior temporal region (Steele & Weller, 1993). However, with anatomical evidence of input to PON, the question becomes: does the pupillary system have meaningful responses to cortical input? Practically, it is well established that pupils respond to arousal and cognitive state (Cash-Padgett *et al.*, 2018), and pupillary response delays in isoluminant colour exchange (Young & Alpern, 1980; Carle *et al.*, 2013) imply notable cortical input from colour integration. Finally the question has been quite elegantly answered by Heywood et al. who demonstrated that cortical lesion to the inferior temporal region of a monkey abolishes isoluminant chromatic exchange response but not luminant achromatic response, demonstrating that cortical lesions may indeed be detected by the pupillary pathway with selective stimuli (Heywood *et al.*, 1998). Given there is strong evidence in monkeys for pupillary detection of a specific cortical lesion, it would be interesting to

ascertain if this is true in human stroke patients, who may have more varying damage affecting analogous regions in addition to other cortical input pathways.

This project aims to explore visual field responses in stroke, pituitary tumour, and AION using two traditional perimeters: HFA and MFA, and compare them to novel mfPOP responses in terms of assessing consistency and diagnostic ability, while also exploring the possibility that the subcortical pupillary response pathway receives cortical input.

5.3. Methods

The history of mfPOP and the reasons for its test parameters can be found in the Introduction (1.6.4 *Multifocal methods*). Full methods including recruitment (section 2.1), screening (section 2.2), and mfPOP stimuli, procedures, and output measures (section 2.5.3) are detailed in the General Methods. Here for brevity only an overview of these will be presented. Noting that 1 subject from the stroke group and two from the chiasmal compression group did not complete day 3 of testing, and so do not have Matrix fields or repeat mfPOP reports. Where possible these subjects were still included in the data set, but removed where data was absent or necessary for comparison.

5.3.1. Subjects and screening

Subjects were recruited from multiple hospital and eye clinic sources and informed consent obtained. Subjects were screened for pre-existing ocular conditions, both via questionnaire and clinical assessment. The latter included best corrected visual acuity 6/24 or better, cataract screening, intraocular pressure measurement, fundus photo, and OCT scans of posterior pole and optic nerve head. Groups consisted of stroke (heterogenous cortical lesions) (n = 25), chiasmal compression (n = 11), and AION (n = 10).

5.3.2. Visual field assessment

All subjects completed the 24-2 pattern of the Humphrey Field Analyser [HFA II] (Carl Zeiss Meditec Inc., Dublin, CA; Achromatic SITA-Full perimetry), 24-2 pattern of the Humphrey Matrix frequency-doubling perimeter [MFA II] (Carl Zeiss Meditec, Inc. Dublin, CA), and multifocal pupillographic objective perimetry (mfPOP) on a prototype FDA-cleared ObjectiveFIELD (Konan Medical USA Inc, Irvine CA) with yellow stimuli on yellow background (Y/Y) which measured maximum amplitude of the pupillary response waveform. Subjects had their visual fields tested over 2 days within 2 weeks of each other. On their first day, subjects had HFA and both mfPOP protocols (Y/Y and G/R) tested, and on their second day had MFA and a repeat of both mfPOP protocols. The order of testing was randomised such that standard automated perimetry (SAP; HFA or MFA) was tested first on one of the days and mfPOP on the other. The analysis for this chapter only uses the more established Y/Y stimuli, as the G/R protocol was of novel design and control data was unavailable (instead G/R is explored in Chapter 6).

5.3.3. Humphrey Field Analyser (HFA)

Methods for conducting HFA are as described in General Methods (2.5.1 *Humphrey Field Analyser (HFA)*). This comprised testing of the 24-2 format, which tests points 3° either side of the meridians and extends to 21° in every direction, with two additional points nasally to 27°. Goldmann size 3 (0.43° diameter) white light stimuli are used, and the order of presentation was determined by the Swedish Interactive Threshold Algorithm (SITA). Standard operating procedures were used according to the HFA manual. Subjects had their ocular prescription measured by vertometer, and entered into HFA device, which recommended trial lenses used during testing. The right eye was always tested first. Subjects were instructed how to complete testing and asked to fixate on central fixation dot. Gaze tracking was initiated prior to testing where possible, and pupil was centred on reference

marker, with small alterations during testing completed as necessary. Where result had poor validity markers (fixation loss >20% or false positive values >33%), the test was repeated. Threshold values were internally calculated according to the Weber formula of contrast ranging between 0-35 dB.

5.3.4. Matrix Field Analyser (MFA)

Methods for conducting MFA are described in General Methods (2.5.2 *Matrix Field Analyser (MFA)*). This comprised testing of the 24-2 format, similar to HFA above, with the addition of a single central test region whose data was discarded. Stimuli were 5° in diameter, consisting of low spatial frequency sinusoidal gratings which were counter-phase flickered at high temporal frequency (>15 Hz), utilising the frequency doubling effect. The order of presentation was determined by Zippy Estimation by Sequential Testing (ZEST) algorithm, resulting in 15 unevenly spaced values. Standard operating procedures were used according to the MFA manual. Subjects with ocular prescriptions < ±3 dioptres were tested without glasses, while those with larger prescriptions were tested with their glasses on. The right eye was always tested first. Subjects were instructed how to complete testing, asked to focus on central reference cross, and a short demonstration was completed for 30 seconds. Pupil was centred on reference marker and small alterations during testing were completed as necessary. Where result had poor validity markers (fixation >20% or false positive values >33%), the test was repeated. Threshold values were internally calculated according to the Michaelson formula of contrast, ranging between 0-38 dB.

5.3.5. Multifocal Pupillographic Objective Perimetry (mfPOP)

The same testing methods were used as described in Chapter 4 (4.3.2 *Multifocal pupillographic objective perimetry (mfPOP)*), with the exception that direct and consensual responses were now combined using signal-to-noise ratio (SNR) weighted means, as per the recommendation from that chapter. A brief outline of methods will be given here, but for further details, refer to

either Chapter 4 or the General methods, where these have already been set out more expansively.

5.3.5.1. Testing protocol and settings

Ambient light was kept constant, and ocular lenses to the nearest 3 spherical dioptres were used. Vergence was aligned to optical infinity. Patients were instructed to maintain focus on a central marker, that they could blink throughout but should minimise it during testing (9 × 45 s segments), instead utilising the breaks (7 s between segments).

Both eyes were tested simultaneously using independent stimuli displayed at 60 frames/s and recorded at 60 frames/s which was interpolated to 30 frames/s. If pupils were obscured by eyelashes or blinking, data was removed, and if less than 85% of stimuli had data, the segment was repeated.

Stimuli were yellow patches averaging 150 cd/m^2 (Y/Y) on a yellow background averaging 10 cd/m^2. A standard layout of 44 regions was used in the shape of partially overlapping segmented annuli which had larger peripheral stimuli (see General Methods, Figure 2.21). Presentation of the stimuli were divided into 8 sections: left and right eye, left and right hemifield, and odd and even rings. Presentations were in clustered volleys (Sabeti *et al.*, 2014), which are temporally sparse stimuli that may be spatially near (see General Methods, Figure 2.22). On average, 50% of regions within a section were activated for 33 ms with a 250 ms delay between each volley, sequentially rotating through presentations in each section. In effect, each test region was activated on average every 4 s for a total of ~90 presentations over 360 s total test duration.

5.3.5.2. Signal extraction and processing

The output signal was processed into response amplitude using a multiple linear regression method as described elsewhere (James, 2003; James *et al.*, 2005; Ruseckaite *et al.*, 2005).

Responses were normalised to a 3.5 mm average to account for resting differences between subjects (James *et al.*, 2012). Amplitudes (μm) were converted into dB using the generalised logarithmic transform to stabilise variance and account for small dilations (see Chapter 4, 4.3.2.2 *Signal extraction and processing*). Direct and consensual components were combined, weighted according to their SNR computed using the *t*-statistic calculated from the per-region responses and the standard error (SE) from the regressive response estimation process. The 44 region mfPOP map was converted to the 54 region HFA map of 24-2 format using weighted averages according to the relative contribution of the overlapping areas. This resulted in directly comparable points between all three devices and all in dB units, although with notably different definitions of contrast and dB scaling.

5.3.6. Analysis

Visual field maps based on the 24-2 format were produced for each subject and device by using a simple greyscale plot on the same scale of 0–35 dB. This is analogous to plots produced from the HFA and MFA devices but has been produced independently from the raw data for direct comparison. Examples are shown (Figure 5.3) which outline the first of each: left homonymous hemianopia (HH), right HH, chiasmal compression field damage, and AION field damage.

5.3.6.1. Principal curves

To investigate relationships between devices, scatterplots were generated with principal curves fitted for each device and protocol with pooled data across disease states. Principal curves begin with the first principal component and then iteratively bend this fit to ensure equal points on either side of the curve with respect to the local normal. Principal curves were selected as an unbiased measure of trend which may conform to any shape (Gerard & Fischer, 2011) and were produced using the princurv function in R using the parameters threshold 100 and maxiterations 1000 (as per (Wall *et al.*, 2010) in comparing field analysers). This revealed non-

linear relationships between all devices, but good linear internal consistency between mfPOP protocols. It was then investigated whether removal of the 0 dB points (which fall below the dynamic range of measurement and so are artificially correlated) changed the relationships. Removal of 0 dB points resulted in a near-linear relationship between HFA and MFA, and produced logarithmic curves between HFA or MFA against mfPOP.

5.3.6.2. Bland–Altman

Bland–Altman plots were produced for each disease state and device to highlight differences between devices and avoid the effect of regression to the mean. Plots were produced with overall mean difference between devices with 95% CI range, as well as percentile values of

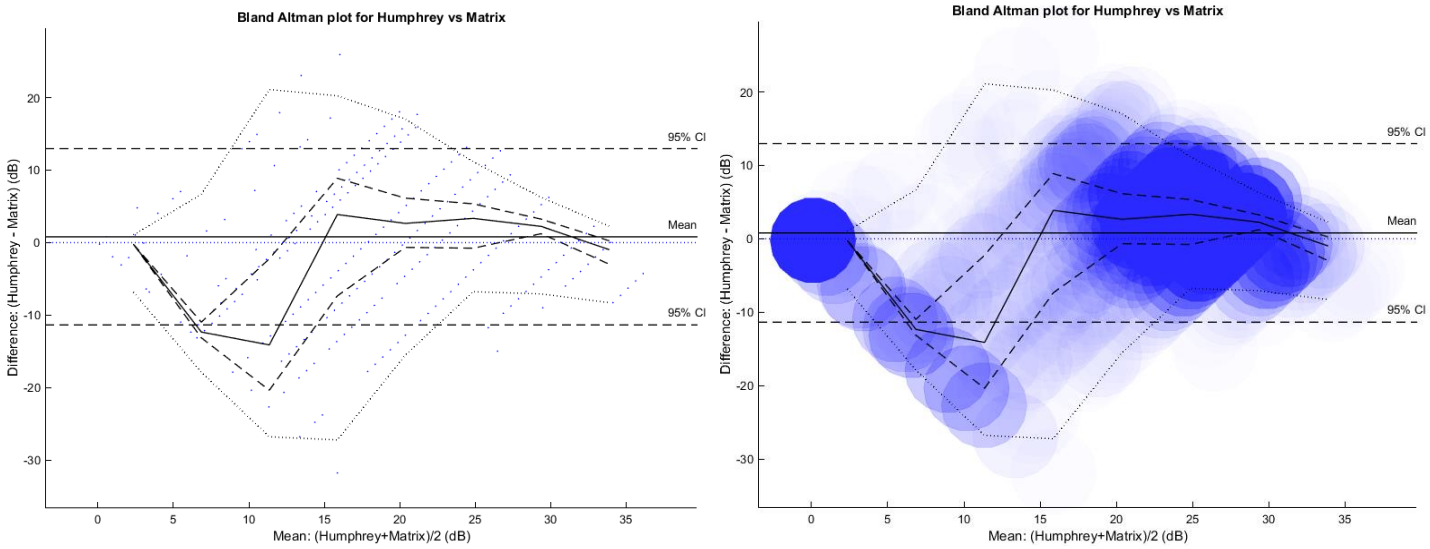

Figure 5.1: Example Bland–Altman plots with (left) single dot data points and (right) semi-transparent enlarged data points to highlight overlap and data dense regions.

5%, 25%, 50%, 75%, and 95% plotted across the range of binned abscissa to highlight areas of elevated variability. Because MFA is limited to 15 possible responses and HFA to 30, using single points does not create a representative view of where the data densities are (see Figure 5.1) and so larger semi-transparent points were used in Matlab with alpha 0.01 and size 5000 to better gauge areas of relative density. Also note the large density of points at (0,0), which are due to 0 dB readings in HFA and MFA. As with scatter plots, these were removed given that they are a truncation of actual scores and are not comparable with continuous mfPOP. Also

note the diagonal lines of data, which exist due to a result for one device (for example HFA 0 dB) having many possible results in the other device (for example MFA 0, 2, 3, 6, 7, 10, 12, 13, 18 dB), which when plotting their average against their difference will result in diagonal placements of points as seen in Figure 5.1.

5.3.6.3. Hemifield ratios

As it is well established in stroke that post-LGN damage typically presents with homonymous field damage (with the most extreme form being homonymous hemianopia), homonymous defects are a classic and effective means to identify post-chiasmal stroke. All three perimeters produce fields with different contrast and ranges, which might make homonymous field identification challenging. In order to compare a machine's ability to identify stroke, a hemifield ratio may be calculated by comparing either the left hemifields of both eyes over the right hemifields or vice versa, depending on the side of damage. To account for either possibility, the minimum of both options was taken, which represents the ratio showing the most damage (see Figure 5.2 top). This was in part done because we did not know with confidence which field was expected to show a hemianopic defect, especially where the field damage due to the stroke was mild. Also, some of the patients had suffered multiple strokes and so strokes were not necessarily confined to a particular half of the posterior pole of the cortex.

A full and complete hemianopia will have a hemifield ratio of 0, and a completely normal field where there is no field damage will have a ratio of 1. This ratio can then be used in receiver operator characteristics (ROC) plots (heading 5.3.6.4) to highlight which devices are most effective at detecting hemifield damage, and in an intraclass correlation coefficients (ICC) table (heading 5.3.6.5) to compare correlation between devices.

While not as well defined as stroke, this principle can be extended to typical field damage in pituitary tumour, which is stereotypically bitemporal or unilateral temporal, and AION which is typically unilateral altitudinal. Therefore, using these assumptions, hemifield ratios can be calculated for chiasmal compression and AION as well (Figure 5.2).

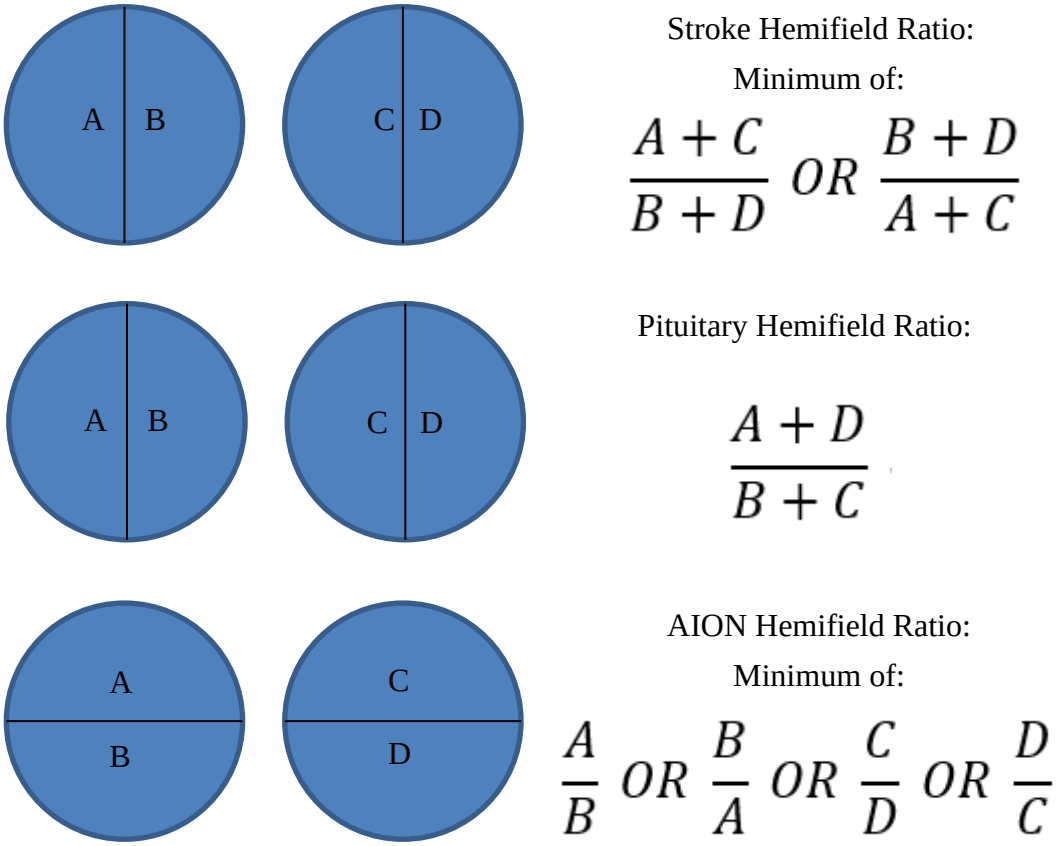

Figure 5.2: Hemifield ratio calculations for stroke (top), chiasmal compression (middle), and AION (bottom). Each ratio assumes typical field damage based on the anatomical location of the damage, with stroke resulting in either right of left homonymous hemianopic damage, chiasmal compression with bitemporal hemianopic damage, and AION with either superior or inferior loss in a single eye. Where more than one possibility is possible, the minimim of the possible ratios is used, which represents the one which explains the most damage.

5.3.6.4. Receiver operator characteristics (ROC)

The same approach as detailed in Chapter 3 (3.3.2 *Receiver operator characteristics and thresholds*) was used utilising the same program and output format, except using the hemifield ratio as the measure. ROC plots sensitivity against false positive ratio (FPR; 1 – specificity)

over the full range of thresholds which could be used to separate two populations. First the smallest threshold is trialled, corresponding to the smallest hemifield ratio in the group, and subjects are tallied to generate sensitivity and FPR values. Sequentially larger thresholds are trialled, gradually correctly identifying more stroke subjects (increasing sensitivity), while also incorrectly classifying control subjects as stroke (increasing FPR). Once the plot is completed, the area under the curve (AUC) can be calculated to assess the overall effectiveness of the test measure, and standard deviation (SD), *Z*-scores, and *p*-values may be calculated to suggest if tests a statistically difference than chance. A diagram showing two theoretical distributions for ROC plots ranging from chance (AUC = 0.500) to perfect separation (AUC = 1.000) is shown in Chapter 3 (Figure 3.1). Output plots include a bootstrap (sample with replacement) with 100,000 repeats to provide the standard deviation measures, which is displayed in 2D histogram heatmap with logarithmic scale (top left) with the mean ± 1 SD plotted below (bottom left), while a similar bootstrap and 2D histogram of threshold values for hemifield ratio is plotted (top right), with the mean ± 1 SD plotted below (bottom right).

5.3.6.5. Intraclass correlation coefficients (ICC)

To more clearly compare devices and to highlight whether they showed the same general locations of hemifield damage, *intraclass correlation coefficients* (ICC) were calculated from hemifield ratios for each disease. ICCs were calculated in Matlab using the 'C-k' category designed to measure the consistency of measures which are averages of *k* independent measures on randomly selected objects. Resulting correlations were presented with calculated *p*-values.

5.4. Results

5.4.1. 24-2 field maps

HFA and MFA thresholds (dB) were plotted against mfPOP pupillary constriction amplitudes (dB) for repeat 1 and 2 in all subjects. Visual field plots were manually reviewed and inspected

for correlation, with Figure 5.3 showing an example for the first: left HH, right HH, chiasmal compression field damage, and AION field damage. Before looking at the analysis of the subjects in their amalgamated form, it is important to first look at the output for visual field agreement visually, as in clinical practice. In nearly all fields, visual inspection shows that HFA and MFA are highly correlated, with this being most apparent in stroke, but also with reasonable correlation in AION and pituitary. Fields from mfPOP generally showed a poor correlation, but there was more subtle agreement in some cases of complete HH, but not in homonymous quadrantanopia or scotomas. Some reportedly clear field on HFA and MFA demonstrated some degree of hemianopia on mfPOP, but this was also true in the control group, suggesting this is simply noise. In stroke, 8/13 largely normal fields on HFA/MFA were also largely normal on mfPOP, while of the damaged fields, 2/4 of the HH showed a moderate match and 0/8 of the quadrantanopias and scotomas showed matched field loss. In pituitary fields, mfPOP showed 2/5 overtly damaged fields having a partial/weak match, with 2/6 largely clear fields in HFA/MFA also being clear in mfPOP (although many were noisy). For AION fields, all subjects had some field damage, with 3/10 demonstrating some agreement between HFA/MFA and mfPOP while the other 7 were unclear or mismatched. These are summarised in a table (Table 5.1) to facilitate comparison between devices.

Summary of visual field correlations by visual inspection

		HFA vs MFA		HFA vs mfPOP		MFA vs mfPOP	
Stroke	Clear	10/13	77%	8/13	62%	8/13	62%
	Homonymous hemianopia	4/4	100%	2/4	50%	2/4	50%
	Homonymous quadrantanopia	4/4	100%	0/5	0%	0/4	0%
	Scotoma	3/3	100%	0/3	0%	0/3	0%
	Total	**22/24***	**92%**	**10/25**	**40%**	**10/24***	**42%**
Pituitary	Clear	4/5	80%	2/6	33%	2/5	40%
	Temporal loss	4/4	100%	1/5	20%	1/4	25%
	Total	**8/9***	**89%**	**3/11**	**27%**	**3/9***	**33%**
AION	Clear	0/0	0%	0/0	0%	0/0	0%
	Altitudinal	6/7	86%	1/7	14%	1/7	14%
	Mixed	2/3	67%	1/3	33%	1/3	33%
	Total	**9/10**	**90%**	**4/10**	**40%**	**2/10**	**0%**

Table 5.1: Summary of subjective visual field correlation by visual inspection. Comparisons were made between Humphrey (HFA), Matrix (MFA), and mfPOP. The asterisk (*) indicates where results exist for one test but not the other in the comparison, (there is one instance of missing MFA in the stroke group and two in the pituitary group, from subjects who did not complete testing). Totals for each class are presented at the bottom of each row. Percentages are graded in green such that 0% is clear and 100% is intensely green. This reveals that HFA and MFA have the best correlation, and that mfPOP has a poor correlation generally, with slightly better correlation in clear fields and homonymous hemianopias.

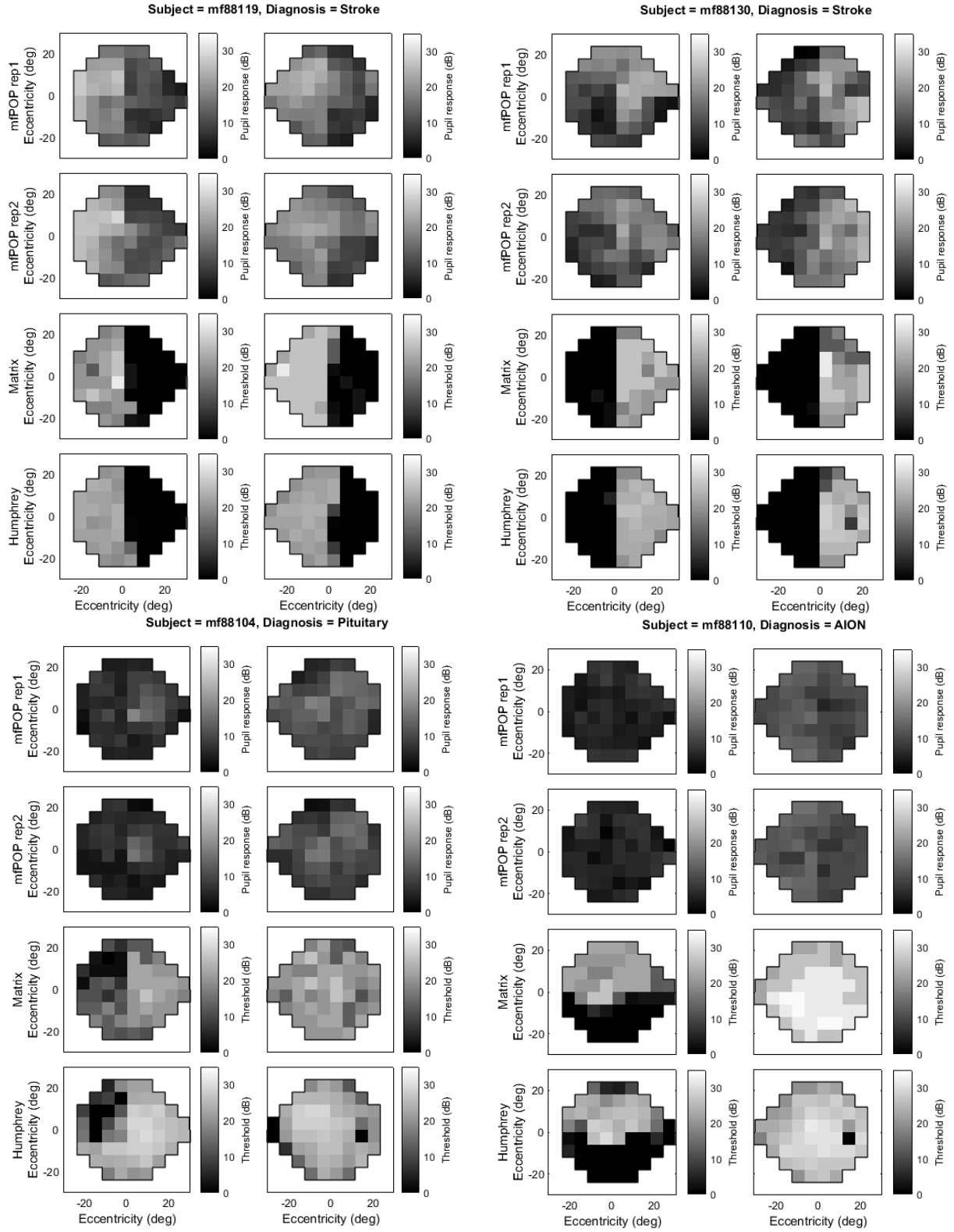

Figure 5.3: Visual fields maps in 24-2 format for the first subject in each disease group with stereotypical field loss: the first stroke right HH (top left), first stroke left HH (top right), first pituitary temporal field damage (bottom left), and first AION altitudinal damage (bottom right). Each set of fields includes mfPOP repeat 1 (row 1), mfPOP repeat 2 (row 2), Matrix (row 3), and Humphrey (row 4) using the same greyscale bar (0–35 dB).

5.4.2. Principal curve scatter plots

Figure 5.4 directly compares 24-2 points between devices by producing scatter plots of all field points, using a dB scale (noting that scales and contrast differ between devices). HFA, MFA, and mfPOP by repeat are compared, with associated principal curves (PC). The principal curve is a non-bias fit which iteratively flexes to ensure the same number of points map to each side. The graph includes all data points, including 0 dB results which represent the maximum contrast capability of HFA and MFA devices, while mfPOP is not limited by such constraints.

The left column (A, B) show HFA against mfPOP repeat 1 and 2. There are similar trends between HFA and both mfPOP repeats, with a logarithmic-like shape. Looking at the data there are two prominent areas of density: one in the range 25–35 dB HFA which represent largely normal results spread over most of the mfPOP range (10–40 dB), and another along the bottom at 0 dB HFA representing complete field loss covering much of the mfPOP range. It is clear there is a poor correlation, with the principal curve indicating that mfPOP has variety whereas there is little in HFA. There is a sudden change where HFA trends towards 0, where many of its points reside, while the mfPOP spread is only marginally reduced. The hyperflex of the PC is probably spurious due to the limited number of data points in this range.

The right column (D, E) show MFA against mfPOP repeat 1 and 2. The generalised shape is very similar to that in HFA (sharp curve) but is slightly more linear. There is less pooling of the data into two domains, with greater spread in MFA than in HFA, although the apparent horizontal banding is due to results in MFA being limited to only 15 possibilities.

The bottom row (C, F) compares HFA vs MFA and shows a complex sigmoidal relationship. Initially there is a roughly linear relationship at high values until ~20 dB, after which there is greater variation in HFA, before both trend towards 0. This may be due to the large number of

values at 0 dB in both devices. While not the focus of these comparisons, mfPOP repeat 1 was compared to repeat 2, and showed a highly linear correlation, which is further investigated in Chapter 6.

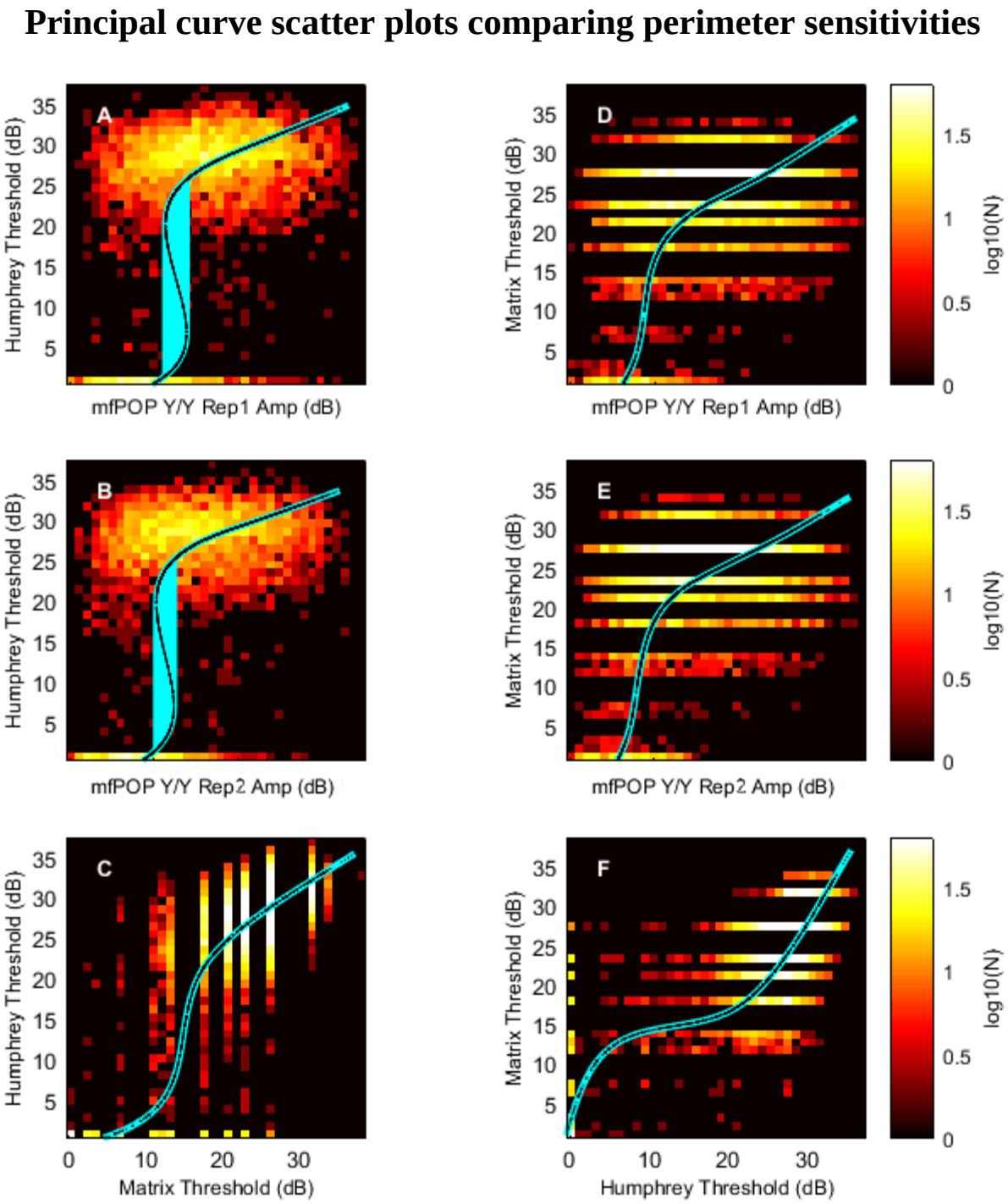

Figure 5.4: Principal curve scatter plots of Humphrey, Matrix, and mfPOP with 0 dB data points included. Graphs A–C show Humphrey against mfPOP repeat 1, mfPOP repeat 2, and Matrix. Graphs D–F show Matrix against mfPOP repeat 1, mfPOP repeat 2, and Humphrey. Heatmaps (2D histograms) show relative density of data on a logorithmic scale, and have fitted principal curves shown in teal with the black line showing data points fitted to the curve. Note that C and F are rotated versions of the same graph.

Due to the large effect of 0 dB points on the data, and the consideration that these are not true 0-dB points, but rather a result of clipping the range of these machines, it is worth investigating whether removal of these points reveals different trends between the machines.

Accordingly, Figure 5.5 shows similar scatter plots to Figure 5.4, with the 0 dB points removed. Scatter plots of HFA, MFA, and mfPOP repeats with associated principal curves are displayed.

The left column (A, B) compares HFA against both mfPOP repeats. Removal of the 0 dB points appears to have quite substantially altered the shape of the curve so that it is no longer anchored at 0 dB. However, it still maintains the general logarithmic shape, which is more modest and appears to give a better fit. At HFA of ~25 dB, the mfPOP covers most of its range of 10–40 dB with a gradient of near zero showing no correlation before arcing downward with a large change in HFA at lower thresholds and having a *y*-intercept at ~12 dB. This shape shows that as mfPOP decreases, HFA remains constant until about 10 dB, after which there is rapid deterioration in HFA scores. If both devices were assumed to be measuring underlying damage, this would be consistent with HFA having input from overlapping retinal cells with redundancy (all RGC), while mfPOP input (ipRGC) has less redundancy, such that small amounts of damage affect mfPOP but do not affect HFA – until no redundancy remains and there is a steep decline. This possibility is further explored in the discussion.

The right column (D, E) compares MFA against both mfPOP repeats. Removal of the 0 dB points has more modestly affected MFA so that its gradients are less steep, and it now closely approximates the general shape of HFA and mfPOP. While HFA is very flat at 25 dB over the mfPOP range of 10–40 dB, MFA has a modest shallow linear gradient before also arcing downwards with an intercept near the origin (0,0). This adds weight to the consideration of redundancy, given that the MFA is said to target M_y cells more sensitive to cellular loss and with less overlapping fields (less redundancy). A key difference between HFA and MFA is that

there is a greater range of data below 20 dB in MFA, which likely accounts for the steeper arc and which makes sense given that the MFA uses the Michelson formula with dB conversion which is effectively mathematically double that of the HFA which uses the Weber formula for contrast.

The bottom rows (C, F) compare HFA and MFA, revealing that there is a much more linear correlation when the 0 dB points are removed. At the higher end of the thresholds, the curve has a 1:2 linear relationship, with HFA falling from 35 to 25 dB (a 10 dB range), while MFA has fallen from 40 to 20 dB (a 20 dB range), consistent with the Michelson and Weber contrast calculations, then shifting to a steeper gradient closer to a 1.3 : 1 ratio (HFA : MFA).

Principal curve scatter plots comparing perimeter sensitivities (no 0 db points)

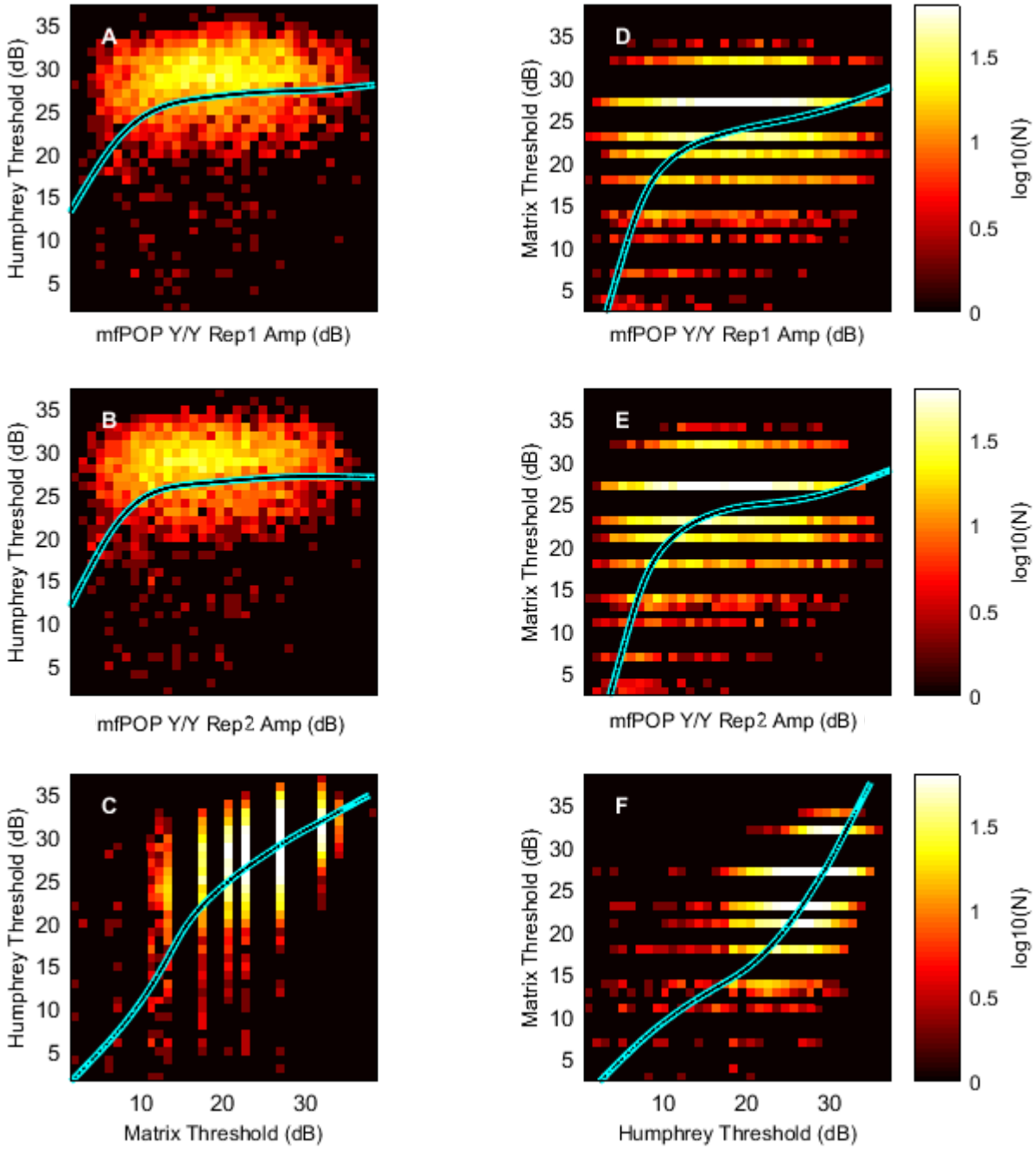

Figure 5.5: Principal curve scatter plots of Humphrey, Matrix, and mfPOP with 0 dB data points removed. Graphs A–C show Humphrey against mfPOP repeat 1, mfPOP repeat 2, and Matrix. Graphs D–F show Matrix against mfPOP repeat 1, mfPOP repeat 2, and Humphrey. Heatmaps (2D histograms) show relative density of data on a logorithmic scale, and have fitted principal curves shown in teal, with the black line showing data points fitted to the curve. Note that C and F are rotated versions of the same graph. Curves appear less extreme after the 0 dB points are removed, and Humphrey and Matrix have a near linear relationship.

5.4.3. Bland–Altman plots

Figures 5.6 – 5.8 show Bland–Altman plots of subjects for each of stroke, chiasmal compression, and AION. They compare HFA, MFA, and mfPOP thresholds using large dots with partial transparency to highlight areas of density. Trendlines fitted to percentile values of 5%, 25%, 50%, 75%, and 95% for each of the binned abscissa values, effectively make a series of box and whisker plots with trends in percentiles across the range. Each of the graphs are discussed sequentially below, with a summary table of their mean and confidence intervals (CI) presented at the end (Table 5.2).

Figure 5.6 shows Bland–Altman plots of stroke patients comparing HFA, MFA, and mfPOP. (A) shows HFA vs MFA, which has the most linear relationship of the comparisons (most stable across the testing range), with the smallest mean difference of 1.87 dB and the smallest 95% CI range of 20.19 dB. The median (50% – solid line) for binned abscissa values shows a good linear agreement between HFA and MFA for means of 17–34 dB, with MFA then exceeding HFA for values <17 dB. (B) shows HFA vs mfPOP, which has the least linear relationship of the comparisons (unstable across testing range), with the largest mean difference of 9.24 dB and largest 95% CI range of 33.38 dB. The median for binned abscissa shows that HFA exceeds mfPOP through most of the upper range, with this being most prominent at 15–20 dB after which the means <11 dB show mfPOP exceeds HFA. There is little to no linear agreement. (C) shows MFA vs mfPOP, which has an intermediate relationship which is less linear than (A) and more linear than (B), with intermediate mean difference of 6.77 dB (similar to before) and equally largest 95% CI range of 33.30 dB. The median for binned abscissa shows there is some linear component at means of 14–21 dB, but that MFA exceeds mfPOP through the entire range except at means <7 dB. Overall, HFA and MFA have a large linear segment with near 0 dB difference and the smallest CI range; MFA and mfPOP have a small linear segment with MFA moderately exceeding mfPOP over most of the range and large CI range;

and HFA and mfPOP have minimal linear segments with HFA greatly exceeding mfPOP over most of the range and large CI range.

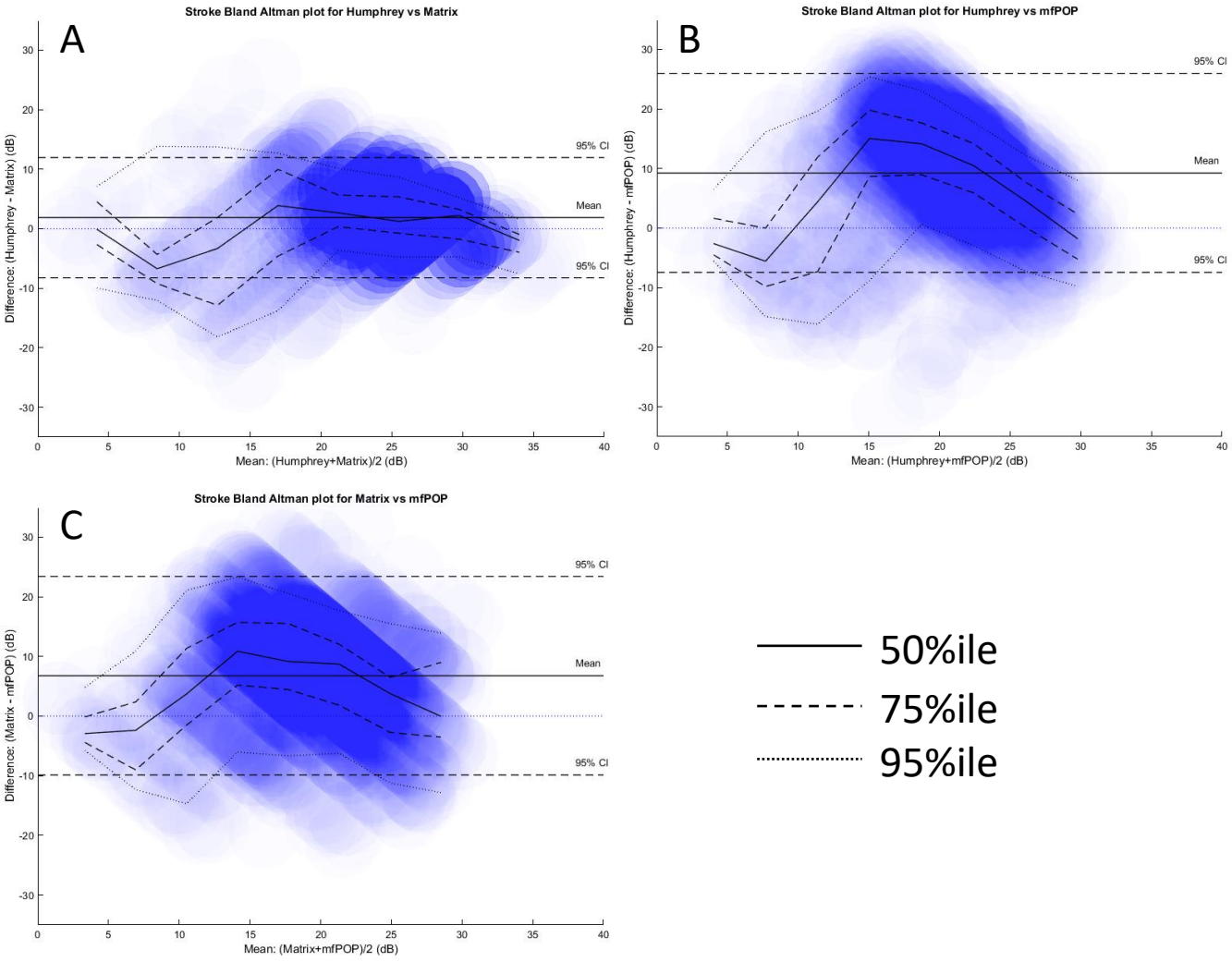

Figure 5.6: Stroke Bland–Altman plots for comparisons of HFA, MFA, and mfPOP with 0 dB points removed. Points are represented by large partially transparent dots with overlapping fields, showing areas of density as darker blue. Overall mean and 95% CI are the labelled horizontal lines (full and dashed). Running auto-binned median (full), and percentiles 75% (dashed), and 95% (dotted) are also presented for comparison. Note that scales have been matched to allow direct comparison between graphs. (A) shows HFA vs MFA, (B) shows HFA vs mfPOP, and (C) shows MFA vs mfPOP.

Figure 5.7 shows Bland–Altman plots of pituitary patients comparing HFA, MFA, and mfPOP. (A) shows that HFA vs MFA has some linearity with the smallest mean difference of 3.84 dB and the smallest 95% CI range of 19.30 dB. HFA vs MFA median demonstrates a somewhat linear relationship initially from a mean of 22–33 dB, with a general trend that HFA gradually

exceeds MFA until a mean of 14 dB at which point it reverses, which is a similar trend to HFA vs MFA in stroke. The lower percentile CI at 14 dB is also markedly shifted from the remainder of the graph, and while it is generally a point of maximal difference in most graphs, this is much larger, perhaps suggesting that an outlier is present in this dataset (due to only a few data points being present in this range). (B) shows HFA vs mfPOP, which has the least linear relationship of the comparisons, with the largest mean difference of 11.36 dB and the equally largest 95% CI range of 25.04 dB. The median shows that HFA exceeds mfPOP through the entire range except at mean values <10 dB, with this being most prominent in the 13–20 dB range, which is also the range where there is linearity. (C) shows MFA vs mfPOP, which has some linearity with an intermediate mean difference of 7.23 dB and the equally largest 95% CI range of 25.54 dB. The median shows good linearity across most of the range spanning means of 9–27 dB with MFA exceeding mfPOP across the entire range except at points <5 dB. There is no evidence of an outlier in the 1% percentile suggesting the outliers present in the previous graphs originated from HFA. Overall, HFA and MFA have a reasonably linear segment with a small difference and best agreement, although HFA modestly exceeds MFA over much of the range; MFA and mfPOP also have a large reasonably linear segment with intermediate difference and poorer agreement with MFA substantially exceeding mfPOP over the entire range; and HFA vs mfPOP having minimal linear segments with HFA greatly exceeding mfPOP over most of the range with poor agreement. Trends in these graphs largely align with

comparisons made in stroke, although MFA vs mfPOP in this instance performed notably better.

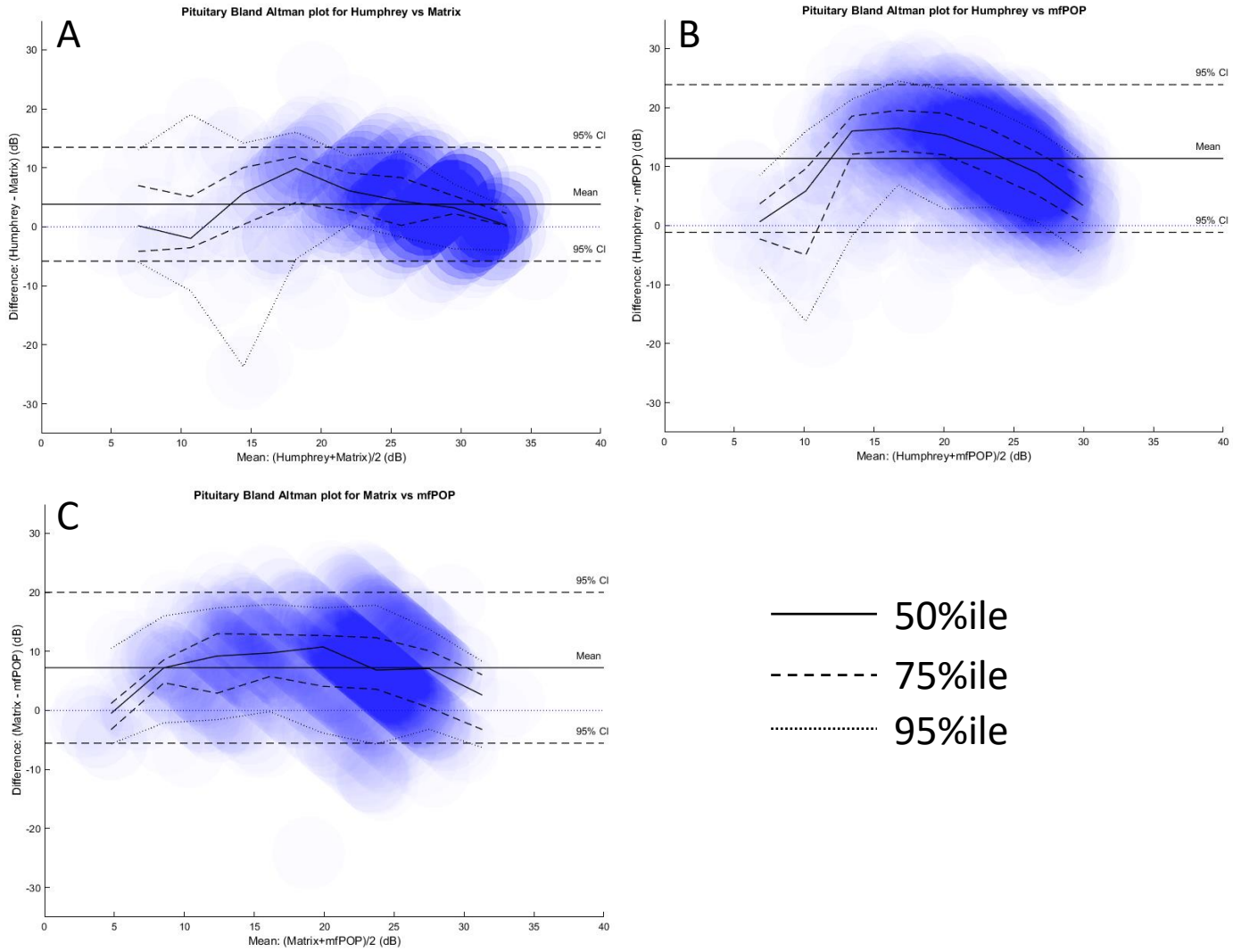

Figure 5.7: Pituitary Bland–Altman plots for comparisons of HFA, MFA, and mfPOP with 0 dB points removed. Points are represented by large partially transparent dots with overlapping fields, showing areas of density as darker blue. Overall mean and 95% CI are the labelled horizontal lines (full and dashed). Running auto-binned median (full), and percentiles 75% (dashed), and 95% (dotted) are also presented for comparison. Note that scales have been matched to allow direct comparison between graphs. (A) shows HFA vs MFA, (B) shows HFA vs mfPOP, and (C) shows MFA vs mfPOP.

Figure 5.8 shows Bland–Altman plots of AION patients comparing HFA, MFA, and mfPOP. (A) shows HFA vs MFA, which has the most linear relationship of the comparisons with a small mean difference of 4.30 dB and smallest 95% CI range of 24.90 dB. The median shows good agreement between HFA and MFA for means over most of the range, with HFA exceeding MFA modestly over the range except at extremes of <4 dB and >32 dB. (B) shows HFA vs mfPOP, which has a nonlinear relationship with the largest mean difference of 8.82 dB and the largest 95% CI range of 39.69 dB. The median shows there is minimal linearity and poor agreement, with HFA substantially exceeding mfPOP over the central range of means of 12–23 dB and mfPOP modestly exceeding HFA at the extremes. Notably, there is a very large 5% percentile range dipping to –15 dB despite the median being 17 dB, suggesting that while HFA generally exceeds mfPOP there is quite substantial variation, and this is consistent with having the equally largest 95% CI of all comparisons in all graphs. (C) shows MFA vs mfPOP, which has a similarly poor relationship to (B) with a nonlinear relationship, small mean difference of 4.12 dB, and an equally large CI range of 40.27 dB. The median shows there is minimal linearity and poor agreement, with MFA substantially exceeding mfPOP over the central range of means of 8–20 dB and mfPOP modestly exceeding MFA at the extremes. There are also particularly wide scores at 95% and 5%, similar to (B). Overall, HFA and MFA have linearity over most of the range with the smallest difference and CI range; MFA and mfPOP as well as HFA and mfPOP have minimal linear segments; and HFA and MFA exceed mfPOP over much of the range with larger differences and very large CI ranges. Trends in AION largely concur with those in stroke and pituitary, highlighting that HFA and MFA have good overall agreement, that MFA and mfPOP have poor agreement, and that HFA and mfPOP have very poor agreement.

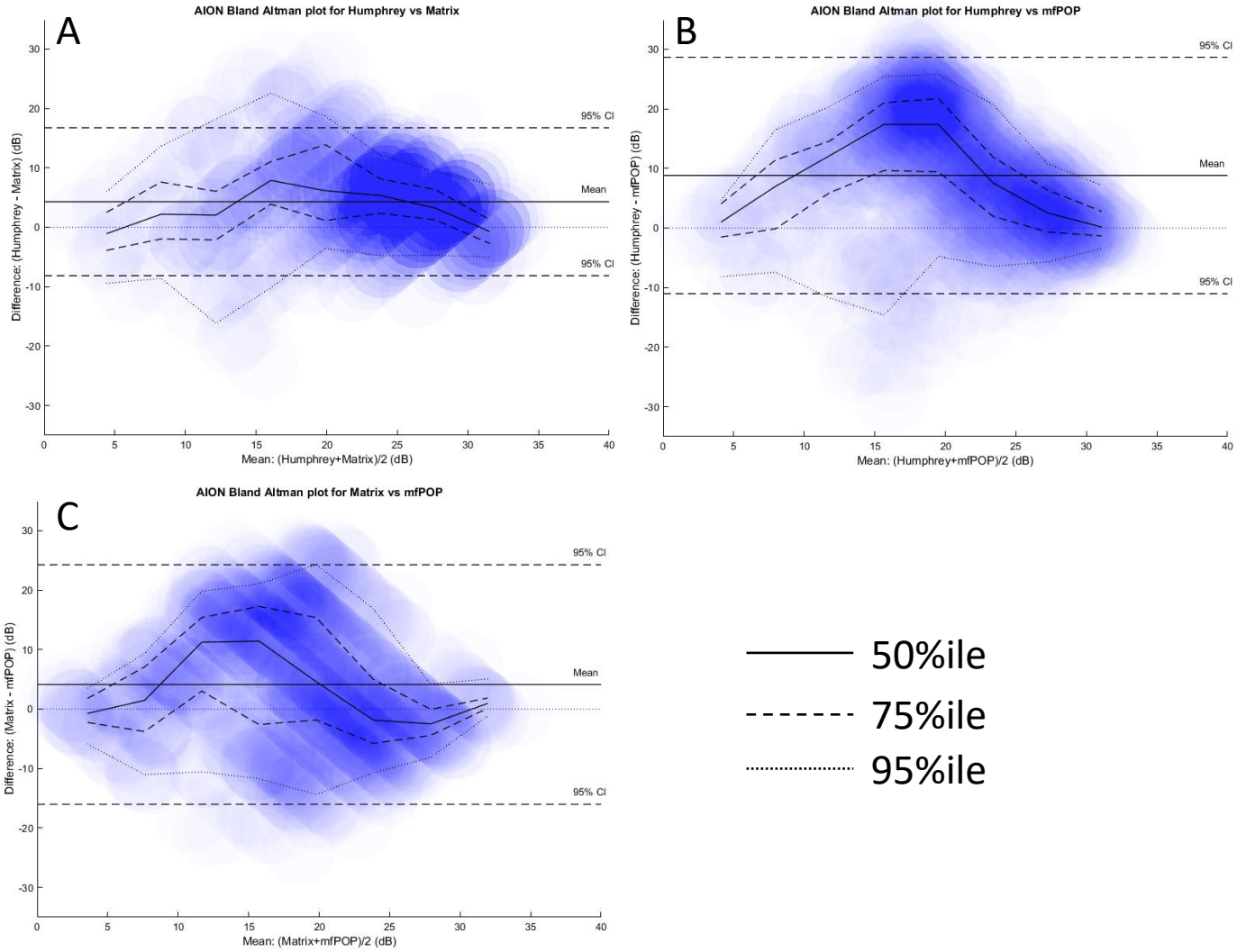

Figure 5.8: AION Bland–Altman plots for comparisons of HFA, MFA, and mfPOP with 0 dB points removed. Points are represented by large partially transparent dots with overlapping fields, showing areas of density as darker blue. Overall mean and 95% CI are the labelled horizontal lines (full and dashed). Running auto-binned median (full), and percentiles 75% (dashed), and 95% (dotted) are also presented for comparison. Note that scales have been matched to allow direct comparison between graphs. (A) shows HFA vs MFA, (B) shows HFA vs mfPOP, and (C) shows MFA vs mfPOP.

A summary of the mean and CI range for each device and each condition is presented in Table 5.2 for easy comparison. Here one can clearly observe that HFA and MFA correlate better with each other than either does with mfPOP.

Table of mean and CI values by disease and device

Comparison	Measure (dB)	HFA vs MFA	HFA vs mfPOP	MFA vs mfPOP
Stroke	Mean	1.87	9.24	6.77
	CI range	20.19	33.38	33.3
Pituitary Tumour	Mean	3.84	11.36	7.23
	CI range	19.3	25.04	25.54
AION	Mean	4.3	8.82	4.12
	CI range	24.9	39.69	40.27

Table 5.2: Mean and confidence interval (CI) range for each disease type and device comparison. Values are colour-coded according to value relative to other results, with white being smallest and red being largest. Colouring reveals HFA with MFA have relatively small means and CIs in all conditions, while MFA with mfPOP show intermediate values, and HFA with mfPOP show larger values.

5.4.4. Receiver operator characteristics plots using hemifield ratios

Receiver operator characteristics represent sensitivity (correctly identified abnormal results) against false positive ratio (FPR; incorrectly identified abnormal results) in order to characterise how effective a test is at distinguishing between two groups (in this case stroke subjects and control subjects). It tests all possible thresholds which might be used to demarcate between groups, and plots the sensitivity and FPR throughout, with the summary measure being the area under the curve (AUC), so that 0.500 is complete chance and 1.000 perfect separation. Stroke hemifield ratio was calculated as the smaller of the ratio of left sides over right sides (or vice versa) consistent with typical homonymous defects (see methods Figure 5.2). This ratio was then used to produce the ROC plots.

Hemifield ROC plots for HFA (Figure 5.9 A, C) show there is a high sensitivity of 59% at minimal FPR of 2%, after which there is only a modest increase over the range at below chance rates, suggesting all those with obvious homonymous defects were rapidly detected and those without were not easily discernible from controls. The threshold ROC plots for HFA (Figure

5.9 B, D) show a sharp asymptotic-like threshold rapidly increasing to 0.94 at 2% FPR, this demonstrates the large bulk of homonymous defects can be detected at or below ratios of 0.94 and that minimal FPR occurs until ratios are very near 1, so one can be confident that even modest deviation from normal is pathologic. The area under the curve (AUC) of 0.842 is relatively large with small variation, which is significantly greater than chance.

In hemifield ROC plots for MFA, (Figure 5.10 A, C) there is moderately-high sensitivity of 44% at minimal FPR of 2%, after which there is categorisation at roughly chance rate, with homonymous defects being rapidly detected and those without not easily being discernible from controls. The threshold ROC plots for MFA (Figure 5.10 B, D) show a sharp asymptotic-like threshold rapidly increasing to 0.93 at 2% FPR, then gradually increasing towards 1; this demonstrates that most of the homonymous defects can be detected at or below a ratio of 0.93. There is also minimal FPR increase until values are quite near 1, so one can be confident that even modest deviations from normal are pathologic. The AUC of 0.844 is relatively large, on a par with HFA, with a lower sensitivity initially but a steeper gradient thereafter and achieving 100% earlier.

Hemifield ROC plots for mfPOP (Figure 5.11 A, C) with poor initial sensitivity of 13% at FPR of 2% and falling to chance level (40% sensitivity at 40% FPR) – compared to 84% sensitivity in both HFA and MFA at the same FPR value. Considering that SD roughly aligns with chance even at the best regions, the test appears to perform no better than chance, with a near-chance AUC of 0.531 which is non-significant. Threshold ROC plots for mfPOP (Figure 5.11 B, D) show that large deviations with ratios of <0.63 are needed before one can be confident that there is a deviation, and FPR rapidly increases linearly with ratios >0.68, demonstrating there is a substantial degree of homonymous-like fields in controls that are indistinguishable from fields in stroke.

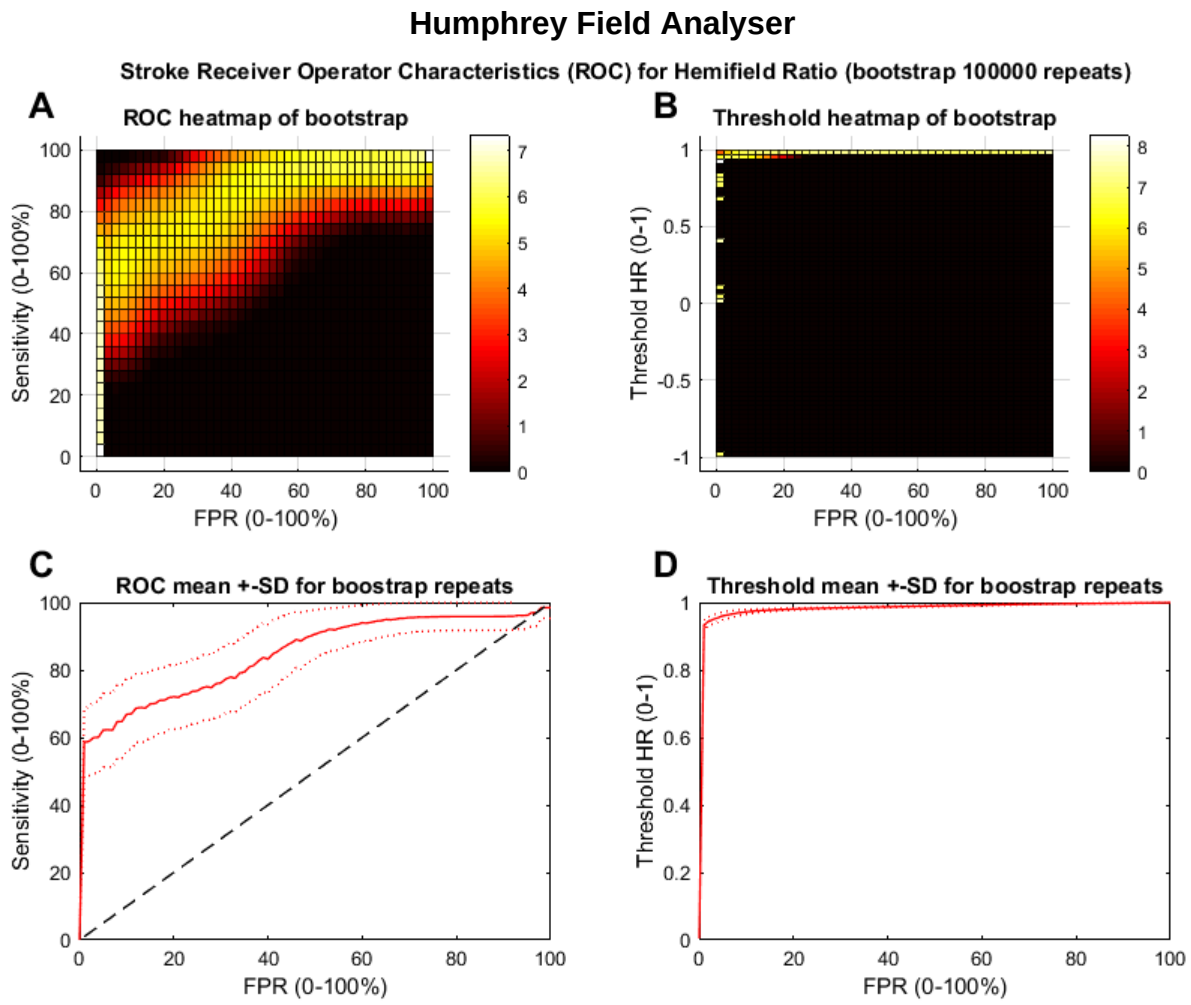

Figure 5.9: Stroke HFA ROC plots using hemifield ratio, with 100,000 repeat bootstrap. Dashed line represents chance (where a test has no diagnostic capacity). (A) shows log-scale heatmap of the ROC with bootstrap demonstrating variability and general trend, with (C) showing the resulting mean ± SD allowing calculation of area under the curve (AUC). (B) shows threshold heatmap highlighting what threshold is used for calculation of the sensitivity/FPR values, together with (D) using the mean and ±SD.

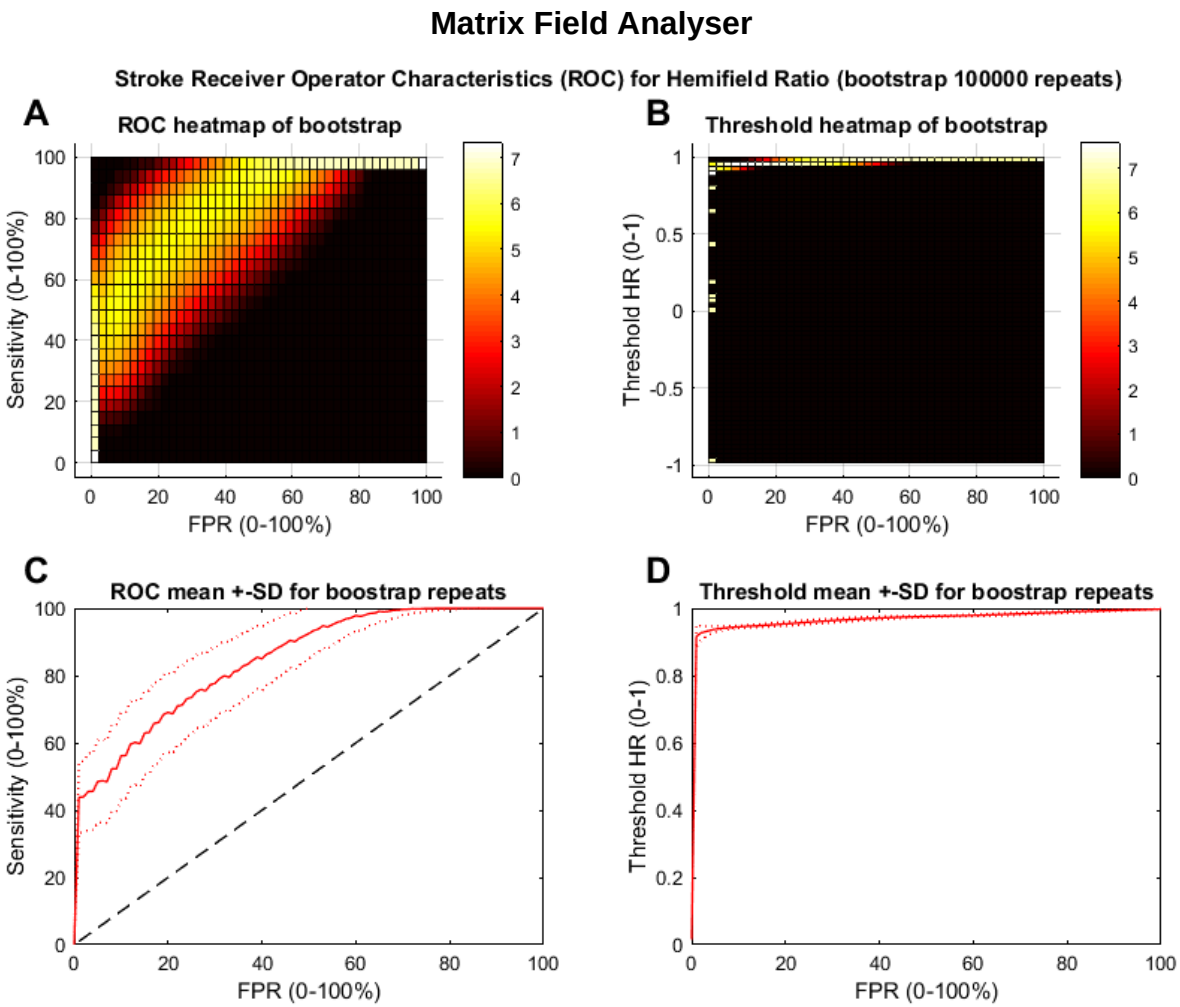

Figure 5.10: Stroke Matrix ROC plots using hemifield ratio with 100k repeat bootstrap. Dashed line represents chance (where a test has no diagnostic capacity). (A) shows log-scale heatmap of the ROC with bootstrap demonstrating variability and general trend with (C) showing the resulting mean ±SD allowing calculation of area under the curve (AUC). (B) shows threshold heatmap highlighting what threshold is used for calculation of the sensitivity/FPR values together with (D) using the mean and ±SD.

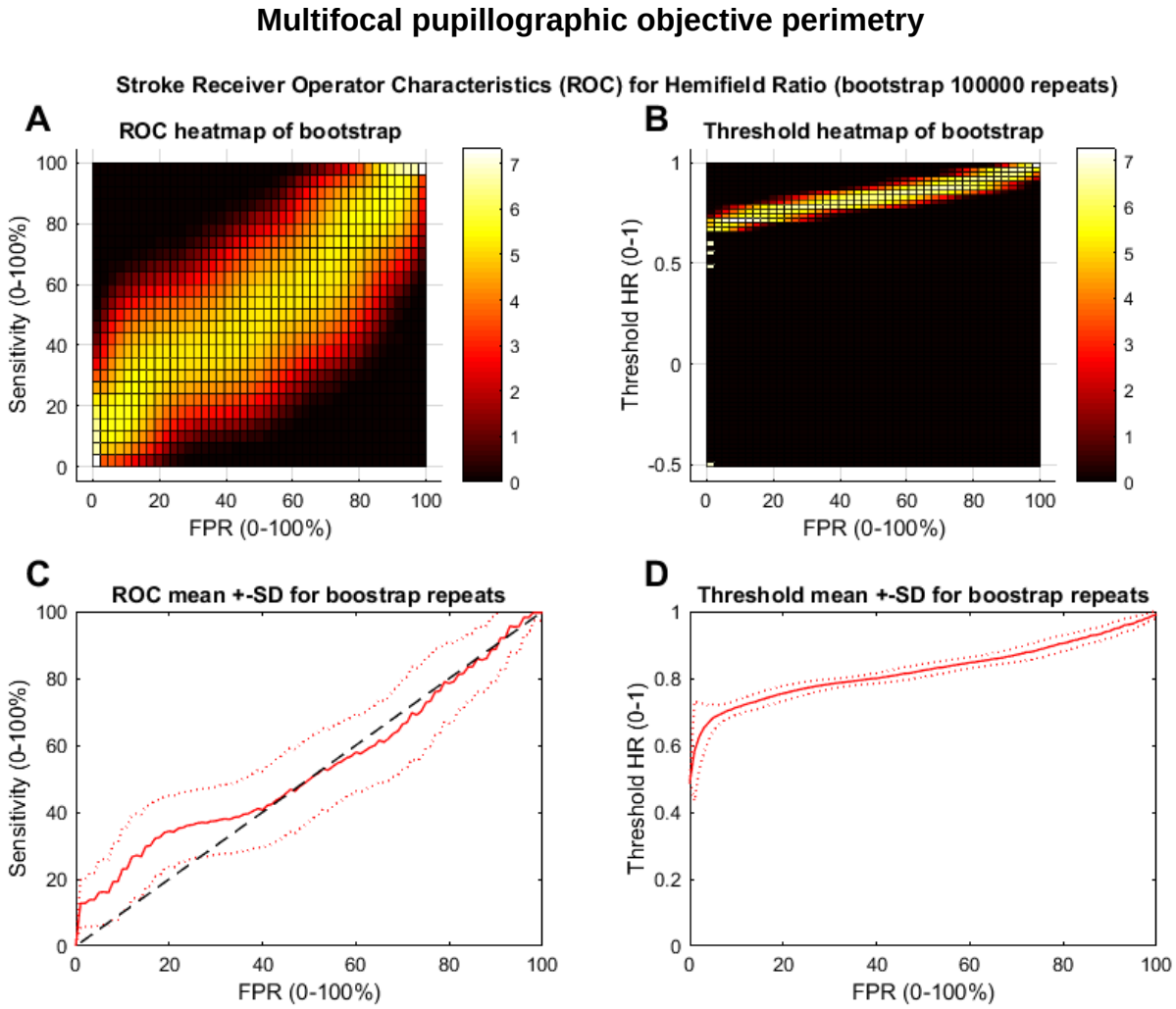

Figure 5.11: Stroke mfPOP ROC plots using hemifield ratio with 100k repeat bootstrap. Dashed line represents chance (where a test has no diagnostic capacity). (A) shows log-scale heatmap of the ROC with bootstrap demonstrating variability and general trend with (C) showing the resulting mean ±SD allowing caluclation of area under the curve (AUC). (B) shows threshold heatmap highlighting what threshold is used for calculation of the sensitivity/FPR values together with (D) using the mean and ±SD.

Stroke		FPR 2	5	10	20	AUC (Mean)	AUC (SD)	Z-score	P-val (Z>z)
HFA	Sensitivity	59	62	67	72	**0.842**	0.071	4.798	8.01E-07
	SD	10	11	11	10			Sig P<0.0001	
	Threshold	0.94	0.96	0.97	0.98				
	SD	0.01	0.01	0.01	0.00				
MFA	Sensitivity	44	49	56	69	**0.844**	0.063	5.459	2.40E-08
	SD	11	12	13	12			Sig P<0.0001	
	Threshold	0.93	0.94	0.94	0.95				
	SD	0.02	0.01	0.00	0.01				
mfPOP	Sensitivity	13	16	23	34	**0.531**	0.108	0.289	0.386
	SD	7	10	12	11			Not Sig	
	Threshold	0.63	0.68	0.71	0.76				
	SD	0.10	0.04	0.02	0.02				

Table 5.3: Summary results and statistics from homonymous hemifield ROC plots in stroke for HFA, MFA, and mfPOP. Sensitivities at FPR of 2, 5, 10, and 20% are provided for comparison given that high FPR would not be acceptable in medical testing for stroke. Total area under curve (AUC) for each device is presented with SD, *Z*-score, and *p*-value for AUC exceeding chance level.

Table 5.3 shows summary results and statistics for hemifield ROC plots in stroke for each device. As per the graphs, sensitivities in HFA are high at low FPR throughout; in MFA starting lower and increase to match HFA at 20% FPR; while mfPOP has relatively low sensitivities. All devices have similar variability in sensitivity (SD) across these low FPR values. Total AUC was high in HFA/MFA with highly significant results $p<0.0001$, while mfPOP has near-chance AUC and greater variability with a non-significant result $p = 0.386$. Thresholds are highest in HFA throughout, with MFA a near second, with both devices have very small amount of variability; however, mfPOP has much lower thresholds with a linear increase and larger amount of variation initially, gradually reducing to rest at roughly double HFA/MFA. Graphs for hemifield ROC plots in pituitary and AION were also produced but not included; instead a table summarising parameters is provided below. Note that the definition for a pituitary hemifield is the lesser of temporal fields/nasal fields (or vice versa); the definition for an AION hemifield is the lesser of superior left/inferior left (or vice versa) or superior right/inferior right (or vice versa), so that stereotypical fields are less well defined than with stroke.

Pituitary		FPR 2	5	10	20	AUC (Mean)	AUC (SD)	Z-score	P-val (Z>z)
HFA	Sensitivity	49	54	55	55	**0.742**	0.117	2.061	1.97E-02
	SD	16	15	15	15			Sig P<0.02	
	Threshold	0.92	0.93	0.94	0.95				
	SD	0.02	0.01	0.01	0.01				
MFA	Sensitivity	71	82	90	99	**0.966**	0.026	17.904	3.89E-72
	SD	16	15	12	5			Sig P<0.0001	
	Threshold	0.98	1.00	1.01	1.02				
	SD	0.01	0.01	0.01	0.01				
mfPOP	Sensitivity	4	16	25	34	**0.545**	0.145	0.308	0.379
	SD	9	15	15	15			Not Sig	
	Threshold	0.59	0.88	0.96	0.99				
	SD	0.28	0.13	0.03	0.02				

Table 5.4: Summary results and statistics from bitemporal hemifield ROC plots in chiasmal compression for HFA, MFA, and mfPOP. Sensitivities at FPR of 2, 5, 10, and 20% are provided for comparison. Total area under curve (AUC) for each device is presented with SD, *Z*-score, and *p*-value for AUC exceeding chance level.

Table 5.4 shows results and statistics from temporal hemifield ROC plots in chiasmal compression for each device. Note that unlike stroke and AION, which used minimums of reciprocal ratios so that the maximum threshold was 1, pituitary is a single ratio of temporal fields over nasal fields and so may exceed 1. HFA demonstrated a good ability to detect initially, with sensitivity of 49% at FPR 2% but only increased marginally thereafter until ~40% FPR at which level it was near to chance. Total AUC was 0.742 which was marginally significant at $p<0.02$. The *p*-values suggest that thresholds below 0.92 are highly diagnostic, while anything above that will have limited utility. MFA demonstrated excellent ability to detect both initially and throughout, with sensitivity of 71% at an FPR 2%, reaching 99% sensitivity at 20% FPR. AUC was excellent at 0.966 and was highly significant – an interesting and unexpected result. Thresholds were near 1, demonstrating that MFA is very sensitive in detecting temporal hemifield damage even when very minute and that this is a good measure for detection. mfPOP demonstrated a poor ability to detect initially with 4% sensitivity at FPR

of 2% and closely following chance-level throughout the range (a non-significant result). Threshold was lower than in other devices, showing that it was not uncommon to have bitemporal hemifields which are dimmer than nasal hemifields in normal controls.

AION		FPR 2	5	10	20	AUC (Mean)	AUC (SD)	Z-score	P-val (Z>z)
HFA	Sensitivity	75	85	90	91	**0.912**	0.078	5.288	6.18E-08
	SD	14	14	10	9			Sig P<0.0001	
	Threshold	0.84	0.90	0.93	0.95				
	SD	0.05	0.03	0.02	0.01				
MFA	Sensitivity	68	78	81	82	**0.885**	0.083	4.650	1.66E-06
	SD	15	14	12	12			Sig P<0.0001	
	Threshold	0.84	0.88	0.90	0.92				
	SD	0.05	0.02	0.01	0.01				
mfPOP	Sensitivity	10	17	23	28	**0.533**	0.142	0.2324	0.408
	SD	10	13	14	14			Not Sig	
	Threshold	0.49	0.66	0.71	0.74				
	SD	0.23	0.09	0.03	0.02				

Table 5.5: Summary results and statistics from altidinal hemifield ROC plots in AION for HFA, MFA, and mfPOP. Sensitivities at FPR of 2, 5, 10, and 20% are provided for comparison. Total area under curve (AUC) for each device is presented with SD, *Z*-score, and *p*-value for AUC exceeding chance level.

Table 5.5 shows results and statistics from altitudinal hemifield ROC plots in AION for each device. This ratio was calculated as the minimum of super/inferior (or vice versa) ratios for either eye, since field deficits may present unilaterally. HFA demonstrates good sensitivity of 75% at an FPR of 2%, rapidly increasing to a sensitivity of 90% at FPR 10%, after which there was negligible further increase. AUC was very high at 0.912, which was highly significant. HFA thresholds showed that values <0.90 are fairly diagnostic, although caution should be made for values >0.93 as FPR rapidly increases after this. MFA demonstrated good sensitivity of 68% at FPR of 2%, rapidly increasing to a sensitivity of 81% at a FPR 10%, after which there was only a marginal further increase – very similar to HFA in morphology. MFA AUC was marginally less than HFA at 0.885, while still being highly significant. MFA thresholds

show similar trends to HFA, being fairly diagnostic at values <0.88 with a sharp increase in FPR for thresholds >0.90. mfPOP demonstrated poor ability to detect initially with sensitivity of 10% at FPR 2% and closely followed the chance-line after 20% FPR, with an AUC near chance of 0.533 which is non-significant. mfPOP thresholds showed a high degree of variability in controls, with the majority of controls having thresholds in the 0.75–1 range, with ratios as low as 0.66 still having 10% FPR as compared to 0.90 and 0.88 in HFA/MFA.

5.4.5. Intraclass correlation by hemifield ratios

Although a direct point-to-point comparison of devices has been done, given that mfPOP used a derived version to generate 24-2 plots it is reasonable to consider than perhaps individual points do not correlate but that general regions/patterns of damage do. Intraclass correlation coefficients (ICC) were calculated to identify whether the stereotypical regions damaged in each disease correlated well between devices. This was completed using the Matlab ICC function of type 'C-k': *The degree of consistency for measurement that are average of k independent measurements made under the fixed levels of column factor*.

Results are shown in Table 5.6.

ICC for hemifield ratios				
		HFA vs MFA	HFA vs mfPOP	MFA vs mfPOP
Stroke	r-correl	0.985	0.495	0.550
	p-value	1.67E-15	0.054	0.034
Pituitary	r-correl	0.923	-0.056	-0.097
	p-value	7.72E-04	0.533	0.550
AION	r-correl	0.962	0.521	0.559
	p-value	7.53E-06	0.131	0.106

Table 5.6: Intraclass correlation coefficients and associated *p*-values for comparisons between each device. Cells are colour-coded to highlight those in green as highly significant, those in yellow as near-significant, and those in red as non-significant.

ICCs for HFA vs MFA were high in all disease states, with stroke being the most highly correlated followed closely by AION and pituitary, with all results being highly significant. For HFA vs mfPOP, results were mixed with moderate correlation in stroke and AION with near-significant results, while pituitary was negatively correlated and was non-significant. For MFA vs mfPOP, results were similar to HFA but slightly more favourable, with stroke and AION being near-significant and marginally significant, and pituitary again being negatively correlated with a non-significant result. These are generally consistent with point-to-point comparisons and further support that there is a good correlation between HFA and MFA, whereas mfPOP does not correlate well with either, although marginally better in MFA.

5.5. Discussion

While an analysis on the population scale would be absolutely worth doing, the 24-2 raw field maps provide a good measure of what clinicians might see in practice when looking at individual patients, and so visual inspection is an important part of deciding which devices work well.

Visually, HFA and MFA have very good agreement with respect to damage location and morphology through all conditions, although there were a couple of instances of mismatch where one demonstrated something the other did not. mfPOP showed some general hemianopic trends to side matching HFA/MFA in stroke when there was complete/near-complete homonymous hemianopia, but otherwise did not correlate well with quadrantanopias or smaller damaged areas in any condition. It was however noticed that in many of the fields where some damage was apparent on HFA/MFA, that mfPOP showed a noisy reduction in the entire field, although it was often difficult to discern given the high level of noise.

This is an interesting result given that the traditional subcortical pupillary pathway branches before the LGN and therefore would not be expected to detect post-LGN damage without cortical input. Anatomical studies show there is cortical input to the pretectal olivary nucleus within the pretectum (Gamlin, 2006), it has been demonstrated that removal of the cortex in macaques can affect pupil dynamics (Heywood *et al.*, 1998), and response delays in isoluminant colour exchange (Carle *et al.*, 2013; Rosli *et al.*, 2018) suggest mfPOP may be affected by cortical input. However, results in this study using the mfPOP Y/Y protocol did not demonstrate this. The inconsistency in mfPOP to show pupillary changes in hemianopias, the absence of any correlation in quadrantanopias, and the at-chance AUC values from ROC show that cortical stroke is only minimally detected by this test. It would then seem that perhaps pupil fields and visual fields might be dissociated in these disorders, as has been reported in

other ocular diseases like Leber hereditary optic neuropathy , which shows complete retention of pupil response despite the visual field loss due to minimal damage to ipRGC (Bremner *et al.*, 1999; Bremner *et al.*, 2001; Nissen *et al.*, 2015). However, since a several hemianopia subjects did show a degree of correlation, there must be some means by which damage is detectable in this system. Another study looking at pupillometry in response to a single large stimulus (10 degrees diameter) presented in the damaged field of stroke patients also revealed mixed results. Some stroke patients showed pupillary responses, while others showed minimal responses, with no obvious reason for this division (Sahraie *et al.*, 2013). Certainly, a simple argument that different cortical strokes result in different loss of cortical input is a likely possibility, but perhaps doesn't explain why same sided hemianopias between patients do not show similar patterns, or why no quandrantanopias show concordance with automated perimetry.

One consideration is that the stimuli employed in this study have sufficiently large contrast to induce a pupil response of the blind hemifield, while not being consciously aware of stimuli. Several studies addressing blindsight in a patient with a cortical lesions resulting in hemianopia have demonstrated that large stimuli presented for long periods can be detectable by the patient and result in pupillary constriction, especially where flicker is employed (Weiskrantz *et al.*, 1991; Barbur *et al.*, 1994). While this is intriguing, there are several key differences between their approach and mfPOP, most notable stimuli were presented for 500ms compared to only 33ms in mfPOP, and flicker was employed, while mfPOP does not use flicker. While these may not be directly comparable, it may still be worth investigating if smaller sized stimuli with lower contrast may show better attenuation of signal in blind hemifields.

Another further possibility is as subcortical pathways remain intact after stroke initially, pupillometry may not align with the field defects, but after atrophy to retinal pathways back to the retina following stroke, retinal input to ipRGC may be affected. This would result in

pupillometry being diminished in blind hemifields, and that this might explain the variable extent of alignment of pupillometry with visual field damage. Removal of striate cortex has been demonstrated to have a time-course related to the atrophy of the LGN in monkeys (Cowey, 1974; Cowey *et al.*, 1999; Johnson & Cowey, 2000) and lesions in occipital cortex of humans using MRI have demonstrated shrinkage of the optic tract (Bridge *et al.*, 2011; Cowey *et al.*, 2011) and even thinning of the retinal nerve fibre layer (RNFL) on OCT scans (Jindahra *et al.*, 2009). It is therefore theoretically possuble that this degeneration might include cells with input to the pupillary pathway, and thereby perturb the subcortical pupillary response sufficiently to facilitate crude detection on mfPOP. Results from a recent study looking at the time course of human retrograde degeneration in homonymous hemianopia demonstrated an initial sharp decrease in the first two years followed by linear thinning thereafter, while in quadrantanopias or smaller, there was no discernible thinning at all (Jindahra *et al.*, 2012). Continuing with the hypothesis that this degeneration affects pupillary input, this then provides a strong argument for why mfPOP might be able to similarly detect some HH damage, although it might not detect quadrantanopias or smaller defects. While this issue was not addressed in these studies, brain MRIs, including diffusion tensor imaging of cortical tracts, was performed on our subjects and future analysis of these might provide further insight into the hypothesis.

Principal curves were explored for relationships between devices. In the first iteration which included all data points, HFA had a complex curve relationship with mfPOP, hyperflexing back on itself, which does not intuitively make sense. Looking more closely at the scatter plot, there were two areas of dense data – one being at the HFA's upper range of 25–35 dB spread over the entire mfPOP range, and another at HFA's lower range at 0 dB, again with a substantial spread in mfPOP, and these appear to be the factors causing this flex. This was confirmed by the second iteration with 0 dB data points removed, showing a relationship with no correlation initially at high normal HFA values, and then a sharp decline in HFA over a small mfPOP

range. Given that HFA thresholds are calculated using the maximal luminance it can display (3178 cd/m^2) as 0 dB (Fredette *et al.*, 2015), it is clear that a 0 dB score is not a true null response, as more intense lights might still allow detection of the stimulus. There is thus a floor effect, at which true thresholds are grouped into 0 dB as the limit of the testing range is reached. It is then reasonable to only compare tests within their range and exclude points affected by this floor (i.e. 0 dB points). In looking at MFA with mfPOP, in the first iteration there was again a pooling of data at the 0 dB range, but otherwise the data was more widely spread throughout the MFA range (albeit striated due to a limitation of 15 output thresholds). After removing the 0 dB data points in the second iteration, the relationship was less dramatically shifted than in HFA, but modestly less steep and in good alignment with HFA trends. In comparing HFA vs MFA with all data, there was a sigmoidal relationship which appears to be due to 0-points in MFA all being 0 dB points in HFA, but HFA having many 0 dB points which are spread over the MFA range. While they both have floor effects, it is well established that MFA has a greater dynamic range than HFA in glaucoma (Wall *et al.*, 2009), and this result suggests the same is true of neurological disease. Once 0 dB points are removed, they show a nearly linear relationship, with a slight flexion at 20 dB HFA / 15 dB MFA. The gradient is initially roughly 2:1 for MFA:HFA, which is consistent with the different dB conversion rates of 20*log(contrast) vs 10*log(attenuation), thereafter becoming closer to 1:1, perhaps due to the HFA's smaller dynamic range. Considering that mfPOP has been correlated with RNFL thickness (structural damage) (Kolic *et al.*, 2013), and that both HFA and MFA are known to measure threshold for detection (functional damage), this may explain the shape of their relationship. It is known that there are many overlapping fields in the retina (Wassle & Boycott, 1991; Gauthier *et al.*, 2009; Soo *et al.*, 2011), with the coverage factor suggesting dendritic overlap of 3–4 cells for a given region (Wassle, 2004), such that damage to a single cell does not result in field loss (redundancy). However, every cell lost would result in a decrease in

RNFL thickness once its axon degenerates, creating a structural loss. It follows that if one were to plot RNFL thickness against perception, one might see structural damage occurring while the perceptual signal remained constant – until a critical point was reached where no redundancy remains and perception rapidly declined (Hart & Becker, 1982; Kerrigan-Baumrind *et al.*, 2000). This may explain the sharply curved relationship between mfPOP and HFA, as HFA is a perceptual measure with redundancy and mfPOP has been shown to have a more linear relationship with RNFL (Kolic *et al.*, 2013). Likewise, it may also underpin why MFA has a similar relationship with mfPOP as with HFA, although with more linearity – that is, MFA remains a perceptual measure with some redundancy, but it was originally created to target M_y said to have less redundancy (Maddess & Henry, 1992; Johnson, 1994; Johnson & Samuels, 1997; Wall *et al.*, 2002; Yoon *et al.*, 2012).

Bland–Altman plots collectively demonstrated similar finding to the scatter plots, with HFA and MFA having the most agreement and smallest mean difference, while HFA and mfPOP showed the worst agreement and largest mean difference, with MFA and mfPOP having marginal agreement and intermediate mean differences. Between diseases, pituitary appeared to have the least variability overall, but may have been confounded by the relatively few data points having heavy field damage. This also explains its particularly large 1% CI at means of 10–15 dB as an outlier in a small dataset. Stroke had a similar degree of variation to pituitary but with more data points, and AION showed much wider confidence intervals and greater variability. Greatest variability in HFA vs MFA for all diseases was in the 12–15 dB range, which roughly aligns with the flexion point on their principal curve plots. In HFA or MFA plots against mfPOP, there was no consistent point of maximal variation, with generally large variation throughout. In terms of means, HFA > MFA > mfPOP for all conditions, which would make sense given the pooling of data at the upper range in the scatter plots while MFA and mfPOP were both more evenly spread throughout their range. It should be noted that in stroke

it is common to see a fairly sharp demarcation between normal and complete deficit, thereby generating two distinct data pools – as opposed to say AION or glaucoma which have many grey-intermediate damage regions which give a spread of data.

In assessing which device is most effective at detecting a disorder, it can be difficult when there is no gold standard to compare against, but one method is to reduce each field to a single number and generate a ROC curve. While Mean Defect (MD) has been used repeatedly in HFA and MFA, it does not take into account if the shape of the field defect is typical for that disease nor does it control for the possibility that the person has brighter or dimmer fields generally. Hemifield ratios provide an interesting in between case which only considers field damage typical of the disease and is naturally normalised to the person's unaffected regions (because it is a ratio of one side to the other). HFA and MFA demonstrated a high and significant AUC, demonstrating that even small deviations (6–7%) from equality between hemifields is highly diagnostic. In terms of selecting which would be more appropriate, although MFA is very marginally better than HFA in terms of total AUC, for FPR values which are be likely to be acceptable (<20%), HFA demonstrates a better profile, reaching 59% sensitivity at an FPR of 2%, compared to MFA's 44%. mfPOP, on the other hand, did not perform so favourably, with an AUC marginally above chance and a non-significant result. Looking at a graph of thresholds, mfPOP demonstrates that many of the control subjects have partial HH-like fields, meaning this noise makes it very difficult to pick up damaged fields. In complete or near-complete HH, there were fields which were discernible in mfPOP, and this explains the initial increase in ROC curves above baseline, but, similar to visual inspection, there was limited ability to correctly identify any damage in those with smaller defects seen on HFA or MFA.

ROC plots using hemifield ratios for pituitary revealed that while HFA performed fine with a significant result, MFA quite dramatically outperformed HFA with an AUC of 0.966 reaching 99% sensitivity at 20% FPR. mfPOP again performed at chance level with a non-significant

result. It was very interesting to note that MFA sensitivity here even outperformed visual inspection, with approximately half the subjects having no apparent damage on Matrix field. Most of the subjects had been identified as having a pituitary tumour through visual field testing and had demonstrated field deficits prior to surgery, after which many completely resolved. This suggests that perhaps there was retained subtle damage and that MFA, in combination with hemifield ratios, is very sensitive to these subtle differences and so may permit earlier detection. In attempting to explain why MFA performed so well in this test, it is worth thinking about its design. Matrix was reported to stimulate a subset of magnocellular cells called M_y (Maddess & Henry, 1992; Johnson & Samuels, 1997). M_y comprise 15–25% of the magnocellular response, are large in diameter, and have minimal coverage factor (Crook *et al.*, 1988), being suggested to be sensitive to glaucomatous damage and insensitive to other neurological disease (Maddess & Henry, 1992). While this premise has been challenged (Anderson & Johnson, 2002; White *et al.*, 2002), it continues to be debated (Maddess, 2011a). Whether M_y cells are the population of interest or not, the principle that the MFA stimulus targets a cell type which has a low convergence factor might well explain why MFA appears to detect subtle differences which HFA is insensitive to.

ROC plots using hemifield ratios for AION revealed that HFA and MFA perform well with high AUC for both devices, with significant results. HFA performed slightly better than MFA, with larger AUC and larger sensitivities over a useful FPR range, initially reaching 75% sensitivity at 2% FPR compared with MFA's 68%. mfPOP performed on a par with previous diseases, with no significant difference from chance.

Overall, the ROC plots reveal that HFA is likely to be the most useful in stroke and AION, while MFA has excellent sensitivity and is most useful in chiasmal compression. mfPOP was not able to discern disease states using hemifield ratios, and thresholds show substantial noise which could mislead clinicians to false conclusions.

While agreement between the devices was determined with point-to-point correlations, the general location of field damage had not been compared. Using the same hemifield ratios utilised in ROC plots, the mfPOP device was compared with other devices using intraclass correlation coefficients (ICCs). Results were consistent with pointwise analysis, with HFA and MFA having excellent correlation in stroke and AION, and very good correlation in chiasmal compression; while mfPOP comparisons were not well correlated, although marginally better against MFA than HFA. While one of the results for MFA vs mfPOP did reach significance at the 5% level, this was marginal and, considering the degree of correlation between the other two devices, this should not be overanalysed. It is also perhaps worth noting that the slightly lower correlation in HFA vs MFA for the 1 group is consistent with the biggest difference in AUC for these machines, likely due to the exceptional performance MFA demonstrated in pituitary detection.

It is interesting to note that mfPOP performed so poorly in the subcortical damage groups of AION and chiasmal compression, when it has been reported effective in damage to the retina in glaucoma (Carle *et al.*, 2011b; Carle *et al.*, 2015), age-related macular degeneration (Sabeti *et al.*, 2011; Maddess *et al.*, 2012b; Rosli *et al.*, 2012), and diabetic retinopathy (Sabeti *et al.*, 2015). The first consideration would be if the anterior damage groups in this study were not severe enough to demonstrate damage. However, given damage was demonstrated on SAP devices, and they were wound effective in separating from controls, this does not seem adequate to explain the findings. Another reason this might be is the diseases AION and chiasmal compression both result in damage to the optic nerve, as opposed to predominantly retinal damage. However, success in glaucoma would imply such damage might be detectable. The other key different is using a method able to consider the location of the damage, rather than simply presence of damage. To date mfPOP studies have largely used the ‘worst *n* regions’ in ROC plots to demonstrate effectiveness, where *n* has varied considerably between studies.

This approach is limited, as it only shows whether your vision is worse than controls, not whether the pattern of field loss is consistent with the disease being assessed. It therefore may provide excellent ROC results for separating diseases from control groups, but would not be effective in separating between the mixed ocular disorders which present to clinicians. Given stroke patients have more typical patterns of field loss, the approach in this study has instead been to assess whether typical field loss is demonstrated in affected patients. This has revealed that mfPOP does not show patterns of loss consistent with stroke, but does appear to show generally dimmer responses in some patients. This can likely explain why this study has not shown as favourable results as in other diseases assessed using mfPOP, and provides a challenge for mfPOP to overcome to be useful in clinical practice.

A limitation in this study is the relatively small numbers of subjects in each group, some of which do not have overt field damage. While this has hindered more definitive conclusions, measuring the same cohort with other devices has allowed a fair comparison despite a heterogenous population. It would have been interesting to note how well the other mfPOP protocol (green stimuli on red background, G/R) performed if control data were collected, given that colour components have been demonstrated to be abolished by a specific cortical lesion in macaques (Heywood *et al.*, 1998). If there was more time, collection of G/R data would facilitate this analysis. Likewise, MRI data was collected but was not able to be analysed at this time. A future direction might be to investigate how structural damage varied between those that appeared to show some mfPOP correlation and those that did not.

5.6. Conclusion

HFA and MFA correlate very well with each other in all conditions, while mfPOP did not correlate well with either HFA or MFA, although marginally better with MFA. This may be due to mfPOP measuring structural damage while HFA and MFA measure perceptual damage.

HFA and MFA performed well at detecting conditions using hemifield ratios, with HFA slightly out-performing MFA in stroke and AION, whereas MFA substantially out-performed HFA in pituitary. mfPOP was not effective at distinguishing disease states based on hemifield ratios, and as things currently stand, cannot contribute to the diagnosis of stroke, chiasmal compression, or AION. Visual inspection suggested that mfPOP demonstrated some correlation in complete/near-complete homonymous hemianopia, which suggests some detection of post-LGN damage, with a likely hypothesis being retrograde degeneration, which can only be seen in hemianopia but not in quadrantanopia or smaller. Further investigation is necessary using MRI data to confirm this hypothesis.

References

Ali EN, Maddess T, James AC, Voicu C & Lueck CJ. (2014). Pupillary response to sparse multifocal stimuli in multiple sclerosis patients. *Mult Scler* **20,** 854-861.

Ali EN, Maddess TL, Martin K, Borbelj A & Lueck CJ. (2015). Pupillary response to sparse multifocal stimuli in epilepsy patients. In *4th annual saudi epilepsy society conference*, ed. Al-Baradie RS, pp. 74-78. Neurosciences, Riyadh.

Anderson AJ & Johnson CA. (2002). Mechanisms isolated by frequency-doubling technology perimetry. *Invest Ophthalmol Vis Sci* **43,** 398-401.

Anderson AJ & Johnson CA. (2006). Comparison of the asa, mobs, and zest threshold methods. *Vision Res* **46,** 2403-2411.

Artes PH, Hutchison DM, Nicolela MT, LeBlanc RP & Chauhan BC. (2005). Threshold and variability properties of matrix frequency-doubling technology and standard automated perimetry in glaucoma. *Invest Ophth Vis Sci* **46,** 2451-2457.

Artes PH, Iwase A, Ohno Y, Kitazawa Y & Chauban BC. (2002). Properties of perimetric threshold estimates from full threshold, sita standard, and sita fast strategies. *Invest Ophth Vis Sci* **43,** 2654-2659.

Barbur JL, Harlow AJ & Weiskrantz L. (1994). Spatial and temporal response properties of residual vision in a case of hemianopia. *Philos Trans R Soc Lond B Biol Sci* **343,** 157-166.

Bell A, James AC, Kolic M, Essex RW & Maddess T. (2010). Dichoptic multifocal pupillography reveals afferent visual field defects in early type 2 diabetes. *Invest Ophth Vis Sci* **51,** 602-608.

Benevento LA & Davis B. (1977). Topographical projections of the prestriate cortex to the pulvinar nuclei in the macaque monkey: An autoradiographic study. *Exp Brain Res* **30,** 405-424.

Benevento LA & Rezak M. (1976). The cortical projections of the inferior pulvinar and adjacent lateral pulvinar in the rhesus monkey (macaca mulatta): An autoradiographic study. *Brain Res* **108,** 1-24.

Benevento LA, Rezak M & Santos A. (1977). An autoradiographic study of the projections of the pretectum in the rhesus monkey (macaca mulatta): Evidence for sensorimotor links to the thalamus and oculomotor nuclei. *Brain Res* **127,** 197-218.

Berezina TL, Khouri AS, Kolomeyer AM, Clancy PS & Fechtner RD. (2011). Peripheral visual field thresholds using humphrey field analyzer program 60-4 in normal eyes. *Eur J Ophthalmol* **21,** 415-421.

Bremner FD, Shallo-Hoffmann J, Riordan-Eva P & Smith SE. (1999). Comparing pupil function with visual function in patients with leber's hereditary optic neuropathy. *Invest Ophthalmol Vis Sci* **40,** 2528-2534.

Bremner FD, Tomlin EA, Shallo-Hoffmann J, Votruba M & Smith SE. (2001). The pupil in dominant optic atrophy. *Invest Ophthalmol Vis Sci* **42,** 675-678.

Bridge H, Jindahra P, Barbur J & Plant GT. (2011). Imaging reveals optic tract degeneration in hemianopia. *Invest Ophthalmol Vis Sci* **52,** 382-388.

Carle CF, James AC, Kolic M, Essex RW & Maddess T. (2015). Blue multifocal pupillographic objective perimetry in glaucoma. *Invest Ophthalmol Vis Sci* **56,** 6394-6403.

Carle CF, James AC, Kolic M, Loh YW & Maddess T. (2011a). High-resolution multifocal pupillographic objective perimetry in glaucoma. *Invest Ophthalmol Vis Sci* **52,** 604-610.

Carle CF, James AC, Kolic M, Loh YW & Maddess T. (2011b). High-resolution multifocal pupillographic objective perimetry in glaucoma. *Invest Ophth Vis Sci* **52,** 604-610.

Carle CF, James AC & Maddess T. (2013). The pupillary response to color and luminance variant multifocal stimuli. *Invest Ophth Vis Sci* **54,** 467-475.

Cash-Padgett T, Azab H, Yoo SBM & Hayden BY. (2018). Opposing pupil responses to offered and anticipated reward values. *Anim Cogn* **21,** 671-684.

Chauhan BC & Johnson CA. (1999). Test-retest variability of frequency-doubling perimetry and conventional perimetry in glaucoma patients and normal subjects. *Invest Ophthalmol Vis Sci* **40,** 648-656.

Coombes C, Sabeti F, Baker L, Cheung V, Chiou M, Kolic M, James A, Nolan C & Maddess T. (2012). Clinical utility of multifocal pupillographic objective perimetry in type 1 diabetes. *Clin Exp Ophthalmol* **40,** 108-108.

Cowey A. (1974). Atrophy of retinal ganglion cells after removal of striate cortex in a rhesus monkey. *Perception* **3,** 257-260.

Cowey A, Alexander I & Stoerig P. (2011). Transneuronal retrograde degeneration of retinal ganglion cells and optic tract in hemianopic monkeys and humans. *Brain* **134,** 2149-2157.

Cowey A, Stoerig P & Williams C. (1999). Variance in transneuronal retrograde ganglion cell degeneration in monkeys after removal of striate cortex: Effects of size of the cortical lesion. *Vision Res* **39,** 3642-3652.

Crook JM, Lange-Malecki B, Lee BB & Valberg A. (1988). Visual resolution of macaque retinal ganglion cells. *J Physiol* **396,** 205-224.

Dineen JT & Hendrickson A. (1983). Overlap of retinal and prestriate cortical pathways in the primate pretectum. *Brain Res* **278,** 250-254.

Distler C & Hoffmann KP. (1989). The pupillary light reflex in normal and innate microstrabismic cats, ii: Retinal and cortical input to the nucleus praetectalis olivaris. *Vis Neurosci* **3,** 139-153.

Fredette MJ, Giguere A, Anderson DR, Budenz DL & McSoley J. (2015). Comparison of matrix with humphrey field analyzer ii with sita. *Optometry and vision science : official publication of the American Academy of Optometry* **92,** 527-536.

Gamlin PDR. (2006). The pretectum: Connections and oculomotor-related roles. *Prog Brain Res* **151,** 379-405.

Gardiner SK, Demirel S, Goren D, Mansberger SL & Swanson WH. (2015). The effect of stimulus size on the reliable stimulus range of perimetry. *Transl Vis Sci Technol* **4,** 10.

Gauthier JL, Field GD, Sher A, Shlens J, Greschner M, Litke AM & Chichilnisky EJ. (2009). Uniform signal redundancy of parasol and midget ganglion cells in primate retina. *J Neurosci* **29,** 4675-4680.

Gerard B & Fischer A. (2011). Parameter selection for principal curves. *HAL archives-ouvertes*.

Hart WM, Jr. & Becker B. (1982). The onset and evolution of glaucomatous visual field defects. *Ophthalmology* **89,** 268-279.

Heijl A, Lindgren A & Lindgren G. (1989). Test-retest variability in glaucomatous visual fields. *Am J Ophthalmol* **108,** 130-135.

Hepworth LR & Rowe FJ. (2018). Programme choice for perimetry in neurological conditions (popin): A systematic review of perimetry options and patterns of visual field loss. *Bmc Ophthalmol* **18,** 241.

Heywood CA, Nicholas JJ, LeMare C & Cowey A. (1998). The effect of lesions to cortical areas v4 or ait on pupillary responses to chromatic and achromatic stimuli in monkeys. *Exp Brain Res* **122,** 475-480.

Holden AL & Fitzke FW. (1988). Image size in the fundus: Structural evidence for wide-field retinal magnification factor. *The British journal of ophthalmology* **72,** 228-230.

Horani A, Frenkel S & Blumenthal EZ. (2007). Test-retest variability in visual field testing using frequency doubling technology. *Eur J Ophthalmol* **17,** 203-207.

Huang CQ, Carolan J, Redline D, Taravati P, Woodward KR, Johnson CA, Wall M & Keltner JL. (2008). Humphrey matrix perimetry in optic nerve and chiasmal disorders: Comparison with humphrey sita standard 24-2. *Invest Ophthalmol Vis Sci* **49,** 917-923.

James AC. (2003). The pattern-pulse multifocal visual evoked potential. *Invest Ophth Vis Sci* **44,** 879-890.

James AC, Kolic M, Bedford SM & Maddess T. (2012). Stimulus parameters for multifocal pupillographic objective perimetry. *J Glaucoma* **21,** 571-578.

James AC, Ruseckaite R & Maddess T. (2005). Effect of temporal sparseness and dichoptic presentation on multifocal visual evoked potentials. *Visual Neurosci* **22,** 45-54.

Jindahra P, Petrie A & Plant GT. (2009). Retrograde trans-synaptic retinal ganglion cell loss identified by optical coherence tomography. *Brain* **132,** 628-634.

Jindahra P, Petrie A & Plant GT. (2012). The time course of retrograde trans-synaptic degeneration following occipital lobe damage in humans. *Brain* **135,** 534-541.

Johnson CA. (1994). Selective versus nonselective losses in glaucoma. *J Glaucoma* **3 Suppl 1,** S32-44.

Johnson CA & Samuels SJ. (1997). Screening for glaucomatous visual field loss with frequency-doubling perimetry. *Invest Ophthalmol Vis Sci* **38,** 413-425.

Johnson H & Cowey A. (2000). Transneuronal retrograde degeneration of retinal ganglion cells following restricted lesions of striate cortex in the monkey. *Exp Brain Res* **132,** 269-275.

Kerrigan-Baumrind LA, Quigley HA, Pease ME, Kerrigan DF & Mitchell RS. (2000). Number of ganglion cells in glaucoma eyes compared with threshold visual field tests in the same persons. *Invest Ophthalmol Vis Sci* **41,** 741-748.

Kim TW, Zangwill LM, Bowd C, Sample PA, Shah N & Weinreb RN. (2007). Retinal nerve fiber layer damage as assessed by optical coherence tomography in eyes with a visual field defect detected by frequency doubling technology perimetry but not by standard automated perimetry. *Ophthalmology* **114,** 1053-1057.

Kolic M, Chain A, James A, Maddess T & Carle C. (2013). Structure and function in multifocal pupillographic objective perimetry (mfpop). *Invest Ophth Vis Sci* **54**.

Lueck C, Ali E, Carle C & Maddess T. (2014). Effects of stimulating melanopsin-containing retinal ganglioncells in migraine patients using multifocal objective pupillometry. *J Clin Neurosci* **21,** 2048.

Maddess T. (2011a). Frequency-doubling technology and parasol cells. *Invest Ophth Vis Sci* **52,** 3759-3759.

Maddess T. (2011b). The influence of sampling errors on test-retest variability in perimetry. *Invest Ophthalmol Vis Sci* **52,** 1014-1022.

Maddess T. (2014). Modeling the relative influence of fixation and sampling errors on retest variability in perimetry. *Graefe's archive for clinical and experimental ophthalmology = Albrecht von Graefes Archiv fur klinische und experimentelle Ophthalmologie* **252,** 1611-1619.

Maddess T, Ali E, James A, Voicu C, Janke A & Lueck C. (2012a). The application of pupillary response to sparse multifocal stimuli in monitoring multiple sclerosis patients. *Neurology* **78**.

Maddess T, Bedford SM, Goh XL & James AC. (2009). Multifocal pupillographic visual field testing in glaucoma. *Clin Exp Ophthalmol* **37,** 678-686.

Maddess T, Essex RW, Kolic M, Carle CF & James AC. (2013). High- versus low-density multifocal pupillographic objective perimetry in glaucoma. *Clin Exp Ophthalmol* **41,** 140-147.

Maddess T & Henry GH. (1992). Performance of nonlinear visual units in ocular hypertension and glaucoma. *Clin Vision Sci* **7,** 371-383.

Maddess T, Saikal A, Kolic M, Carle CF, Essex RW, James AC & Sabeti F. (2012b). Diagnostic accuracy of multifocal pupillographic objective perimetry (mfpop) in early age-related macular degeneration. *Clin Exp Ophthalmol* **40,** 129-129.

Medeiros FA, Sample PA & Weinreb RN. (2004). Frequency doubling technology perimetry abnormalities as predictors of glaucomatous visual field loss. *Am J Ophthalmol* **137,** 863-871.

Nissen C, Ronnback C, Sander B, Herbst K, Milea D, Larsen M & Lund-Andersen H. (2015). Dissociation of pupillary post-illumination responses from visual function in confirmed opa1 c.983a > g and c.2708_2711delttag autosomal dominant optic atrophy. *Frontiers in neurology* **6,** 5.

Numata T, Maddess T, Matsumoto C, Okuyama S, Hashimoto S, Nomoto H & Shimomura Y. (2017). Exploring test-retest variability using high-resolution perimetry. *Transl Vis Sci Technol* **6,** 8.

Pearce JG & Maddess T. (2016). Retest variability in the medmont m700 automated perimeter. *Optometry and vision science : official publication of the American Academy of Optometry* **93,** 272-280.

Rosli Y, Bedford SM, James AC & Maddess T. (2012). Photopic and scotopic multifocal pupillographic responses in age-related macular degeneration. *Vision Res* **69,** 42-48.

Rosli Y, Carle CF, Ho Y, James AC, Kolic M, Rohan EMF & Maddess T. (2018). Retinotopic effects of visual attention revealed by dichoptic multifocal pupillography. *Sci Rep* **8,** 2991.

Ruseckaite R, Maddess T, Danta G, Lueck CJ & James AC. (2005). Sparse multifocal stimuli for the detection of multiple sclerosis. *Ann Neurol* **57,** 904-913.

Sabeti F, James AC, Carle CF, Essex RW, Bell A & Maddess T. (2017). Comparing multifocal pupillographic objective perimetry (mfpop) and multifocal visual evoked potentials (mfvep) in retinal diseases. *Sci Rep* **7,** 45847.

Sabeti F, James AC, Essex RW & Maddess T. (2013). Multifocal pupillography identifies retinal dysfunction in early age-related macular degeneration. *Graefe's archive for clinical and experimental ophthalmology = Albrecht von Graefes Archiv fur klinische und experimentelle Ophthalmologie* **251,** 1707-1716.

Sabeti F, Maddess T, Essex RW & James AC. (2011). Multifocal pupillographic assessment of age-related macular degeneration. *Optometry Vision Sci* **88,** 1477-1485.

Sabeti F, Maddess T, Essex RW, Saikal A, James AC & Carle CF. (2014). Multifocal pupillography in early age-related macular degeneration. *Optometry and vision science : official publication of the American Academy of Optometry* **91,** 904-915.

Sabeti F, Nolan CJ, James AC, Jenkins A & Maddess T. (2015). Multifocal pupillography identifies changes in visual sensitivity according to severity of diabetic retinopathy in type 2 diabetes. *Invest Ophthalmol Vis Sci* **56,** 4504-4513.

Sahraie A, Trevethan CT, MacLeod MJ, Urquhart J & Weiskrantz L. (2013). Pupil response as a predictor of blindsight in hemianopia. *Proc Natl Acad Sci U S A* **110,** 18333-18338.

Soo FS, Schwartz GW, Sadeghi K & Berry MJ, 2nd. (2011). Fine spatial information represented in a population of retinal ganglion cells. *J Neurosci* **31,** 2145-2155.

Steele GE & Weller RE. (1993). Subcortical connections of subdivisions of inferior temporal cortex in squirrel monkeys. *Vis Neurosci* **10,** 563-583.

Taravati P, Woodward KR, Keltner JL, Johnson CA, Redline D, Carolan J, Huang CQ & Wall M. (2008). Sensitivity and specificity of the humphrey matrix to detect homonymous hemianopias. *Invest Ophthalmol Vis Sci* **49,** 924-928.

Wall M, Doyle CK, Zamba KD, Artes P & Johnson CA. (2013). The repeatability of mean defect with size iii and size v standard automated perimetry. *Invest Ophthalmol Vis Sci* **54,** 1345-1351.

Wall M, Neahring RK & Woodward KR. (2002). Sensitivity and specificity of frequency doubling perimetry in neuro-ophthalmic disorders: A comparison with conventional automated perimetry. *Invest Ophth Vis Sci* **43,** 1277-1283.

Wall M, Woodward KR, Doyle CK & Artes PH. (2009). Repeatability of automated perimetry: A comparison between standard automated perimetry with stimulus size iii and v, matrix, and motion perimetry. *Invest Ophthalmol Vis Sci* **50,** 974-979.

Wall M, Woodward KR, Doyle CK & Zamba G. (2010). The effective dynamic ranges of standard automated perimetry sizes iii and v and motion and matrix perimetry. *Arch Ophthalmol* **128,** 570-576.

Wassle H. (2004). Parallel processing in the mammalian retina. *Nat Rev Neurosci* **5,** 747-757.

Wassle H & Boycott BB. (1991). Functional architecture of the mammalian retina. *Physiol Rev* **71,** 447-480.

Weber J & Dobek K. (1986). What is the most suitable grid for computer perimetry in glaucoma patients? *Ophthalmologica* **192,** 88-96.

Weiskrantz L, Harlow A & Barbur JL. (1991). Factors affecting visual sensitivity in a hemianopic subject. *Brain* **114 (Pt 5),** 2269-2282.

White AJ, Sun H, Swanson WH & Lee BB. (2002). An examination of physiological mechanisms underlying the frequency-doubling illusion. *Invest Ophthalmol Vis Sci* **43,** 3590-3599.

Yoon MK, Hwang TN, Day S, Hong J, Porco T & McCulley TJ. (2012). Comparison of humphrey matrix frequency doubling technology to standard automated perimetry in neuro-ophthalmic disease. *Middle East Afr J Ophthalmol* **19,** 211-215.

Young RSL & Alpern M. (1980). Pupil responses to foveal exchange of monochromatic lights. *J Opt Soc Am* **70,** 697-706.

Chapter 6: Analysis of time-to-peak response in pupillometry waveforms, and comparison with response amplitude in stroke, chiasmal compression, and AION

6.1. Abstract

6.1.1. Purpose

Multifocal pupillographic objective perimetry (mfPOP) uses changes in pupil diameter in response to light stimuli to measure sensitivity of the visual field. This results in a pupil response waveform for each region measured across 2 seconds, and the waveform is then used to derive measures that can be used to assess the visual field. In previous experiments the amplitude of this waveform was called the peak response. It is also possible to measure the latency of this peak response, called the time-to-peak (TTP). While amplitude is perhaps the most intuitive measure, there may also be useful information in the TTP.

In previous experiments, yellow stimuli on a yellow background (Y/Y) were used, giving purely luminance-based stimuli, while another protocol is presented here, with green stimuli on a red background (G/R) with a mixed luminance and colour exchange signal. While both colour and luminance pupil responses receive cortical input, it appears cortical input dominates in isoluminant colour exchange, whereas subcortical input dominates in luminance-only responses. Thus, the G/R protocol provides a plausible means for detecting stroke damage, whereas Y/Y was ineffectual (see Chapter 5). The extent of colour exchange compared to luminance has also been associated with increased TTP, suggesting that this measure might

provide additional utility for detecting cortical damage. This chapter compares amplitude (Amp) and TTP measures across both protocols of Y/Y and G/R, testing whether there are any useful relationships and notable features. Additionally, given the large degree of noise in results presented in Chapter 5, repeat sessions will be evaluated as a measure of internal consistency and reproducibility.

6.1.2. Methods

Subjects with complete data sets for groups [stroke (n = 24), pituitary (n = 11), and AION (n = 10)] were tested using multifocal pupillographic objective perimetry (mfPOP) with either yellow stimuli on a yellow background (Y/Y) or green stimuli on a red background (G/R), with average stimuli luminance of 150 cd/m^2 and average background 10 cd/m^2. Pupillary responses had their peak amplitude measured (Amp) and their latency measured as time-to-peak (TTP; latency). Amp was converted from absolute measures (μm) to relative measures of dB to allow comparison with the Humphrey Field Analyser (HFA) results. Pupillary responses had direct and consensual components combined in terms of signal-to-noise-ratio weighted means. Means across repeats were taken where appropriate and converted from 44-region mfPOP fields into 54-region HFA 24-2 format by proximity weighting. Results were plotted on visual field maps with a colour- or grey-scale map.

6.1.3. Results

In stroke patients, G/R showed response amplitudes 2.2 dB smaller and TTP values 11.2 ms greater than Y/Y, with similar trends in chiasmal compression and AION. Comparing direct and consensual, both Y/Y and G/R protocols showed that direct exceeded consensual temporally, and consensual exceeded direct nasally (except for Y/Y in stroke where nasal regions were equivalent). TTP showed relatively smaller proportional differences between direct and consensual responses, which had whole fields (from one eye) showing a bias towards either direct or consensual in 60–63% of eyes (and frequently being reciprocal between fellow

eyes). There were moderate–strong relationships between Y/Y and G/R for Amp and TTP across all disease types, with Pearson correlation coefficients in the range 0.530–0.849. Aggregate results comparing Amp and TTP for each protocol showed curvilinear response with no correlation ($r^2 < 0.06$), but individual plots showed positive linear correlations in 21/24 for Y/Y stroke and 19/24 for G/R stroke. Results for pituitary and AION were similar, with Y/Y showing greater Pearson scores than in G/R generally. Repeats showed high correlations for all protocols, measures, and conditions ($r \geq 0.7$, except G/R TTP in stroke with $r = 0.491$).

6.1.4. Conclusions

Pupil responses from G/R correlate well with Y/Y stimuli in terms of Amp and TTP, with marginally smaller amplitude and greater latency on average. Contraction anisocoria varies according to hemifield in both Y/Y and G/R, with temporal fields showing direct > consensual and nasal fields with consensual > direct. Differences between direct and consensual in terms of latency are small and tend to affect the whole field of any eye, often with reciprocal results in the fellow eye, which is likely due to anatomical variation. There is a positive correlation between Amp and TTP in the majority of subjects, suggesting damaged regions show smaller amplitudes and increased latency. Repeats show a mostly high degree of correlation, with Y/Y outperforming G/R. No approach appears to have good visual correlation with HFA results.

6.2. Introduction

In chapter 5, the traditional visual field devices, the Humphrey Field Analyser (HFA) and the Matrix Field Analyser (MFA), were compared to multifocal pupillographic objective perimetry (mfPOP) using the most straightforward protocol and measure – the standardised amplitude (Amp) of pupil constrictions in response to a luminance-only based protocol comprising bright yellow stimuli on a dimmer yellow background (Y/Y). Chapter 5 revealed that neither HFA nor MFA sensitivities appeared to correlate well with responses to the mfPOP protocol, that it had limited utility in predicting stroke, and suggested that these devices may be measuring different things. It was suggested that HFA and MFA measure perception, which is sensitive to any damage to processes that input to the cortex (or to the cortex itself), whereas the mfPOP Y/Y protocol appears to measure structural damage predominantly within the subcortical pupillary pathway (in which afferent components project to the pretectum prior to the LGN), making it relatively insensitive to cortical or posterior pathway damage.

As previously mentioned, in monkeys there is extensive anatomical evidence that there is input from both striate and extrastriate vision areas to the pretectal olivary nucleus (PON), as reviewed by Gamlin (Gamlin, 2006). This includes input from occipital cortex (V1) (Benevento & Rezak, 1976; Benevento *et al.*, 1977; Distler & Hoffmann, 1989), visual association cortices V2–5 (Benevento & Davis, 1977; Benevento *et al.*, 1977; Dineen & Hendrickson, 1983), and the inferior temporal region (Steele & Weller, 1993). It would therefore seem plausible that stroke damage may affect the pupillary response, despite the poor sensitivity of the Y/Y protocol using Amp.

It is known that changing colour at the same luminance (isoluminant colour exchange) evokes a bidirectional pupillary constriction, such that a red stimulus on a green background (R/G) or a green stimulus on a red background (G/R) both result in constriction (Young & Alpern, 1980;

Barbur *et al.*, 1992; Barbur *et al.*, 1998; Carle *et al.*, 2013). Further, it was shown that these typically have a peak response ~40–50 ms later than with luminance protocols (Gamlin *et al.*, 1998; Carle *et al.*, 2011).

The reported delay between activity in primary visual cortex (V1) and association cortex (V4) appears to be in the order of 20–30 ms (McClurkin & Optican, 1996; McClurkin *et al.*, 1996). Such an activation time between V1 and V4 is in a similar range to that of the increased latency observed in colour exchange, and it has been suggested that this delay might represent cortical processing of colour (Gamlin *et al.*, 1998; Carle *et al.*, 2011). Further, Heywood et al. demonstrated that a cortical lesion can abolish the isoluminant colour exchange response without damaging the luminant achromatic response (Heywood *et al.*, 1998). A stimulus with a colour component might then provide useful information not apparent with a pure luminance stimulus, and response delays might provide an alternative way to detect differences not apparent in the response's amplitude.

Input to intrinsically photoreceptive retinal ganglion cells (ipRGC) comes both from intrinsic sensitivity predominantly in the blue part of the spectrum (slow, tens of seconds) and cone input (rapid, <2 seconds) from all cone types (Pickard & Sollars, 2012; Sand *et al.*, 2012). This essentially makes ipRGC sensitive to changes in red/green/yellow, especially for rapid responses. In that sense Y/Y stimuli involve only luminance changes and probably focus only on subcortical input, while isoluminant colour exchange stimuli involve colour changes only and focus on cortical pathways.

Naturally, there is pupil constriction to a pure increase in luminance, such as with a yellow stimulus on a yellow background (Y/Y). Where there are larger increases in luminance, there are larger pupillary constrictions, and very large differences in luminance (order of ~2 log units) can result in shorter latencies of response (Bergamin & Kardon, 2003). The addition of

colour exchange to luminance stimuli marginally increases amplitudes, but what is interesting is that the latency of response measured by time-to-peak (TTP) appears to also be greater when there is more colour-exchange component and less luminance component (Barbur *et al.,* 1992; Barbur *et al.,* 1998; Carle *et al.,* 2013). It has also been noted that while there is a bidirectional response, both the amplitude response and latency are larger when presenting G/R compared to R/G (Carle *et al.,* 2013). It can therefore be understood why the same paper suggested that a suitable candidate for assessing the combined function of cortical and subcortical pathways might be a mixed component comprised of relatively high luminance green stimuli on a relatively lower luminance red background (Carle *et al.,* 2013).

In this study G/R is defined as a bright green stimulus of average 150 cd/m^2 on a dim red background of average 10 cd/m^2, thereby combining both colour and luminance. This compares to the Y/Y protocol used in earlier chapters, where there was a similarly bright yellow stimulus (150 cd/m^2) on a similarly dim yellow background (10 cd/m^2), representing luminance change, but without any colour exchange component. The G/R protocol was used (in addition to the Y/Y protocol utilised in earlier chapters) in order that we might compare potential changes in Amp and TTP due to damage within the subcortical pathway (such as from chiasmal compression and AION) or the cortical pathway (stroke). In addition, we wanted to explore whether the protocols (Y/Y and G/R) and measures (Amp and TTP) had any significant relationships or notable features.

It is expected that, due to cortical colour processing, the G/R protocol might have longer latencies than Y/Y, and might better reflect cortical damage in the stroke cohort. It would be reasonable to infer that cortical damage might result in decreased amplitude due to smaller pupillary input, and reduced latency due to a smaller colour component input, thus relying more heavily on the faster luminance component. Here, this aspect will be investigated in two ways:

by producing visual field plots for all subjects and visually inspecting them; and by comparing amalgamated visual field plots, box and whisker plots, and scatter plots.

In the pituitary and AION groups, damage is anterior and is expected to affect both subcortical and cortical pathways. While long latencies are still expected in the G/R protocol compared to Y/Y, it is expected that damage will result in decreased amplitude but minimal changes in TTP (given that the input from colour and luminance might be equally reduced but still proportionate). Throughout, results for chiasmal compression and AION will be presented along with stroke for comparison purposes.

6.3. Methods

A history of mfPOP and reasoning for test parameters can be found in the Introduction chapter: Multifocal methods heading. Full methods including recruitment (section 2.1), screening (section 2.2) and mfPOP stimuli, procedures and output measures (section 2.5.3) are detailed in General Methods. As all procedures are unchanged from previous chapters, this section will focus only on the novel G/R protocol and analyses used in this chapter.

It is first worth reiterating the three groups involved here: each subject within each disease group for which there was a complete data set (stroke, $n = 24$; pituitary, $n = 11$; and AION, $n = 10$). Stroke was defined (according to General Methods) as cortical damage, and no subject with demonstrated cerebellar damage or damage anterior to the optic chiasm was included. The stroke group is otherwise a heterogenous population, preferentially but not exclusively selected for occipital lesions. The pituitary group demonstrate chiasmal compression on the optic nerve (shown either through MRI or visual field testing consistent with disorder) which may or may not have resolved post-treatment. AION is defined according to the best clinical judgement of the treating ophthalmologist, and may involve a single eye or both eyes.

Measures not used in previous chapters will be touched on here, but for complete details the reader is referred to the General Methods section. The stimulus parameters are summarised in Table 6.1.

Protocol	Stimuli / Background Colour	Stimuli / Background Luminance (cd/m2)	Luminance Contrast	Stimulis Duration	Stimulus Frequency	Percentage Activation	Single region frequency	Presentation method	Stimulus grid
Y/Y	Yellow / Yellow	150 / 10	88%	33 ms	4 / s	50%	0.25 / s	Temporally sparse volleys	44-region overlapping
G/R	Red / Green	150 / 10	88%	33 ms	4/ s	50%	0.25 / s	Temporally sparse volleys	44-region overlapping

Table 6.1: Stimulus parameters for protocols Y/Y and G/R. Note that the only difference between them are the stimuli and background colours. Stimuli average 150 cd/m^2 presented on a background averaging 10 cd/m^2 for 33 ms at a rate of 4/s (every 250 ms), where only an average of 50% of the regions are activated. Presentations are grouped according to left and right eye, left and right hemifield, and odd or even stimulus grids, such that there are 8 sequential stimuli before any single region can be reactivated (minimum 2 seconds, average 4 s between stimuli). These are described as temporally sparse volleys presented in the 44-region overlapping grid as outlined in General Methods Figure 2.17.

For each of the 44 test regions in mfPOP, direct and consensual pupillary responses are measured over a two-second period (Figure 6.1).

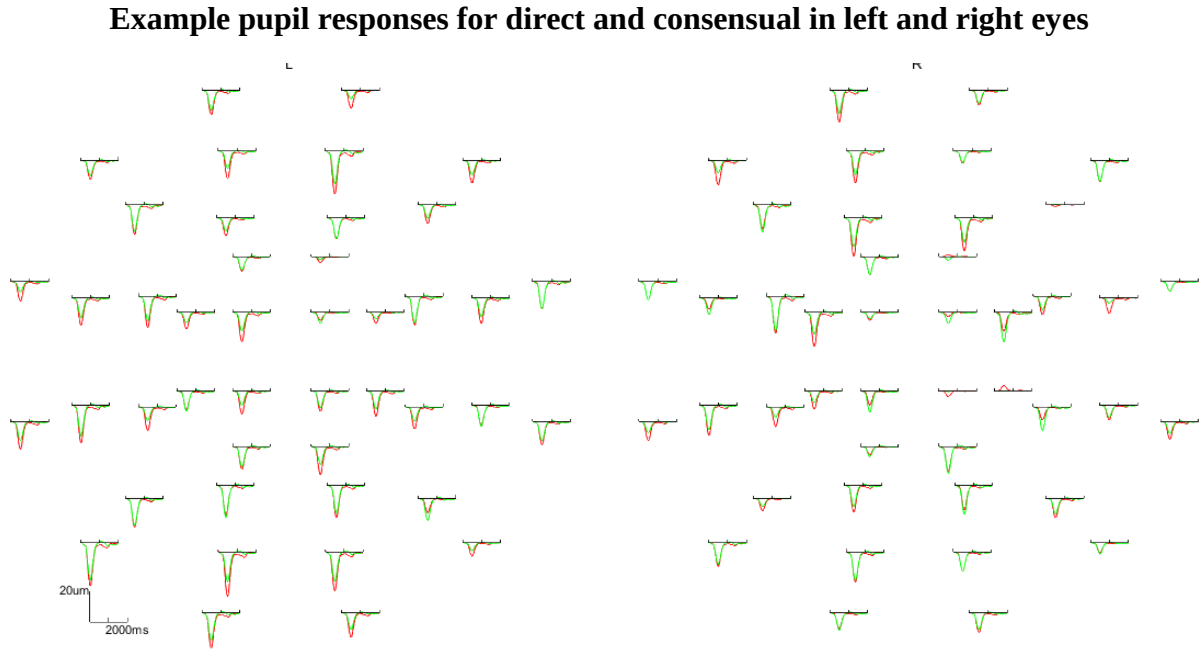

Figure 6.1: Left (L) and right (R) eye, showing direct (red) and consensual (green) pupillary responses over time. Note the scale in the lower left corner. Each of the 44 regions for each eye has a direct and consensual response curve lasting up to 2 s. From this, measures of amplitude (Amp) and time-to-peak (TTP) can be derived.

Pupillary responses to stimuli presented in each of the 44 test regions were estimated for each eye (left and right), each component (direct and consensual), each protocol (Y/Y and G/R), and each repeat (rep 1 and rep 2). From these response curves, measures of amplitude (Amp) and time-to-peak (TTP) can be extracted (Figure 6.2).

Example pupil responses for direct and consensual in a single region of left eye

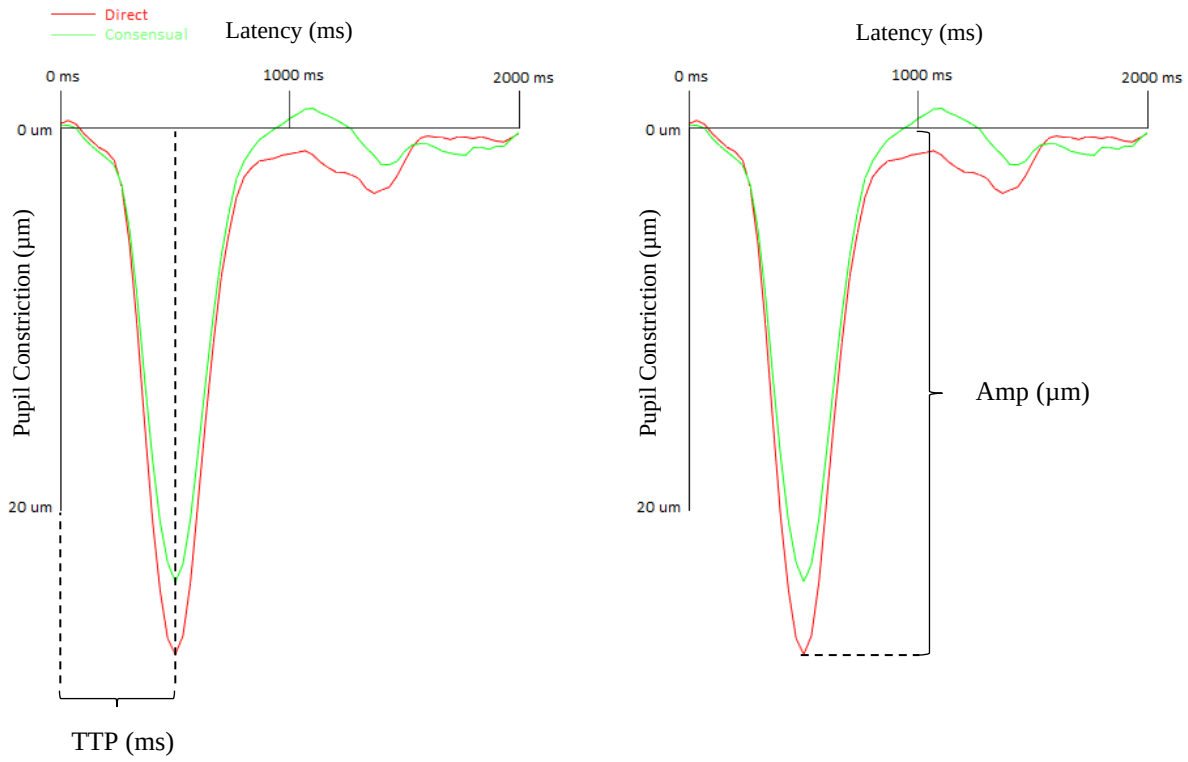

Figure 6.2: Example of pupillary responses for direct (red) and consensual (green) for a single region of the 44 test regions with stimulus onset at 0 ms. The time-to-peak (TTP) is highlighted on the left (measured in milliseconds, ms), while the amplitude (Amp) is indicated on the right as the maximum pupil constriction (in micrometers, µm).

As in previous chapters, amplitude is converted into dB units using a generalised log transform and rescaled to be cover the same range as the Humphrey Field Analyser (HFA). TTP is left in units of ms. Both Amp and TTP measures have direct and consensual components combined by weighting them according to their signal-to-noise ratio (SNR), where SNR is defined as the measure divided by its variance. Where repeats are combined, they are combined by the mean

of the two repeats. Lastly, the 44 region mfPOP results are translated by area-weighted means into the 54 region 24-2 design of the HFA. Where averages of the cohort are given, they are after the preliminary data processing mentioned above and relate only to a single disease.

Results for these regions are presented as fields which show the 54 regions according to eccentricity, in either linear grayscale, in colour with 128 degrees of colour difference, or in the case of ratios, as a colour scale in 64 shades of red (larger direct than consensual) and in 64 shades of blue (larger consensual than direct). In the case of ratios, a value of 1 is represented by white and darker colours represent more extreme ratios. Unless otherwise stated, graphs of averages clip the scale according to the maximum and minimum values presented in that plot only and thus cover the full range, while when individual subject plots are given, the scales are clipped to the maximum and minimum values for that entire disease cohort and so may not cover the entire range, but allow comparison between subjects.

For direct and consensual ratios measuring TTP, differences occurred between eyes. To better quantify this, a threshold percentage of regions where direct > consensual (or vice versa) was calculated to allow an eye to be considered ‘polarised’ rather than simply showing random noise. A binomial distribution was used to calculate the threshold using the following technique: 50% probability of success (direct/consensual ratio could only be above 1 or below 1) based on 54 trials (number of regions in field) and a cumulative probability of <0.01 as an acceptable α-value. This calculation gave the threshold as ≥ 36 (more than two-thirds of the 54 points) for an eye to be considered polarised. Using this threshold, tables were produced showing the number of polarised fields.

6.4. Results

6.4.1. Individual field plots for both protocols and measures

Initially, to investigate gross trends in the data, visual field plots comparing Amplitude (Amp) and time-to-peak (TTP) across the protocols Y/Y and G/R were created, alongside those for the Humphrey Field Analyser (HFA), for the three disease states – stroke, pituitary tumour, and AION. An example set showing the first-tested stroke subject with left hemianopia, the first stroke subject with right hemianopia, and the first pituitary and AION subjects with field damage according to HFA are shown in Figure 6.3 (equivalent to the subjects used in Chapter 5).

Chapter 5 indicated that mfPOP Amp Y/Y correlated poorly with HFA, so the Y/Y results are displayed here only for comparison. In terms of Amp, it appears that Y/Y and G/R are relatively similar, which is expected given they both have the same difference in luminance between stimulus and background, and luminance appears to be the main driver of changes in Amp. TTP values for Y/Y and G/R agree only crudely, but G/R appears to have greater latencies (darker in figure), which is consistent with the G/R protocol involving more synapses and a longer pathway (due to cortical processing of colour). An interesting and notable feature is that in some stroke patients, pupillary responses to G/R mfPOP stimuli in regions which had lower sensitivity on HFA exhibit smaller constriction amplitudes (darker) as well as shorter TTPs (darker), consistent with the expectation that cortical damage results in loss of colour input.

6.4.2. Average data by disease: field plots and box and whisker plots

This initial look at the data suggests some extra interesting comparisons. It would be useful to see if the apparent trends in Y/Y and G/R protocols show up consistently in the amalgamated dataset. Averages for stroke (n = 24), pituitary (n = 11), and AION (n = 10) are shown in Figures 6.4–6.6. Y/Y Amp appears to have marginally larger responses than G/R Amp across

both eyes and all three disease types. Although the individual points do not match especially well, general regions such as quadrants appear to show similar gradients of light and dark regions, indicating there is some signal within the background noise. G/R TTP appears to have longer delays than Y/Y TTP, consistent with individual results. Comparing patterns, they crudely align, with similar gradients of light visible when quadrants are compared. Comparing both measures (Amp and TTP) from either protocol, some selected subjects in the stroke cohort (such as mf88130 below) appear to show marginally smaller latency (darker) in regions where Amp is smaller (darker), although this is very noisy and shows inconsistencies. The G/R protocol also appears to have smaller amplitudes (darker Amp) and larger latency (brighter TTP) than its Y/Y equivalents throughout all three disease types. To confirm these relationships, box and whisker plots of Amp and TTP measures for Y/Y and G/R were produced (see Figure 6.7).

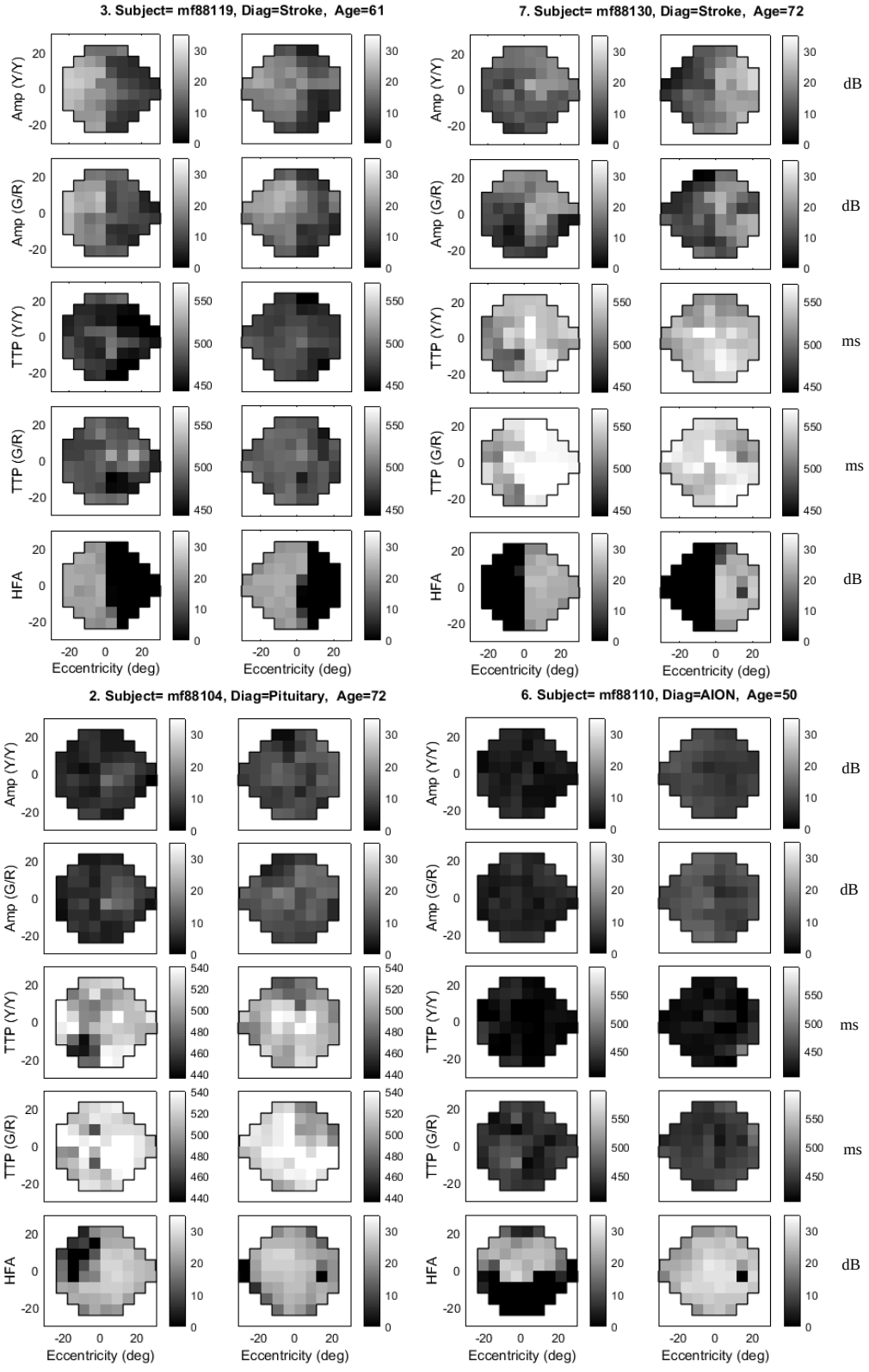

Figure 6.3: Each plot shows four variations of mfPOP (Amp for Y/Y and G/R; TPP for Y/Y and G/R) and Humphrey field analyser response. The scale of each plot is adjusted so the range covers the maximum and minimum for that group (stroke, pituitary, and AION), with both Amp plots and both TTP plots having shared scales for direct comparison. Selected subjects match those presented in Ch 5, with the first stroke subject with right hemianopia (top left: mf88119), first left hemianopia (top right: mf88130), first chiasmal compression subject with temporal field damage (bottom left: mf88104), and first AION subject with altitudinal damage (mf88110).

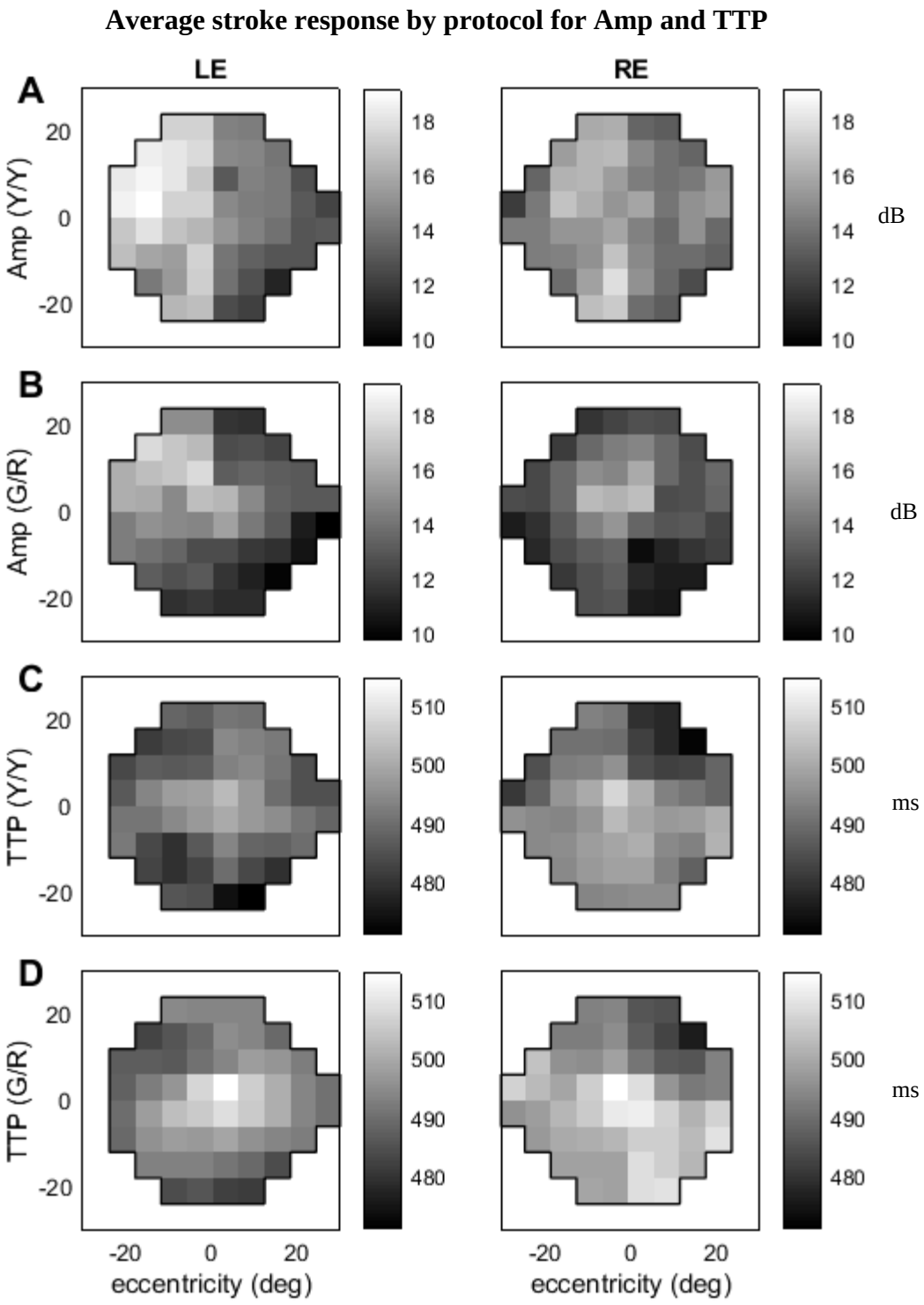

Figure 6.4: Plots showing mean values across all stroke subjects (*n* = 24) for each protocol [yellow/yellow (Y/Y) and green/red (G/R)] and each measure [amplitude (Amp) and time-to-peak (TTP)]. Scale is the maxima and minima from combined Amp data for Amp plots and from combined TTP data for TTP plots, so that the plots have shared scales for direct comparison.

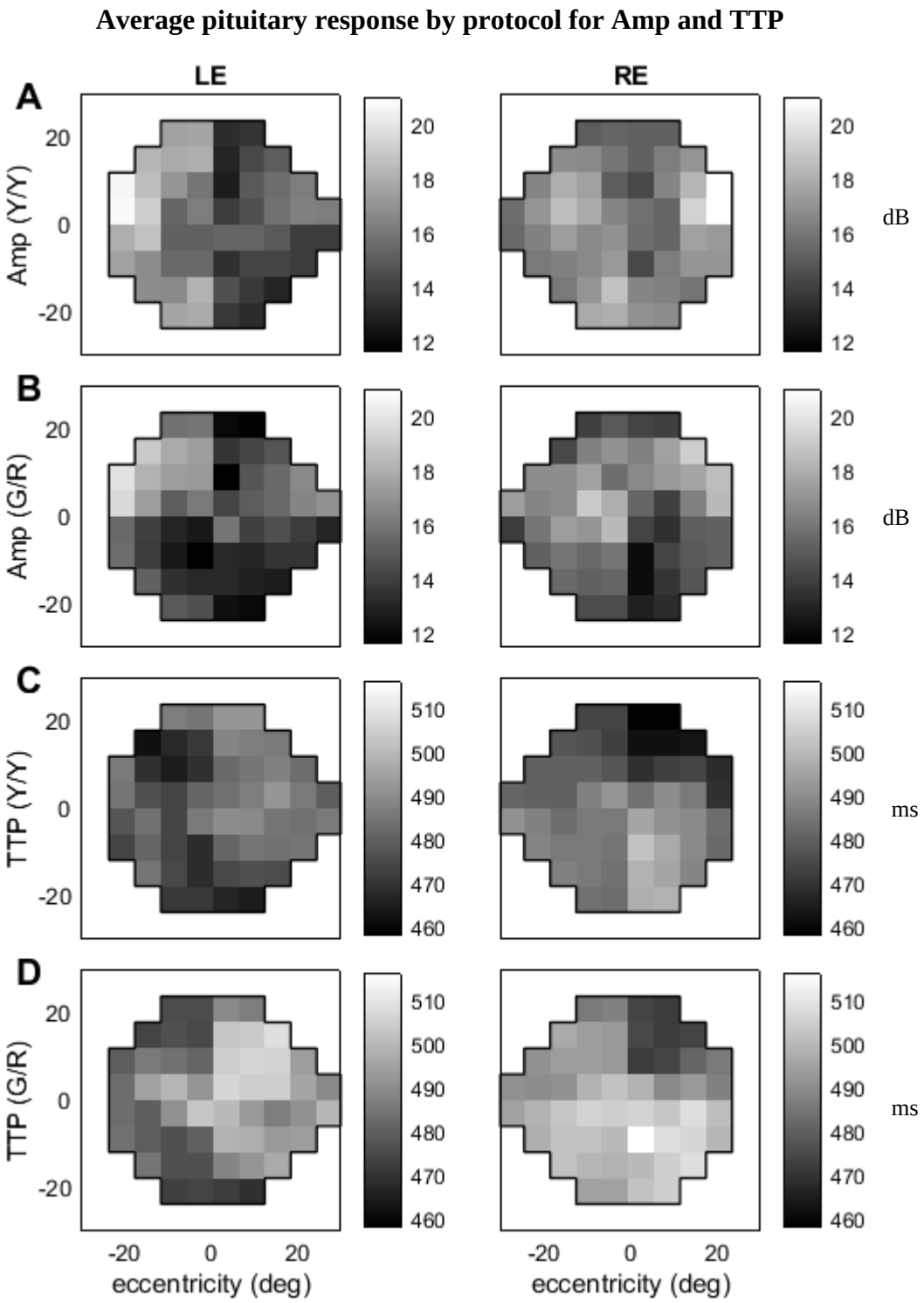

Figure 6.5: Mean values across all chiasmal compression subjects (*n* = 11) for each protocol [yellow/yellow (Y/Y) and green/red (G/R)] and each measure [amplitude (Amp) and time-to-peak (TTP)]. Scale is the maxima and minima from combined Amp data for Amp plots and from combined TTP data for TTP plots, so that these each have shared scales for direct comparison.

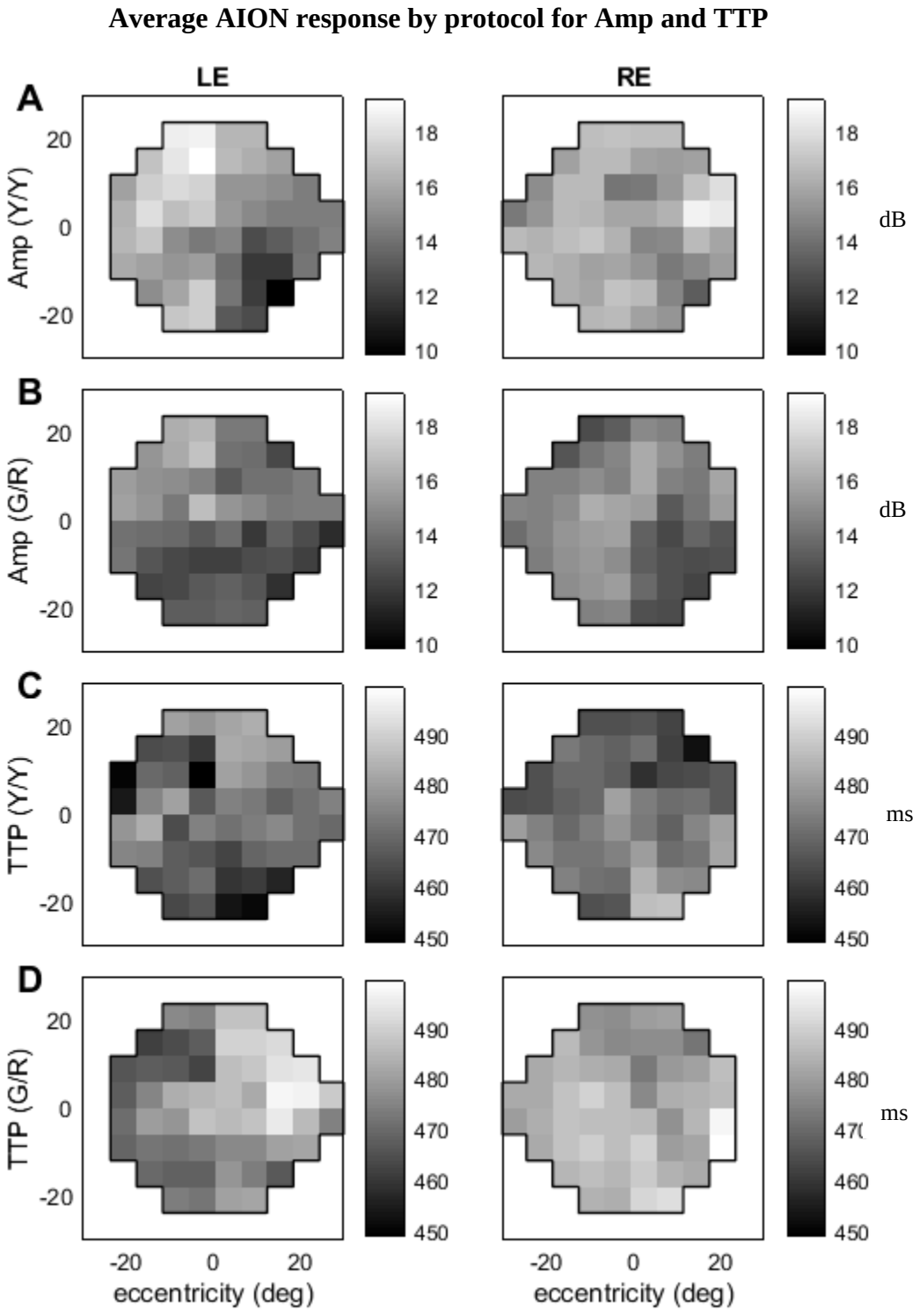

Figure 6.6: Mean values across all anterior ischemic optic neuropathy (AION) subjects (*n* = 10) for each protocol [yellow/yellow (Y/Y) and green/red (G/R)] and each measure [amplitude (Amp) and time-to-peak (TTP)[. Scale is the maxima and minima from combined Amp data for Amp plots and from combined TTP data for TTP plots, so that these each have shared scales for direct comparison.

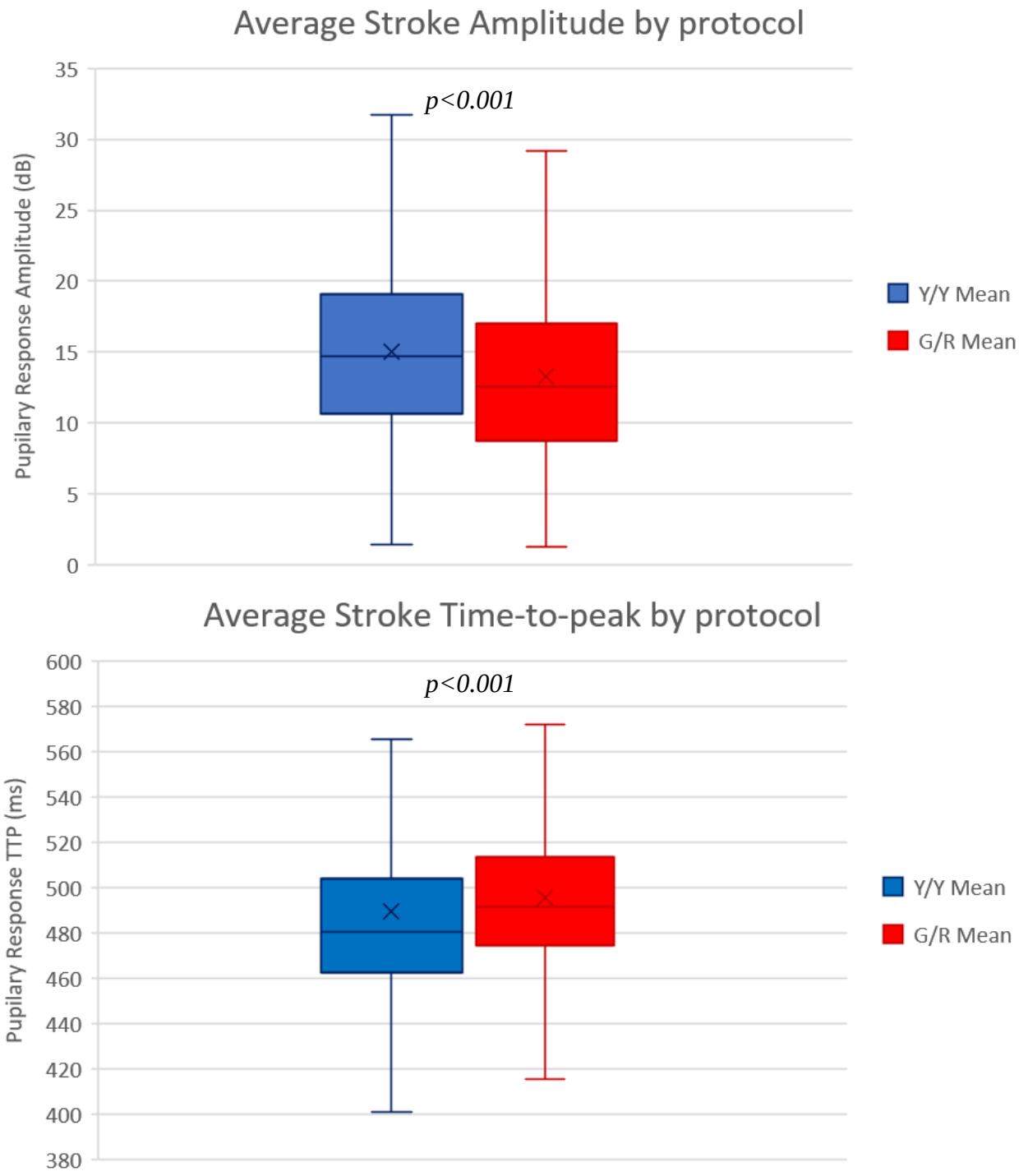

Figure 6.7: Box and whisker plots for (top left) Y/Y amplitude, (top right) G/R amplitude, (bottom left) Y/Y time to peak, and (bottom right) G/R time to peak. Means were taken over repeats. The box is centered on the median, with X representing the mean, and extends to upper and lower quartiles. Whiskers represent minimum and maximum values up to 1.5 times above and below the interquartile range. For amplitude, G/R has a median 2.2 dB below that of Y/Y, which is also reflected in the mean and quartiles. For time to peak, G/R has a median latency 11.2 ms greater than Y/Y, which is also reflected in the mean and quartiles. P-values for difference in means were calculated with highly significant difference *p<0.001* for both plots.

The results from the box and whisker plots match observations from visual inspection of individual and amalgamated field plots: the G/R protocol has marginally smaller responses (–2.2 dB median difference) and marginally greater latency (11.2 ms median difference) compared to their Y/Y counterparts. The greater latency is expected and consistent with controls tested previously, but the decreased amplitude is novel, since controls previously showed marginally greater amplitudes. This might be explained by G/R detecting some stroke damage in selected subjects, so that individual results suggest decreased Amp and shorter TTP, which is also reflected in the average results (a reduction in Amp and TTP compared to controls). Because controls showed only slightly larger Amp values in G/R compared to Y/Y, any damage is readily reflected as a smaller Amp. Controls for TTP had larger differences between G/R and Y/Y, so while these differences appear reduced in the stroke population, their G/R remains longer than Y/Y in terms of latency.

Results for chiasmal compression and AION show similar trends, with median differences for Amp of –1.3 dB for Y/Y and –1.7 dB for G/R, while the corresponding figures for TTP are 12.2 ms and 5.1 ms. As these groups would not be expected to have cortical damage, this suggests that perhaps the decreased latency is not due to lack of cortical input, but may relate to an intrinsically longer latency in the G/R protocol.

6.4.3. Direct and consensual components

When investigating direct and consensual amplitude responses in Chapter 3, it was found that direct and consensual varied throughout the field, and it was demonstrated that SNR-weighted means were an appropriate way of fairly amalgamating these components. Given that there is also a difference between the Y/Y and G/R protocols, it seems worthwhile to investigate whether any prominent differences in direct and consensual responses occur in the G/R protocol and in TTP measures. For the stroke group, graphs of fields for Y/Y and G/R, direct and consensual, are plotted for Amp in Figure 6.8 and for TTP in Figure 6.9.

When Y/Y Amp is broken into direct and consensual components, results are subtle, but again they show features previously highlighted in Chapter 3: that direct exceeds consensual temporally and consensual marginally exceeds direct nasally (further investigated as ratios next). Also note the larger response on the left side of both fields, which is a consequence of the order of stimulus presentation, showing larger responses to the first presentation within each eye due to gain control. These effects persist through all three disease types and across both protocols – although they are more apparent in the Y/Y protocol. It should be made clear this effect is independent and distinct to any differences noted between direct and consensual components, and this is further covered in the discussion.

Neither Y/Y or G/R show the same features using TTP for direct and consensual, nor do they have any obvious patterns, other than to say direct and consensual appear to align well. Plots from pituitary and AION did not show any additional information and so were omitted in favour of the direct consensual ratios which demonstrate these features more clearly.

Stroke average pupil response amplitude by protocol for direct and consensual

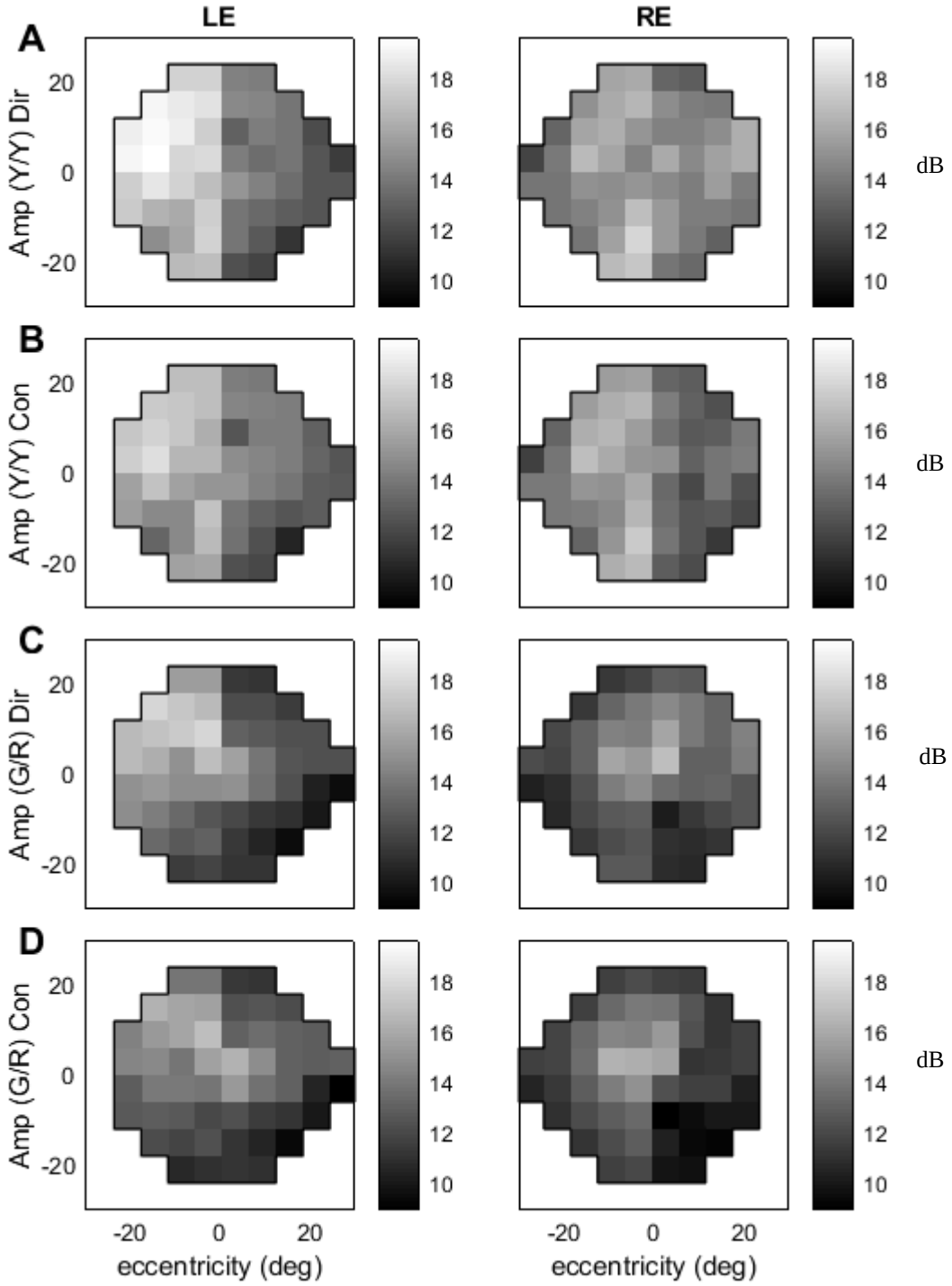

Figure 6.8: Mean Amp values across all stroke subjects (*n* = 24) for yellow stimuli on yellow background (Y/Y) direct and consensual components, and green stimuli on red background (G/R) direct and consensual components. Scale was taken as the maxima and minima from combined Amp data of all displayed plots so that these each have shared scales for direct comparison.

Stroke average pupil response TTP by protocol for direct and consensual

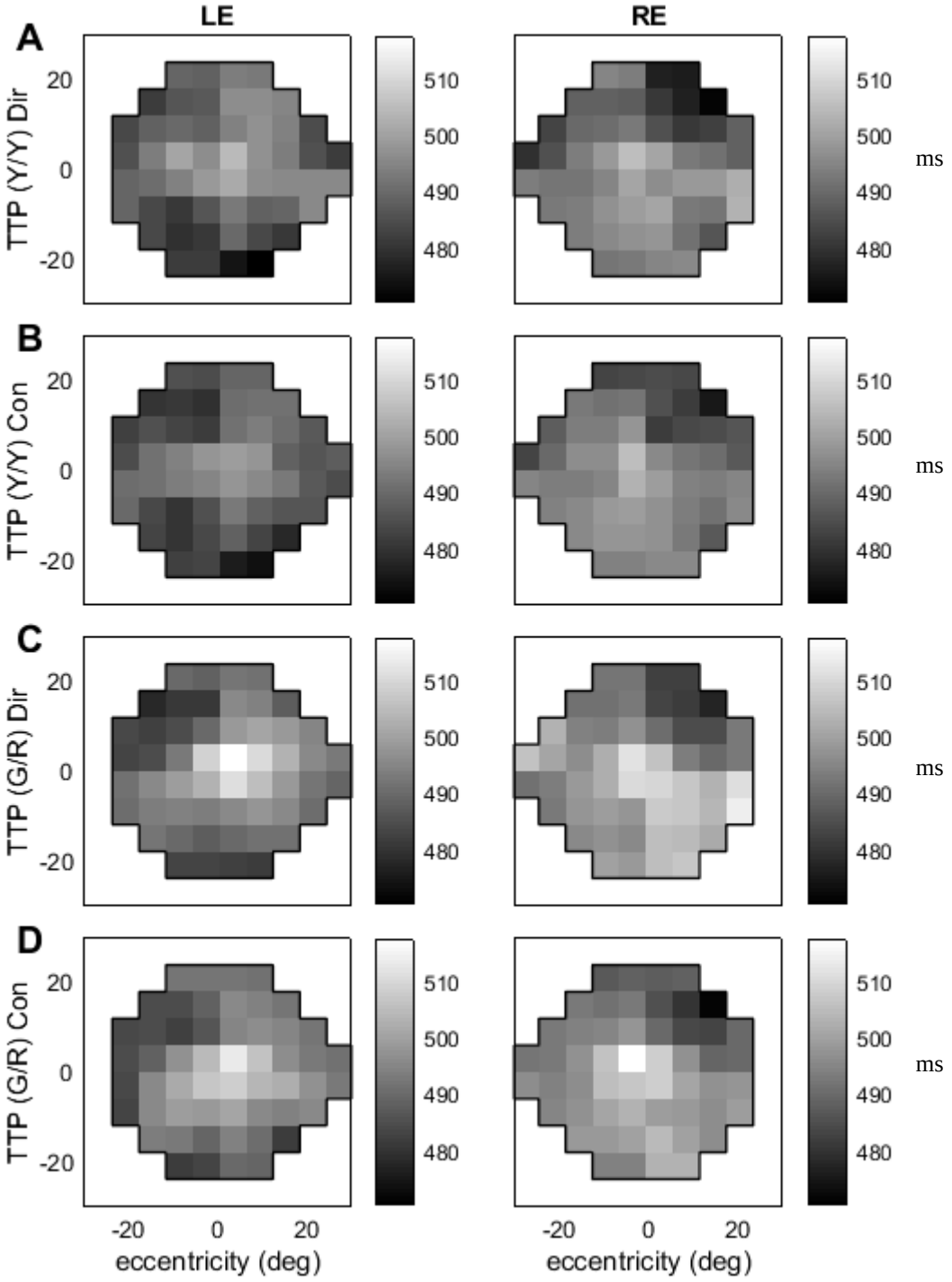

Figure 6.9: Mean TTP values across all stroke subjects (*n* = 24) for yellow stimuli on yellow background (Y/Y) direct and consensual components and green stimuli on red background (G/R) direct and consensual components. Scale was taken as the maxima and minima from combined TTP data of all displayed plots so that these each have shared scales for direct comparison.

With features again showing a difference between direct and consensual according to hemifield, it is worth viewing the direct / consensual ratios, which previously highlighted the hemifield differences in the Y/Y Amp protocol. Fields with plotted ratios for Y/Y and G/R using both measures of AMP and TTP, with shared scale across all four variants were produced for each disease type in Figures 6.10–6.12.

As shown previously for the Y/Y Amp results, in the all groups direct exceeds consensual in temporal regions, while in nasal regions, for the stroke group consensual and direct are roughly equal; however, in the pituitary and AION groups consensual exceeds direct.

For the G/R Amp results we see that very similar features are highlighted, with slightly enhanced contraction anisocoria reflecting the marginally larger differences between direct and consensual in both temporal and nasal regions. In the stroke group, the nasal region now matches the other disease groups with consensual exceeding direct nasally.

Looking at the TTP values across all groups, the ratios are proportionately much smaller than those in Amp, showing only very subtle differences of 2–3% above or below equivalence, while Amp shows differences as great as 20%. To better examine whether any trends exist within the TTP data, the contrast was enhanced by producing separate scales for these results, which are reiterated in Figures 6.14–6.15. The subtle differences in TTP results do not align with Amp at all, and appear to poorly correlate between protocols. Stroke TTP results seem close to random noise, although the Y/Y appears to show that for the left eye many results have direct > consensual, while the fellow right eye shows consensual > direct; the issue is unclear in G/R. Conversely, in chiasmal compression both protocols show consensual > direct for the left eye, while the right eye shows direct > consensual. For AION, only the G/R protocol shows this effect, while it is unclear in the Y/Y. It would appear there are some underlying effects causing differences between eyes, but these appear inconsistent between the groups.

Stroke ratio of direct and consensual response across protocols – fixed scale

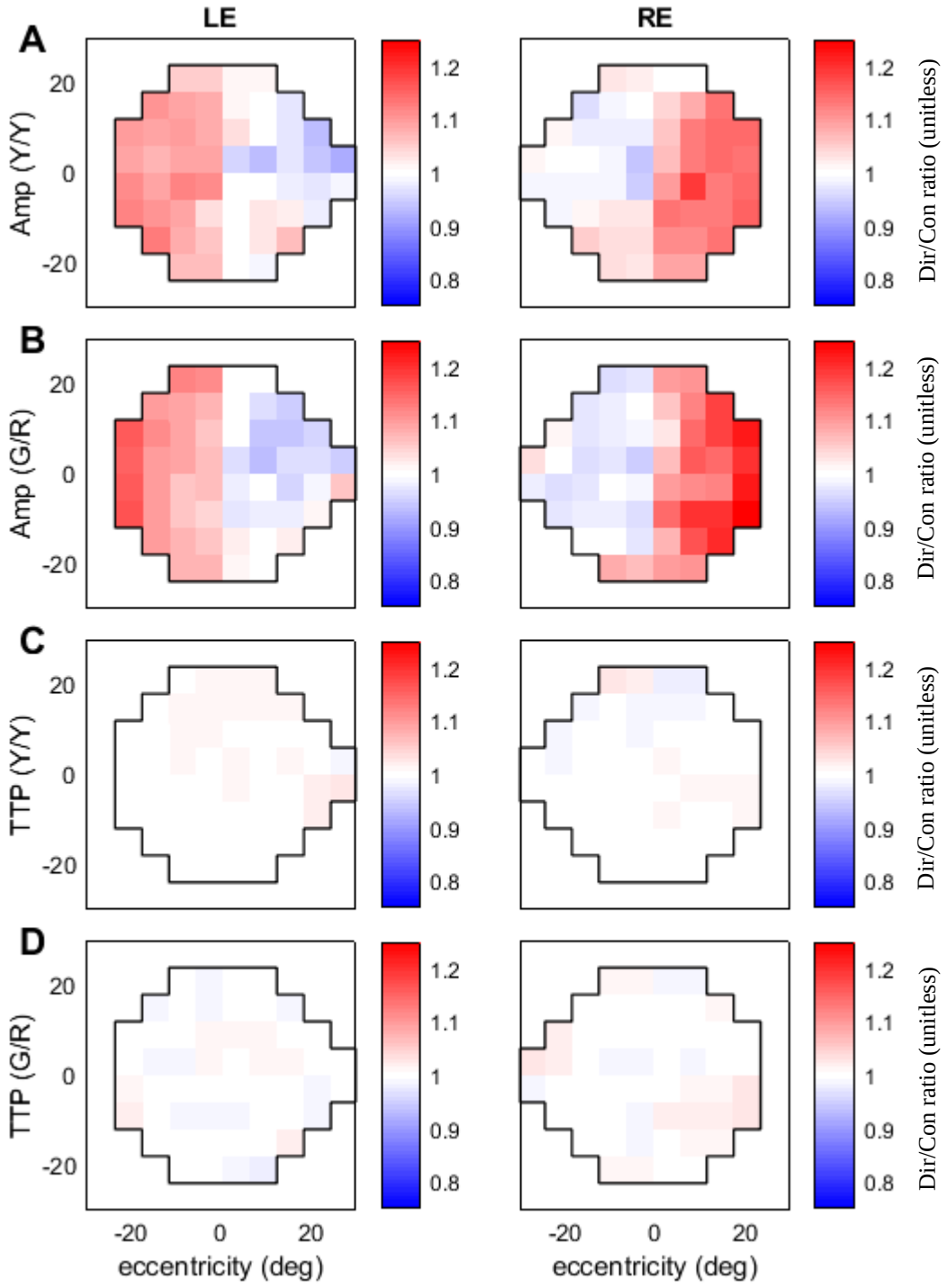

Figure 6.10: Stroke subjects (n = 24) mean direct / consensual ratios for protocols yellow stimuli on yellow background (Y/Y) and green stimuli on red background (G/R), using amplitude (Amp), and time-to-peak (TTP) measures of pupillary response. A common scale was used across all plots according to the minima and maxima ratio values to allow direct comparison. Direct exceeding consensual is shown in red and consensual exceeding direct in blue.

Pituitary ratio of direct and consensual response across protocols – fixed scale

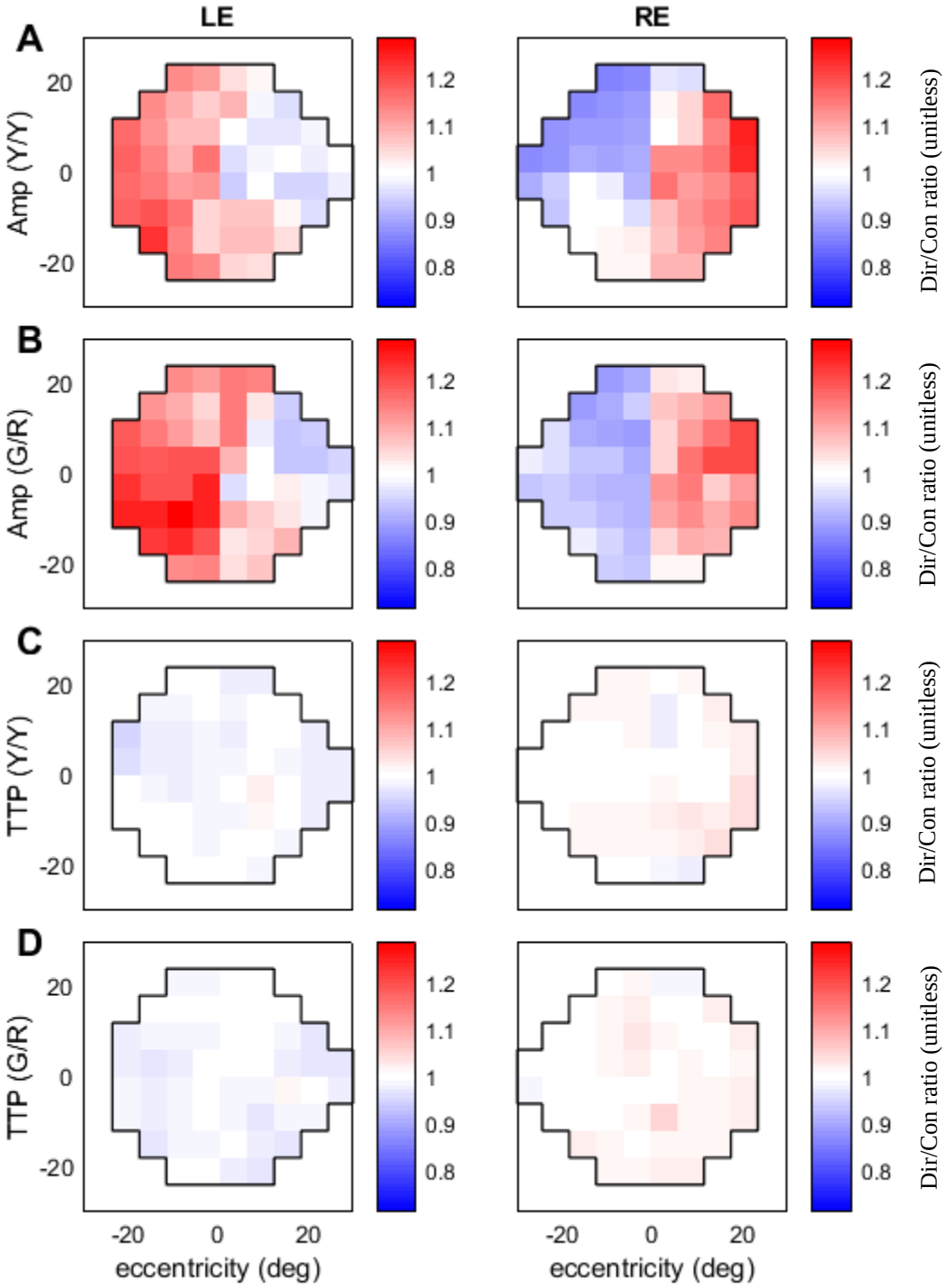

Figure 6.11: Pituitary subjects (*n* = 11) mean direct / consensual ratios for protocols yellow stimuli on yellow background (Y/Y) and green stimuli on red background (G/R), using amplitude (Amp) and time-to-peak (TTP) measures of pupillary response. A common scale was used across all plots according to the minima and maxima ratio values to allow direct comparison. Direct exceeding consensual is shown in red and consensual exceeding direct in blue.

AION ratio of direct and consensual response across protocols – fixed scale

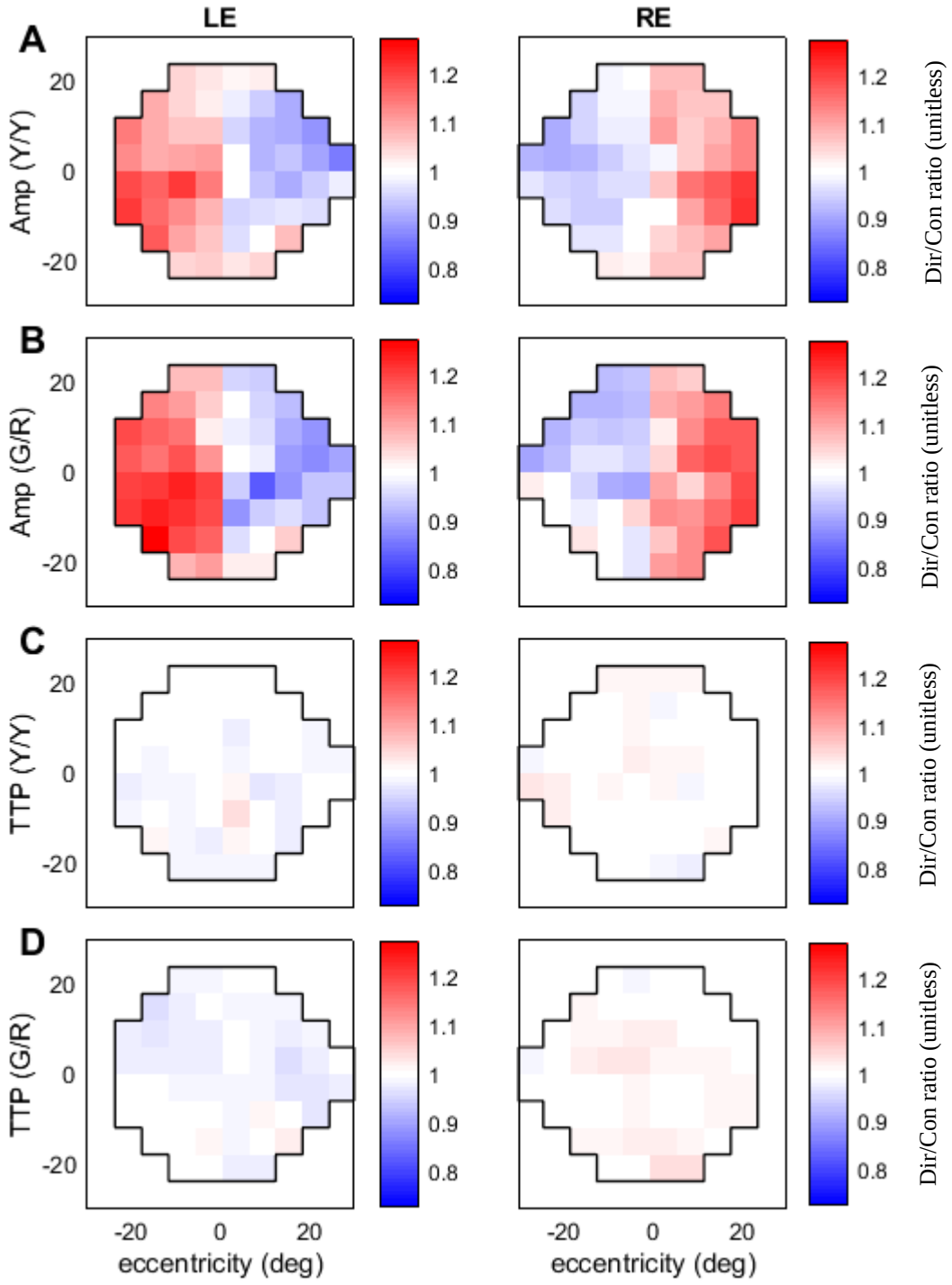

Figure 6.12: AION subjects (*n* = 10) mean direct / consensual ratios for protocols yellow stimuli on yellow background (Y/Y) and green stimuli on red background (G/R), using amplitude (Amp) and time-to-peak (TTP) measures of pupillary response. A common scale was used across all plots according to the minima and maxima ratio values to allow direct comparison. Direct exceeding consensual is shown in red and consensual exceeding direct in blue.

Stroke ratio of direct and consensual time-to-peak – variable scale

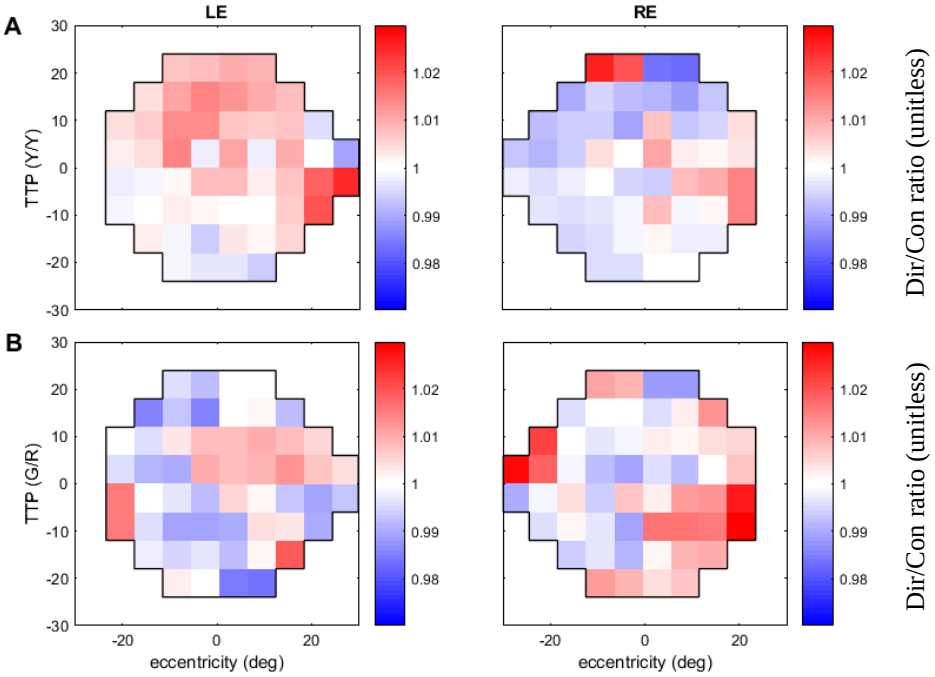

Figure 6.14: Stroke subjects (*n* = 24) mean direct / consensual TTP ratios for protocols yellow stimuli on yellow background (Y/Y) and green stimuli on red background (G/R). Scale is adjusted to the minima and maxima TTP averages in order to increase constrast.

Pituitary ratio of direct and consensual time-to-peak – variable scale

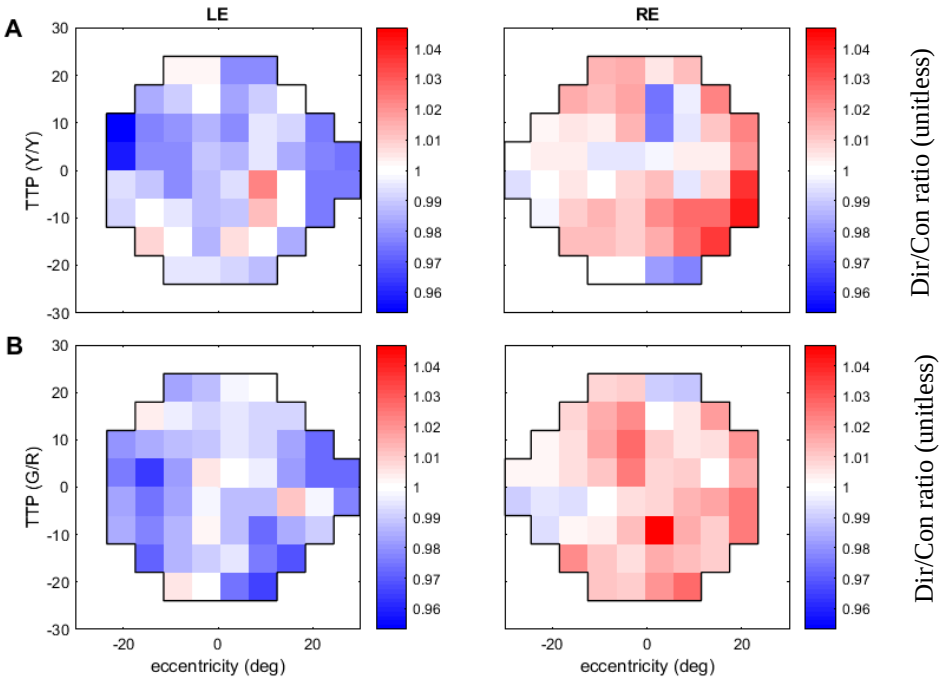

Figure 6.13: Pituitary subjects (*n* = 11) mean direct / consensual TTP ratios for protocols yellow stimuli on yellow background (Y/Y) and green stimuli on red background (G/R). Scale is adjusted to the minima and maxima TTP averages in order to increase constrast.

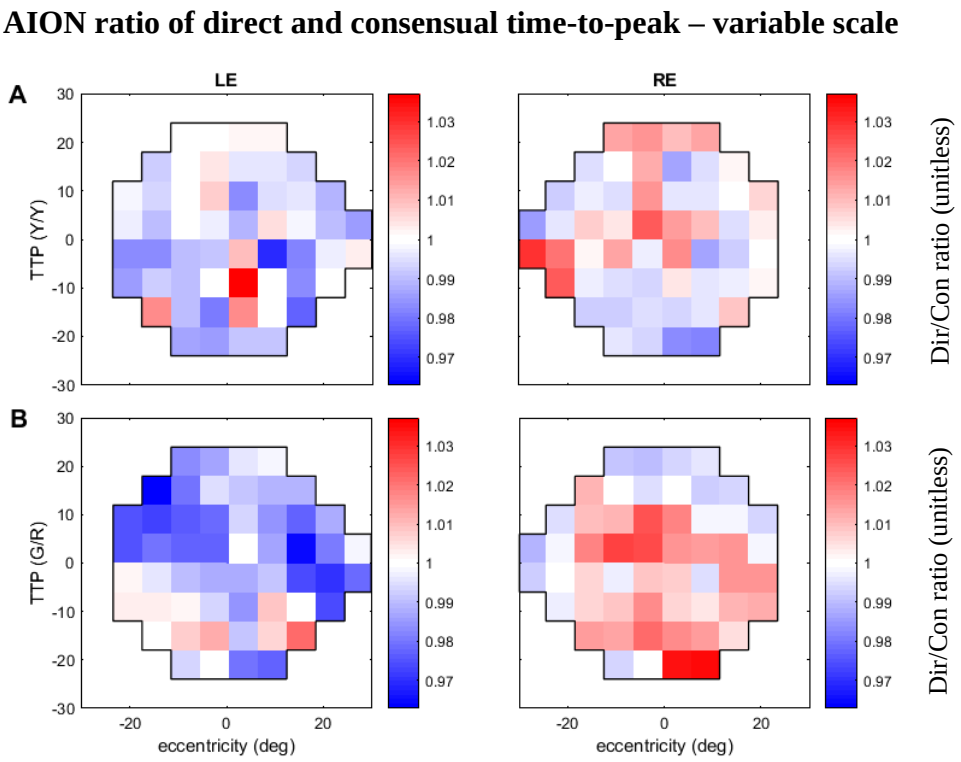

Figure 6.15: AION subjects (*n* = 10) mean direct / consensual TTP ratios for protocols yellow stimuli on yellow background (Y/Y) and green stimuli on red background (G/R). Scale is adjusted to the minima and maxima TTP averages in order to increase constrast.

6.4.4. Bias in latency: apparent polarisation according to eye

To further investigate why there may be subtle differences between the TTP averages of left eye and right eye for direct and consensual ratios, plots for each subject were individually generated and inspected. These showed even greater polarity than the average plots, with many plots having direct exceeding consensual (red) or consensual exceeding direct (blue) throughout most of an eye, and often being reciprocal – so that if one eye had a bias towards larger direct responses (red), the other was biased towards larger consensual (blue), although sidedness and extent appeared to vary.

A quantitative assessment was done using a binomial distribution as outlined in the methods, which set the threshold for a field be polarised as ≥ 36/54 at a probability of <0.01. Using this

threshold, tables were produced for showing the number of polarised fields for each of the three conditions and these are presented below as Tables 6.2–6.4**.**

Results show that fields are polarised in 60–63% of eyes, and they were not overtly affected by protocol (Y/Y or G/R), type of polarisation (dir > con [red] or con > dir [blue]), or the affected eye.

Comparing stroke bias for direct and consensual TTP in Table 6.2 for individuals to the average bias in Figure 6.10, provides a suggestion as to why the averages were less clear: because polarisation might occur in either direction in a given subject, these frequently cancel out, leaving the amalgamated results less polarised than the individual subject results. Investigating repeats, it was found that the vast majority of those which showed polarisation in first testing also showed the same polarisation in repeat testing, suggesting it is unlikely to be noise. These results were compared to apparent field damage from the HFA and seemed to be independent of damage and disease type. It is unknown why this polarisation occurs, but it could relate to asymmetrical sympathetic input to the EWN.

Stroke				
Protocol	**Eye**	**Polarisation**	**Ratio**	**Percentage**
By protocol, eye and polarisation				
Y/Y	Left	Dir > Con	11 / 23	48%
	Left	Con > Dir	5 / 23	22%
	Right	Dir > Con	6 / 23	26%
	Right	Con > Dir	8 / 23	35%
G/R	Left	Dir > Con	4 / 23	17%
	Left	Con > Dir	9 / 23	39%
	Right	Dir > Con	7 / 23	30%
	Right	Con > Dir	5 / 23	22%
Any protocol by eye and polarisation				
Any	Left	Dir > Con	15 / 23	65%
	Left	Con > Dir	14 / 23	61%
	Right	Dir > Con	13 / 23	57%
	Right	Con > Dir	13 / 23	57%
Any polarisation by protocol and eye				
Y/Y	Left	Any	16 / 23	70%
	Right		14 / 23	61%
G/R	Left		13 / 23	57%
	Right		12 / 23	52%
Any protcol, any polarisation by eye				
Any	Left	Any	29 / 46	63%
	Right		26 / 46	57%
Any protocol, any eye, any polarisation				
Any	Any	Any	55 / 92	60%

Table 6.2: Summary polarisation data for stroke time-to-peak (TTP) direct / consensual ratio, highlighting the number of eyes which have ≥36 regions (≥66%) where dir > con (in red) or where con > dir (in blue). Results are broken down by protocol (Y/Y or G/R), eye (left or right), and type of polarisation (red or blue). They are then presented by summing protocols to investigate whether there is a bias towards one polarisation or the other, and then by summing by polarisation to see if there is a bias towards one protocol or the other. The total sum of left eye and right eye are used to assess bias between the eyes, and finally the sum total is presented. Results in the final column are coloured according to size, with darker red representing larger values within each category.

Pituitary				
Protocol	**Eye**	**Polarisation**	**Ratio**	**Percentage**
By protocol, eye and polarisation				
Y/Y	Left	Dir > Con	1 / 8	13%
	Left	Con > Dir	4 / 8	50%
	Right	Dir > Con	3 / 8	38%
	Right	Con > Dir	1 / 8	13%
G/R	Left	Dir > Con	2 / 8	25%
	Left	Con > Dir	4 / 8	50%
	Right	Dir > Con	3 / 8	38%
	Right	Con > Dir	2 / 8	25%
Any protocol by eye and polarisation				
Any	Left	Dir > Con	3 / 8	38%
	Left	Con > Dir	8 / 8	100%
	Right	Dir > Con	6 / 8	75%
	Right	Con > Dir	3 / 8	38%
Any polarisation by protocol and eye				
Y/Y	Left	Any	5 / 8	63%
	Right		4 / 8	50%
G/R	Left		6 / 8	75%
	Right		5 / 8	63%
Any protcol, any polarisation by eye				
Any	Left	Any	11 / 16	69%
	Right		9 / 16	56%
Any protocol, any eye, any polarisation				
Any	Any	Any	20 / 32	63%

Table 6.3: Summary of polarisation data for chiasmal compression time-to-peak (TTP) direct / consensual ratio, highlighting the number of eyes which have ≥36 regions (≥66%) where dir > con (in red) or where con > dir (in blue). Results are broken down by protocol (Y/Y or G/R), eye (left or right), and type of polarisation (red or blue). They are then presented by summing protocols to investigate whether there is a bias towards one polarisation or the other, then by summing by polarisation to see if there is a bias towards one protocol or the other. The total sum of left eye and right eye are used to assess bias between eyes, and finally the sum total is presented. Results in final column are coloured according to size, with darker red representing larger values within each category.

AION				
Protocol	**Eye**	**Polarisation**	**Ratio**	**Percentage**
By protocol, eye and polarisation				
Y/Y	Left	Dir > Con	3 / 10	30%
	Left	Con > Dir	5 / 10	50%
	Right	Dir > Con	3 / 10	30%
	Right	Con > Dir	3 / 10	30%
G/R	Left	Dir > Con	2 / 10	20%
	Left	Con > Dir	4 / 10	40%
	Right	Dir > Con	3 / 10	30%
	Right	Con > Dir	2 / 10	20%
Any protocol by eye and polarisation				
Any	Left	Dir > Con	5 / 10	50%
	Left	Con > Dir	9 / 10	90%
	Right	Dir > Con	6 / 10	60%
	Right	Con > Dir	5 / 10	50%
Any polarisation by protocol and eye				
Y/Y	Left	Any	8 / 10	80%
	Right		6 / 10	60%
G/R	Left		6 / 10	60%
	Right		5 / 10	50%
Any protcol, any polarisation by eye				
Any	Left	Any	14 / 20	70%
	Right		11 / 20	55%
Any protocol, any eye, any polarisation				
Any	Any	Any	25 / 40	63%

Table 6.4: Summary polarisation data for AION time-to-peak (TTP) direct / consensual ratio, highlighting the number of eyes which have ≥36 regions (≥66%) where dir > con (in red) or where con > dir (in blue). Results are broken down by protocol (Y/Y or G/R), eye (left or right), and type of polarisation (red or blue). They are then presented by summing protocols to indicate whether there is a bias towards one polarisation or the other, then by summing by polarisation to see if there is a bias towards one protocol or the other. The total sum of left eye and right eye are used to assess bias between eyes, and finally the sum total is presented. Results in final column are coloured according to size, with darker red representing larger values within each category.

6.4.5. Correlation between protocols (Y/Y and G/R)

Now that the key differences in direct and consensual responses between protocols have been highlighted, it is interesting to look for correlation between protocols. Recall that both protocols (Y/Y and G/R) using Amp appeared to broadly align, although G/R had smaller mean amplitudes, and that using TTP they also appeared to align, although G/R had larger mean latencies. These relationships will now be formally reviewed in scatter plots (Figures 6.16–6.19). In comparing stroke protocols Y/Y (ordinate) and G/R (abscissa) using Amp, a Pearson correlation coefficient of r = 0.762 demonstrates a strong relationship, with a linear fit appearing suitable and with the trendline mostly below unity for the majority of points. This is consistent with G/R having smaller responses than Y/Y. The stroke Y/Y (ordinate) and G/R (abscissa) for TTP has a moderate correlation (r = 0.530), which appears to be mostly linear but is skewed by several more extreme points in the range 550–800 ms on the Y/Y protocol corresponding to much smaller G/R points in the 300–500 ms range. This was investigated and found to be largely due to a single subject with discordant results – if the graph is replotted with that subject removed, the Pearson correlation improves dramatically to r = 0.647 and a more linear correlation appears, consistent with results from chiasmal compression (r = 0.699) and AION (r = 0.849) shown in Figure 6.17. For all conditions, the trendline has a gradient less than unity, but this trendline crosses unity *after* the bulk of the data points. This is therefore consistent with the bulk of points having greater latencies in G/R, particularly at smaller values, while at the larger end of values the G/R has marginally smaller latencies.

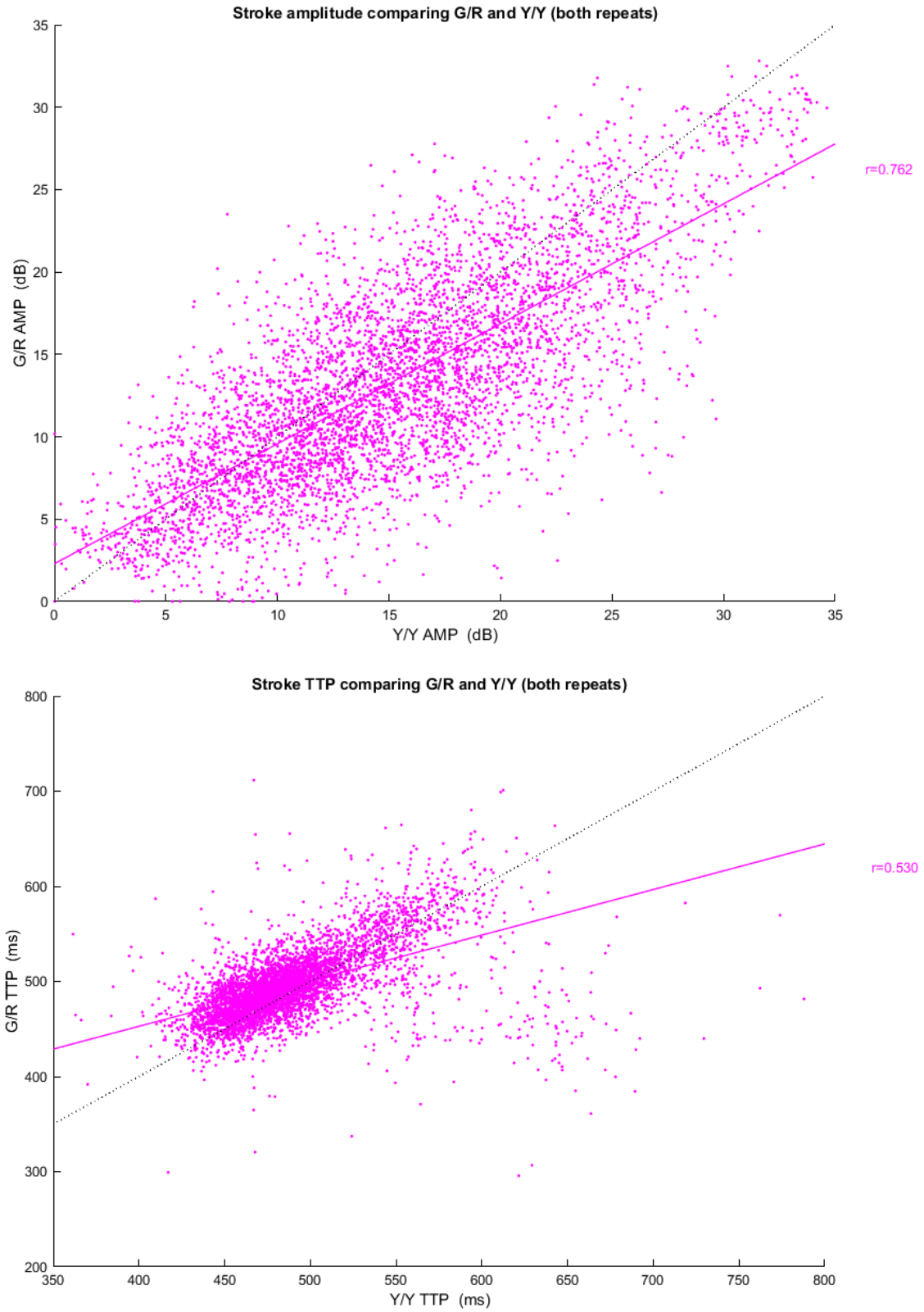

Figure 6.16: Scatter plots for the stroke cohort comparing protocols Y/Y against G/R for amplitude (Amp, top), and time-to-peak (TTP, bottom). Line of unity is represented by the black dotted line, and the least squares correlation line is plotted with Pearson correlation coefficient (*r*) included.

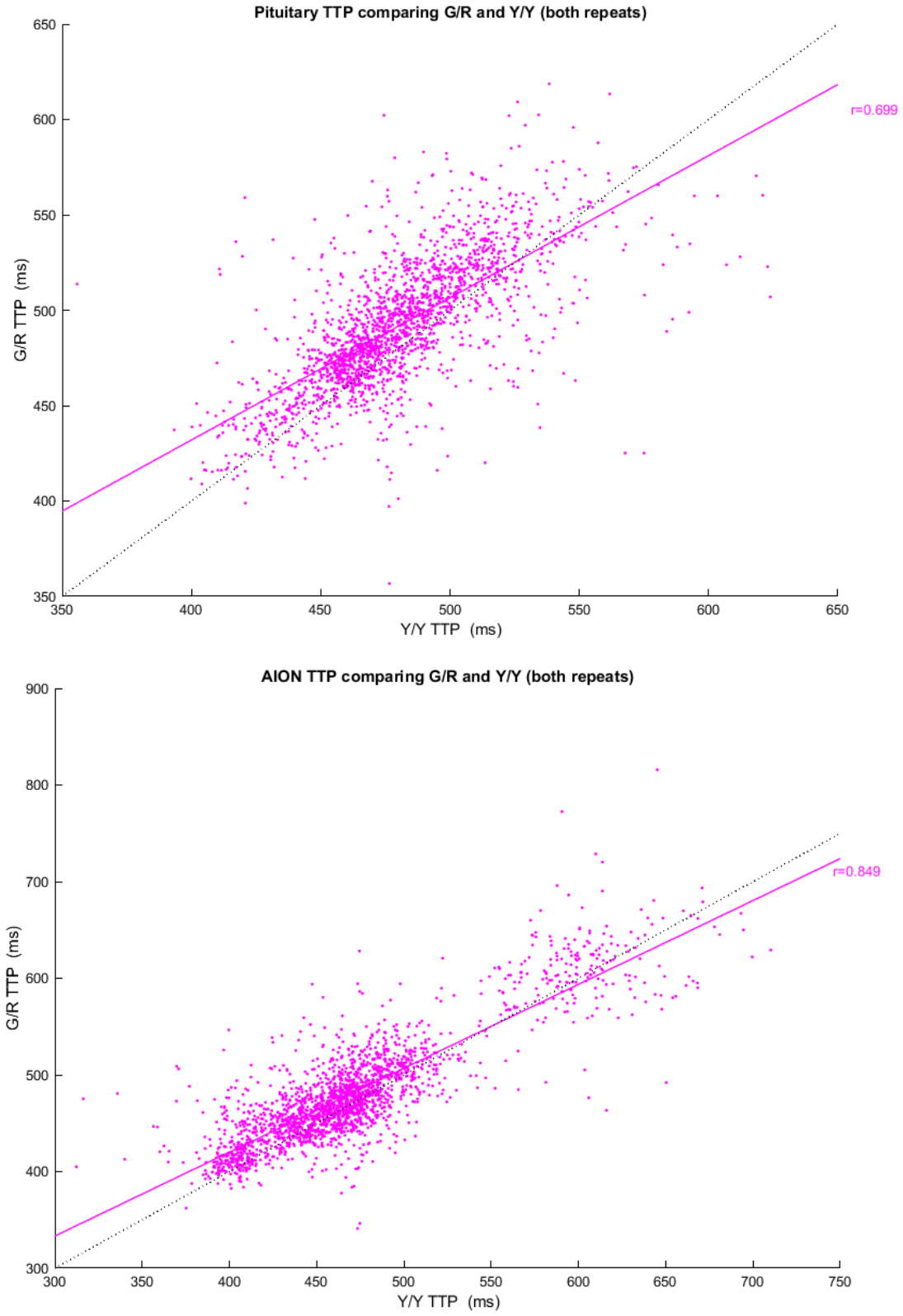

Figure 6.17: Scatter plots for the pituitary (top) and AION (bottom) cohorts comparing protocols Y/Y against G/R using time-to-peak (TTP). Line of unity is represented by black dotted line, and least squares correlation line is plotted with Pearson correlation coefficient (*r*) included.

6.4.6. Correlation between measures (Amp and TTP)

The other feature that was noted on visual inspection was that some areas showing smaller Amp responses appeared to show some decreased latency (albeit small) in selected stroke subjects, while there was small increase in latency for selected pituitary subjects – although noise might have been the explanation. Therefore, it is interesting to investigate whether these relationships are formally true within the larger cohort. Figure 6.18 presents a scatter plot for stroke subjects comparing Amp (ordinate) and TTP (abscissa) for Y/Y and for G/R protocols. A quadratic fit appeared to show a very poor relationship, with correlation coefficients r^2 = 0.050 for Y/Y and r^2 = 0.055 for G/R, suggesting TTP is independent of Amp. Since this was not consistent with individual results, this was further explored by producing scatter plots for each subject individually (see Table 6.5) which tells a very different story. Individually, 21 of 24 subjects show positive linear correlation, mostly in the r = 0.2–0.4 range, with only 2 showing a negative correlation. What becomes apparent on inspection is that there is substantial variation between people, and that this can cause spurious associations when plotted in aggregate. The G/R protocol was analysed in the same way (see Table 6.6) with overall poorer correlations (but still overwhelmingly positive), with 19 of 24 subjects having a positive correlation mostly in the range r = 0.1–0.3. Results for chiasmal compression and AION were also completed but for brevity not included – these showed similar trends to the stroke group, with the majority of correlations positive and the Y/Y protocol showing, overall, higher Pearson correlation values than G/R. This new evidence suggests that there is a positive linear association between Amp and TTP for most subjects, although the extent of this relationship varies between subjects.

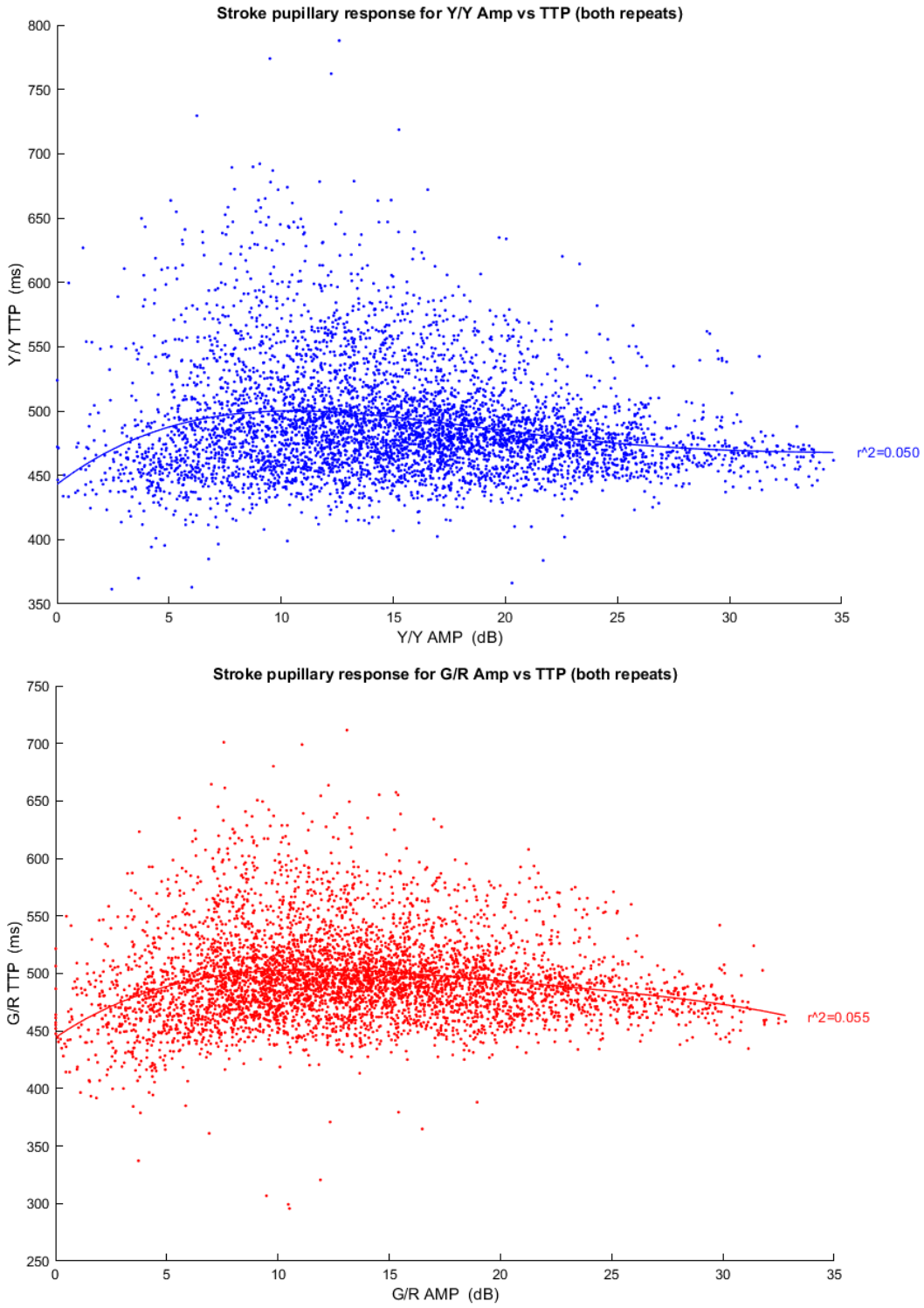

Figure 6.18: Scatter plots for the stroke cohort of Y/Y protocol (top, blue) and G/R protocol (bottom, red) comparing amplitude (Amp) against time-to-peak (TTP). Linear fits were first considered but did not fit the data well at the extremes. Quadratic polynomial fits were applied after inspection of polynomial fits of orders 1–7 after demonstrating that lesser orders provided poorer fit and higher orders did not add value to the fit. Coefficient of determination (r^2) values were calculated for fits, which were r = 0.050 for Y/Y and r = 0.055 for G/R, showing relatively poor fits due to substantial noise.

Stroke - Pearson correlation (r) for Amp vs TTP (Y/Y)			
Subject #	Pearson (r)	Subject #	Pearson (r)
1	0.191	13	-0.32
2	0.215	14	0.041
3	0.441	15	0.285
4	0.065	16	0.665
5	0.34	17	0.272
6	0.324	18	0.21
7	0.304	19	0
8	0.171	20	0.3
9	0.062	21	0.198
10	0.501	22	-0.147
11	0.451	23	0.32
12	0.378	24	0.585

Table 6.5: Pearson correlation coefficients for individual patient plots (n = 24) of yellow stimuli on a yellow background (Y/Y) amplitude (Amp) against time-to-peak (TTP). Values are then coloured by their size where –1 is full red, 0 is white, and 1 is full green. There were 21/24 subjects who showed a positive correlation.

Stroke - Pearson correlation (r) for Amp vs TTP (G/R)			
Subject #	Pearson (r)	Subject #	Pearson (r)
1	0.045	13	-0.048
2	0.174	14	0.286
3	0.062	15	0.211
4	-0.057	16	0.626
5	0.236	17	0.243
6	0.266	18	-0.021
7	0.232	19	0.626
8	-0.113	20	0.018
9	0.110	21	0.158
10	0.200	22	-0.198
11	0.141	23	0.388
12	0.327	24	0.392

Table 6.6: Pearson correlation coefficients for individual patient plots (n = 24) of red stimuli on a green background (G/R) comparing amplitude (Amp) against time-to-peak (TTP). Values are coloured by their size, where –1 is full red, 0 is white, and 1 is full green. There were 19/24 patients who showed a positive correlation.

6.4.7. Correlation between repeats (Rep 1 and Rep 2)

The final comparison which needs to be explored is between repeats, giving a measure of internal consistency. Both Y/Y repeats for Amp and G/R repeats for Amp show strong correlation, with high Pearson coefficients $r = 0.821$ and $r = 0.794$ respectively (Figure 6.19). Both have gradients below unity, but with the intersection occurring roughly in the middle of the data so that between repeats there is a similar number of points above and below unity. For the Y/Y repeats for TTP, a tight linear correlation close to unity was found, with strong correlation $r = 0.800$ (Figure 6.20). G/R repeats using TTP did not fare so well, being plagued by outlier points in repeat 1 which had substantially higher latencies than the second repeat (even when subjects with the most extreme results were removed) and showed only moderate correlation $r = 0.491$. Overall, repeats did show correlation, but with quite a lot of noise, so that if a single test is to be reliable, this aspect will need further reduction, particularly in the G/R protocol.

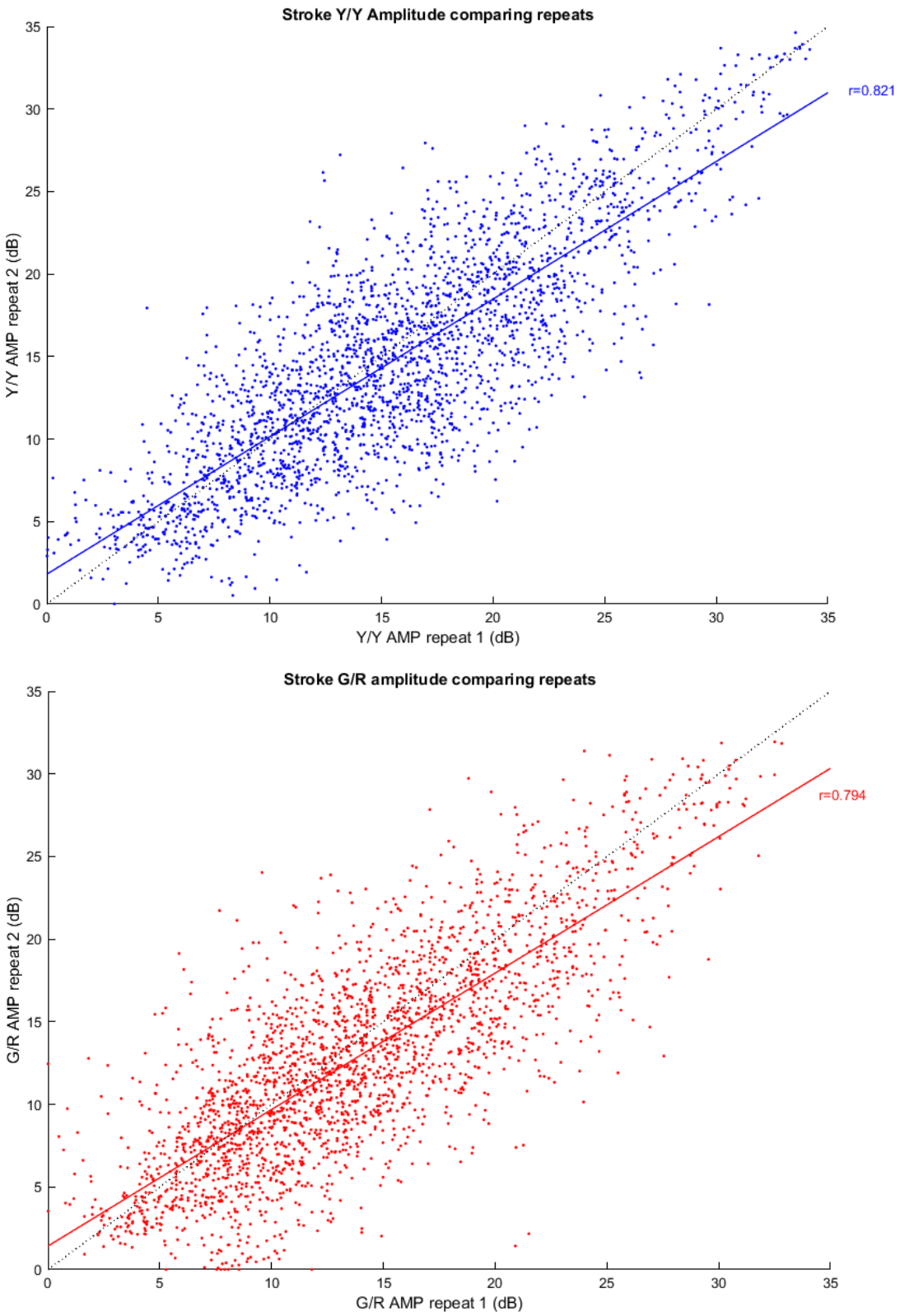

Figure 6.19: Scatter plots for the stroke cohort using amplitude (Amp) and comparing Y/Y repeats (top, blue) and G/R repeats (bottom, red). The line of unity is represented by the black dotted line and the least squares correlation is plotted together with the Pearson correlation coefficient (*r*).

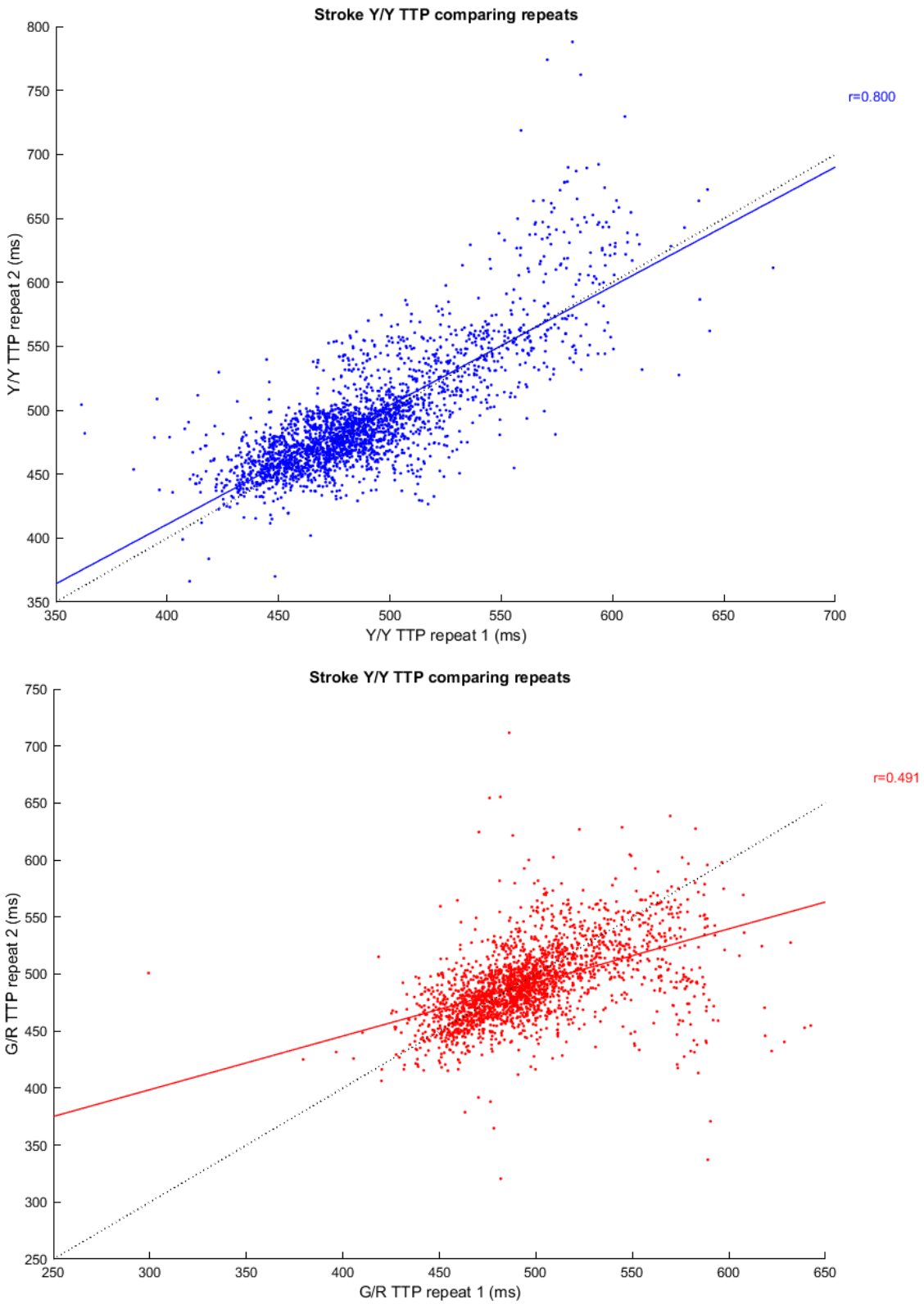

Figure 6.20: Scatter plots for the stroke cohort using time-to-peak (TTP) and comparing Y/Y repeats (top, blue) and G/R repeats (bottom, red). The line of unity is represented by the black dotted line and the least squares correlation is plotted along with the Pearson correlation coefficient (*r*).

6.5. Discussion

Initial inspection of individual subjects (examples in Figure 6.3) and their amalgamated results (Figures 6.4–6.6**)** showed that the G/R protocol produced smaller amplitudes and greater latencies compared with Y/Y. This was confirmed in box and whisker plots of stroke patients (Figure 6.7), revealing differences in median amplitude of 2.2 dB and in median TTP of 11.2 ms, with similar trends in pituitary and AION plots. Comparing these findings with the literature, results here used a background luminance of 10 cd/m^2 and stimuli of 150 cd/m^2 for both Y/Y and G/R protocols, while the nearest comparison used stimuli of 290 cd/m^2 on either a background of 115 cd/m^2 (Y-hi/Y-mid) or 10 cd/m^2 (Y-hi/Y-lo) (Carle *et al.*, 2013). Y-hi/Y-mid uses different luminance values for both stimuli and background, but with a similar absolute difference between stimuli and background (Δ = +175 cd/m^2) compared to ours (Δ = +140 cd/m^2), while Y-hi/Y-lo uses the same background but with a stronger stimulus (Δ = +280 cd/m^2). In this instance it is not the absolute luminance difference which matters, but rather the contrast of the stimulus with the background which induces pupillary constriction. Luminance contrast can be calculated using the Michaelson formula: $C = (L_{max} - L_{min}) / (L_{max} + L_{min})$ often used for gratings or where there are an even number of high and low contrast areas, or the Weber formula $C = (L_{max} - L_{min}) / L_{background}$ used for bright stimuli on an extensive background (MacIntyre & Cowan, 1992; Pelli & Bex, 2013). As stimuli are active in up to 50% of possible regions at a given time either contrast formula might be appropriate, although Weber may be preferable in this instance as there are frequently less than 50% active. Comparing protocols (Table 6.7) reveals that Y-hi/Y-lo is the closest match for comparison.

	Protocols		
	Data	Y-hi/Y-mid	Y-hi/Y-lo
Stimuli	150	290	290
Background	10	115	10
Michaelson	**0.88**	0.43	**0.93**
Weber	**14**	1.52	**28**

Table 6.7: Differences between stimuli and background for the Y/Y experimental protocol (stimuli 150 cd/m^2 on a background 10 cd/m^2) and two other experimental approaches: Y-hi/Y-mid (stimuli 290 cd/m^2 on 115 cd/m^2 background) and Y-hi/Y-lo (stimuli 290 cd/m^2 on a background 10 cd/m^2) along with their Michaelson and Weber luminance contrasts. Highlighted in bold are the most comparable parameters.

Results for controls from the previous study using the Y-hi/Y-lo protocol have a mean Amp of ~13.6 dB and TTP ~445 ms (Carle *et al.*, 2013) compared to our current results in stroke of Amp 16.5 dB and TTP 491 ms. In the G/R protocol the previous results for G-hi/G-lo Amp were ~14.0 dB and for TTP ~460 ms (Carle *et al.*, 2013) compared to our Amp 14.2 dB and TTP 497 ms. It is reassuring that the results have a similar range despite the differences in protocols and populations. It is worth noting that when comparing means of G/R and Y/Y in the previous study and our study, both data sets show an increase in latency within the G/R protocol (+16 ms in previous study and +6 ms in the current study); however for Amp, the previous study showed minimal change (+0.3 dB) and the current study shows a decrease (–1.8 dB). In trying to resolve why there is a difference in reported Amp, the first thing to note is that the variability in results between studies is different. In the previous study, the standard error equated to ~6% of reported values in both Amp and TTP, while in the current study standard errors were ~6% of reported values for TTP, but up to 45% for Amp. This may reflect the fact we are measuring stroke patients, many of which have visual field damage and so include regions which may be diminished or hypersensitive compared to those with normal vision. This variation makes it difficult to interpret whether the decrease is meaningful.

An initial review of individual results appeared to show regions appearing damaged on HFA showed some decreased Amp and TTP values. While this was hidden in the amalgamated results, individual correlations support this observation, showing a positive correlation between Amp and TTP in the large majority, particularly for the G/R protocol. A tentative explanation might be that shallower amplitudes have slower constriction velocities and so their TTP is wider. However, although pupillary response velocity does scale with amplitude (Bremner, 2012), the pupillary response waveform has been shown to be isomorphically scaled – that is every component of its shape remains constant (Semmlow & Stark, 1973; Semmlow *et al.*, 1975; Maddess, 2012), demonstrating that delays in TTP are real and not simply an artefact of wider pupillary responses. Comparing this positive Amp and TTP relationship to the original expectation – that cortical damage would result in both decreased Amp and TTP – appears to support this. Likewise, it was considered that G/R likely utilises a greater cortical input than Y/Y, which is again supported by a greater proportion and stronger correlations in the G/R protocol. But equally, the results for Y/Y should not be overlooked, because applying the same argument, it would suggest that there is also a cortical component to this 'luminance pathway'. Comparing G/R and Y/Y can then be thought of in a less absolute way: it is not 'subcortical luminance' and 'cortical colour exchange' but rather a matter of shifting the balance of the cortical and subcortical components they both produce, either more towards cortical in G/R or more towards subcortical in Y/Y.

Direct and consensual components were explored across both protocols and measures (Figures 6.10–6.12). The previously noted Amp Y/Y contraction anisocoria from Chapter 3 (in which there are hemifield differences) was also demonstrated in the Amp G/R protocol, with broadly similar distribution and a marginally more prominent magnitude. For G/R, the relationship of direct > consensual temporally and consensual > direct nasally was demonstrated across all diseases, and similarly for Y/Y except for the nasal regions of stroke (which were nearly equal).

This is consistent with the literature in which temporal contraction anisocoria is consistent across studies while nasal fields vary (Smith & Smith, 1980; Wyatt & Musselman, 1981; Cox & Drewes, 1984; Martin *et al.,* 1991; Schmid *et al.,* 2000; Carle *et al.,* 2011). TTP did not follow this trend, which intuitively makes sense, given that the difference between direct and consensual responses is predominantly due to differential input from the pretectal olivary nucleus (PON) to the Edinger–Westphal Nucleus (EWN) but does not involve any additional pathways or synapses. TTP showed only very small deviations from direct and consensual equivalence throughout all tested fields, having ratios that were in the range 0.96–1.04 and mostly near 1, whereas the Amp ratios were in the range 0.8–1.2. When the scales were adjusted to make clearer these finer degrees of latency difference (Figures 6.14–6.15), it was found that a large number were polarised (whole field having ratios above 1 or ratios below 1) within a single eye. Eyes would mostly have longer latencies for direct in one eye and longer latencies for consensual in the other, with the direction seemingly at random. On the whole, 60–63% of eyes were polarised through all three disease states and both protocols (Tables 6.2–6.4). While it should be noted these are only small changes in TTP (mostly <30 ms), with so many subjects showing polarisation, and consistency between repeats on different days, it would appear this effect is real. It does not appear to be attributable to the device settings, given the variation in sidedness and extent, nor does it seem to correlate to a protocol, eye, or visual field damage as shown by HFA, but rather it seems likely to be due to intrinsic differences between subjects. While differences between eyes has been reported for combined pupillary components, a difference between eyes for direct and consensual latency does not appear to have been reported by others. A difference in the inter-eye latency for time of onset of pupillary response has been shown in normal subjects to be about 5–10 ms, while there are larger responses in the range 20–60 ms for those with optic neuritis, with larger intensity stimuli having smaller differences (Bergamin & Kardon, 2003). In the stroke group, the average inter-eye latency was 6.8 ms,

falling in the middle of the expected range. Differences between direct and consensual for a single eye averaged over all regions were very variable between subjects and were as large as 30 ms in some eyes; averaging these differences across subjects resulted in a right eye mean difference for direct and consensual of 8.2 ms and a left eye mean difference of 7.6 ms. This suggests that the bulk of the difference in latency between eyes appears to be due to differences in the direct and consensual responses between eyes, giving rise to the commonly observed reciprocal nature of the difference between eyes. While these differences in latency could be due to variable degrees of myelination affecting conduction velocity, their often reciprocal nature suggests anatomical differences such that when one pathway becomes longer, the other becomes shorter.

Consistent with the individual results, correlation between repeats for each protocol (Y/Y and G/R) showed a strong relationship across all conditions (stroke, chiasmal compression, and AION) using both measures (Amp and TTP), except there was only moderate correlation in TTP for the stroke group (Figures 6.19–6.20). This appeared to be due to a number of aberrant results far from the main pool of data where G/R repeat 1 greatly exceeded G/R repeat 2. In investigating the source of this anomaly, a single subject was shown to contribute most of these points, and correlation improved notably if replotted without this subject's results (although no valid reason to exclude them was found). Despite this, the lower correlation coefficients for G/R suggest it is a slightly less reliable measure than its Y/Y counterpart.

It would have been useful to create a G/R receiver operating characteristic (ROC) curve for detection of each of the disease states (as done for Y/Y in Chapter 5), but unfortunately there is no control data to permit this. Although this data could still be collected, the methods used in this current study for Amp analysis seem unlikely to be useful – because there is a strong correlation between Y/Y and G/R amplitude and Y/Y is poor in detecting any of these diseases. The TTP results show much less correlation with Amp (in both protocols), but they also showed

a poor visual correlation with the HFA results, and so it would be surprising if they were to perform well in an ROC analysis.

Considering that there were indeed longer delays in the G/R protocol than the Y/Y, it is worth reviewing the results of an experiment done previously comparing G/R and R/G. Carle et al. tested equiluminant R/G and G/R protocols with luminances of 90, 115, and 140 cd/m^2 and measured Amp and TTP values (Carle *et al.*, 2013). Results demonstrated that the G/R protocol had consistently larger responses and longer latencies – demonstrating that there is a bi-directional response heavily biased towards G/R. The authors suggested that this could be due to chromatic adaptation of cone photoreceptors, so that due to the wavelengths of the tested colours, a green background would enhance activation of red stimuli rather than the reverse. What they did not consider was how this same effect might impact the increased latency noted in G/R compared to R/G. There is a fixed delay in opsin activation which depends on a protein cascade ending in cell hyperpolarisation, a process which occurs in the order of ~20-50ms in cones (van Hateren & Lamb, 2006) and ~100ms in rods to reach peak hyperpolarisation (Arshavsky & Wensel, 2013) after which neurotransmitter release ceases and signal transduction is complete. Intuitively, it then follows that a Y/Y stimulus already has these mechanisms partially activated through the background luminance, so the time required for activation is reduced compared to a G/R protocol (where predominantly new cones need to be activated from rest). However, the much larger portion of the 500-600ms time until peak pupillary constriction is due to delays in iris constriction. The prediction is that the greater the luminance component, the more cross-activation of cones at rest, and the faster the response. Likewise, while less background activation occurs in any colour exchange stimuli, R/G has greater background activation than G/R, and so would be predicted to have shorter delays in activation. This would account for the longer delays we observed in G/R compared to Y/Y. It would also account for the findings of Carle et al. which suggest that greater colour opponency

and reduced luminance result in greater delays, and also why G/R is more responsive in amplitude and has longer latencies than R/G. Further investigation with other colour varieties may confirm if this is in fact the case.

In this context, it is worth considering here the results from Chapter 4, which discussed higher visual function (HVF) deficits, since colour was highlighted as one of the two common deficits. Given that colour provides input to the pupillary response (Heywood *et al.*, 1998), and that the previous chapter suggested colour vision was commonly impaired in the same cohort of subjects for which we now see pupillary impairment (decreased Amp and TTP), it is reasonable to suppose that colour impairment and pupillary impairment may be related. Further, associations of TTP with areas of field damage were more obvious in the G/R group, reinforcing the idea that the G/R protocol has greater cortical involvement. If the colour centre were damaged, the question as to why no subject had complete colour loss (achromatopsia) in HVF arises, but it is true that many had more subtle impairments. Since visual field damage naturally prevents testing of colour vision in that region, and damage to the colour centre without field defects is uncommon, it is strange that colour has been affected so commonly in the seeing field. If colour is considered to be processed bilaterally, then unilateral damage might impair colour in the seeing field; however, this does not make sense when unilateral damage generally causes hemiachromatopsia (colour loss on a single side of homonymous fields) contralaterally (similar to field loss) (Damasio & Damasio, 1986; Kolmel, 1988; Paulson *et al.*, 1994; Short & Graff-Radford, 2001). Alternatively, if one thinks of areas which are necessary for colour, such as posterior aspect of inferior temporal (IT) which when damaged appears to cause cerebral achromatopsia, and others that contribute to colour quality, then perhaps this might better explain what these results demonstrate. Noting the heterogeneity of the stroke cohort also might explain the variation in responses: why some subjects show

damage in Amp and TTP somewhat congruent with visual field damage, while others show no such relationship.

The original premise behind these experiments was that the pupils receive input from the cortex and that cortical damage may be able to be detected using appropriate pupillary stimuli. Some evidence for cortical input to pupillary mechanisms was presented in the introduction, with one elegant paper from Heywood and colleagues unequivocally demonstrating this. Their paper showed that removal of the rostral inferior temporal (IT) cortex of a rhesus monkey removed chromatic pupillary response but spared luminance response (Heywood *et al.*, 1998). Further, they demonstrated that removal of a different region of visual association cortex (V4) did not cause changes to either type of stimuli. The point here is that while there is cortical input to the pupillary response, this cortical input appears to be specialised information from particular regions, such as colour exchange from IT cortex. While a colour exchange protocol may be useful in detecting those with damage to a single area providing colour input to the pupil response, there is no evidence that it can detect damage to other cortical areas. Further, combining colour exchange with luminance (as done in our protocol) means that even if the appropriate cortical region were damaged and the colour component abolished, the luminance component would remain, making it harder to distinguish the response from what is already a noisy response compared to standard automated perimetry.

In summary, the results from Chapter 5 exploring Y/Y Amp and correlating it with visual field damage showed that this was not a good measure; hence a potentially better candidate, G/R TTP, was tested. This definitely showed that a few subjects had decreased TTP which aligned with field damage; however, the majority did not have this pattern, and even in those which did, there was a high degree of noise, making this relationship difficult to establish. There is a large amount of data processing involved in extracting mfPOP raw data and adapting it into a useable form comparable with the Humphrey and Matrix devices, and some steps of this

processing seem likely to add noise – for example, in using weighted means to translate 44 regions into 54 regions. Likewise, the combination of luminance and colour exchange pathways makes it harder to isolate what the causes of changes in responses noted in the stroke group. In future analyses, it may be worth performing isoluminant colour exchange and luminance-only testing, and less heavily processing the data, to see whether this gives less background noise and better performance.

6.6. Conclusion

Pupillary responses from G/R stimuli correlate well with Y/Y stimuli in terms of Amp and TTP, with marginally smaller amplitude and greater latency overall. Trends in direct and consensual responses for both Y/Y and G/R protocols show contraction anisocoria according to hemifield using amplitude measures, but these are not reflected in TTP measures. TTP appears to show, in 60–63% of eyes, subtle differences in direct and consensual responses throughout a significant (p<0.01) number of regions within a single eye, and often with a reciprocal relationship in the fellow eye. These trends in TTP were not associated with either eye or protocol and appear to be anatomical differences between subjects.

Aggregate results comparing Amp against TTP did not show a relationship, but assessment of individual subjects showed that the vast majority had a moderate–strong correlation for Y/Y and a weak–moderate correlation for G/R. Repeats for each protocol and measure generally showed high Pearson values in the range 0.7–0.8 (except for G/R TTP in stroke, which was much smaller at 0.49). The additional G/R protocol and measures of TTP do not, appear to correlate well visually with HFA fields; a few subjects do show a weak relationship, although it is very noisy. The G/R protocol in its current form appears unlikely to have much better utility in identifying stroke than its Y/Y Amp counterpart, although it might have potential if the stimuli were further refined and data processing was streamlined.

References

Arshavsky VY & Wensel TG. (2013). Timing is everything: Gtpase regulation in phototransduction. *Invest Ophthalmol Vis Sci* **54,** 7725-7733.

Barbur JL, Harlow AJ & Sahraie A. (1992). Pupillary responses to stimulus structure, colour and movement. *Opthalmic and Physiological Optics* **12,** 137-141.

Barbur JL, Wolf J & Lennie P. (1998). Visual processing levels revealed by response latencies to changes in different visual attributes. *Proc Biol Sci* **265,** 2321-2325.

Benevento LA & Davis B. (1977). Topographical projections of the prestriate cortex to the pulvinar nuclei in the macaque monkey: An autoradiographic study. *Exp Brain Res* **30,** 405-424.

Benevento LA & Rezak M. (1976). The cortical projections of the inferior pulvinar and adjacent lateral pulvinar in the rhesus monkey (macaca mulatta): An autoradiographic study. *Brain Res* **108,** 1-24.

Benevento LA, Rezak M & Santos A. (1977). An autoradiographic study of the projections of the pretectum in the rhesus monkey (macaca mulatta): Evidence for sensorimotor links to the thalamus and oculomotor nuclei. *Brain Res* **127,** 197-218.

Bergamin O & Kardon RH. (2003). Latency of the pupil light reflex: Sample rate, stimulus intensity, and variation in normal subjects. *Invest Ophthalmol Vis Sci* **44,** 1546-1554.

Bremner FD. (2012). Pupillometric evaluation of the dynamics of the pupillary response to a brief light stimulus in healthy subjects. *Invest Ophthalmol Vis Sci* **53,** 7343-7347.

Carle CF, James AC & Maddess T. (2013). The pupillary response to color and luminance variant multifocal stimuli. *Invest Ophth Vis Sci* **54,** 467-475.

Carle CF, Maddess T & James AC. (2011). Contraction anisocoria: Segregation, summation, and saturation in the pupillary pathway. *Invest Ophthalmol Vis Sci* **52,** 2365-2371.

Cox TA & Drewes CP. (1984). Contraction anisocoria resulting from half-field illumination. *Am J Ophthalmol* **97,** 577-582.

Damasio AR & Damasio H. (1986). Hemianopia, hemiachromatopsia and the mechanisms of alexia. *Cortex* **22,** 161-169.

Dineen JT & Hendrickson A. (1983). Overlap of retinal and prestriate cortical pathways in the primate pretectum. *Brain Res* **278,** 250-254.

Distler C & Hoffmann KP. (1989). The pupillary light reflex in normal and innate microstrabismic cats, ii: Retinal and cortical input to the nucleus praetectalis olivaris. *Vis Neurosci* **3,** 139-153.

Gamlin PDR. (2006). The pretectum: Connections and oculomotor-related roles. *Prog Brain Res* **151,** 379-405.

Gamlin PDR, Zhang HY, Harlow A & Barbur JL. (1998). Pupil responses to stimulus color, structure and light flux increments in the rhesus monkey. *Vision Res* **38,** 3353-3358.

Heywood CA, Nicholas JJ, LeMare C & Cowey A. (1998). The effect of lesions to cortical areas v4 or ait on pupillary responses to chromatic and achromatic stimuli in monkeys. *Exp Brain Res* **122,** 475-480.

Kolmel HW. (1988). Pure homonymous hemiachromatopsia. Findings with neuro-ophthalmologic examination and imaging procedures. *Eur Arch Psychiatry Neurol Sci* **237,** 237-243.

MacIntyre B & Cowan WB. (1992). A practical approach to calculating luminance contrast on a crt. *ACM Trans Graph* **11,** 336–347.

Maddess T. (2012). Pupil dynamics and response amplitude: Only size matters. *Invest Ophth Vis Sci* **53,** 7644-7644.

Martin TI, Kardon RI & Thompson HS. (1991). Unequal direct and consensual pupillary responses to hemiretinal stimuli. *Invest Ophth Vis Sci* **32,** 1124.

McClurkin JW & Optican LM. (1996). Primate striate and prestriate cortical neurons during discrimination. I. Simultaneous temporal encoding of information about color and pattern. *J Neurophysiol* **75,** 481-495.

McClurkin JW, Zarbock JA & Optican LM. (1996). Primate striate and prestriate cortical neurons during discrimination. Ii. Separable temporal codes for color and pattern. *J Neurophysiol* **75,** 496-507.

Paulson HL, Galetta SL, Grossman M & Alavi A. (1994). Hemiachromatopsia of unilateral occipitotemporal infarcts. *Am J Ophthalmol* **118,** 518-523.

Pelli DG & Bex P. (2013). Measuring contrast sensitivity. *Vision Res* **90,** 10-14.

Pickard GE & Sollars PJ. (2012). Intrinsically photosensitive retinal ganglion cells. *Rev Physiol Bioch P* **162,** 59-90.

Sand A, Schmidt TM & Kofuji P. (2012). Diverse types of ganglion cell photoreceptors in the mammalian retina. *Prog Retin Eye Res* **31,** 287-302.

Schmid R, Wilhelm B & Wilhelm H. (2000). Naso-temporal asymmetry and contraction anisocoria in the pupillomotor system. *Graef Arch Clin Exp* **238,** 123-128.

Semmlow J, Hansmann D & Stark L. (1975). Variation in pupillomotor responsiveness with mean pupil size. *Vision Res* **15,** 85-90.

Semmlow J & Stark L. (1973). Pupil movements to light and accommodative stimulation: A comparative study. *Vision Res* **13,** 1087-1100.

Short RA & Graff-Radford NR. (2001). Localization of hemiachromatopsia. *Neurocase* **7,** 331-337.

Smith SA & Smith SE. (1980). Contraction anisocoria: Nasal versus temporal illumination. *The British journal of ophthalmology* **64,** 933-934.

Steele GE & Weller RE. (1993). Subcortical connections of subdivisions of inferior temporal cortex in squirrel monkeys. *Vis Neurosci* **10,** 563-583.

van Hateren JH & Lamb TD. (2006). The photocurrent response of human cones is fast and monophasic. *BMC Neuroscience* **7,** 34.

Wyatt HJ & Musselman JF. (1981). Pupillary light reflex in humans: Evidence for an unbalanced pathway from nasal retina, and for signal cancellation in brainstem. *Vision Res* **21,** 513-525.

Young RSL & Alpern M. (1980). Pupil responses to foveal exchange of monochromatic lights. *J Opt Soc Am* **70,** 697-706.

Chapter 7: Integrative discussion

Chapter 1 provided a background to the visual pathways, processing in higher visual centres, how neurological disease affects these pathways, and introduced both traditional visual field testing and multifocal pupillographic objective perimetry. The topic of functional specialisation of visual association cortices was covered, with isolated deficits in a range of visual functions being highly suggestive of processing in this way (see Chapter 3 introduction for a list of over 20 such examples). Despite many such reports, completely isolated functional deficits remain rare (Vaina, 1995). The distributive model of processing – that multiple areas take part in visual processing – would also appear to have some weight, with selective stimuli activating many cortical areas (McKeefry *et al.*, 1997; Furlan & Smith, 2016). Combining both these concepts, it is a logical progression to believe that multiple areas are involved in processing but that one final area is necessary for perception. If this is the case, the question becomes: does damage to such processing areas result in more subtle defects, which are not examined during routine clinical practice? (Rowe, 2016). This question was addressed in Chapter 1, revealing that it appears to be the case, with depth perception and colour being the primary measures affected. Receiver operator characteristics plots and principal component analysis both suggested that stereofly, randot, and Ishihara were the most useful tests, noting that stereofly and randot appear to measure the same thing and so only one is necessary. It also addressed potential improvements in the current testing regimens, such as larger well Farnsworth–Munsell and a wider dynamic range for Cambridge Facial Memory Test.

A visual deficit known to be common in neurological disease is visual field loss, both in stroke (Zhang *et al.*, 2006; Chen *et al.*, 2009; Gall *et al.*, 2010; Luu *et al.*, 2010; Rowe *et al.*, 2013; Glisson, 2014) and other subcortical diseases like chiasmal compression (Walsh, 1990; Wang

et al., 2008; Kasputyte *et al.*, 2013) and AION (Hayreh & Zimmerman, 2008; Cullen & Chung, 2012; Pahor & Pahor, 2016). To assess these, perimetry is commonly used. In covering the history behind these perimetry devices, common use has progressed from simple confrontational testing (Reader & Harper, 1976), to manual perimetry (Goldmann) (Trope & Britton, 1987), through to automated perimetry with multiple iterations (Johnson *et al.*, 2011; Hepworth & Rowe, 2018; Bevers *et al.*, 2019). In parallel to the more recent iterations of perimetry, the extensive work on multifocal visual evoked potentials ultimately led to the development of multifocal pupillography (for review see Chapter 1, section 1.6.4 *Multifocal methods*). Two key areas of mfPOP development have been its use to non-invasively probe human physiology and its use in ocular disease, both of which are addressed in Chapters 4 and 5 respectively.

Early work with other devices noted that pupil responses in direct were greater than consensual (Lowenstein, 1954; Smith *et al.*, 1979; Fan *et al.*, 2009). Further exploration led to the conclusion that direct consistently exceeded consensual in the temporal field, but results were mixed nasally, some showing consensual marginally exceeding direct (Cox & Drewes, 1984; Martin *et al.*, 1991) while others have shown equivalence (Smith & Smith, 1980; Wyatt & Musselman, 1981; Schmid *et al.*, 2000; Carle *et al.*, 2011b). Investigation with mfPOP has not only produced similar results, but has gone on to produce a model of how these differences occur, proposing it relates to luminance of the stimuli (Carle *et al.*, 2011b) and, more recently, that the majority of the gain control exists at the EWN (Carle *et al.*, 2019). While this finding was investigated in controls, it remained untested in neurological disease. This thesis has investigated stroke, chiasmal compression, and AION, and reveals that these naso-temporal differences in pupillary components persist. It further raises the possibility that the higher density input from the nasal retina (temporal field) explains why the bias towards direct in the temporal field is larger than the bias towards consensual in the nasal field.

In terms of mfPOP use in ocular disease, the device appears to function well in a range of retinal disorder including glaucoma (Maddess *et al.*, 2007; Maddess *et al.*, 2009), AMD (Carle *et al.*, 2011a; Sabeti *et al.*, 2011; Rosli *et al.*, 2012; Sabeti *et al.*, 2014), and diabetic retinopathy (Bell *et al.*, 2010; Carle *et al.*, 2015; Sabeti *et al.*, 2015). Some initial tests with multiple sclerosis (Ali *et al.*, 2014; Maddess & Lueck, 2017) and migraine (Lueck *et al.*, 2014) also show some promise.

If mfPOP is to be the future replacement for standard automated perimetry such as Humphrey perimetry, it must first demonstrate it is at least as good as these devices in the full range of conditions for which perimetry is currently used. It is therefore essential to determine the performance of mfPOP in some of the more common neurological disorders which produce visual field deficits (specifically stroke, chiasmal compression, and AION). Chapter 5 addressed this question, with results demonstrating that the Humphrey and Matrix devices highly correlate, while neither correlate well with mfPOP. Further, in assuming typical field loss for each disease, Humphrey and Matrix were able to detect these disorders, while mfPOP was not. Large variations even in control fields made differentiation very difficult with the mfPOP approach.

It is then worth considering other approaches to using mfPOP which might better detect cortical changes. As there is evidence from anatomical studies of cortical input to the pupillary system at the PON (Benevento & Rezak, 1976; Benevento & Davis, 1977; Benevento *et al.*, 1977; Dineen & Hendrickson, 1983; Distler & Hoffmann, 1989; Steele & Weller, 1993; Gamlin, 2006), which demonstrate that colour exchange induces pupillary constriction (Barbur *et al.*, 1992; Barbur *et al.*, 1998; Carle *et al.*, 2013) and that colour-exchange has delayed responses (Gamlin *et al.*, 1998; Carle *et al.*, 2011b), it has been proposed that colour exchange may preferentially utilise cortical input to the pupillary system. This is further supported by direct evidence in macaques that a cortical lesion can induce colour-exchange-specific deficits while

retaining luminance responses (Heywood *et al.*, 1998). These studies, and a closely related study using isoluminant colour exchange (Carle *et al.*, 2013), informed the design of Chapter 6, which addressed whether coloured stimuli (G/R), and the alternative measure of time-to-peak (latency) gave any promising differences from the luminance-only approach (Y/Y) used in Chapter 5. The population as a whole revealed that the G/R protocol had smaller responses and longer latencies compared to the Y/Y, consistent with the concept that cortical damage lessens cortical input to the pupillary system (thereby reducing amplitude and shifting the balance of input towards the faster subcortical luminance pathway). However, this line of argument is questionable, given similar results found with both chiasmal compression and AION, which are subcortical lesions. While a more definitive repeat analysis using receiver operator curves for the G/R protocol was not possible (because no control dataset was available), visual comparison with Humphrey fields also did not show promise, with mfPOP showing that only a couple of subjects with full hemianopias had mildly congruent damage. While alternative approaches and methods may reveal more sensitive measures, we are forced to conclude that the studies here were unable to demonstrate that mfPOP was effective in stroke, chiasmal compression, or AION.

Nevertheless, comparing results between chapters, some understanding has emerged. It is first worth considering how the higher visual function (HVF) deficits in Chapter 3 relate to the visual field defects in Chapter 5. While the degree of visual field deficits did not prevent appropriate completion of HVF tasks, it is questionable whether in real situations where rapid decision-making is necessary (such as stepping down stairs), that visual field damage might add to the lack of visual information. Interaction of deficits would be consistent with prolonged and reduced functional rehabilitation in those with visual field defects (Riggs *et al.*, 2007). These combined deficits also seem probable, given the proximity of the primary visual cortex to the association cortices (Zeki, 2003). Combined deficits in HVF have also been reported,

frequently grouping colour vision deficits and facial recognition deficits (Bouvier & Engel, 2006), and also suggesting that those with loss of motion sensitivity also have decreased stereopsis (Vaina *et al.*, 2010). This is consistent with the concept of two pathways of processing: dorsal (superiorly towards V5) and ventral (inferiorly towards V4). While the small numbers in this study make it difficult to say, this was evident in the principal component analysis, where the first principal components grouped stereovision tests (stereofly and randot) most closely with motion (kinematogram) [dorsal pathway], and the second grouped colour (Farnsworth–Munsell) with facial recognition (CFMT) [ventral pathway]. The intention of Chapter 3 was to investigate subtotal HVF deficits under the premise that such deficits may be more diffusely located than the functionally specialised regions reported in complete deficits. Since subtle defects were grouped similarly to complete deficits, this implies (perhaps weakly) that these diffuse regions may affect the dorsal and ventral processing pathways, such that damage in a given pathway might subtlety impair function in both domains. It would be interesting to explore this concept further in future analysis of the MRI data collected, and more definitively with a larger study that can use the suggestions from this pilot and provide the resolution necessary for firmer evidence.

The results in Chapter 4 regarding the effect of naso-temporal differences on pupillary components was similar to controls, even in chiasmal compression. This is surprising given that chiasmal compression is expected to reduce responses bitemporally. In this chapter it was noted that not many of the subjects in the pituitary group had overt field deficits on Humphrey field testing, and that this might relate to the lack of evidence for damage to pupillary components. However, in Chapter 5, it was shown that Matrix was exceptionally effective in detecting chiasmal compression, despite there being no obvious field loss. This means that more subtle loss is likely to be present, which mfPOP was unable to detect, as discussed in Chapter 5. So perhaps the persistence of naso-temporal differences is a reflection of mfPOP

not being sensitive to loss rather than to absence of damage. This would make sense in the context of blind-sight, where the person is functionally blind but appears to have subconscious capacity to respond to stimuli they are unable to see. It has been reported that cells which may be involved in this subconscious visual ability are the ipRGC (Van Gelder, 2008), which are also involved in the pupillary response. If these ipRGC persist through substantial retinal loss, as blind-sight suggests they do, then this might explain why the pupillary response was insensitive to both pituitary and AION damage. It at least poses the question: to what extent are ipRGC affected in neurological disorders? Certainly in cortical stroke, it has been established that there is retrograde degeneration to the retina due to lack of feedback (Jindahra *et al.*, 2012), but as ipRGC project subcortically, this cell population may be unaffected. It would be worth studying the behaviour of ipRGC in both retinal and neurological diseases to clarify why mfPOP appears effectual in some conditions and not others.

Chapter 5 directly compared perimeter devices and assessed their effectiveness in differentiating stroke, chiasmal compression, and AION using the typical pattern of field loss expected for these conditions. This is a different approach than has been used previously in mfPOP studies, where often the 'worst *n* regions' has been used in receiver operator characteristics, where *n* has ranged considerably between studies (Maddess *et al.*, 2009; Bell *et al.*, 2010; Sabeti *et al.*, 2011, 2012; Maddess *et al.*, 2013; Carle *et al.*, 2015). While this parameter appears quite effective at differentiating between various retinal conditions and controls, and may even show up progression, this approach is limited. The reason is that it is only a binary differentiator, in other words all conditions lead to worsening of the worst *n* regions, meaning it has great difficulty (or impossibility) in differentiating between conditions, since the pattern of field loss is not considered. Clinically, this is extremely important, given that not all patients present for follow-up of a known condition; rather, many present with an unknown disease which requires diagnosis. In future analysis, it would be informative to review

the results in these chapters using the *n*-worst regions. Likewise it would be worth reviewing data for a mixed disease population, perhaps employing typical patterns of loss as was presented here, to determine if mfPOP might be used to differentiate between diseases (in addition to its established role in differentiating between disease and controls).

Chapter 6 explored alternative mfPOP stimuli and measures, employing G/R stimuli with both colour and luminance components. The principle at work here was that colour change might preferentially stimulate cortical pupillary input. Taking into consideration the results from Chapter 3, which revealed colour to be one of the more prominently affected functions in stroke, it is worth considering how G/R stimuli might be affected by this. As discussed earlier, removal of a particular section of macaque cortex analogous to the human inferior temporal (IT; thought to process colour) selectively impaired chromatic responses but not achromatic luminance changes, while similar experiments with V4 did not (Heywood *et al.*, 1998). It would seem that a complete lesion to IT can dramatically affect pupillary response, while lesion of an adjacent area in the same ventral pathway does not. Considering that colour defects in this cohort was mostly subtle, it does not appear as if there were an isolated IT lesion in this cohort, although, as discussed above, grouping according to dorsal and ventral pathways does seem likely. It then follows that any damage that does not lesion the IT is unlikely to result in pupillary changes. While several subjects with full homonymous hemianopias who completed G/R mfPOP testing did show some alignment with Humphrey fields, quadrantanopias and scotomas (which were more frequent) did not. It would be indeed worthwhile to analyse the MRI data from these selected subjects, in order to determine if the IT region was affected, and whether this might support pupillary changes in response to cortical lesions in humans.

Conclusion

This thesis set out to explore testing visual deficits in neurological disease, and to address the lack of information in the literature surrounding subtle HVF in stroke and visual field assessment using pupillometry in common neurological diseases.

Chapter 3 sought to pilot a study screening for common HVF, and determine which HVF (if any) show deficits, which tests are effective in measuring these, and how those tests might be improved towards a larger and more concrete study in the future. The chapter reveals that there are common HVF deficits in stereopsis and colour, which can be detected using Ishihara, stereofly, and randot. Several improvements were suggested, including selection of stereofly over randot, larger well set for Farnsworth-Munsell, and more sensitive CFMT by using racially specific versions and more distractor images.

Chapter 4 sought to determine if direct and consensual pupil components retained naso-temporal differences in neurological diseases, explore the physiology behind these differences, and investigate how they might be combined into a single measure for clinical practice. The chapter reveals that naso-temporal differences are retained in stroke, chiasmal compression, and AION, suggests that temporal bias appears greater than nasal bias due to density of retinal input, and shows that SNR weighted means are an appropriate means to combine signals without discarding data and with minimal bias.

Chapter 5 sought to compare the perimetry devices of Humphrey, Matrix, and mfPOP, correlate their fields, seek an understanding of why any differences exist, and determine which are most effective in detection of stroke, chiasmal compression, and AION. The chapter reveals that Humphrey and Matrix correlate well, while mfPOP does not correlate with either of the other two devices. It appears this may relate to mfPOP measuring structural damage to ipRGC which

may be resistant to damage, while standard automated perimetry measure perceptual damage. Both Humphrey and Matrix were effective in detection of all tested neurological disorders, with Humphrey being marginally better in pituitary and AION, while Matrix was exquisitely sensitive to chiasmal compression, while mfPOP was poor throughout. Results from this study have not been promising, and suggest that mfPOP is inferior to current methods in detection of visual field loss in stroke, chiasmal compression, and AION.

Chapter 6 sought to determine if an alternate mfPOP approach using colour exchange stimuli (G/R), or the alternate measure of pupillary latency (time-to-peak; TTP) reveal any differences compared to the traditional testing of luminance only (Y/Y). The chapter reveals that G/R protocol has marginally smaller Amps and marginally larger TTP, but otherwise correlate well with each other. It notes there are biases in direct and consensual responses between eyes that are largely reciprocal in nature, and that individuals appear to show a positive relationship between Amp and TTP in all conditions. Lastly it shows the there is moderate-strong correlation between repeats, although with substantial noise.

Overall this thesis has substantially contributed to the knowledge of visual impairment in neurological diseases, and suggested some interesting new topics to explore. Notably, whether colour and depth should be routinely tested in clinical practice, whether retinal density plays a role in pupillary component naso-temporal bias, whether hemifield ratios might be an effective means for early detection of chiasmal compression, and whether G/R delays are actually caused by cortical processing.

References

Ali EN, Maddess T, James AC, Voicu C & Lueck CJ. (2014). Pupillary response to sparse multifocal stimuli in multiple sclerosis patients. *Mult Scler* **20,** 854-861.

Barbur JL, Harlow AJ & Sahraie A. (1992). Pupillary responses to stimulus structure, colour and movement. *Opthalmic and Physiological Optics* **12,** 137-141.

Barbur JL, Wolf J & Lennie P. (1998). Visual processing levels revealed by response latencies to changes in different visual attributes. *Proc Biol Sci* **265,** 2321-2325.

Bell A, James AC, Kolic M, Essex RW & Maddess T. (2010). Dichoptic multifocal pupillography reveals afferent visual field defects in early type 2 diabetes. *Invest Ophth Vis Sci* **51,** 602-608.

Benevento LA & Davis B. (1977). Topographical projections of the prestriate cortex to the pulvinar nuclei in the macaque monkey: An autoradiographic study. *Exp Brain Res* **30,** 405-424.

Benevento LA & Rezak M. (1976). The cortical projections of the inferior pulvinar and adjacent lateral pulvinar in the rhesus monkey (macaca mulatta): An autoradiographic study. *Brain Res* **108,** 1-24.

Benevento LA, Rezak M & Santos A. (1977). An autoradiographic study of the projections of the pretectum in the rhesus monkey (macaca mulatta): Evidence for sensorimotor links to the thalamus and oculomotor nuclei. *Brain Res* **127,** 197-218.

Bevers C, Blanckaert G, Van Keer K, Fils JF, Vandewalle E & Stalmans I. (2019). Semi-automated kinetic perimetry: Comparison of the octopus 900 and humphrey visual field analyzer 3 versus goldmann perimetry. *Acta Ophthalmol* **97,** e499-e505.

Bouvier SE & Engel SA. (2006). Behavioral deficits and cortical damage loci in cerebral achromatopsia. *Cereb Cortex* **16,** 183-191.

Carle CF, James AC, Kolic M, Essex RW & Maddess T. (2015). Blue multifocal pupillographic objective perimetry in glaucoma. *Invest Ophthalmol Vis Sci* **56,** 6394-6403.

Carle CF, James AC, Kolic M, Loh YW & Maddess T. (2011a). High-resolution multifocal pupillographic objective perimetry in glaucoma. *Invest Ophth Vis Sci* **52,** 604-610.

Carle CF, James AC & Maddess T. (2013). The pupillary response to color and luminance variant multifocal stimuli. *Invest Ophth Vis Sci* **54,** 467-475.

Carle CF, James AC, Rosli Y & Maddess T. (2019). Localization of neuronal gain control in the pupillary response. *Frontiers in neurology* **10,** 203.

Carle CF, Maddess T & James AC. (2011b). Contraction anisocoria: Segregation, summation, and saturation in the pupillary pathway. *Invest Ophthalmol Vis Sci* **52,** 2365-2371.

Chen CS, Lee AW, Clarke G, Hayes A, George S, Vincent R, Thompson A, Centrella L, Johnson K, Daly A & Crotty M. (2009). Vision-related quality of life in patients with complete homonymous hemianopia post stroke. *Top Stroke Rehabil* **16,** 445-453.

Cox TA & Drewes CP. (1984). Contraction anisocoria resulting from half-field illumination. *Am J Ophthalmol* **97,** 577-582.

Cullen JF & Chung SH. (2012). Non-arteritic anterior ischaemic optic neuropathy (na-aion): Outcome for visual acuity and visual field defects, the singapore scene 2. *Singapore Med J* **53,** 88-90.

Dineen JT & Hendrickson A. (1983). Overlap of retinal and prestriate cortical pathways in the primate pretectum. *Brain Res* **278,** 250-254.

Distler C & Hoffmann KP. (1989). The pupillary light reflex in normal and innate microstrabismic cats, ii: Retinal and cortical input to the nucleus praetectalis olivaris. *Vis Neurosci* **3,** 139-153.

Fan X, Miles JH, Takahashi N & Yao G. (2009). Sex-specific lateralization of contraction anisocoria in transient pupillary light reflex. *Invest Ophthalmol Vis Sci* **50,** 1137-1144.

Furlan M & Smith AT. (2016). Global motion processing in human visual cortical areas v2 and v3. *J Neurosci* **36,** 7314-7324.

Gall C, Franke GH & Sabel BA. (2010). Vision-related quality of life in first stroke patients with homonymous visual field defects. *Health Qual Life Out* **8**.

Gamlin PDR. (2006). The pretectum: Connections and oculomotor-related roles. *Prog Brain Res* **151,** 379-405.

Gamlin PDR, Zhang HY, Harlow A & Barbur JL. (1998). Pupil responses to stimulus color, structure and light flux increments in the rhesus monkey. *Vision Res* **38,** 3353-3358.

Glisson CC. (2014). Visual loss due to optic chiasm and retrochiasmal visual pathway lesions. *Continuum (Minneap Minn)* **20,** 907-921.

Hayreh SS & Zimmerman MB. (2008). Nonarteritic anterior ischemic optic neuropathy: Natural history of visual outcome. *Ophthalmology* **115,** 298-305 e292.

Hepworth LR & Rowe FJ. (2018). Programme choice for perimetry in neurological conditions (popin): A systematic review of perimetry options and patterns of visual field loss. *Bmc Ophthalmol* **18,** 241.

Heywood CA, Nicholas JJ, LeMare C & Cowey A. (1998). The effect of lesions to cortical areas v4 or ait on pupillary responses to chromatic and achromatic stimuli in monkeys. *Exp Brain Res* **122,** 475-480.

Jindahra P, Petrie A & Plant GT. (2012). The time course of retrograde trans-synaptic degeneration following occipital lobe damage in humans. *Brain* **135,** 534-541.

Johnson CA, Wall M & Thompson HS. (2011). A history of perimetry and visual field testing. *Optometry and vision science : official publication of the American Academy of Optometry* **88,** E8-15.

Kasputyte R, Slatkeviciene G, Liutkeviciene R, Glebauskiene B, Bernotas G & Tamasauskas A. (2013). Changes of visual functions in patients with pituitary adenoma. *Med Lith* **49,** 132-137.

Lowenstein O. (1954). Alternating contraction anisocoria; a pupillary syndrome of the anterior midbrain. *AMA Arch Neurol Psychiatry* **72,** 742-757.

Lueck C, Ali E, Carle C & Maddess T. (2014). Effects of stimulating melanopsin-containing retinal ganglioncells in migraine patients using multifocal objective pupillometry. *J Clin Neurosci* **21,** 2048.

Luu S, Lee AW, Daly A & Chen CS. (2010). Visual field defects after stroke a practical guide for gps. *Aust Fam Physician* **39,** 499-503.

Maddess T, Bedford SM, Goh XL & James AC. (2009). Multifocal pupillographic visual field testing in glaucoma. *Clin Exp Ophthalmol* **37,** 678-686.

Maddess T, Essex RW, Kolic M, Carle CF & James AC. (2013). High- versus low-density multifocal pupillographic objective perimetry in glaucoma. *Clin Exp Ophthalmol* **41,** 140-147.

Maddess T, Goh XL & James AC. (2007). Luminance and chromatic multifocal pupillographic perimetry. In *ARVO annual meeting*, pp. 1628. Investigative ophthalmology and visual science.

Maddess T & Lueck CJ. (2017). Multiple sclerosis seen through new eyes. *Clin Exp Ophthalmol* **45,** 9-11.

Martin TI, Kardon RI & Thompson HS. (1991). Unequal direct and consensual pupillary responses to hemiretinal stimuli. *Invest Ophth Vis Sci* **32,** 1124.

McKeefry DJ, Watson JDG, Frackowiak RSJ, Fong K & Zeki S. (1997). The activity in human areas v1/v2, v3, and v5 during the perception of coherent and incoherent motion. *Neuroimage* **5,** 1-12.

Pahor A & Pahor D. (2016). [clinical findings in patients with non-arteritic anterior ischemic optic neuropathy (na-aion) under 50 years of age]. *Klin Monbl Augenheilkd* **233,** 66-71.

Reader AL & Harper DG. (1976). Confrontation visual-field testing. *Jama-J Am Med Assoc* **236,** 250-250.

Riggs RV, Andrews K, Roberts P & Gilewski M. (2007). Visual deficit interventions in adult stroke and brain injury - a systematic review. *Am J Phys Med Rehab* **86,** 853-860.

Rosli Y, Bedford SM, James AC & Maddess T. (2012). Photopic and scotopic multifocal pupillographic responses in age-related macular degeneration. *Vision Res* **69,** 42-48.

Rowe F. (2016). Visual effects and rehabilitation after stroke. *Community Eye Health* **29,** 75-76.

Rowe FJ, Wright D, Brand D, Jackson C, Harrison S, Maan T, Scott C, Vogwell L, Peel S, Akerman N, Dodridge C, Howard C, Shipman T, Sperring U, Macdiarmid S & Freeman C. (2013). A prospective profile of visual field loss following stroke: Prevalence, type, rehabilitation, and outcome. *BioMed research international* **2013,** 719096.

Sabeti F, Maddess T, Essex RW & James AC. (2011). Multifocal pupillographic assessment of age-related macular degeneration. *Optometry Vision Sci* **88,** 1477-1485.

Sabeti F, Maddess T, Essex RW & James AC. (2012). Multifocal pupillography identifies ranibizumab-induced changes in retinal function for exudative age-related macular degeneration. *Invest Ophthalmol Vis Sci* **53,** 253-260.

Sabeti F, Maddess T, Essex RW, Saikal A, James AC & Carle CF. (2014). Multifocal pupillography in early age-related macular degeneration. *Optometry and vision science : official publication of the American Academy of Optometry* **91,** 904-915.

Sabeti F, Nolan CJ, James AC, Jenkins A & Maddess T. (2015). Multifocal pupillography identifies changes in visual sensitivity according to severity of diabetic retinopathy in type 2 diabetes. *Invest Ophthalmol Vis Sci* **56,** 4504-4513.

Schmid R, Wilhelm B & Wilhelm H. (2000). Naso-temporal asymmetry and contraction anisocoria in the pupillomotor system. *Graef Arch Clin Exp* **238,** 123-128.

Smith SA, Ellis CJ & Smith SE. (1979). Inequality of the direct and consensual light reflexes in normal subjects. *The British journal of ophthalmology* **63,** 523-527.

Smith SA & Smith SE. (1980). Contraction anisocoria: Nasal versus temporal illumination. *The British journal of ophthalmology* **64,** 933-934.

Steele GE & Weller RE. (1993). Subcortical connections of subdivisions of inferior temporal cortex in squirrel monkeys. *Vis Neurosci* **10,** 563-583.

Trope GE & Britton R. (1987). A comparison of goldmann and humphrey automated perimetry in patients with glaucoma. *The British journal of ophthalmology* **71,** 489-493.

Vaina LM. (1995). Akinetopsia, achromatopsia and blindsight: Recent studies on perception without awareness. *Synthese* **105,** 253-271.

Vaina LM, Sikoglu EM, Soloviev S, LeMay M, Squatrito S, Pandiani G & Cowey A. (2010). Functional and anatomical profile of visual motion impairments in stroke patients correlate with fmri in normal subjects. *J Neuropsychol* **4,** 121-145.

Van Gelder RN. (2008). Non-visual photoreception: Sensing light without sight. *Curr Biol* **18,** R38-39.

Walsh TJ. (1990). *Visual fields: Examination and interpretation*. Oxford University Press, Oxford, United Kingdom.

Wang HB, Sun W, Fu Z, Si ZC, Zhu YF, Zhai GD, Zhao GY, Xu SC & Pang Q. (2008). The pattern of visual impairment in patients with pituitary adenoma. *J Int Med Res* **36,** 1064-1069.

Wyatt HJ & Musselman JF. (1981). Pupillary light reflex in humans: Evidence for an unbalanced pathway from nasal retina, and for signal cancellation in brainstem. *Vision Res* **21,** 513-525.

Zeki S. (2003). Improbable areas in the visual brain. *Trends Neurosci* **26,** 23-26.

Zhang XJ, Kedar S, Lynn MJ, Newman NJ & Biousse V. (2006). Homonymous hemianopia in stroke. *J Neuro-Ophthalmol* **26,** 180-183.